UNIVERSITY OF COPENHAGEN
FACULTY OR DEPARTMENT

PhD thesis

Global volcanism as seen in ice cores during the last glacial cycle

Sulfate magnitude, climate forcing and probability of recurrence

Jiamei Lin

Supervisor: Anders Svensson

Submitted on: October 1st, 2022

This thesis has been submitted to the PhD School of The Faculty of Science, University of Copenhagen

Abstract – English

Historical large sulfur-rich volcanic eruptions disturbed the radiation budget, blocked incoming sunlight, cooled the surface, altered the precipitation and temperature in the earth system due to the sulfuric acid aerosols in the atmosphere. The Younger Toba Tuff eruption, the largest volcanic eruption in the Quaternary, has been suggested to have induced an abrupt climate oscillation as the effect of long lifetime and large scale stratospheric sulfate aerosols in atmospheric circulation and the following feedbacks in ocean dynamics and sea ice. Humans have limited knowledge about the sulfate magnitude, the frequency, and the probability of the occurrence of such large volcanic eruptions.The past volcanic sulfate signals are recorded in the ice sheets. The sulfate magnitude, climate forcing, and timing of the explosive volcanic eruptions can be reconstructed from an array of Greenland and Antarctic ice cores that cover the last glacial period. That will be beneficial for understanding the volcanic impact on climate and useful for forecasting future volcanic hazards.

This dissertation extends the volcanic sulfate deposition in Greenland and Antarctica during the second half of the last glacial period and the early Holocene (60-9 ka), and estimates the emission strength, the frequency, and the climatic forcing of large volcanic eruptions. There are 69 volcanic eruptions that have stronger emissions strength than that of the Tambora, 1815 AD eruption (Chapter 2).

Second, this dissertation compiles all available ice-core sulfate records and published sulfur isotope records to pinpoint, constrain the magnitude, and characterize the ~74 ka Toba eruption, which is proposed to be the largest volcanic eruption in the Quaternary. The estimated volcanic stratospheric sulfate loading of the eruption is 535 ± 96 Tg, that is 3.3 times that of the Samalas 1258 AD, 6.3 times that of the Tambora 1815 AD, and 9.7 times that of the Pinatubo 1991 AD. The continuous time-series of volcanic sulfate deposition, sulfur emission strength, and volcanic radiative forcing are derived for the period of 74.8-73.8 ka (Chapter 3).

Third, this dissertation estimates the recurrence rate and probability of global sulfur-rich volcanism based on the ice-core bi-hemispheric volcanic records over the Holocene and the last glacial periods (Chapter 4). In a statistical approach, the mean return time is estimated to be 434 years for volcanic eruptions larger than the Tambora 1815 AD eruption, and the probability of this magnitude eruption being observed in the next 100 years is around 19%.

Abstract – Danish

Historiske store svovlholdige vulkanudbrud har forstyrret strålingsbudgettet, blokeret for indkommende sollys, afkølet overfladen og ændret nedbør og temperatur i jordsystemet på grund af svovlsyreaerosoler i atmosfæren. Det yngre Toba Tuff-udbrud, det største vulkanudbrud i kvartæret, er blevet foreslået at have forårsaget en pludselig klimasvingning som følge af langvarige og store stratosfæriske sulfataerosoler i atmosfærisk cirkulation og de efterfølgende feedbacks i havets dynamik og havisen. De tidligere vulkanske sulfatsignaler er registreret i indlandsisen. Mennesket har begrænset viden om sulfatmængden, hyppigheden og sandsynligheden for sådanne store vulkanudbrud. Sulfatstørrelsen, klimapåvirkningen og tidspunktet for de eksplosive vulkanudbrud kan rekonstrueres ud fra en række grønlandske og antarktiske iskerner, der dækker den sidste istid. Det vil være gavnligt for forståelsen af den vulkanske indvirkning på klimaet og nyttigt til at forudsige fremtidige vulkanske farer.

Denne afhandling udvider den vulkanske sulfataflejring i Grønland og Antarktis i anden halvdel af den sidste istid og den tidlige holocæn (60-9 ka) og estimerer emissionsstyrken, hyppigheden og den klimatiske påvirkning af store vulkanske udbrud. Der er 69 vulkanudbrud, som har en større emissionsstyrke end Tambora-udbruddet i 1815 e.Kr. (kapitel 2).

For det andet samler denne afhandling alle tilgængelige sulfatoptegnelser fra vulkanske iskerner og offentliggjorte svovlisotopoptegnelser med henblik på at identificere og begrænse størrelsen og karakterisere Toba-udbruddet på ~74 ka, som foreslås at være det største vulkanudbrud i kvartæret. Den anslåede vulkaniske stratosfæriske sulfatbelastning fra udbruddet er 535 ± 96 Tg, hvilket er 3,3 gange så meget som Samalas 1258 e.Kr., 6,3 gange så meget som Tambora 1815 e.Kr. og 9,7 gange så meget som Pinatubo 1991 e.Kr. De kontinuerlige tidsserier af vulkansk sulfatdeposition, svovlemissionens styrke og den vulkanske strålingsforcing er udledt for perioden 74,8-73,8 ka (kapitel 3).

For det tredje vurderes i denne afhandling gentagelsesfrekvensen og sandsynligheden for global svovlrig vulkanisme på grundlag af de bi-hemisfæriske vulkanske optegnelser fra iskerne i Holocæn og de sidste istider (kapitel 4). I en statistisk tilgang anslås den gennemsnitlige genkomsttid at være 434 år for vulkanudbrud større end Tambora-udbruddet i 1815 e.Kr., og sandsynligheden for at et udbrud af denne størrelsesorden vil blive observeret inden for de næste 100 år er ca. 19 %.

Publications and author contributions

This thesis is comprised by three research articles in Chapters 2 to 4.

Chapter 2- Magnitude, frequency and climate forcing of global volcanism during the last glacial period as seen in Greenland and Antarctic ice cores (60-9 ka)

***Lin, J.**, Svensson, A., Hvidberg, C. S., Lohmann, J., Kristiansen, S., Dahl-Jensen, D., Steffensen, J. P., Rasmussen, S. O., Cook, E., Kjær, H. A., Vinther, B. M., Fischer, H., Stocker, T., Sigl, M., Bigler, M., Severi, M., Traversi, R., and Mulvaney, R.: Magnitude, frequency and climate forcing of global volcanism during the last glacial period as seen in Greenland and Antarctic ice cores (60–9 ka), Clim. Past, 18, 485–506, https://doi.org/10.5194/cp-18-485-2022, 2022.*

Author contributions: The initial idea was designed by AS. Datasets were collected by AS and JL. JL analyzed the data and created the figures. JL and AS prepared the paper. All authors contributed to the discussion and commented on the paper.

Chapter 3- Pinpointing the ~74 ka Toba eruption from ice cores and estimating the volcanic radiative forcing of the 74.8-73.8 ka period

***Jiamei Lin**, Peter M. Abbott, Michael Sigl, Jørgen P. Steffensen, Robert Mulvaney, Mirko Severi, Anders Svensson*

This manuscript is under review in the peer-reviewed journal Quaternary Science Review at 1st May, 2022.

Author contributions: All the authors contribute to this manuscript. JL wrote the paper with AS. JL analysed the data and create figures. AS, JL, JP, RM, MS were involved to obtain the applied datasets. All authors contribute the comments on the paper.

Chapter 4- Recurrence rates and probability of global sulfur-rich volcanism as seen from ice cores

***Jiamei Lin**, Anders Svensson, Johannes Lohmann*

This manuscript is in final step of preparation to be submitted at a peer-reviewed journal

Author contributions: All the authors contribute to this manuscript. JL designed and wrote the paper. JL analysed the data and create figures. AS revised the papers. All authors contribute the comments on the paper.

Co-author contributions of research papers out of this thesis:

Svensson, A., ***Lin, J.****, Sinnl, G., Dahl-Jensen, D., Steffensen, J. P., Rasmussen, S. O., Vinther, B. M., Cook, E., Kjær, H. A., Muscheler, R., Kipfstuhl, S., Wilhelms, T. F., Fischer, H., Bigler, M., Sigl, M., Landais, A., Parrenin, F., Buizert, C., McConnell, J. R., Severi, M., Mulvaney, R.: Bipolar volcanic ice-core synchronization of the last glacial cycle (In prepare)*

Johannes Lohmann, ***Jiamei Lin****, Bo M. Vinther, Sune O. Rasmussen and Anders Svensson.: Climatic impact of volcanic eruptions during the last glacial period inferred from Greenland and Antarctic ice cores (In prepare).*

Sigl, M., Abbott, P., Adolphi, F., Albertl, G., Chellman, N., Baillie, Michael G. L., Burke, A., Cole-Dai, Jihong, Cook, E., Davies, S., Gabriel, I., Helmick, M., Horhold, M., Innes, H., Jungclaus, J., Kuger, K., Nicolussi, K., Kurbarov, A., ***Lin, J.****, Mcconnell, J., Pearson, C., Plunker, G., Salzer M., Severi, M., Svensson, A., Timmerck, C., Toohey, M.: Timing of Holocene volcanic eruptions and their radiative aerosol forcing (In prepare).*

Eliza Cook, Johannes Lohmann, Vera Ponomareva, Maxim Portnyagin, ***Jiamai Lin****, Anders Svensson, Michael Sigl, Elliott Street, Joseph Harrison.: Early Holocene explosive Kamchatkan volcanism cooled climate in the Northern Hemisphere (In prepare).*

Acknowledgments

Many thanks to my supervisor Ander Svensson for his advice, support and help over the past three years and proofreading for this thesis.

I would like to thank Prof. Kirstin Krüger at the university of Oslo (UIO), who gave me invaluable and dispassionate advice in my research work during my Ph.D exchange.

I would like to thank all the people in PICE. Such a nice research group and equal research environment.

A big thank for my office colleagues - Tamara, Julien and Gulia. Great time working and hang out together.

A big thank to my friends in Copenhagen, Alan, Jianwei Qi, Paul, Ying Yu, Shanzhong Han, Liu Jian, Wang Lu, Sara, Stefano, Tania and Kirsten. You guys are sunlight in my spare life.

I would like to thank Tomas Zoega at UIO for his nice comments on the first chapter of this thesis, and the others at UIO. I had a wonderful summer there.

Many thanks to my parents, my grandpa, my sister and brother. Your support and careness rise my up over the past three years.

Abbreviations

AICC 2012	Antarctic Ice Core Chronology
ECM	Electrical Conductivity Measurement
DEP	Dielectrical Profiling
VEI	Volcanic Explosivity Index
Toba	Youngest Toba Tuff
NEEM	North Greenland Eemian Ice Drilling
GICC05	Greenland Ice Core Chronology 2005
SH	Southern Hemisphere
NH	Northern Hemisphere
WDC	WAIS Divide
TE-CFA	Trace Element Continuous Flow Analysis
LGM	Last Glacial Maximum
DO	Dansgaard Oeschger
AMOC	Atlantic Meridional Overturning Circulation
VSSL	Volcanic Stratospheric Sulfate Loading
TAL	Talos Dome
IC	Ion Chromatography
FIC	Fast Ion Chromatography
CFA	Continous Flow Analysis
ICP-MS	Inductively Coupled Plasma Mass Spectrometers

List of figures

Contents

Chapter 1

Chapter content

The state of the art of ice-core volcanic records

Explosive volcanic eruptions are one of the major forcings of climate change. Their sulfate aerosols scatter the solar radiation back to space causing short or long term climate cooling, both regionally or globally (Robock, 2000). Large explosive volcanic eruptions induce climatic hazards, leading to economic loss, famines and pandemics in human societies (Luterbacher and Pfister, 2015; Rampino and Self, 1992; Guillet et al., 2017; Tejedor et al., 2021). The 1815 AD Tambora eruption caused extreme weather 'the year without a summer' and led to famines and malnutrition (Luterbacher and Pfister, 2015). The Youngest Toba Tuff (Toba) eruption that occurred some 74 thousand years before present (BP) in Indonesia is one of the largest eruptions in the Quaternary Period (2.58 million years ago to present; Paine et al., 2021; Storey et al., 2012). Its magnitude in terms of Volcanic Explosivity Index (VEI) is estimated to 8.8 and it has been related to 'a human bottleneck' (Rampino and Self, 1992). The largest volcanic eruptions with a magnitude of VEI-8 occur very rarely and have not been observed in the last two millennia (Papale, 2018; Sigl et al., 2013). Compared to water vapor, carbon dioxide, ash and dust emitted from a volcano, volcanic sulfur-containing gas and sulfate aerosols play an important role in the atmosphere as they influence the long-term global radiation budget (Swingedouw et al., 2017). Volcanic eruptions have been proven as one of the main drivers of climate variability through direct volcanic aerosol forcing and possible feedbacks from ocean dynamics and sea ice (Sigl et al., 2015; Baldini et al., 2015). In the past 2500 years, the climatic cooling caused by explosive volcanic eruptions and observed from tree ring proxies, is proportional to the magnitude of the volcanic forcing related to the stratospheric volcanic sulfate aerosol loading, which is mostly quantified from ice-core sulfate records (Sigl et al., 2015). Ice cores are useful for tracing the eruption age and assessing the post volcanic sulfate deposition with high accuracy, possibly linking it to other climate proxies, such as water isotopes and tree-rings, to estimate the volcanic climatic impact.

In this chapter, I introduce the polar ice sheets and the deep ice-core projects in Section 1.1. In Section 1.2, I introduce the climate variability during the last glacial cycle.Then follows an overview of ice-core dating methods applied in Greenland and Antarctica in Section 1.3. In Section 1.4, I provide an overview of the regional volcanic synchronizations in Greenland and Antarctic ice cores and the bi-hemisphere volcanic matching. In Section 1.5, I provide an overview of ice-core sulfate and sulfur record measurements and go through the reconstruction

of historical ice-core volcanic records. In Section 1.6, I introduce the climate response to large historical volcanic eruptions by the application of temperature proxies and volcanic climatic models.

1.1 Ice sheets and deep ice core projects

1.1.1 Ice sheets are archives of past climate

The Greenland and Antarctic ice sheets are beautiful climate archives of the earth's system. Ice sheets comprise about 99% of all continental glaciers on earth and play an important role in the climate system. The ice volume of the Antarctic ice sheet, equals to 58 m potential sea level rise, which is about 17 times that of the Greenland ice sheet (Fretwell et al., 2013). The thickest part of the Antarctic ice sheet is about 4000 m thick and around 3000 m in Greenland (Fig. 1.1). The ice sheets are commonly described by two zones – the accumulation and ablation zone. The accumulation zone is the area of snowfall accumulating and exceeding the losses from ablation, such as melting, sublimation and evaporation. In polar dry snow zones, the ice layers are generally not disturbed by ice melt and ice flow. The climate records are well perserved in these zones with long time series and high resolution. These sequenced climate archives in the ice sheets are formed in a long process, where snow is gradually transformed into firn and ice and concealed with impurity and air mass, reflecting regional and remote climate conditions. The transition from firn to ice varies with density and the density for pure glacier ice is approximately 917 kg m^{-3}.

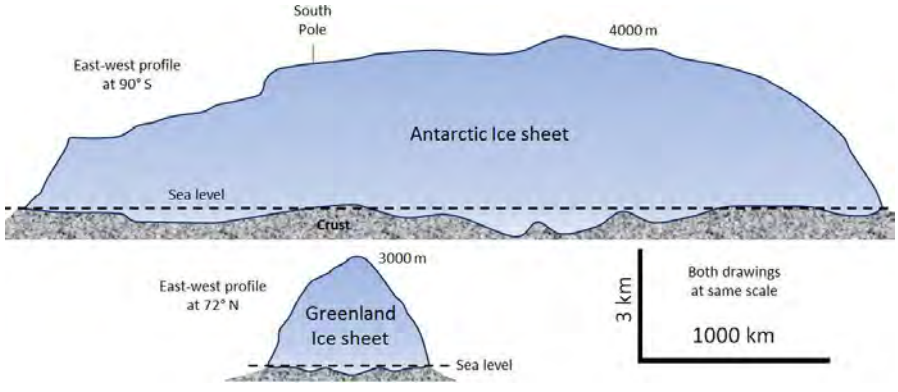

Figure 1.1 Greenland and Antarctic cross-sectional profiles - both drawn on the same scale. [https://opentextbc.ca/geology/chapter/16-2-how-glaciers-work/]

Polar ice sheets are dynamic bodies of flowing and deforming ice. Snow accumulates on the ice sheet's surface and is compressed into firn and ice in the upper ~100 m of the ice sheet. The

ice flows due to its own gravity as snow accumulates in the ice sheet. The ice flows from the central part of the ice sheet to the ice margin where it melts, runs off or calves as an iceberg (Fig. 1.2). The annual ice layers continue to thin with depth as more ice is accumulated and ice flows by its own weight. The ice flow model reconstruction depends on the past accumulation rate that vary with climate and are difficult to reconstruct precisely. The ice layer thinning function at specific ice core site can be approximated using the Dansgaard – Johnsen flow model (Dansgaard and Johnsen, 1969; Fudge et al., 2016; Gkinis et al., 2016; Hvidberg et al., 1997; Veres et al., 2013). From an ice flow model, the annual layer thinning and the depth-age relationship can be deduced.

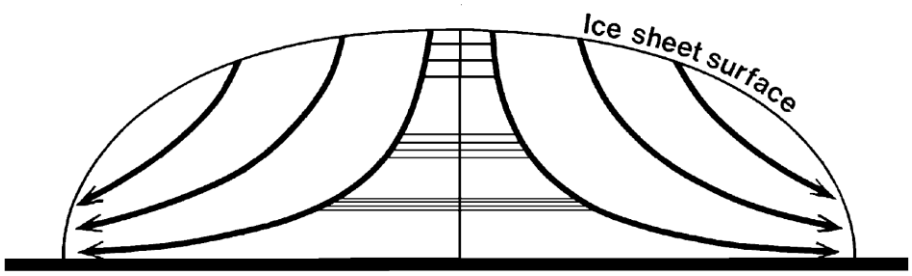

Figure 1.2 A sketch of the cross section of Greenland and Antartic ice sheet shows the ice accumulation and ablation, the ice layer thinning and ice flow process.

Ice cores preserve past climate conditions, such as the atmospheric composition of gases, the atmopsheric dust content, the water isotopic composition, proxies for past solar activity, and the occurrence of explosive volcanic eruptions in terms of acidity and tephra. The past volcanic activities can be traced through liquid conductivity, electrical conductivity measurments (ECM), Di-Electric Properties (DEP), non-sea salt sulfate and the other impurities. The climate response to volcanic eruptions can be traced through ice-core parameters of water isotopes, gases, major soluble ions or particle size and composition of dust that indicate the source of air mass. The following give a short introduction to some of the above-mentioned parameters:

a) Water isotopes ($\delta^{18}O$ and δD): The $\delta^{18}O$ (δD) is the isotopic ratio with regard to a standard value of oxygen (hydrogen). The isotopic composition of polar ice cores reflects the evaporation and condensation processes, providing information on the past temperature in the polar region (Dansgaard, 1964). The deuterium-excess ($\delta D - 8 * \delta^{18}O$) is determined by the water isotopes ($\delta^{18}O$ and δD) measured from polar ice cores, which identifies the moisture source within the hydrological cycle (Masson-Delmotte et al., 2005).

b) Chemical impurities: the dissolved chemicals in the ice core, including major ions NH_4^+ , Na^+, Ca^{2+}, NO_3^-, and SO_4^{2-}, can be analyzed through Ion Chromatography (IC), Fast Ion Chromatography (FIC), Inductively Coupled Plasma Mass Spectrometers (ICP-MS) and Continous Flow Analysis (CFA) system (Legrand and Mayewski, 1997; Röthlisberger et al., 2000). The composition of major ions in the ice cores may provide information on the past atmospheric circulation. The Ca^{2+} mainly originates from terrestrial sources. The Na^+ and Cl^- are of sea-salt origin, and the NH_4^+ is mainly of bacterial decomposition origin. The NO_3^- is from biomass burning, bacterial decomposition in soils, and lightning strikes. In addition to volcanism, the SO_4^{2-} is of marine biogenic activity or continental biogenic emissions origin. The chemical records of high-resolution in seasonal or annual cycle can be used to construct the ice core choronology.

c) Gases: the air trapped in bubbles of the ice sheet provides the composition and concentration of the past atmopheric gases, including the main greenhouse gases - CO_2, CH_4 and N_2O. The composition of gases in the past atmosphere and their isotopes that were retrived from air bubbles within ice cores show past climatic variation. For instance, the concentration of greenhouse gases referred from the Antarctic ice core is lower in pre-industrial periods than present (Rubino et al., 2019). Over the last glacal period, the temperature co-variant with CO_2 indicates the relationship between CO_2 and temperature (Parrenin et al., 2013; Petit et al., 1999). Furthermore, the radiocarbon dating of CO_2 can be used as an abosolute dating method for ice core timescales. The global synchronous change in the methane records can be used to align the ice-core timescales from both poles (Buizert et al., 2018).

d) DEP measurments of ice cores provide the ice-core's electrial conductivity and permittivity. The DEP record relates to the ice-core acidity, as well as ammonium and salt contents of the ice (Moore et al., 1992; Moore et al.,1994). ECM measures the ice acidity records using an electrical current (Hammer, 1980; Moore et al., 1992). The ECM current is converted to ice acidity by using the equation between H^+ and acidity, suggested by Hammer (1980). The ECM is high, when the ice has a high acid content, e.g. from volcanic eruptions. The conductivity measurements of DEP and ECM records are valuable indicatiors of volcanic events and can be used to support the volcanic tephra layer investigation (McConnell et al., 2020). Additionally, the DEP and ECM analytical methods are non-destructive for ice cores.

1.1.2 Deep ice core projects in Greenland and Antarctica

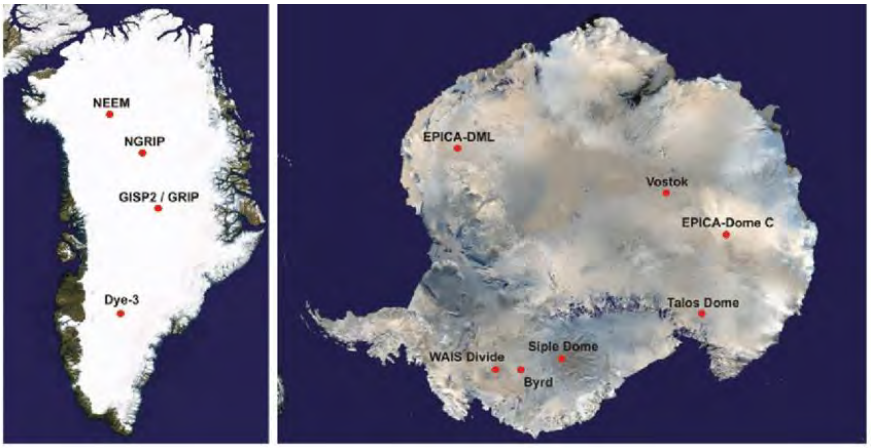

Figure 1.3 The ice core drilling sites in Greenland (NGRIP, NEEM, GRIP, GISP2 and Dye 3) and in Antarctica (Vostok, EPICA Dronning Maud Land; EPICA Dome C, Siple Dome, Talos Dome, Byrd and West Antarctic Ice Sheet Divide) (Winckler and Severinghaus, 2013).

The locations of some of the ice-core drilling projects in polar ice sheets are shown in Fig. 1.3, including the NGRIP, NEEM, GRIP, GISP2 and Dye 3 from Greenland, and the EPICA Dome C (EDC), EPICA Dronning Maud Land (EDML), West Antarctic Ice Sheet Divide (WDC), Vostok, Siple Dome, Talos Dome (TAL) and Byrd from Antarctica. The oldest ice core from Antarctica spans from the Holocene back to the Lower Pleistocene (EPICA community members, 2004), whereas, the oldest Greenland ice core covers the Holocene and Upper Pleistocene (NGRIP Project Members, 2004). The time series of sulfate or sulfur records, that are used to quantify volcanic sulfate magnitude over the last glacial cycle in this thesis, are mainly from seven deep ice cores of Greenland and Antarctica. A brief introduction is given in the following:

In Greenland, the NGRIP ice core was drilled on the ice divide on a flat basal topography (NGRIP Project Members, 2004). Due to basal melting, the annual layer thickness in the deeper part of this core is higher than that of the GISP2 and GRIP at the corresponding ages. The NGRIP core is 3085 m long and the oldest ice age is dated back to 120 kyr. The GISP2 and GRIP were drilled on the Summit. The depth of the GISP2 is 3053 m (Grootes et al., 1993). The GRIP is a 3029 m long core, and there is distubance in the deeper part of the ice core near the bedrock (Stauffer, 1993). The NEEM ice core reached bedrock at 2537 m and is dated back to the Emian interglacial period (NEEM community members, 2013).

In East Antarctica, two deep ice core projects are used to extend volcanic records in this work: one is at Dome C (EDC, 75.1S, 123.32E, 3270 m; EPICA community members, 2004), and the

other is in the Dronning Maud Land area (EDML, 75.00S, 0.07E, 2882 m; EPICA community members, 2006). EDC has the longest climate archive, dating back to 800 kyr (Jouzel et al., 2007), providing 740 kyr of chemical impurities (Wolff et al., 2006). In West Antarctica, the WDC ice core reached the depth of 3405 m, the ice age covering the last 68 kyr (WAIS Divide Project Members, 2013, 2015). The WDC ice core was drilled in an area with a high snow accumulation rate (200 kg m^{-2} yr^{-1}) to obtain high-resolution climatic proxies, compared to that of EDML (68 kg m^{-2} yr^{-1}) and that of EDC (23-34 kg m^{-2} yr^{-1}), which has retrieved high temporal climate information, comparable to the quality of Greenland ice cores.

1.2 Climate of the last glacial cycle

The climate of the last glacial cycle is revealed in detail by Greenland and Antarctic ice-core water isotopic records thanks to their high resolution and well-constrained chronologies (Fig. 1.4). The last glaical period occurred from the end of the Eemian (115 ka b2k, before 2000 AD) which was 1-2 °C warmer than present, to the onset of the Holocene about 11.7 ka b2k (Rasmussen et al., 2014). The last deglaciation was in the climate transtion from the cold state of the last glaciation to the warm state of the early Holocene, which occurred between 12.9 and 11.7 ka b2k. The Last Glacial Maximum (LGM), occurring during the 19.0 - 26.5 ka, has some of the lowest temperature of the last glacial period with the greatest ice sheet extents (Clark et al., 2009). A combination of geochemical proxies and climate models shows that the global mean cooling constraint in the LGM is in the range of -6.5 °C to -5.7 °C (Tierney et al., 2020). The Henrich events are the millennial-scale abrupt global climate events in the last glacial period that is related to the large discharge events of icebergs from the surrounding ice sheet in North Atlantic (Fig. 1.4; Hemming, 2004; Bond et al., 1992). The associated large amounts of melting fresh water released from icebergs likely changed the density-driven ocean circulation of the North Atlantic Ocean, that is believed to have been weaken or shut down the circulation during the Henrich events.

During the last glacial cycle, the climate was charaterized by multiple centennial- to millennial-scale cold-warm oscillations, called Dansgaard-Oeschger (DO) events occurring from the end of Eemian to the end of Youngers Dryas (Dansgaard et al., 1982; Fig. 1.4). In Greenland, there are 25 major DO events, each consisting of a mild climate state followed by a cold climate state, called, respectively, Greenland Interstadial (GI) and Greenland Stadial (GS), recorded by temperature proxies in Northern Hemisphere (Rasmussen et al., 2014). The climate response of DO-events is documented in the paleo-records in the Northern Hemisphere as well as in the low

latitudes. For example, 63 individual stalagmites across Europe, South America and Asia, show imprints of these climate oscillations, with stronger signals in the high latitudes of the Northern Hemisphere (Corrick et al., 2020).

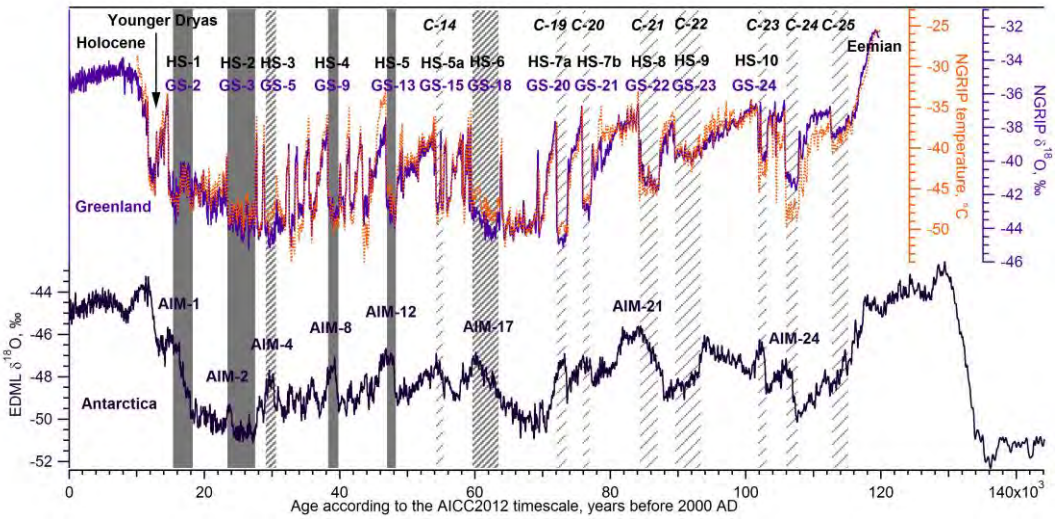

Figure 1.4 Records of abrupt climate oscillations in last glacial cycle. Grey vertical bands represent major Heinrich events. The $\delta^{18}O$ in purple color is from Greenland NGRIP core. The $\delta^{18}O$ in black color is from EDML core in east Antarctica. [https://en.wikipedia.org/wiki/Heinrich_event]

Associated with DO-events, the temperature changes out of phase between the Antarctica and the Northern Hemisphere. Antarctica was warming up when Greenland was in a cold state, while it was cooling off when Greenland was in a warm state, a mechanism modeled by the bipolar seesaw (Stocker & Johnsen, 2003). For bipolar seesaw, during a Greenland warm phase, heat is exported from the Southern Hemisphere (SH) to the North Atlantic through the Atlantic Meridional Overturning Circulation (AMOC), similar to the present climate. When Greenland is a cold phase, there is more heat accumulated in the SH due to the weaker AMOC (Pedro et al., 2018; Schneider et al., 2014). The Antarctic climate response to DO-events is hypothesized in two modes - a homogeneous oceanic 'bipolar seesaw' mode and an atmospheric mode that is in phase with DO-events in Northern Hemisphere (Buizert et al., 2018). In addition, the Antarctic climate response lags the midpoint of Greenland abrupt warming transitions of $\delta^{18}O$ by 1-2 centuries (Svensson et al., 2020).

1.3 Ice core dating

An ice core chronology makes the basis for interpretation of ice-core climate information and for comparison to the other climate archives. Several methods have been employed for dating the

ice: comparison of temperature proxies or chemical records, annual layer counting, ice flow models, snow accumulation and firn densification models, constrained by age markers.

1.3.1 Greenland ice core dating

The Greenland Ice Core Chronology 2005 (GICC05) is a timescale based on high-resolution annual layer counting covering the past 60 kyr. In the Holocene back to 7.9 ka, the layer counting is based on the DYE-3, the NGRIP and the GRIP cores using water isotopic records (Vinther et al., 2006). In the 7.9-14.8 ka period, the stratigraphic timescale is counted using high resolution CFA records from the NGRIP and the GRIP cores (Rasmussen et al., 2006). Back to 60.2 ka, the NGRIP core has been annually counted using the CFA dataset together with the visual stratigraphy record (Svensson et al., 2008) (Fig. 1.5). Beyond 60 ka, the GICC05 timescale is extended using the ss09sea-modeled age scale (Wolff et al., 2010), where the annual accumulation rate is derived from water isotopic records (NGRIP Members, 2004). An improved ice-core chronology GICC2021 for the last 3800 years has been obtained by annual layer counting in six deep and three shallow Greenland ice cores (Fig. 1.6). Compared to the GICC05 timescale, the GICC2021 timescale is about 15 years younger at 3800 years before present, but for the upper 800 years, the above two time scales are almost identical (Sinnl et al., 2022).

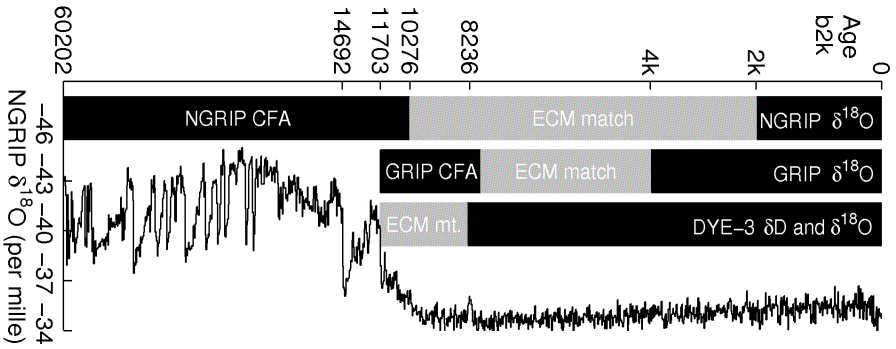

Figure 1.5 Ice cores and the applied records used for obtain GICC05 time scale.
[https://www.iceandclimate.nbi.ku.dk/research/strat_dating/annual_layer_count/gicc05_time_scale/]

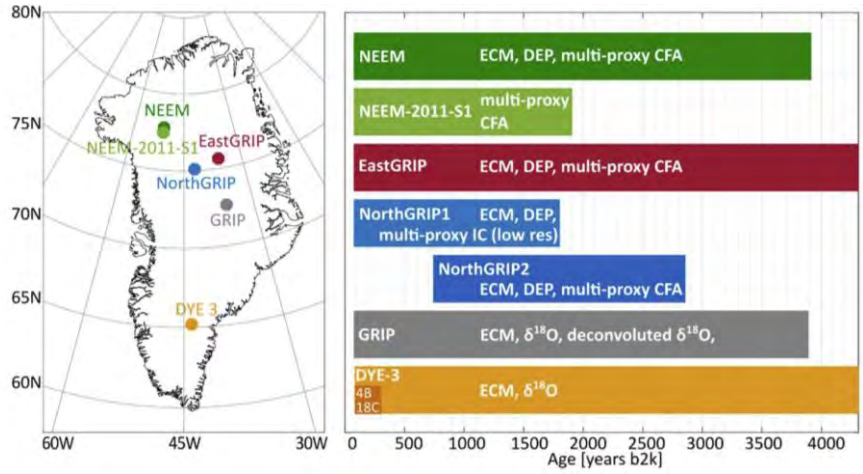

Figure 1.6 Ice cores and the applied records used to obtain the GICC2021 time scales that covers the last 3800 years (Sinnl et al., 2022).

1.3.2 Antarctic ice core dating

Records from Vostok, Talos Dome, EDML and EDC ice cores in Antarctica and from the NGRIP core in Greenland are employed in building the 0-120 ka section of the Antarctic Ice Core Chronology (AICC2012). Stratigraphic markers - ice stratigraphic links, gas stratigraphic links, cosmogenic age markers and Δdepth markers - are used to synchronize ice cores (Fig. 1.7). The gas- and ice- phase age minor offset years may be a few centuries between in the AICC2012 gas and ice chronologies, where the gases are younger than the surrounding ice, due to gas diffusion in the firn above the close-off depth at 50-120 m (depending on ice-core site characters; Witrant et al., 2011). The AICC2012 and GICC05 time scales are tied together for the last 60.2 ka, and beyond that the AICC2012 is independent of the GICC05 timescale. Thanks to a high number of stratigraphic ice markers (^{10}Be, volcanogenic sulphate and tephra) used to constrain the timescale, the AICC2012 deviates at most by 5 years from the GICC05 time scale, in the last 60 kyr (Veres et al., 2013).

The WD2014 chronology is based on annual layers counting in the upper part (0-2850 m) of the WDC ice core, using high-quality proxies, back to 31.2 ka BP (Sigl et al., 2016). Below 2850 m, the WD2014 is based on methane gas markers that are synchronized to the GICC05 (Buizert et al., 2015). The WD2014 timescale is consistently younger than the GICC05 in most periods in the Holocene.

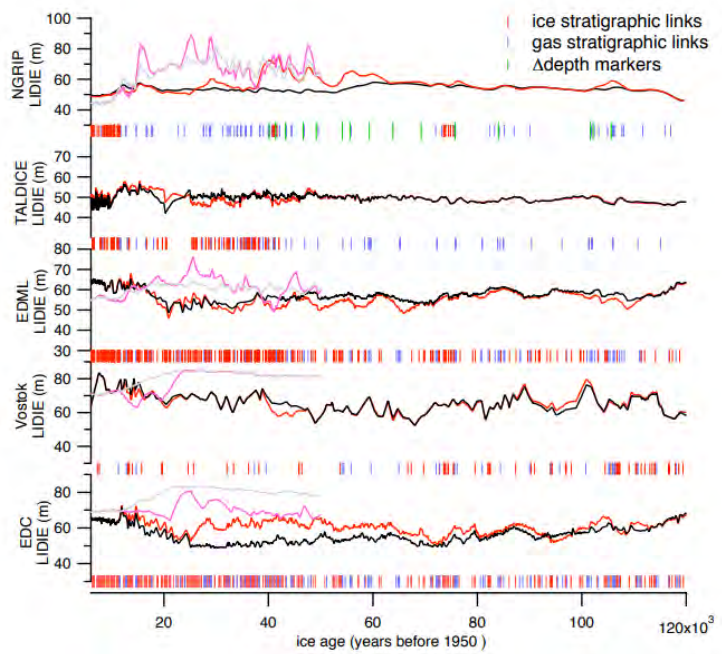

Figure 1.7 The stratigraphic markers from the five ice cores applied for the AICC2012 chronology. The green, red, and blue vertical bars indicate Δdepth markers, ice stratigraphic links, and gas stratigraphic links, respectively (Veres et al., 2013).

1.4 Volcanic synchronization of Greenland and Antarctic ice cores

Volcanic synchronization is based on the identification of a common volcanic footprint in ice cores through tephra, sulfate, sulfur or other acidity records. Patterns of volcanic events are identified in several ice cores within Greenland (or within Antarctica) by counting the annual layers between adjacent volcanic events or by a smooth and continous depth to depth relationship between ice cores (Fig. 1.8; Svensson et al., 2020; Seierstad et al., 2014; Buizert et al., 2018). These volcanic stratigraphic markers are mostly identified among regional ice cores (i.e. cores within Greenland) and very challenging to identify the common volcanic events between Greenland and Antarctic ice cores. For the ice cores in a regional area, the magnitude of the acidity signals are often comparable among ice cores, giving more confidence in the volcanic matching. For the volcanic synchronization of bipolar ice cores, the smooth variation in ice-core annual layer thickness and the similar number of annual layers between volcanic tie-points is applied in these matching (Svensson et al., 2020).

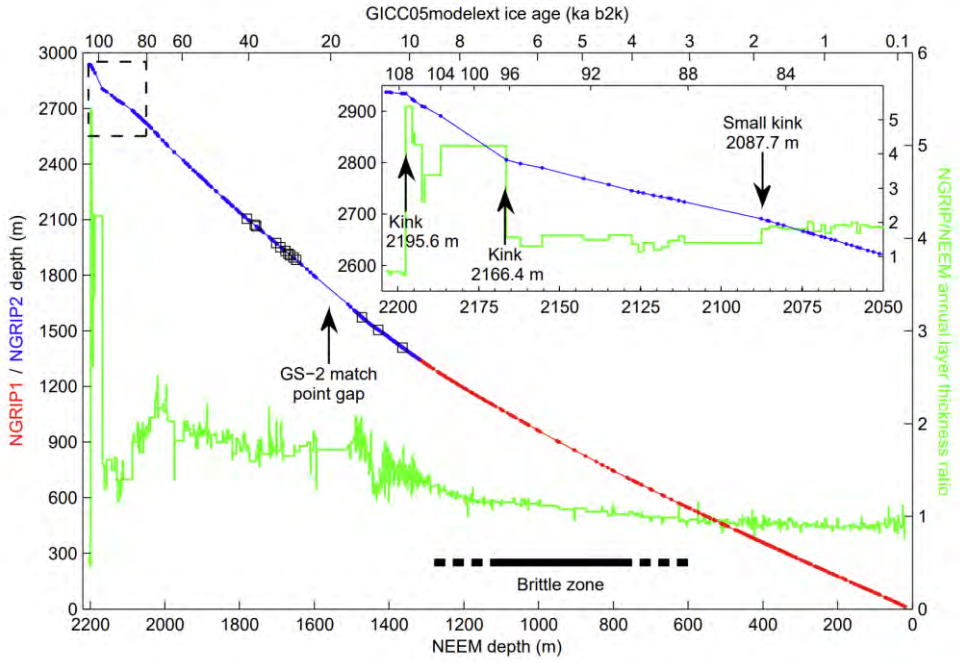

Figure 1.8 Smooth and continous depth to depth relationship between the NGRIP core (red+blue) and the NEEM core, that were matched by tephra (black squares) and chemical stratigraphic match points (dots) (Seierstad et al., 2014).

1.4.1 Hemispheric ice-core volcanic synchronization

In Greenland, the stratigraphic matching procedure is to identify and match common volcanic events by the profiles of sulfate or sulfur, tephra, ECM, DEP, and conductivity records (Svensson et al., 2008; Rasmussen et al., 2013; Vinther et al., 2006; Seierstad et al., 2014). These volcanic tie-points and other chemical tie-points, such as DEP or ECM based match points, have been employed to establish and transfer the GICC05 time scale in the past 60 kyr. The synchronization between the NEEM and the NGRIP cores has been employed in the non-disturbed section of the cores (Rasmussen et al., 2013) and there are 787 acidity or tephra tie-points over the past 100 kyr, mainly volcanic match points, identified using ECM and DEP records. The synchronization of the GRIP, NGRIP and GISP2 ice cores covers the past 104 kyr by linking distinct volcanic sulfate events and other impurity events (Seierstad et al., 2014). There are around 900 marker horizons between the three cores in addition to 24 volcanic ash tie-points.

In Antarctica, the deep ice cores have been synchronized (Winski et al., 2019; Ruth et al., 2007a; Severi et al., 2007; Buizert et al., 2018). Compared to volcanic tie points among Greenland ice cores, there is lower density of volcanic tie points in Antarctic ice cores due to the lower resolution ice-core impurity records and the lower occurrence of regional explosive

volcanic eruptions in the SH. The volcanic linking has been made from the EDC ice core to the TAL/EDML/DF/Vostok cores for the last glacial period (Severi et al., 2007; Ruth et al., 2007; Parrenin et al., 2012b), and the linking from the WDC ice core to the EDC / EDML / TAL / DF ice core (Buizert et al., 2018). During the 10-61 ka interval, 773 volcanic tie-points were identified between WDC and EDML, and 396 tie-points were identified between WDC and EDC. Over the last 52 kyr, there were about 200 common volcanic signatures identified between EDC and EDML ice cores (Severi et al., 2007). The 'EDML1' timescale is derived from the EDC timescale by stratigraphic matching in the past 128 kyr and 322 common volcanic stratigraphic signals were identified in the two cores (Ruth et al., 2007).

1.4.2 Bi-hemispheric ice-core volcanic synchronization

The bi-hemispheric (bipolar) matching is based on the constrained gas- and ^{10}Be - synchronization between Greenland and Antarctic ice cores (Svensson et al., 2013; Buizert et al., 2018). In Greenland, the abrupt climate of DO events can be seen in high-resolution water isotope and methane concentration records in the last glacial period. The Antarctic methane records show a similar pattern to that of Greenland abrupt climate events because methane is a well mixed gas in the atmosphere (Capron et al., 2010; Blunier et al., 2007; Schwander and Stauffer, 1984). The Antarctic methane records can thus be aligned to the Greenland climate records in identical pattern. The abrupt changes of methane concentrations at the onset of DO events can be applied as stratigraphic links for synchronization of time scales between both the two poles. It has been employed between Greenland and WDC (Buizert et al., 2018), between NGRIP and Vostok (Landais et al., 2006), between NGRIP and EDML (Capron et al., 2010; Lemieux-Dudon et al., 2010) and between NGRIP and TALDICE (Buiron et al., 2011). This was also employed in linking ice cores in Antarctica between EDC and Vostok (Loulergue et al., 2007; Lemieux-Dudon et al., 2010), between EDC and EDML (Loulergue et al., 2007), between EDML and TALDICE (Schupbach et al., 2011), and between EDC and TALDICE (Buiron et al., 2011; Schupbach et al., 2011; Parrenin et al., 2012a). The weakness of this approach is that there is an offset age between the ice age and the gas age that varies with temperature and accumulation that can be estimated from firn modelling (Blunier et al., 2007; Schwander and Stauffer, 1984).

In addition, cosmogenic signals are used to constrain and synchronize the Greenland and Antarctic time scale, making them more precise. The detected cosmogenic signals (^{10}Be) in polar ice cores are mostly in the Holocene period (Mekhaldi et al., 2015; Sigl et al., 2015; Steinhilber

et al., 2012), and in the last glacial period there is a cosmogenic signal – Laschamp geomagnetic excursion, that the Earth magnetic field diminished in some centuries occurred about 41 kyr ago (Raisbeck et al., 2017). Two weaker cosmogenic events have recently been identified in NGRIP and WDC ice cores, that are useful for obtaining a better synchronization between Greenland and Antarctica in the last glacial maximum (Sinnl et al., 2022, under review).

A more precise synchronization of Greenland and Antarctic timescales can be obtained through the identification of common volcanic signals in both poles and annual layer counting between events. This approach has been applied for bipolar ice core synchronization during the second half of the last glacial period (12-60 kyr; Svensson et al., 2020; Fig. 1.9). The bi-hemisphere volcanic signals matching was firstly practiced in the Holocene period between the NGRIP core and EDML core (Vinther et al., 2012), and was constrained by the Laschamp geomagnetic excursion back at around 41 ka as well as the Toba volcanic eruption that occurred at ~74 ka (Svensson et al., 2013). This improved bipolar ice-core synchronization has been provided a decadal-scale precision of the phasing of the climate between the two hemispheres, while there are no bipolar volcanic match points reported in the Last Glacial Maximum (Svensson et al., 2020).

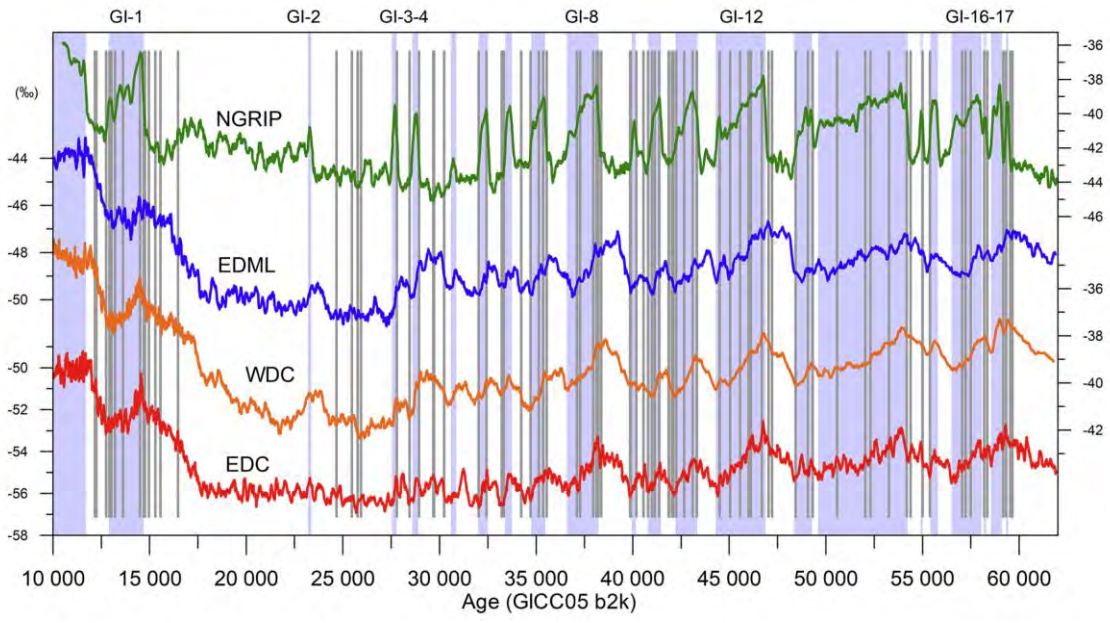

Figure 1.9 Identified bipolar volcanic match points from Greenland (NGRIP) and Antarctic (EDML, WDC, and EDC) ice cores in the period of 60-9 ka b2k (vertical grey lines). The climate records (δ ^{18}O) are shown in green (Greenland), blue, orange, and red (Antarctica) colors (Svensson et al., 2020).

1.5 Reconstruction of ice-core volcanic records

1.5.1 Ice-core sulfate records

Volcanic eruptions can inject large amounts of sulfur-containing gases into the atmosphere, and most of them are in the form of hydrogen sulfide and sulfur dioxide. The gases are photochemically oxidized, dissolved into droplets, formed into sulfate aerosols through micro-chemical and physical processes and deposited on the polar ice sheets (Rampino and Self, 1984; Robock, 2000). The sulfate (or sulfur) records measured from polar ice cores may have three major sources – marine sources, volcanic emissions, and terrestrial sources before the industrial era (Cole-Dai, 2010).

The ice-core volcanic sulfate is significantly above the background level (Hammer, 1997) and non-volcanic sulfate is characterized by periodical and seasonal variability. A common method to separate volcanic sulfate signals from sulfate background is to apply a low pass filter (Gao et al., 2008; Sigl et al., 2014; Cole-Dai et al., 2021). The SO_4^{2-} concentration in polar ice cores can be measured by Ion Chromatography (IC), Fast Ion Chromatography (FIC), Inductively Coupled Plasma Mass Spectrometers (ICP-MS) and Continous Flow Analysis (CFA) system.

In Greenland, the ice-core sulfate record from the NEEM-S1 core has been analyzed using CFA covering the past 2500 years (Sigl et al., 2013). For NGRIP, the sulfate concentration has been obtained by the CFA system over the last glacial period (Bigler, 2004; Röthlisberger et al., 2000). For GISP2 and a second discrete NGRIP profile, SO_4^{2-} was obtained from discrete samples by IC (Clausen et al., 1997; Mayewski et al., 1993; Siggaard-Andersen, 2004).

In Antarctica, sulfate or sulfur records have been obtained from three deep ice cores (WDC, EDC and EDML) for the entire Holocene and last glacial periods. For WDC, sulfur was measured by ICP-MS coupled to a CFA system (Sigl et al., 2016; Sigl et al., 2022). For EDC and EDML, the SO_4^{2-} was measured by FIC coupled to a CFA system (Severi et al., 2015).

1.5.2 Historical volcanism evaluated from ice cores

Ice-core sulfate records are good proxies to identify the occurrence of historical volcanic eruptions. Compared to petrological evidence, the number of volcanic signals and assessment of volcanic sulfate magnitude from ice cores are in a better constraint (Palais and Sigurdsson, 1989). Several individual unipolar volcanic lists have been reconstructed using the Greenland and Antarctic ice cores (Table 1.1).

Table 1.1 Unipolar volcanic lists derived from Greenland and Antarctic ice cores.

Time period	Ice core	Location	Analytical method, effective depth resolution	Number of events	References
165 - 1997AD	Four ice cores + 13 snow pits	Dronning Maud Land, East Antarctica	IC	49	Traufetter et al., 2004
50BC - 1950AD	Law Dome	Law Dome, East Antarctica	IC, 2.5 cm	45	Plummer et al., 2012
last millennium	GV7	Northern Victoria land	IC, 5 cm	24	Nardin et al., 2020
last 2000 yrs	WDC06A | NEEM-S1	WAIS Divide, West Antarctica | Greenland	CFA-ICP-MS	133|138	Sigl et al., 2013
last 2000 yrs	19 ice core sites	Antarctica		166	Sigl et al., 2014
2144BC - 1968AD	Plateau Remote	Plateau Remote, East Antarctica	IC, 4 cm	54	Cole-Dai et al., 2000
45,000 yrs	EDC96	Dome C, East Antarctica	FIC-IC, 4 cm	283	Castellano et al., 2004
110,000 yrs	GISP2	Greenland	IC, 20 cm	850	Zielinski et al., 1996
10,000 BP - 2000 AD	Siple Dome	Siple Dome A, West Antarctica	IC, 20 cm	168	Kurbatov et al., 2006
0 - 11,000 BP	WDC	WAIS Divide	ICP-MS	426	Cole-Dai et al., 2021
200 kyr	EDC	Dome C, East Antarctica	IC | FIC-IC, 2-6 cm	678	Wolff et al., 2022

The global volcanic lists have been reconstructed from polar ice-core sulfate records under the requirement that all ice core records should be aligned to a common timescale (Sigl et al., 2015; Sigl et al., 2013). In the past 2500 years, 283 individual volcanic events have been detected. Among them, 81 global volcanic eruptions (bi-hemispheric/bipolar eruptions) have been identified with accurate eruption timing and climate forcing, and 5 large volcanic eruptions have exceeded the volcanic forcing of the Tambora 1815 eruption (Fig. 1.10). Toohey and Sigl. (2017) reconstructed the volcanic stratospheric sulfur injections and aerosol optical depth from 500 BC to 1900 AD using an array of Greenland and Antarctic ice cores, including the approximate eruption latitude and magnitude for major eruptions.

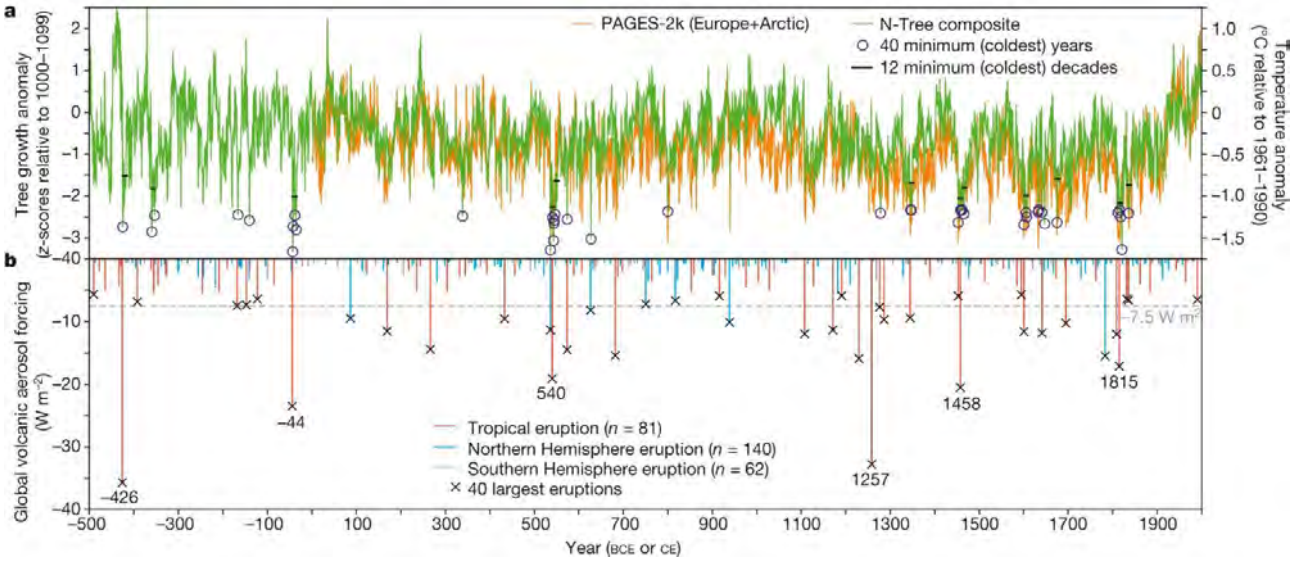

Figure 1.10 Global volcanic forcing and Northern Hemisphere temperature estimated from tree-ring records during the past 2,500 years (Sigl et al., 2015).

From 9500 BC to 1900 AD, stratospheric sulfur injections, eruption latitudes, and the aerosol optical depth of global volcanism have recently been reconstructed using the ice-core sulfate or sulfur records from NGRIP, GISP2, EDC, and EDML (Sigl et al., 2022). In total, 850 volcanic eruptions have been identified with stratospheric sulfur injections over 1 Tg. Among them, there are 329 bipolar volcanoes located in the low latitudes, 426 unipolar volcanoes located in the Northern Hemisphere, and 88 unipolar volcanoes located in the Southern Hemisphere (Fig. 1.11). These reconstructions provide comprehensive information about the historical sulfur-rich explosive volcanic eruptions with low discrepancies in terms of the eruption timing and magnitude.

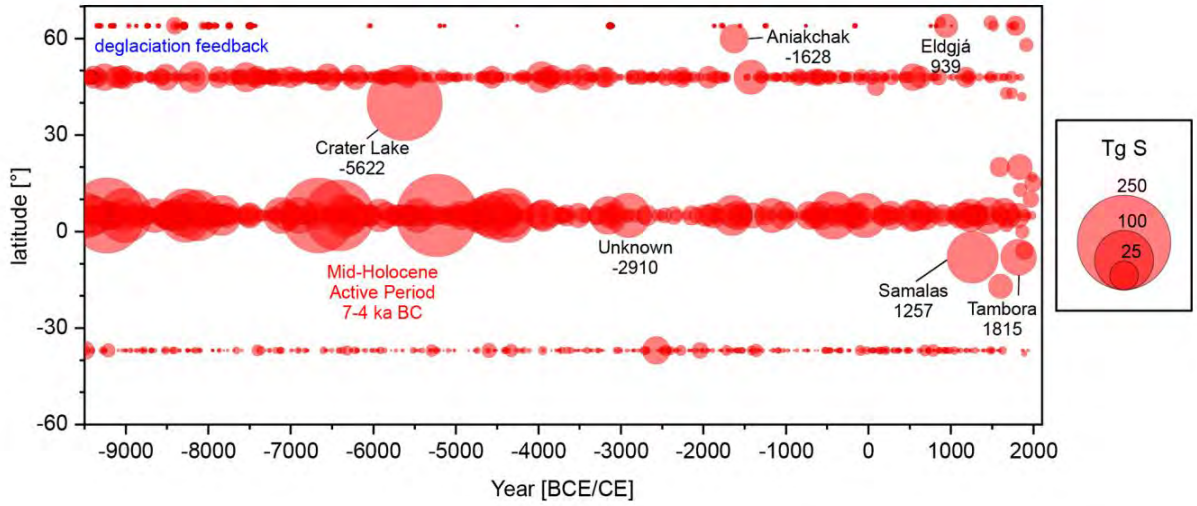

Figure 1.11 Global volcanic sulfur injections in the stratosphere, that were calculated from bipolar volcanic sulfate fallout, with the approximate erupted latitudes in the whole Holocene period. Large volcanic eruptions are marked (Sigl et al., 2022).

In the last millennia, the ice-core volcanic records can be dated with high accuracy from ice-core chronologies and can often be assigned to the location and timing of known eruptions. In the last 2500 years, the five largest volcanic events identified in ice cores are the unknown (426 BC), Samalas (Indonesian,1257 AD), Okmok (Alaska, 43 BC), Kuwea (Vanuatu, 1458 AD) and unknown (540 AD), all of them exceeding the stratospheric volcanic sulfate loading of the Tambora (1815 AD) eruption in Indonesia (Sigl et al., 2015; Mcconnell et al., 2020).

When available, geochemical information about tephra in ice cores can be used to identify the location of the ice-core volcanic eruptions. Many ice-core volcanic signals are linked to the Icelandic volcanoes by the identified tephra layers in the ice cores, including Veiðivötn (1477 AD; Abbott et al., 2021), Eldgjá (939–940 AD; Oppenheimer et al., 2018; Zielinski, 1995) and Katla (822 AD; Büntgen et al., 2017; Plunkett et al., 2020). In additional to the Icelandic

volcanoes, some ice-core volcanic signals are linked to the known volcanic eruptions, including the Samalas, 1257 AD (Lavigne et al., 2013), Changbaishan, 946 AD (Oppenheimer et al., 2017; Sun et al., 2014), Mt Churchill, 853 AD (Jensen et al., 2014), Ilopango, 431 AD (Smith et al., 2020), Okmok, 43 BC (McConnell et al., 2020), Aniakchak, 1628 BC (Pearce et al., 2004; McAneney and Baillie, 2019; Plunkett and Pilcher, 2018; Pearson et al., 2022), Mazama, 5677 ± 150 BC (Zdanowicz et al., 1999), and Khangar, 5922 ± 50 BC (Cook et al., 2018).

In the Holocene, two volcanic eruptions in the extratropical NH with the strongest sulfur injections were the Aniakchak (1628 BC) and Eldgjá (939–940 AD). There are 8 sulfur-rich explosive eruptions with stratopheric sulfur emissions stronger than that of the Samalas, 1257 AD, clustered in the early Middle Holocene (Sigl et al., 2022).

1.6 Volcanic impact on climate

1.6.1 Volcanic forcing reconstruction based on ice cores

Sulfur-containing gases emitted from explosive eruptions into the stratosphere, oxidize to sulfuric acid vapor, convert to sulfate aerosols and liquid droplets, scatter the short-wave solar radiation back to space, and reflect long-wave solar radiation back to Earth, leading to cooling of the Earth's surface (Timmreck et al., 2012; Robock, 2000; Kremser et al., 2016). The stratospheric aerosol optical depth (SAOD) is a measure of the stratospheric opacity which can be used to estimate the volcanic radiative forcing. In the Satellite Era, the SAOD has been observed as a continuous record from 1979 to 2018 and compiled in the database of the Global Spaced-based Stratospheric Aerosol Climatology (GloSSAC) (Thomason et al., 2008; Kovilakam et al., 2020). Before the Satellite Era, the volcanic radiative forcing has been obtained mainly from ice-core volcanic sulfate depositions. The stratospheric sulfate loading is estimated from ice-core volcanic sulfate deposition using a calibration factor of spatial distribution of sulfate deposition from Gao et al. (2007), and the volcanic forcing is derived from the stratospheric sulfate loading based on idealized volcanic aerosol models (Toohey et al., 2016; Aubry et al., 2020).

These idealized volcanic aerosol models are basically box models (Gao et al., 2008; Toohey et al., 2016; Aubry et al., 2020), where the box (stratosphere) is separated into several latitude and altitude regions. After a sulfur injection into the box, processes of the evolution of sulfate from SO_2, the mixing between different regions, and the aerosol loss to the troposphere are considered. One such model, the Easy Volcanic Aerosol (EVA), is an idealized model (Toohey

et al., 2016), using the parameters from ice cores - amount of sulfur injections, emission latitudes and the timing of the past eruptions - to estimate the SAOD (Toohey & Sigl, 2017). The sulfur injections height is not considered in this model. In EVA, the relationship between the sulfur injection mass and the volcanic forcing is calculated from the characteristics of the 1991 Mount Pinatubo eruption (e.g., the latitude or the altitude of injection, e.g., Marshall et al., 2019; Toohey et al., 2019). A later idealized model, EVA-H, use an extended methodology from the EVA, calibrating the volcanic radiative forcing from the ice core constraints parameter based on dataset of mass of SO_2, location, and altitude of volcanic sulfur emissions over 1978–2015 (Aubry et al., 2020). The EVA_H model is limited by the parameters calculated from the eruptions over 1978–2015. The above models only rely on a few parameters and the propagated uncertainty is straightforward.

A time series of volcanic forcing covering the past 1,500 years has been reconstructed using 53 Greenland and Antarctic ice cores (Gao et al., 2008). The latest reconstruction of SAOD from volcanic eruptions provides the monthly and latitudinal SAOD time series over the past 2,500 years (Toohey & Sigl, 2017) and 11,500 years (Sigl et al., 2022). The SAOD datasets derived from ice core sulfate depositions do not consider the aerosol-chemistry and microphysical effects (Crowley & Unterman, 2013; Gao et al., 2008; Toohey & Sigl, 2017; Sigl et al., 2022).

The ice-core volcanic forcing is estimated from SAOD by assuming a linear relationship calibrated by climate model simulations of the 1991 eruption of Mt. Pinatubo (Hansen et al., 2005). As the volcanic radiative forcing derived from SAOD among others depends on the cloud cover, insolation and surface albedo (Andersson et al., 2015), this simple relationship doesn't take into account the eruption latitudes, sulfur emission strengths, emission altitudes, and eruption seasons (Marshall et al., 2019; Toohey et al., 2011, 2013). A nonlinear relationship between SAOD and volcanic radiative forcing is suggested by multiple aerosol-chemistry-climate simulations with SO_2 emissions ranging between 10 and 100 Tg, eruption latitude ranging from 80°S to 80°N, and eruption altitude ranging between 15–18 km and 25–28 km (Marshall et al., 2020). Compared to the constant factor of Hansen et al. (2005), the total time-integrated volcanic radiative forcing derived by the multiple aerosol-chemistry-climate simulations is 79% when used for volcanic eruptions over the past 2500 years (Fig. 1.12).

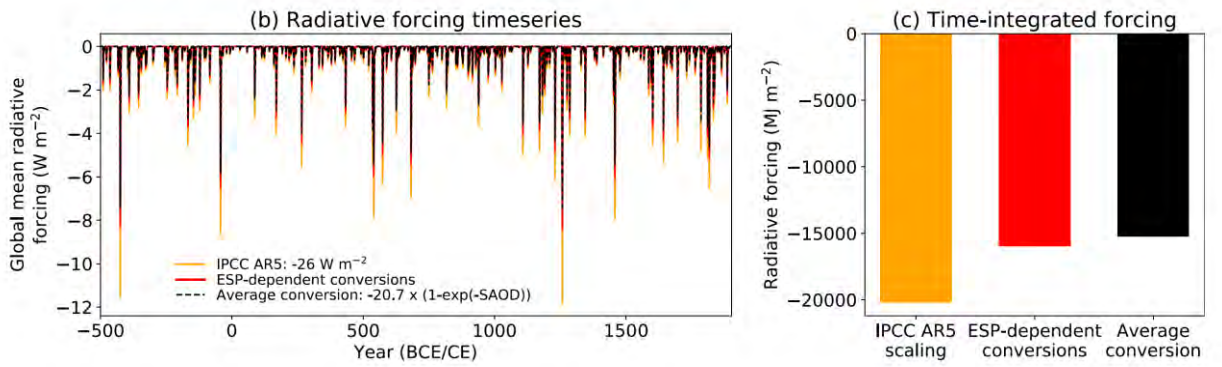

Figure 1.12 Volcanic forcing calculated from the SAOD using the constant scaling factor (orange) and using nonlinear scaling factor (red) (Marshall et al., 2020).

1.6.2 Observations and climate proxies

Large sulfur-rich explosive volcanic eruptions are one of the main drivers of climate variability, that has been revealed in the temperature records (Crowley, 2000; Briffa et al., 1998; Sigl et al., 2015). We can understand the volcanic impact through the application of tree-ring width proxies, ice-core water isotopes, and marine sediment records, etc.

Ice-core evidence of large explosive volcanic eruptions, combined with a well-dated array of tree-ring width records in the NH over the past 600 years, revealed summer cooling related to the recent volcanic events in 1816 AD, 1884 AD and 1912 AD and to unknown volcanic events that occurred in 1601, 1453, 1452, 1641/42, 1666, 1695 and 1698 AD (Fig. 1.13; Briffa et al., 1998). Quantifying the climate variability for different magnitudes of historical volcanic sulfur-rich eruptions can be resolved through synchronization between ice-core volcanic sulfate records and climate proxies such as tree-ring width records and ice-core water isotopes. With the improvement of ice-core dating and synchronization with the tree-ring width records, the reconstruction of volcanic radiative forcing and past temperature variability reveals the volcanic impact on climate in the past 2500 years (Sigl et al., 2015). The sequenced volcanic-induced cooling proxies (tree-ring width records) have been well connected to the volcanic sulfate magnitude derived from ice-core sulfate records in the past 2,500 years (Fig. 1.10 and Table 1.2). The cooling induced by volcanic eruptions has been observed to be proportional to the volcanic sulfate magnitude of the large explosive eruptions (Fig. 1. 14; Sigl et al., 2015; Toohey et al., 2019).

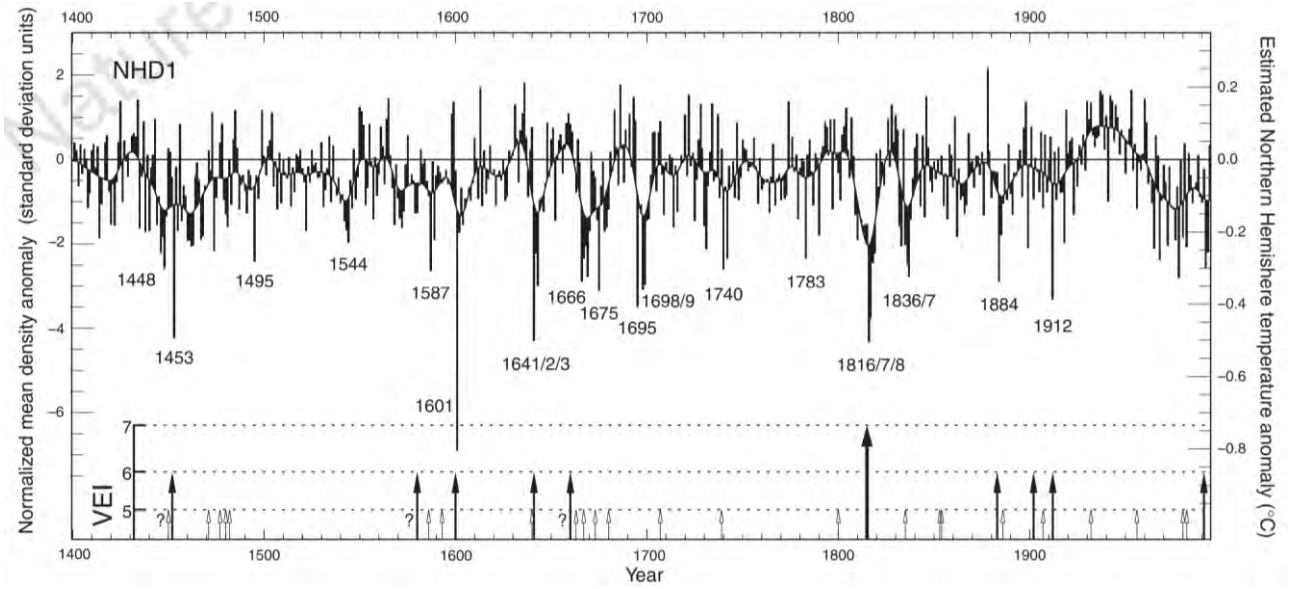

Figure 1.13 NHD1 shows the averge NH tree-ring width records (left-hand axis, standard anomaly values) and the estimated temperature (right-hand axis, standard anomaly values) response to the main explosive volcanic eruptions (VEI 5, 6 and 7; Briffa et al., 1998).

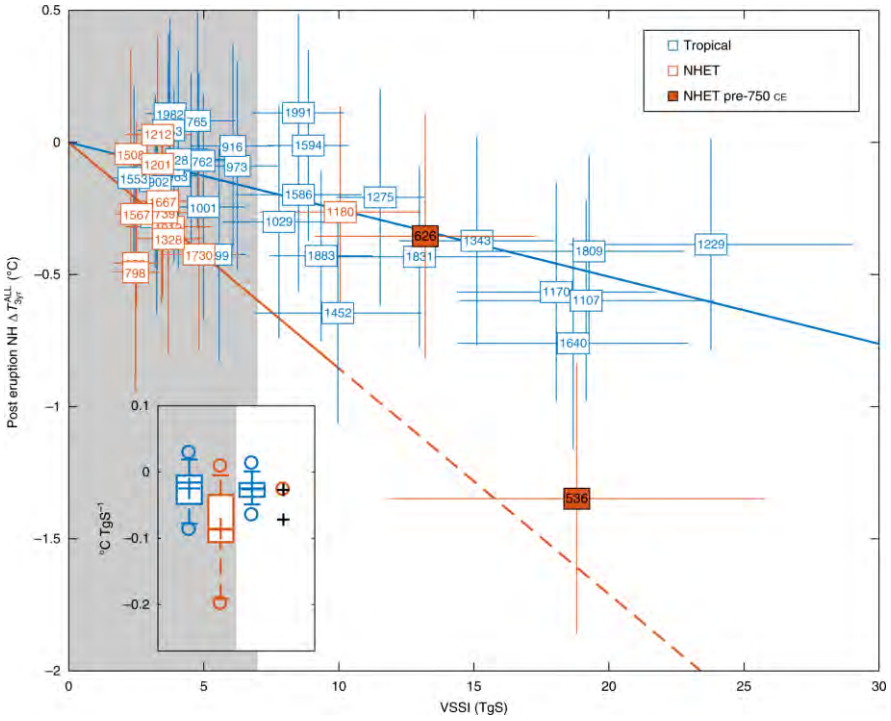

Figure. 1.14 Three-year average NH temperature anomalies, reconstructed by NH tree-ring width records, versus the estimated stratospheric sulfur injections (TgS) of tropical (blue) and NH extratropical (NHET; orange) explosive volcanic eruptions. Number labels show the eruption years (Toohey et al., 2019).

Table 1.2 Large sulfur-rich explosive volcanic eruptions over the past 2,500 years. Years with negative numbers are BC. The average temperature of Europe and the Arctic is associated to the volcanic cold year. Volcanic radiative forcing was estimated by scaling the volcanic sulfate depositions in polar ice sheets for the Pinatubo 1991 (Sigl et al., 2015).

Rank	Year	Volc. SO_4^{2-} Greenland ($kg\ km^{-2}$)	Volc. SO_4^{2-} Antarctica ($kg\ km^{-2}$)	Global forcing* ($W\ m^{-2}$)	Cold year	N-Tree (z scores; 1000-99)	$T_{Europe/Arctic}$ (°C; 1961-90)	Volcano†/ Region
1	-426	99.8	78.2	-35.6	-425	-2.74		UE -426
2	1258	90.4	73.4	-32.8	1258	-1.43	-0.91	Samalas/Indonesia
3	-44	100.6	15.4	-23.2	-43	-3.33		Chiltepe?/Nicaragua
4	1458	39.0	63.6	-20.5	1459	-2.31	-1.03	Kuwae/Vanuatu
5	540	61.2	34.4	-19.1	541	-2.57	-1.48	Ilopango?/El Salvador
6	1815	39.7	45.8	-17.1	1816	-2.51	-1.55	Tambora/Indonesia
7	1230	56.4	23.1	-15.9	1230	-1.71	-0.65	UE 1230
8	1783	135.8		-15.5	1783	-1.16	-0.97	Laki/Iceland
9	682	38.4	38.7	-15.4	682	-0.95	-0.96	Pago?/New Britain
10	574	38.3	34.1	-14.5	574	-2.46	-0.94	Rabaul?/New Britain
11	266	61.0	11.3	-14.5	268	-1.70	-0.72	UE 266
12	1809	34.6	25.4	-12.0	1810	-2.18	-1.23	UE 1809
13	1108	48.3	11.6	-12.0	1109	-1.99	-1.15	UE 1108
14	1641	44.2	14.9	-11.8	1641	-2.31	-1.19	Parker/Philippines
15	1601	39.2	18.7	-11.6	1601	-2.62	-1.50	Huaynaputina/Peru
16	169	39.1	18.4	-11.5	170	-0.80	-0.94	UE 169
17	1171	37.0	19.5	-11.3	1171	-0.91	-0.88	UE 1171
18	536	99.0		-11.3	536	-3.36	-1.74	UE 536
19	1695	28.6	22.5	-10.2	1696	-1.63	-1.28	UE 1695
20	939	88.7		-10.1	940	-1.81	-1.44	Eldgjá/Iceland
21	1286	27.6	20.8	-9.7	1288	-1.49	-0.65	Quilotoa?/Ecuador
22	433	20.6	27.2	-9.6	432	-0.45	-0.25	UE 433
23	87	83.1		-9.5	87	-0.22	-0.49	UE 87
24	1345	27.9	19.1	-9.4	1346	-2.18	-1.48	El Chichon?/Mexico
25	626	72.2		-8.2	627	-3.00	-0.93	UE 626

The climate response to large tropical eruptions since the beginning of the 19th century has been derived from multiple proxies and reconstructions of surface temperature, for the volcanic years of 1809, 1815, 1831, 1835, 1840, 1843, 1883, 1902, 1912, 1924, 1982, and 1991 (Guillet et al., 2017). In the last millennium, tree-ring records and ice-core data were applied to reconstruct the spatial and temporal surface temperature response to large volcanic eruptions. The recent extreme average surface cooling occurred in 1259 AD following the Samalas 1258 AD eruption, reaching -1.2 °C, ranking as the third cooling summer in the last millennium, whereas 1816 AD (-1.2 °C), 1601 AD (-1.2 °C), and 1453 AD (-1 °C) are ranking as the first, the second and seventh coldest summers, and the most severe persistent cooling event is followed by the Samalas eruption (Guillet et al., 2017; Stothers, 1984; Churakova et al., 2014; Büntgen et al., 2016; Sigl et al., 2015).

Volcanic eruptions play an important role in centennial and millennial-scale changes in Greenland temperatures, which are reconstructed using argon and nitrogen isotopes in the Greenland ice cores (Kobashi et al., 2017). The cold climate and mountain glacier growth in Alaska, New Zealand, European Alps, and the southern Andes, growth in the Little Ice Age (LIA) have been related to the enhanced sulfur-rich volcanic activity, potentially resulting in a centennial-scale or longer change of state in Arctic climate by model simulation (Miller et al., 2012). Solar variability is considered to be the primary factor to have induced the LIA (Lean and Rind, 1999), however, Hegerl et al. (2003) states that the enhanced volcanic forcing response to climate is substantially more important.

1.6.3 Climate modelling of volcanic-climate impact

Climate models have high spatial resolutions and are useful tools to capture both the regional and large scale climate impact of large volcanic eruptions. Climate models with complex stratospheric aerosol-chemistry and microphysics modules can simulate the aerosol formation and depletion process from an initial volcanic sulfur injection. Examples of these models are the MAECHAM5-HAM, CESM-WACCM and CESM-WACCM-CARMA. The sulfur emission latitude, the injection season and the altitude are important factors, which can influence the size, transport time, dispersal process and lifetime of volcanic sulfate aerosols, and are critical to quantify the volcanic impact on climate. Changing the eruption parameters to explore the volcanic-climate impact in these models is possible and may be close to the realism (Marshall et al., 2020).

The mass of volcanic sulfur injection and injection latitude of historical volcanic eruptions can be estimated based on ice-core volcanic sulfate depositions. That is important for the climate model experimental setup when investigating the volcanic sulfate cloud formation, transport and deposition processes and the related climate response. Toohey et al. (2013) applied the MAECHAM5-HAM aerosol-climate model to test the sensitivity between the sufur injection strength (ranging from 8.5 to 700 Tg) and the sulfate depositions in Greenland and Antarctica, and found that the ice-core sulfate depositions vary as a function of the sulfate magnitude and the season of the injection. For the large volcanic eruptions, the relationship between Greenland and Antarctic sulfate depositions is nonlinear, with the Greenland sulfate depositions being significantly stronger than that in Antarctica (Fig. 1.15). In MAECHAM5-HAM model simulations, a linear relationship between the stratospheric sulfur injections and peak global

mean AOD is simulated for for smaller volcanic eruptions with 2.5 Mt sulfur injection (Metzner et al., 2014).

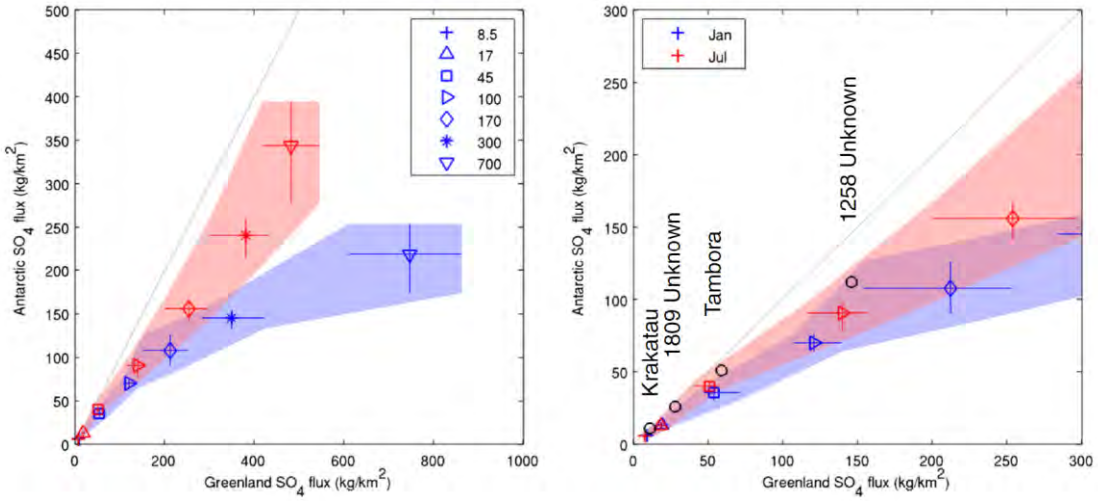

Figure 1. 15 Antarctica vs Greenland mean volcanic sulfate deposition for different stratospheric SO_2 injections (labelled in different shape markers). Shading represents the linearly interpolated envelopes of the range of variability of each experiment (Toohey et al., 2013).

The climate impact of supereruptions has been discussed for decades. The Toba eruption, dated radiometrically to 73.88 ± 0.32 ka (Storey et al., 2012), related to a glacial abrupt climate event (Schulz et al., 1998; Deplazes et al., 2013) and human population bottleneck (Rampino and Self, 1992; Ambrose, 1998). The Los Chocoyos eruption, which occurred in Guatemala at 75 ± 2 ka (De Leon et al., 2021), coupled with the Toba eruption has been suggested to have triggered the Greenland Stadial-20 cooling transition (Paine et al., 2021).

For super-eruptions, the aerosol-climate models can provide a thorough investigation of the climatic and environmental impacts. Experiments with different sulfur injection strengths in the global aerosol climate models show that the volcanic sulfur injection strength is nonlinearly related to the global average SAOD (Fig. 1.16 (a)), although the experimental setups (the eruption date, altitude and latitude) are different among models (Timmreck, 2010; English et al., 2013; Jones et al., 2005; Metzner et al., 2014; Brenna et al., 2020; Robock, 2009). The explanation for the difference could be that following the large magnitude eruptions, aerosols quickly become large-size aerosols and fall out of the atmosphere (Timmreck, 2010). Meanwhile, in the CESM2-WACCM6 model, the smaller-size aerosols have a longer lifetime and have larger SAOD (Brenna et al., 2020). These model simulations consistently demostrate a linear relationship between the surface cooling and peak SAOD (Fig. 1.16 (c)). The sulfur injections is nonlinear to the maximum temperature anomaly. The global mean precipitation anomaly is linearly related to the surface temperature anomaly (Fig. 1.16 (d)), that could be

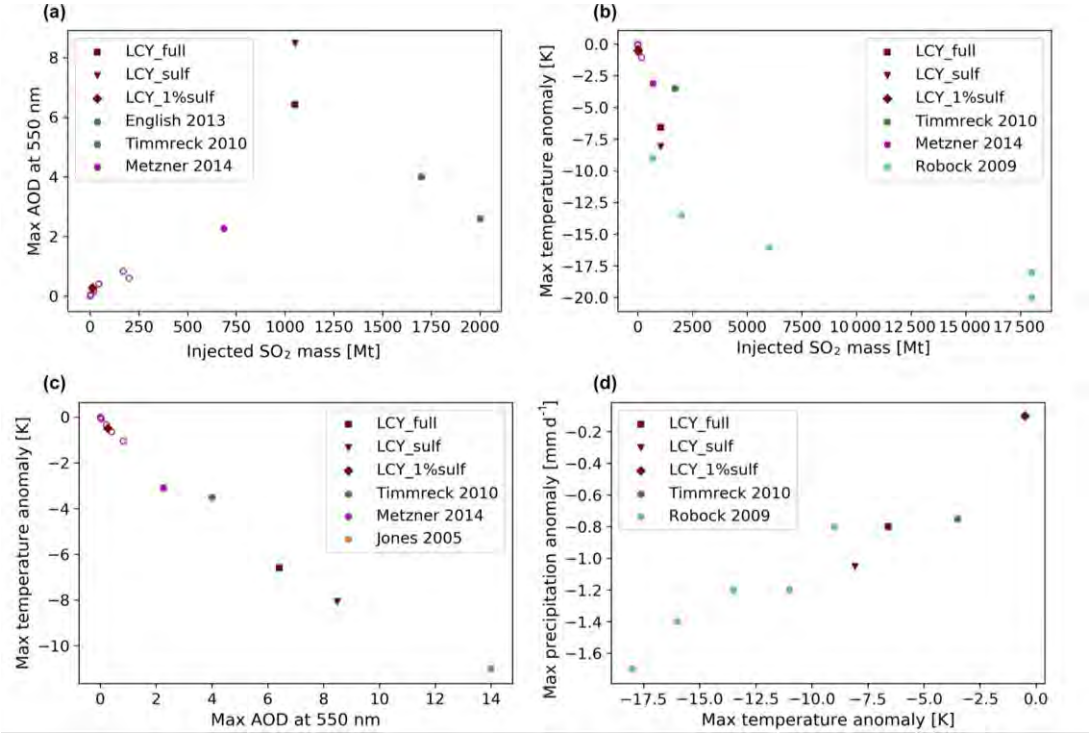

Figure 1.16 Scatterplots of large to extreme volcanic eruption simulations from Robock et al. (2009), Jones et al. (2005), Timmreck et al. (2010), Metzner et al. (2014) and English et al. (2013) (Brenna et al., 2020).

explained as larger cooling coupled with weak global hydrological dynamics, leading to lower precipitation. With 523 ± 94 Mt sulfur, 10 % and 1 % halogen of stratospheric injections in the model simulations (CESM2-WACCM6), Brenna et al. (2020) simulated SAOD above 6, surface precipitation decreased to 25% and sea ice area increased by around 40% in the first three years following the eruption. The Intertropical Convergence Zone was found to shift southward and the recovery time of the ozone layer took 15-30 years.

Climate models coupled with a volcanic aerosol radiative forcing dataset can be low computational cost and make the volcanic forcing is consistent with the other models when testing the climate impact of volcanic eruptions (Timmreck, 2012). The Community Earth System Model (CESM) and the Max Planck Institute Earth System Model (MPI-ESM) are comprehensive and widely used global climate models. Black et al. (2021) set different emission scenarios of volcanic sulfur dioxide gas from 200 to 2,000 Tg for the Toba eruption using CESM 1.3 simulations, that resulted in 2.3 - 4.1 °C global cooling and lasting for five years. Although a significant regional climate disruption follows the Toba eruption in the model, the regional climate in South Africa shows low variablility in temperature and precipitation, which is consistent with paleoclimate proxies (Smith et al., 2018; Jackson et al., 2015).

1.7 References

Abbott, P. M., Plunkett, G., Corona, C., Chellman, N. J., McConnell, J. R., Pilcher, J. R., Stoffel, M., and Sigl, M.: Cryptotephra from the Icelandic Veiðivötn 1477 CE eruption in a Greenland ice core: confirming the dating of volcanic events in the 1450s CE and assessing the eruption's climatic impact, Clim. Past, 17, 565-585, 10.5194/cp-17-565-2021, 2021.

Ambrose, S. H.: Late Pleistocene human population bottlenecks, volcanic winter, and differentiation of modern humans, Journal of Human Evolution, 34, 623-651, 10.1006/jhev.1998.0219, 1998.

Anchukaitis, K. J. and Smerdon, J. E.: Progress and uncertainties in global and hemispheric temperature reconstructions of the Common Era, Quaternary Science Reviews, 286, 107537, https://doi.org/10.1016/j.quascirev.2022.107537, 2022.

Anchukaitis, K. J., Breitenmoser, P., Briffa, K. R., Buchwal, A., Büntgen, U., Cook, E. R., D'Arrigo, R. D., Esper, J., Evans, M. N., Frank, D., Grudd, H., Gunnarson, B. E., Hughes, M. K., Kirdyanov, A. V., Körner, C., Krusic, P. J., Luckman, B., Melvin, T. M., Salzer, M. W., Shashkin, A. V., Timmreck, C., Vaganov, E. A., and Wilson, R. J. S.: Tree rings and volcanic cooling, Nature Geoscience, 5, 836-837, 10.1038/ngeo1645, 2012.

Andersen, K. K., Azuma, N., Barnola, J. M., Bigler, M., Biscaye, P., Caillon, N., Chappellaz, J., Clausen, H. B., DahlJensen, D., Fischer, H., Fluckiger, J., Fritzsche, D., Fujii, Y., Goto-Azuma, K., Gronvold, K., Gundestrup, N. S., Hansson, M., Huber, C., Hvidberg, C. S., Johnsen, S. J., Jonsell, U., Jouzel, J., Kipfstuhl, S., Landais, A., Leuenberger, M., Lorrain, R., Masson-Delmotte, V., Miller, H., Motoyama, H., Narita, H., Popp, T., Rasmussen, S. O., Raynaud, D., Rothlisberger, R., Ruth, U., Samyn, D., Schwander, J., Shoji, H., Siggard-Andersen, M. L., Steffensen, J. P., Stocker, T., Sveinbjornsdottir, A. E., Svensson, A., Takata, M., Tison, J. L., Thorsteinsson, T., Watanabe, O., Wilhelms, F., White, J. W. C., and Project, N. G. I. C.: High-resolution record of Northern Hemisphere climate extending into the last interglacial period, Nature, 431, 147-151, 10.1038/nature02805, 2004.

Augustin, L., Barbante, C., Barnes, P. R. F., Barnola, J. M., Bigler, M., Castellano, E., Cattani, O., Chappellaz, J., DahlJensen, D., Delmonte, B., Dreyfus, G., Durand, G., Falourd, S., Fischer, H., Fluckiger, J., Hansson, M. E., Huybrechts, P., Jugie, R., Johnsen, S. J., Jouzel, J., Kaufmann, P., Kipfstuhl, J., Lambert, F., Lipenkov, V. Y., Littot, G. V. C., Longinelli, A., Lorrain, R., Maggi, V., Masson-Delmotte, V., Miller, H., Mulvaney, R., Oerlemans, J., Oerter, H., Orombelli, G., Parrenin, F., Peel, D. A., Petit, J. R., Raynaud, D., Ritz, C., Ruth, U., Schwander, J., Siegenthaler, U., Souchez, R., Stauffer, B., Steffensen, J. P., Stenni, B., Stocker, T. F., Tabacco, I. E., Udisti, R., van de Wal, R. S. W., van den Broeke, M., Weiss, J., Wilhelms, F., Winther, J. G., Wolff, E. W., Zucchelli, M., and Members, E. C.: Eight glacial cycles from an Antarctic ice core, Nature, 429, 623-628, 10.1038/nature02599, 2004.

Augustin, L., Barbante, C., Barnes, P. R. F., Barnola, J. M., Bigler, M., Castellano, E., Cattani, O., Chappellaz, J., DahlJensen, D., Delmonte, B., Dreyfus, G., Durand, G., Falourd, S., Fischer, H., Fluckiger, J., Hansson, M. E., Huybrechts, P., Jugie, R., Johnsen, S. J., Jouzel, J., Kaufmann, P., Kipfstuhl, J., Lambert, F., Lipenkov, V. Y., Littot, G. V. C., Longinelli, A., Lorrain, R., Maggi, V., Masson-Delmotte, V., Miller, H., Mulvaney, R., Oerlemans, J., Oerter, H., Orombelli, G., Parrenin, F., Peel, D. A., Petit, J. R., Raynaud, D., Ritz, C., Ruth, U., Schwander, J., Siegenthaler, U., Souchez, R., Stauffer, B., Steffensen, J. P., Stenni, B., Stocker, T. F., Tabacco, I. E., Udisti, R., van de Wal, R. S. W., van den Broeke, M., Weiss, J., Wilhelms, F., Winther, J. G., Wolff, E. W.,

Zucchelli, M., and Members, E. C.: Eight glacial cycles from an Antarctic ice core, Nature, 429, 623-628, 10.1038/nature02599, 2004.

Barbante, C., Barnola, J. M., Becagli, S., Beer, J., Bigler, M., Boutron, C., Blunier, T., Castellano, E., Cattani, O., Chappellaz, J., Dahl-Jensen, D., Debret, M., Delmonte, B., Dick, D., Falourd, S., Faria, S., Federer, U., Fischer, H., Freitag, J., Frenzel, A., Fritzsche, D., Fundel, F., Gabrielli, P., Gaspari, V., Gersonde, R., Graf, W., Grigoriev, D., Hamann, I., Hansson, M., Hoffmann, G., Hutterli, M. A., Huybrechts, P., Isaksson, E., Johnsen, S., Jouzel, J., Kaczmarska, M., Karlin, T., Kaufmann, P., Kipfstuhl, S., Kohno, M., Lambert, F., Lambrecht, A., Lambrecht, A., Landais, A., Lawer, G., Leuenberger, M., Littot, G., Loulergue, L., Luthi, D., Maggi, V., Marino, F., Masson-Delmotte, V., Meyer, H., Miller, H., Mulvaney, R., Narcisi, B., Oerlemans, J., Oerter, H., Parrenin, F., Petit, J. R., Raisbeck, G., Raynaud, D., Rothlisberger, R., Ruth, U., Rybak, O., Severi, M., Schmitt, J., Schwander, J., Siegenthaler, U., Siggaard-Andersen, M. L., Spahni, R., Steffensen, J. P., Stenni, B., Stocker, T. F., Tison, J. L., Traversi, R., Udisti, R., Valero-Delgado, F., van den Broeke, M. R., van de Wal, R. S. W., Wagenbach, D., Wegner, A., Weiler, K., Wilhelms, F., Winther, J. G., Wolff, E., and Members, E. C.: One-to-one coupling of glacial climate variability in Greenland and Antarctica, Nature, 444, 195-198, 10.1038/nature05301, 2006.

Baldini, J. U. L., Brown, R. J., and McElwaine, J. N.: Was millennial scale climate change during the Last Glacial triggered by explosive volcanism?, Scientific Reports, 5, 10.1038/srep17442, 2015.

Benson, C. S. 1961. Stratigraphic studies in the snow and firn of the Greenland ice sheet. Folio Geogr. Dan., 9, 13-37.

Bigler, M.: Hochauflösende Spurenstoffmessungen an polaren Eisbohrkernen: Glazio-chemische und klimatische Prozessstudien, PhD dissertation, Physics Institute, University of Bern, Switzerland, 2004.

Bond, G., Heinrich, H., Broecker, W., Labeyrie, L., McManus, J., Andrews, J., Huon, S., Jantschik, R., Clasen, S., Simet, C., Tedesco, K., Klas, M., Bonani, G., and Ivy, S.: Evidence for massive discharges of icebergs into the North Atlantic ocean during the last glacial period, Nature, 360, 245-249, 10.1038/360245a0, 1992.

Black, B. A., Lamarque, J. F., Marsh, D. R., Schmidt, A., and Bardeen, C. G.: Global climate disruption and regional climate shelters after the Toba supereruption, Proceedings of the National Academy of Sciences of the United States of America, 118, 10.1073/pnas.2013046118, 2021.

Blunier, T., Spahni, R., Barnola, J. M., Chappellaz, J., Loulergue, L., and Schwander, J.: Synchronization of ice core records via atmospheric gases, Climate of the Past, 3, 325-330, 10.5194/cp-3-325-2007, 2007.

Braconnot, P., Harrison, S. P., Kageyama, M., Bartlein, P. J., Masson-Delmotte, V., Abe-Ouchi, A., Otto-Bliesner, B., and Zhao, Y.: Evaluation of climate models using palaeoclimatic data, Nature Climate Change, 2, 417-424, 10.1038/nclimate1456, 2012.

Brenna, H., Kutterolf, S., Mills, M. J., and Kruger, K.: The potential impacts of a sulfur- and halogen-rich supereruption such as Los Chocoyos on the atmosphere and climate, Atmospheric Chemistry and Physics, 20, 6521-6539, 10.5194/acp-20-6521-2020, 2020.

Buiron, D., Chappellaz, J., Stenni, B., Frezzotti, M., Baumgartner, M., Capron, E., Landais, A., Lemieux-Dudon, B., Masson-Delmotte, V., Montagnat, M., Parrenin, F., and Schilt, A.: TALDICE-1 age scale of the Talos Dome deep ice core, East Antarctica, Climate of the Past, 7, 1-16, 10.5194/cp-7-1-2011, 2011.

Buizert, C., Cuffey, K. M., Severinghaus, J. P., Baggenstos, D., Fudge, T. J., Steig, E. J., Markle, B. R., Winstrup, M., Rhodes, R. H., Brook, E. J., Sowers, T. A., Clow, G. D., Cheng, H., Edwards, R. L., Sigl, M., McConnell, J.

R., and Taylor, K. C.: The WAIS Divide deep ice core WD2014 chronology - Part 1: Methane synchronization (68-31 kaBP) and the gas age-ice age difference, Climate of the Past, 11, 153-173, 10.5194/cp-11-153-2015, 2015.

Buizert, C., Sigl, M., Severi, M., Markle, B. R., Wettstein, J. J., McConnell, J. R., Pedro, J. B., Sodemann, H., Goto-Azuma, K., Kawamura, K., Fujita, S., Motoyama, H., Hirabayashi, M., Uemura, R., Stenni, B., Parrenin, F., He, F., Fudge, T. J., and Steig, E. J.: Abrupt ice-age shifts in southern westerly winds and Antarctic climate forced from the north, Nature, 563, 681-+, 10.1038/s41586-018-0727-5, 2018.

Büntgen, U., Myglan, V. S., Ljungqvist, F. C., McCormick, M., Di Cosmo, N., Sigl, M., Jungclaus, J., Wagner, S., Krusic, P. J., Esper, J., Kaplan, J. O., de Vaan, M. A. C., Luterbacher, J., Wacker, L., Tegel, W., and Kirdyanov, A. V.: Cooling and societal change during the Late Antique Little Ice Age from 536 to around 660 AD, Nature Geoscience, 9, 231-236, 10.1038/ngeo2652, 2016.

Büntgen, U., Eggertsson, O., Wacker, L., Sigl, M., Ljungqvist, F. C., Di Cosmo, N., Plunkett, G., Krusic, P. J., Newfield, T. P., Esper, J., Lane, C., Reinig, F., and Oppenheimer, C.: Multi-proxy dating of Iceland's major pre-settlement Katla eruption to 822–823 CE, Geology, 45, 783–786, 2017.

Büntgen, U., Allen, K., Anchukaitis, K. J., Arseneault, D., Boucher, É., Bräuning, A., Chatterjee, S., Cherubini, P., Churakova, O. V., Corona, C., Gennaretti, F., Grießinger, J., Guillet, S., Guiot, J., Gunnarson, B., Helama, S., Hochreuther, P., Hughes, M. K., Huybers, P., Kirdyanov, A. V., Krusic, P. J., Ludescher, J., Meier, W. J. H., Myglan, V. S., Nicolussi, K., Oppenheimer, C., Reinig, F., Salzer, M. W., Seftigen, K., Stine, A. R., Stoffel, M., St. George, S., Tejedor, E., Trevino, A., Trouet, V., Wang, J., Wilson, R., Yang, B., Xu, G., and Esper, J.: The influence of decision-making in tree ring-based climate reconstructions, Nature Communications, 12, 3411, 10.1038/s41467-021-23627-6, 2021.

Capron, E., Landais, A., Chappellaz, J., Schilt, A., Buiron, D., Dahl-Jensen, D., Johnsen, S. J., Jouzel, J., Lemieux-Dudon, B., Loulergue, L., Leuenberger, M., Masson-Delmotte, V., Meyer, H., Oerter, H., and Stenni, B.: Millennial and sub-millennial scale climatic variations recorded in polar ice cores over the last glacial period, Climate of the Past, 6, 345-365, 10.5194/cp-6-345-2010, 2010.

Castellano, E., Becagli, S., Jouzel, J., Migliori, A., Severi, M., Steffensen, J. P., Traversi, R., and Udisti, R.: Volcanic eruption frequency over the last 45 ky as recorded in Epica-Dome C ice core (East Antarctica) and its relationship with climatic changes, Global and Planetary Change, 42, 195-205, 10.1016/j.gloplacha.2003.11.007, 2004.

Cook, E., Portnyagin, M., Ponomareva, V., Bazanova, L., Svensson, A., and Garbe-Schönberg, D.: First identification of cryptotephra from the Kamchatka Peninsula in a Greenland ice core: Implications of a widespread marker deposit that links Greenland to the Pacific northwest, Quaternary Sci. Rev., 181, 200–206, 2018.

Cole-Dai, J.: Volcanoes and climate, Wiley Interdisciplinary Reviews-Climate Change, 1, 824-839, 10.1002/wcc.76, 2010.

Cole-Dai, J., Mosley-Thompson, E., Wight, S. P., and Thompson, L. G.: A 4100-year record of explosive volcanism from an East Antarctica ice core, Journal of Geophysical Research: Atmospheres, 105, 24431-24441, https://doi.org/10.1029/2000JD900254, 2000.

Cole-Dai, J., Ferris, D. G., Kennedy, J. A., Michael, S., and McConnell, J.: Comprehensive Record of Volcanic Eruptions in the Holocene (11,000 · years) From the WAIS Divide, Antarctica Ice Core, Journal of Geophysical Research-Atmospheres, 126, 10.1029/2020JD032855, 2021.

Corrick, E. C., Drysdale, R. N., Hellstrom, J. C., Capron, E., Rasmussen, S. O., Zhang, X., Fleitmann, D., Couchoud, I., and Wolff, E.: Synchronous timing of abrupt climate changes during the last glacial period, Science, 369, 963-969, doi:10.1126/science.aay5538, 2020.

Clausen, H. B., Hammer, C. U., Hvidberg, C. S., DahlJensen, D.,Steffensen, J. P., Kipfstuhl, J., and Legrand, M.: A comparison of the volcanic records over the past 4000 years from the Greenland Ice Core Project and Dye 3 Greenland Ice Cores, J. Geophys. Res., 102, 26707–26723, https://doi.org/10.1029/97jc00587, 1997.

Clark, P. U., Dyke, A. S., Shakun, J. D., Carlson, A. E., Clark, J., Wohlfarth, B., Mitrovica, J. X., Hostetler, S. W., and Mccabe, A.: The Last Glacial Maximum, Science, 325, 710 - 714, 2009.

Churakova, O. V., Bryukhanova, M. V., Saurer, M., Boettger, T., Naurzbaev, M. M., Myglan, V. S., Vaganov, E. A., Hughes, M. K., and Siegwolf, R. T. W.: A cluster of stratospheric volcanic eruptions in the AD 530s recorded in Siberian tree rings, Global and Planetary Change, 122, 140-150, https://doi.org/10.1016/j.gloplacha.2014.08.015, 2014.

Danabasoglu, G., Lamarque, J. F., Bacmeister, J., Bailey, D. A., DuVivier, A. K., Edwards, J., Emmons, L. K., Fasullo, J., Garcia, R., Gettelman, A., Hannay, C., Holland, M. M., Large, W. G., Lauritzen, P. H., Lawrence, D. M., Lenaerts, J. T. M., Lindsay, K., Lipscomb, W. H., Mills, M. J., Neale, R., Oleson, K. W., Otto-Bliesner, B., Phillips, A. S., Sacks, W., Tilmes, S., van Kampenhout, L., Vertenstein, M., Bertini, A., Dennis, J., Deser, C., Fischer, C., Fox-Kemper, B., Kay, J. E., Kinnison, D., Kushner, P. J., Larson, V. E., Long, M. C., Mickelson, S., Moore, J. K., Nienhouse, E., Polvani, L., Rasch, P. J., and Strand, W. G.: The Community Earth System Model Version 2 (CESM2), Journal of Advances in Modeling Earth Systems, 12, 10.1029/2019ms001916, 2020.

de Leon, A. C., Schindlbeck-Belo, J. C., Kutterolf, S., Danisik, M., Schmitt, A. K., Freundt, A., Perez, W., Harvey, J. C., Wang, K. L., and Lee, H. Y.: A history of violence: magma incubation, timing and tephra distribution of the Los Chocoyos supereruption (Atitlan Caldera, Guatemala), Journal of Quaternary Science, 36, 169-179, 10.1002/jqs.3265, 2021.

Dansgaard, W. and S. J. Johnsen (1969). “A Flow Model and a Time Scale for the Ice Core from Camp Century, Greenland”. In: Journal of Glaciology 8.53, pp. 215–223.

Dansgaard, W., Clausen, H. B., Gundestrup, N., Hammer, C. U., Johnsen, S. F., Kristinsdottir, P. M., and Reeh, N.: A New Greenland Deep Ice Core, Science, 218, 1273-1277, doi:10.1126/science.218.4579.1273, 1982.

Deplazes, G., Luckge, A., Peterson, L. C., Timmermann, A., Hamann, Y., Hughen, K. A., Rohl, U., Laj, C., Cane, M. A., Sigman, D. M., and Haug, G. H.: Links between tropical rainfall and North Atlantic climate during the last glacial period, Nature Geoscience, 6, 213-217, 10.1038/ngeo1712, 2013.

Fretwell, P., Pritchard, H. D., Vaughan, D. G., Bamber, J. L., Barrand, N. E., Bell, R., Bianchi, C., Bingham, R. G., Blankenship, D. D., Casassa, G., Catania, G., Callens, D., Conway, H., Cook, A. J., Corr, H. F. J., Damaske, D., Damm, V., Ferraccioli, F., Forsberg, R., Fujita, S., Gim, Y., Gogineni, P., Griggs, J. A., Hindmarsh, R. C. A., Holmlund, P., Holt, J. W., Jacobel, R. W., Jenkins, A., Jokat, W., Jordan, T., King, E. C., Kohler, J., Krabill, W., Riger-Kusk, M., Langley, K. A., Leitchenkov, G., Leuschen, C., Luyendyk, B. P., Matsuoka, K., Mouginot, J., Nitsche, F. O., Nogi, Y., Nost, O. A., Popov, S. V., Rignot, E., Rippin, D. M., Rivera, A., Roberts, J., Ross, N.,

Siegert, M. J., Smith, A. M., Steinhage, D., Studinger, M., Sun, B., Tinto, B. K., Welch, B. C., Wilson, D., Young, D. A., Xiangbin, C., and Zirizzotti, A.: Bedmap2: improved ice bed, surface and thickness datasets for Antarctica, The Cryosphere, 7, 375-393, 10.5194/tc-7-375-2013, 2013.

Fudge, T. J., B. R. Markle, K. M. Cuffey, C. Buizert, K. C. Taylor, E. J. Steig, E. D. Waddington, H. Conway, and M. Koutnik (2016), Variable relationship between accumulation and temperature in West Antarctica for the past 31,000 years, Geophys. Res. Lett., 43, 3795–3803, doi:10.1002/2016GL068356.

Gao, C. C., Robock, A., and Ammann, C.: Volcanic forcing of climate over the past 1500 years: An improved ice core-based index for climate models, Journal of Geophysical Research-Atmospheres, 113, 10.1029/2008jd010239, 2008.

Giorgetta, M. A., Jungclaus, J., Reick, C. H., Legutke, S., Bader, J., Bottinger, M., Brovkin, V., Crueger, T., Esch, M., Fieg, K., Glushak, K., Gayler, V., Haak, H., Hollweg, H. D., Ilyina, T., Kinne, S., Kornblueh, L., Matei, D., Mauritsen, T., Mikolajewicz, U., Mueller, W., Notz, D., Pithan, F., Raddatz, T., Rast, S., Redler, R., Roeckner, E., Schmidt, H., Schnur, R., Segschneider, J., Six, K. D., Stockhause, M., Timmreck, C., Wegner, J., Widmann, H., Wieners, K. H., Claussen, M., Marotzke, J., and Stevens, B.: Climate and carbon cycle changes from 1850 to 2100 in MPI-ESM simulations for the Coupled Model Intercomparison Project phase 5, Journal of Advances in Modeling Earth Systems, 5, 572-597, 10.1002/jame.20038, 2013.

Gkinis, V., S. B. Simonsen, S. L. Buchardt, J. W. C. White, and B. M. Vinther (2014). “Water isotope diffusion rates from the NorthGRIP ice core for the last 16,000 years - glaciological and paleoclimatic implications”. In: Earth and Planetary Science Letters 405.

Guillet, S., Corona, C., Stoffel, M., Khodri, M., Lavigne, F., Ortega, P., Eckert, N., Sielenou, P. D., Daux, V., Churakova, O. V., Davi, N., Edouard, J. L., Zhang, Y., Luckman, B. H., Myglan, V. S., Guiot, J., Beniston, M., Masson-Delmotte, V., and Oppenheimer, C.: Climate response to the Samalas volcanic eruption in 1257 revealed by proxy records, Nature Geoscience, 10, 123-+, 10.1038/ngeo2875, 2017.

Hammer, C. U., Clausen, H. B., and Langway, C. C.: 50,000 years of recorded global volcanism, Climatic Change, 35, 1-15, 10.1023/a:1005344225434, 1997.

Hammer, C. U. (1980). Acidity of polar ice cores in relation to absolute dating, past volcanism, and radio–echoes. Journal of Glaciolo, 25(93):359–372.

Hemming, S. R.: Heinrich events: Massive late Pleistocene detritus layers of the North Atlantic and their global climate imprint, Reviews of Geophysics, 42, https://doi.org/10.1029/2003RG000128, 2004.

Ilyina, T., Six, K. D., Segschneider, J., Maier-Reimer, E., Li, H. M., and Nunez-Riboni, I.: Global ocean biogeochemistry model HAMOCC: Model architecture and performance as component of the MPI-Earth system model in different CMIP5 experimental realizations, Journal of Advances in Modeling Earth Systems, 5, 287-315, 10.1029/2012ms000178, 2013.

Jackson, L. J., Stone, J. R., Cohen, A. S., and Yost, C. L.: High-resolution paleoecological records from Lake Malawi show no significant cooling associated with the Mount Toba supereruption at ca. 75 ka, Geology, 43, 823-826, 10.1130/g36917.1, 2015.

Jensen, B. J. L., Pyne-O’Donnell, S., Plunkett, G., Froese, D. G., Hughes, P. D. M., Sigl, M., McConnell, J. R., Amesbury, M. J., Blackwell, P. G., van den Bogaard, C., Buck, C. E., Charman, D. J., Clague, J. J., Hall, V. A.,

Koch, J., Mackay, H., Mallon, G., McColl, L., and Pilcher, J. R.: Transatlantic distribution of the Alaskan White River Ash, Geology, 42, 875–878, 2014.

Jouzel, J., Masson-Delmotte, V., Cattani, O., Dreyfus, G., Falourd, S., Hoffmann, G., Minster, B., Nouet, J., Barnola, J. M., Chappellaz, J., Fischer, H., Gallet, J. C., Johnsen, S., Leuenberger, M., Loulergue, L., Luethi, D., Oerter, H., Parrenin, F., Raisbeck, G., Raynaud, D., Schilt, A., Schwander, J., Selmo, E., Souchez, R., Spahni, R., Stauffer, B., Steffensen, J. P., Stenni, B., Stocker, T. F., Tison, J. L., Werner, M., and Wolff, E. W.: Orbital and millennial Antarctic climate variability over the past 800,000 years, Science, 317, 793-796, 10.1126/science.1141038, 2007.

Jungclaus, J. H., Fischer, N., Haak, H., Lohmann, K., Marotzke, J., Matei, D., Mikolajewicz, U., Notz, D., and von Storch, J. S.: Characteristics of the ocean simulations in the Max Planck Institute Ocean Model (MPIOM) the ocean component of the MPI-Earth system model, Journal of Advances in Modeling Earth Systems, 5, 422-446, 10.1002/jame.20023, 2013.

Kremser, S., Thomason, L. W., von Hobe, M., Hermann, M., Deshler, T., Timmreck, C., Toohey, M., Stenke, A., Schwarz, J. P., Weigel, R., Fueglistaler, S., Prata, F. J., Vernier, J.-P., Schlager, H., Barnes, J. E., Antuña-Marrero, J.-C., Fairlie, D., Palm, M., Mahieu, E., Notholt, J., Rex, M., Bingen, C., Vanhellemont, F., Bourassa, A., Plane, J. M. C., Klocke, D., Carn, S. A., Clarisse, L., Trickl, T., Neely, R., James, A. D., Rieger, L., Wilson, J. C., and Meland, B.: Stratospheric aerosol—Observations, processes, and impact on climate, Reviews of Geophysics, 54, 278-335, https://doi.org/10.1002/2015RG000511, 2016.

Kobashi, T., Menviel, L., Jeltsch-Thommes, A., Vinther, B. M., Box, J. E., Muscheler, R., Nakaegawa, T., Pfister, P. L., Doring, M., Leuenberger, M., Wanner, H., and Ohmura, A.: Volcanic influence on centennial to millennial Holocene Greenland temperature change, Scientific Reports, 7, 10.1038/s41598-017-01451-7, 2017.

Kurbatov, A. V., Zielinski, G. A., Dunbar, N. W., Mayewski, P. A., Meyerson, E. A., Sneed, S. B., and Taylor, K. C.: A 12,000 year record of explosive volcanism in the Siple Dome Ice Core, West Antarctica, Journal of Geophysical Research-Atmospheres, 111, 10.1029/2005jd006072, 2006.

Kovilakam, M., Thomason, L. W., Ernest, N., Rieger, L., Bourassa, A., and Millán, L.: The Global Space-based Stratospheric Aerosol Climatology (version 2.0): 1979–2018, Earth Syst. Sci. Data, 12, 2607-2634, 10.5194/essd-12-2607-2020, 2020.

Landais, A., Waelbroeck, C., and Masson-Delmotte, V.: On the limits of Antarctic and marine climate records synchronization: Lag estimates during marine isotopic stages 5d and 5c, Paleoceanography, 21, 10.1029/2005pa001171, 2006.

Lavigne, F., Degeai, J. P., Komorowski, J. C., Guillet, S., Robert, V., Lahitte, P., Oppenheimer, C., Stoffel, M., Vidal, C. M., Surono, Pratomo, I., Wassmer, P., Hajdas, I., Hadmoko, D. S., and De Belizal, E.: Source of the great A.D. 1257 mystery eruption unveiled, Samalas volcano, Rinjani Volcanic Complex, Indonesia, P. Natl. Acad. Sci. USA, 110, 16742–16747, 2013.

Lean, J. and Rind, D.: Evaluating sun–climate relationships since the Little Ice Age, Journal of Atmospheric and Solar-Terrestrial Physics, 61, 25-36, https://doi.org/10.1016/S1364-6826(98)00113-8, 1999.

Legrand, M. and Mayewski, P.: Glaciochemistry of polar ice cores: A review, Reviews of Geophysics, 35, 219-243, 10.1029/96rg03527, 1997.

Lemieux-Dudon, B., Blayo, E., Petit, J. R., Waelbroeck, C., Svensson, A., Ritz, C., Barnola, J. M., Narcisi, B. M., and Parrenin, F.: Consistent dating for Antarctic and Greenland ice cores, Quaternary Science Reviews, 29, 8-20, 10.1016/j.quascirev.2009.11.010, 2010.

Loulergue, L., Parrenin, F., Blunier, T., Barnola, J. M., Spahni, R., Schilt, A., Raisbeck, G., and Chappellaz, J.: New constraints on the gas age-ice age difference along the EPICA ice cores, 0-50 kyr, Climate of the Past, 3, 527-540, 10.5194/cp-3-527-2007, 2007.

Luterbacher, J. and Pfister, C.: The year without a summer, Nature Geoscience, 8, 246-248, 10.1038/ngeo2404, 2015.

Marshall, L. R., Smith, C. J., Forster, P. M., Aubry, T. J., Andrews, T., and Schmidt, A.: Large Variations in Volcanic Aerosol Forcing Efficiency Due to Eruption Source Parameters and Rapid Adjustments, Geophysical Research Letters, 47, 10.1029/2020gl090241, 2020.

Mayewski, P. A., Holdsworth, G., Spencer, M. J., Whitlow, S., Twickler, M., Morrison, M. C., Ferland, K. K., and Meeker, L. D.: Ice-core sulfate from three northern hemisphere sites: Source and temperature forcing implications, Atmos. Environ. A-Gen., 27, 2915–2919, https://doi.org/10.1016/0960-1686(93)90323-q, 1993.

Masson-Delmotte, V., Jouzel, J., Landais, A., Stievenard, M., Johnsen, S. J., White, J. W. C., Werner, M., Sveinbjornsdottir, A., and Fuhrer, K.: GRIP Deuterium Excess Reveals Rapid and Orbital-Scale Changes in Greenland Moisture Origin, Science, 309, 118-121, doi:10.1126/science.1108575, 2005.

McAneney, J. and Baillie, M.: Absolute tree-ring dates for the Late Bronze Age eruptions of Aniakchak and Thera in light of a proposed revision of ice-core chronologies, Antiquity, 93, 99–112, 2019.

Mekhaldi, F., Muscheler, R., Adolphi, F., Aldahan, A., Beer, J., McConnell, J. R., Possnert, G., Sigl, M., Svensson, A., Synal, H.-A., Welten, K. C., and Woodruff, T. E.: Multiradionuclide evidence for the solar origin of the cosmic-ray events of AD 774/5 and 993/4, Nature Communications, 6, 8611, 10.1038/ncomms9611, 2015.

Moore, J. C., Wolff, E. W., Clausen, H. B., and Hammer, C. U.: The chemical basis for the electrical stratigraphy of ice, Journal of Geophysical Research: Solid Earth, 97, 1887–1896, doi:10.1029/91JB02750, URL https://agupubs.onlinelibrary.wiley.com/doi/abs/10.1029/91JB02750, 1992.

Moore, J. C., Wolff, E. W., Clausen, H. B., Hammer, C. U., Legrand, M. R., and Fuhrer, K.: Electrical response of the Summit-Greenland ice core to ammonium, sulphuric acid, and hydrochloric acid, grl, 21, 565–568, doi: 10.1029/94GL00542, 1994.

McConnell, J. R., Sigl, M., Plunkett, G., Burke, A., Kim, W. M., Raible, C. C., Wilson, A. I., Manning, J. G., Ludlow, F., Chellman, N. J., Innes, H. M., Yang, Z., Larsen, J. F., Schaefer, J. R., Kipfstuhl, S., Mojtabavi, S., Wilhelms, F., Opel, T., Meyer, H., and Steffensen, J. P.: Extreme climate after massive eruption of Alaska's Okmok volcano in 43 BCE and effects on the late Roman Republic and Ptolemaic Kingdom, Proceedings of the National Academy of Sciences, 117, 15 443–15 449, doi: 10. 1073/pnas.2002722117, URL https://www.pnas.org/content/117/27/15443, 2020.

Muller, F. 1962. Zonation in the accumulation area of the glaciers of Axel Heiberg Island, N.W.T., Canada.]. Glaciol., 4(33), 302-311.

Nardin, R., Amore, A., Becagli, S., Caiazzo, L., Frezzotti, M., Severi, M., Stenni, B., and Traversi, R.: Volcanic Fluxes Over the Last Millennium as Recorded in the Gv7 Ice Core (Northern Victoria Land, Antarctica), Geosciences, 10, 10.3390/geosciences10010038, 2020.

Otto-Bliesner, B. L., Brady, E. C., Fasullo, J., Jahn, A., Landrum, L., Stevenson, S., Rosenbloom, N., Mai, A., and Strand, G.: CLIMATE VARIABILITY AND CHANGE SINCE 850 CE An Ensemble Approach with the Community Earth System Model, Bulletin of the American Meteorological Society, 97, 735-754, 10.1175/bams-d-14-00233.1, 2016.

Oppenheimer, C., Orchard, A., Stoffel, M., Newfield, T. P., Guillet, S., Corona, C., Sigl, M., Di Cosmo, N., and Buntgen, U.: The Eldgja eruption: timing, long-range impacts and influence on the Christianisation of Iceland, Clim. Change, 147, 369–381, 2018.

Oppenheimer, C., Wacker, L., Xu, J., Galvan, J. D., Stoffel, M., Guillet, S., Corona, C., Sigl, M., Di Cosmo, N., Hajdas, I., Pan, B., Breuker, R., Schneider, L., Esper, J., Fei, J., Hammond, J. O. S., and Büntgen, U.: Multi-proxy dating the 'Millennium Eruption' of Changbaishan to late 946 CE, Quaternary Sci. Rev., 158, 164–171, 2017.

Paine, A. R., Wadsworth, F. B., and Baldini, J. U. L.: Supereruption doublet at a climate transition, Communications Earth & Environment, 2, 219, 10.1038/s43247-021-00293-6, 2021.

Papale, P.: Global time-size distribution of volcanic eruptions on Earth, Scientific Reports, 8, 10.1038/s41598-018-25286-y, 2018.

Parrenin, F., Barker, S., Blunier, T., Chappellaz, J., Jouzel, J., Landais, A., Masson-Delmotte, V., Schwander, J., and Veres, D.: On the gas-ice depth difference (Delta depth) along the EPICA Dome C ice core, Climate of the Past, 8, 1239-1255, 10.5194/cp-8-1239-2012, 2012a.

Parrenin, F., Petit, J. R., Masson-Delmotte, V., Wolff, E., Basile-Doelsch, I., Jouzel, J., Lipenkov, V., Rasmussen, S. O., Schwander, J., Severi, M., Udisti, R., Veres, D., and Vinther, B. M.: Volcanic synchronisation between the EPICA Dome C and Vostok ice cores (Antarctica) 0–145 kyr BP, Clim. Past, 8, 1031-1045, 10.5194/cp-8-1031-2012, 2012b.

Palais, J. M. and Sigurdsson, H.: Petrologic Evidence of Volatile Emissions from Major Historic and Pre-Historic Volcanic Eruptions, in: Understanding Climate Change, 31-53, https://doi.org/10.1029/GM052p0031, 1989.

Pearce, N. J. G., Westgate, J. A., Preece, S. J., Eastwood, W. J., and Perkins, W. T.: Identification of Aniakchak (Alaska) tephra in Greenland ice core challenges the 1645 BC date for Minoan eruption of Santorini, Geochem. Geophy. Geosy., 5, Q03005, https://doi.org/10.1029/2003GC000672, 2004.

Pearson, C., Sigl, M., Burke, A., Davies, S., Kurbatov, A., Severi, M., Cole-Dai, J., Innes, H., Albert, P. G., and Helmick, M.: Geochemical ice-core constraints on the timing and climatic impact of Aniakchak II (1628 BCE) and Thera (Minoan) volcanic eruptions, PNAS Nexus, https://doi.org/10.1093/pnasnexus/pgac048, 2022. 2022.

Plummer, C. T., Curran, M. A. J., van Ommen, T. D., Rasmussen, S. O., Moy, A. D., Vance, T. R., Clausen, H. B., Vinther, B. M., and Mayewski, P. A.: An independently dated 2000-yr volcanic record from Law Dome, East Antarctica, including a new perspective on the dating of the 1450s CE eruption of Kuwae, Vanuatu, Climate of the Past, 8, 1929-1940, 10.5194/cp-8-1929-2012, 2012.

Plunkett, G., Sigl, M., Pilcher, J. R., McConnell, J. R., Chellman, N., Steffensen, J. P., and Büntgen, U.: Smoking guns and volcanic ash: the importance of sparse tephras in Greenland ice cores, Polar Res., 39, 3511, https://doi.org/10.33265/polar.v39.3511, 2020.

Plunkett, G. and Pilcher, J. R.: Defining the potential source region of volcanic ash in northwest Europe during the Mid- to Late Holocene, Earth-Sci. Rev., 179, 20–37, 2018.

Raisbeck, G. M., Cauquoin, A., Jouzel, J., Landais, A., Petit, J. R., Lipenkov, V. Y., Beer, J., Synal, H. A., Oerter, H., Johnsen, S. J., Steffensen, J. P., Svensson, A., and Yiou, F.: An improved north–south synchronization of ice core records around the 41 kyr 10Be peak, Clim. Past, 13, 217-229, 10.5194/cp-13-217-2017, 2017.

Rampino, M. R. and Self, S.: VOLCANIC WINTER AND ACCELERATED GLACIATION FOLLOWING THE TOBA SUPER-ERUPTION, Nature, 359, 50-52, 10.1038/359050a0, 1992.

Rampino, M.R., and S. Self, 1984: Sulphur-rich volcanic eruptions and stratospheric aerosols. Nature, 310, doi:10.1038/310677a0.

Rasmussen, S. O., Andersen, K. K., Svensson, A. M., Steffensen, J. P., Vinther, B. M., Clausen, H. B., Siggaard-Andersen, M. L., Johnsen, S. J., Larsen, L. B., Dahl-Jensen, D., Bigler, M., Rothlisberger, R., Fischer, H., Goto-Azuma, K., Hansson, M. E., and Ruth, U.: A new Greenland ice core chronology for the last glacial termination, Journal of Geophysical Research-Atmospheres, 111, 10.1029/2005jd006079, 2006.

Rasmussen, S. O., Abbott, P. M., Blunier, T., Bourne, A. J., Brook, E., Buchardt, S. L., Buizert, C., Chappellaz, J., Clausen, H. B., Cook, E., Dahl-Jensen, D., Davies, S. M., Guillevic, M., Kipfstuhl, S., Laepple, T., Seierstad, I. K., Severinghaus, J. P., Steffensen, J. P., Stowasser, C., Svensson, A., Vallelonga, P., Vinther, B. M., Wilhelms, F., and Winstrup, M.: A first chronology for the North Greenland Eemian Ice Drilling (NEEM) ice core, Climate of the Past, 9, 2713-2730, 10.5194/cp-9-2713-2013, 2013.

Rasmussen, S. O., Bigler, M., Blockley, S. P., Blunier, T., Buchardt, S. L., Clausen, H. B., Cvijanovic, I., Dahl-Jensen, D., Johnsen, S. J., Fischer, H., Gkinis, V., Guillevic, M., Hoek, W. Z., Lowe, J. J., Pedro, J. B., Popp, T., Seierstad, I. K., Steffensen, J. P., Svensson, A. M., Vallelonga, P., Vinther, B. M., Walker, M. J. C., Wheatley, J. J., and Winstrup, M.: A stratigraphic framework for abrupt climatic changes during the Last Glacial period based on three synchronized Greenland ice-core records: refining and extending the INTIMATE event stratigraphy, Quaternary Science Reviews, 106, 14-28, 10.1016/j.quascirev.2014.09.007, 2014.

Reick, C. H., Raddatz, T., Brovkin, V., and Gayler, V.: Representation of natural and anthropogenic land cover change in MPI-ESM, Journal of Advances in Modeling Earth Systems, 5, 459-482, 10.1002/jame.20022, 2013.

Robock, A.: Volcanic eruptions and climate, Reviews of Geophysics, 38, 191-219, 10.1029/1998rg000054, 2000.

Robock, A., Ammann, C. M., Oman, L., Shindell, D., Levis, S., and Stenchikov, G.: Did the Toba volcanic eruption of similar to 74 ka BP produce widespread glaciation?, Journal of Geophysical Research-Atmospheres, 114, 10.1029/2008jd011652, 2009.

Röthlisberger, R., Bigler, M., Hutterli, M., Sommer, S., Stauffer, B.,Junghans, H. G., and Wagenbach, D.: Technique for continuoushigh-resolution analysis of trace substances in firn and ice cores,Environ. Sci. Technol., 34, 338–342, 2000.

Ruth, U., Barnola, J. M., Beer, J., Bigler, M., Blunier, T., Castellano, E., Fischer, H., Fundel, F., Huybrechts, P., Kaufmann, P., Kipfstuhl, S., Lambrecht, A., Morganti, A., Oerter, H., Parrenin, F., Rybak, O., Severi, M., Udisti, R., Wilhelms, F., and Wolff, E.: "EDML1": a chronology for the EPICA deep ice core from Dronning Maud Land, Antarctica, over the last 150 000 years, Clim. Past, 3, 475-484, 10.5194/cp-3-475-2007, 2007.

Shindell, D.T., G.A. Schmidt, M.E. Mann, and G. Faluvegi, 2004: Dynamic winter climate response to large tropical volcanic eruptions since 1600. J. Geophys. Res., 109, D05104, doi:10.1029/2003JD004151.

Schneider, D. P., C. M. Ammann, B. L. Otto-Bliesner, and D. S. Kaufman (2009), Climate response to large, high-latitude and low-latitude volcanic eruptions in the Community Climate System Model, J. Geophys. Res., 114, D15101, doi:10.1029/2008JD011222.

Schulz, H., von Rad, U., and Erlenkeuser, H.: Correlation between Arabian Sea and Greenland climate oscillations of the past 110,000 years, Nature, 393, 54-57, 10.1038/31750, 1998.

Schupbach, S., Federer, U., Bigler, M., Fischer, H., and Stocker, T. F.: A refined TALDICE-1a age scale from 55 to 112 ka before present for the Talos Dome ice core based on high-resolution methane measurements, Climate of the Past, 7, 1001-1009, 10.5194/cp-7-1001-2011, 2011.

Schwander, J. and Stauffer, B.: AGE DIFFERENCE BETWEEN POLAR ICE AND THE AIR TRAPPED IN ITS BUBBLES, Nature, 311, 45-47, 10.1038/311045a0, 1984.

Seierstad, I. K., Abbott, P. M., Bigler, M., Blunier, T., Bourne, A. J., Brook, E., Buchardt, S. L., Buizert, C., Clausen, H. B., Cook, E., Dahl-Jensen, D., Davies, S. M., Guillevic, M., Johnsen, S. J., Pedersen, D. S., Popp, T. J., Rasmussen, S. O., Severinghaus, J. P., Svensson, A., and Vinther, B. M.: Consistently dated records from the Greenland GRIP, GISP2 and NGRIP ice cores for the past 104 ka reveal regional millennial-scale delta O-18 gradients with possible Heinrich event imprint, Quaternary Science Reviews, 106, 29-46, 10.1016/j.quascirev.2014.10.032, 2014.

Severi, M., Becagli, S., Castellano, E., Morganti, A., Traversi, R., Udisti, R., Ruth, U., Fischer, H., Huybrechts, P., Wolff, E., Parrenin, F., Kaufmann, P., Lambert, F., and Steffensen, J. P.: Synchronisation of the EDML and EDC ice cores for the last 52 kyr by volcanic signature matching, Climate of the Past, 3, 367-374, 10.5194/cp-3-367-2007, 2007.

Sigl, M., Toohey, M., McConnell, J. R., Cole-Dai, J., and Severi, M.: Volcanic stratospheric sulfur injections and aerosol optical depth during the Holocene (past 11,500 years) from a bipolar ice core array, Earth Syst. Sci. Data Discuss., 2022, 1-45, 10.5194/essd-2021-422, 2022.

Sigl, M., McConnell, J. R., Layman, L., Maselli, O., McGwire, K., Pasteris, D., Dahl-Jensen, D., Steffensen, J. P., Vinther, B., Edwards, R., Mulvaney, R., and Kipfstuhl, S.: A new bipolar ice core record of volcanism from WAIS Divide and NEEM and implications for climate forcing of the last 2000 years, Journal of Geophysical Research-Atmospheres, 118, 1151-1169, 10.1029/2012jd018603, 2013.

Sigl, M., Winstrup, M., McConnell, J. R., Welten, K. C., Plunkett, G., Ludlow, F., Buntgen, U., Caffee, M., Chellman, N., Dahl-Jensen, D., Fischer, H., Kipfstuhl, S., Kostick, C., Maselli, O. J., Mekhaldi, F., Mulvaney, R., Muscheler, R., Pasteris, D. R., Pilcher, J. R., Salzer, M., Schupbach, S., Steffensen, J. P., Vinther, B. M., and Woodruff, T. E.: Timing and climate forcing of volcanic eruptions for the past 2,500 years, Nature, 523, 543-+, 10.1038/nature14565, 2015.

Sigl, M., McConnell, J. R., Toohey, M., Curran, M., Das, S. B., Edwards, R., Isaksson, E., Kawamura, K., Kipfstuhl, S., Kruger, K., Layman, L., Maselli, O. J., Motizuki, Y., Motoyama, H., Pasteris, D. R., and Severi, M.: Insights from Antarctica on volcanic forcing during the Common Era, Nature Climate Change, 4, 693-697, 10.1038/nclimate2293, 2014.

Sigl, M., Fudge, T. J., Winstrup, M., Cole-Dai, J., Ferris, D., McConnell, J. R., Taylor, K. C., Welten, K. C., Woodruff, T. E., Adolphi, F., Bisiaux, M., Brook, E. J., Buizert, C., Caffee, M. W., Dunbar, N. W., Edwards, R.,

Geng, L., Iverson, N., Koffman, B., Layman, L., Maselli, O. J., McGwire, K., Muscheler, R., Nishiizumi, K., Pasteris, D. R., Rhodes, R. H., and Sowers, T. A.: The WAIS Divide deep ice core WD2014 chronology - Part 2: Annual-layer counting (0-31 ka BP), Climate of the Past, 12, 769-786, 10.5194/cp-12-769-2016, 2016.

Siggaard-Andersen, M. L.: Analysis of soluble ions from dust and sea salt over the last glacial cycle in polar deep ice cores, PhD thesis, University of Bremen, 2004.

Sinnl, G., Winstrup, M., Erhardt, T., Cook, E., Jensen, C., Svensson, A., Vinther, B. M., Muscheler, R., and Rasmussen, S. O.: A multi-ice-core, annual-layer-counted Greenland ice-core chronology for the last 3800 years: GICC21, Clim. Past Discuss., 2021, 1-34, 10.5194/cp-2021-155, 2021.

Stocker, T. F., and Johnsen, S. J. (2003), A minimum thermodynamic model for the bipolar seesaw, Paleoceanography, 18, 1087, doi:10.1029/2003PA000920, 4.

Steinhilber, F., Abreu, J. A., Beer, J., Brunner, I., Christl, M., Fischer, H., Heikkila, U., Kubik, P. W., Mann, M., McCracken, K. G., Miller, H., Miyahara, H., Oerter, H., and Wilhelms, F.: 9,400 years of cosmic radiation and solar activity from ice cores and tree rings, Proceedings of the National Academy of Sciences of the United States of America, 109, 5967-5971, 10.1073/pnas.1118965109, 2012.

Stenchikov, G., Hamilton, K., Stouffer, R. J., Robock, A., Ramaswamy, V., Santer, B., and Graf, H. F.: Arctic Oscillation response to volcanic eruptions in the IPCC AR4 climate models, Journal of Geophysical Research-Atmospheres, 111, 10.1029/2005jd006286, 2006.

Stevens, B., Giorgetta, M., Esch, M., Mauritsen, T., Crueger, T., Rast, S., Salzmann, M., Schmidt, H., Bader, J., Block, K., Brokopf, R., Fast, I., Kinne, S., Kornblueh, L., Lohmann, U., Pincus, R., Reichler, T., and Roeckner, E.: Atmospheric component of the MPI-M Earth System Model: ECHAM6, Journal of Advances in Modeling Earth Systems, 5, 146-172, 10.1002/jame.20015, 2013.

Storey, M., Roberts, R. G., and Saidin, M.: Astronomically calibrated Ar-40/Ar-39 age for the Toba supereruption and global synchronization of late Quaternary records, Proceedings of the National Academy of Sciences of the United States of America, 109, 18684-18688, 10.1073/pnas.1208178109, 2012.

Stothers, R. B.: Mystery cloud of AD 536, Nature, 307, 344-345, 10.1038/307344a0, 1984.

Smith, E. I., Jacobs, Z., Johnsen, R., Ren, M., Fisher, E. C., Oestmo, S., Wilkins, J., Harris, J. A., Karkanas, P., Fitch, S., Ciravolo, A., Keenan, D., Cleghorn, N., Lane, C. S., Matthews, T., and Marean, C. W.: Humans thrived in South Africa through the Toba eruption about 74,000 years ago, Nature, 555, 511-+, 10.1038/nature25967, 2018.

Smith, V. C., Costa, A., Aguirre-Diaz, G., Pedrazzi, D., Scifo, A., Plunkett, G., Poret, M., Tournigand, P. Y., Miles, D., Dee, M. W., McConnell, J. R., Sunye-Puchol, I., Harris, P. D., Sigl, M., Pilcher, J. R., Chellman, N., and Gutierrez, E.: The magnitude and impact of the 431 CE Tierra Blanca Joven eruption of Ilopango, El Salvador, P. Natl. Acad. Sci. USA, 117, 26061– 26068, 2020.

Sun, C. Q., Plunkett, G., Liu, J. Q., Zhao, H. L., Sigl, M., McConnell, J. R., Pilcher, J. R., Vinther, B., Steffensen, J. P., and Hall, V.: Ash from Changbaishan Millennium eruption recorded in Greenland ice: Implications for determining the eruption's timing and impact, Geophys. Res. Lett., 41, 694–701, 2014.

Svensson, A., Andersen, K. K., Bigler, M., Clausen, H. B., Dahl-Jensen, D., Davies, S. M., Johnsen, S. J., Muscheler, R., Parrenin, F., Rasmussen, S. O., Roethlisberger, R., Seierstad, I., Steffensen, J. P., and Vinther, B. M.: A 60 000 year Greenland stratigraphic ice core chronology, Climate of the Past, 4, 47-57, 10.5194/cp-4-47-2008, 2008.

Svensson, A., Bigler, M., Blunier, T., Clausen, H. B., Dahl-Jensen, D., Fischer, H., Fujita, S., Goto-Azuma, K., Johnsen, S. J., Kawamura, K., Kipfstuhl, S., Kohno, M., Parrenin, F., Popp, T., Rasmussen, S. O., Schwander, J., Seierstad, I., Severi, M., Steffensen, J. P., Udisti, R., Uemura, R., Vallelonga, P., Vinther, B. M., Wegner, A., Wilhelms, F., and Winstrup, M.: Direct linking of Greenland and Antarctic ice cores at the Toba eruption (74 ka BP), Climate of the Past, 9, 749-766, 10.5194/cp-9-749-2013, 2013.

Svensson, A., Dahl-Jensen, D., Steffensen, J. P., Blunier, T., Rasmussen, S. O., Vinther, B. M., Vallelonga, P., Capron, E., Gkinis, V., Cook, E., Kjaer, H. A., Muscheler, R., Kipfstuhl, S., Wilhelms, F., Stocker, T. F., Fischer, H., Adolphi, F., Erhardt, T., Sigl, M., Landais, A., Parrenin, F., Buizert, C., McConnell, J. R., Severi, M., Mulvaney, R., and Bigler, M.: Bipolar volcanic synchronization of abrupt climate change in Greenland and Antarctic ice cores during the last glacial period, Climate of the Past, 16, 1565-1580, 10.5194/cp-16-1565-2020, 2020.

Swingedouw, D., Mignot, J., Ortega, P., Khodri, M., Menegoz, M., Cassou, C., and Hanquiez, V.: Impact of explosive volcanic eruptions on the main climate variability modes, Global and Planetary Change, 150, 24-45, 10.1016/j.gloplacha.2017.01.006, 2017.

Traufetter, F., Oerter, H., Fischer, H., Weller, R., and Miller, H.: Spatio-temporal variability in volcanic sulphate deposition over the past 2 kyr in snow pits and firn cores from Amundsenisen, Antarctica, Journal of Glaciology, 50, 137-146, 10.3189/172756504781830222, 2004.

Tierney, J. E., Zhu, J., King, J., Malevich, S. B., Hakim, G. J., and Poulsen, C. J.: Glacial cooling and climate sensitivity revisited, Nature, 584, 569-573, 10.1038/s41586-020-2617-x, 2020.

Tejedor, E., Steiger, N. J., Smerdon, J. E., Serrano-Notivoli, R., and Vuille, M.: Global hydroclimatic response to tropical volcanic eruptions over the last millennium, Proceedings of the National Academy of Sciences of the United States of America, 118, 10.1073/pnas.2019145118, 2021.

Timmreck, C., Graf, H. F., Zanchettin, D., Hagemann, S., Kleinen, T., and Kruger, K.: Climate response to the Toba super-eruption: Regional changes, Quaternary International, 258, 30-44, 10.1016/j.quaint.2011.10.008, 2012.

Toohey, M. and Sigl, M.: Volcanic stratospheric sulfur injections and aerosol optical depth from 500 BCE to 1900 CE, Earth System Science Data, 9, 809-831, 10.5194/essd-9-809-2017, 2017.

Toohey, M., Kruger, K., and Timmreck, C.: Volcanic sulfate deposition to Greenland and Antarctica: A modeling sensitivity study, Journal of Geophysical Research-Atmospheres, 118, 4788-4800, 10.1002/jgrd.50428, 2013.

Thomason, L. W., Burton, S. P., Luo, B. P., and Peter, T.: SAGE II measurements of stratospheric aerosol properties at non-volcanic levels, Atmos. Chem. Phys., 8, 983-995, 10.5194/acp-8-983-2008, 2008.

Valcke, S.: The OASIS3 coupler: a European climate modelling community software, Geoscientific Model Development, 6, 373-388, 10.5194/gmd-6-373-2013, 2013.

Veres, D., Bazin, L., Landais, A., Kele, H. T. M., Lemieux-Dudon, B., Parrenin, F., Martinerie, P., Blayo, E., Blunier, T., Capron, E., Chappellaz, J., Rasmussen, S. O., Severi, M., Svensson, A., Vinther, B., and Wolff, E. W.: The Antarctic ice core chronology (AICC2012): an optimized multi-parameter and multi-site dating approach for the last 120 thousand years, Climate of the Past, 9, 1733-1748, 10.5194/cp-9-1733-2013, 2013.

Vinther, B. M., Clausen, H. B., Johnsen, S. J., Rasmussen, S. O., Andersen, K. K., Buchardt, S. L., Dahl-Jensen, D., Seierstad, I. K., Siggaard-Andersen, M. L., Steffensen, J. P., Svensson, A., Olsen, J., and Heinemeier, J.: A

synchronized dating of three Greenland ice cores throughout the Holocene, Journal of Geophysical Research-Atmospheres, 111, 10.1029/2005jd006921, 2006.

Vinther, B. M. , Clausen, H. B. , Kipfstuhl, S. , Fischer, h. , Bigler, M. , Oerter, H. , Wegner, A. , Wilhelms, F. , Severi, M. , Udisti, R. , Beer, J. , Steinhilber, F. , Muscheler, R. , Rasmussen, S. O. and Svensson, A. (2012): An annual layer counted EDML time scale covering the past 16700 years , EGU General Assembly 2012, Vienna, Austria, 23 April 2012 - 27 April 2012 .

Winckler, G. and Severinghaus, J.: Noble Gases in Ice Cores: Indicators of the Earth's Climate History, in, 33-53, 10.1007/978-3-642-28836-4_3, 2013.

Winski, D. A., Fudge, T. J., Ferris, D. G., Osterberg, E. C., Fegyveresi, J. M., Cole-Dai, J., Thundercloud, Z., Cox, T. S., Kreutz, K. J., Ortman, N., Buizert, C., Epifanio, J., Brook, E. J., Beaudette, R., Severinghaus, J., Sowers, T., Steig, E. J., Kahle, E. C., Jones, T. R., Morris, V., Aydin, M., Nicewonger, M. R., Casey, K. A., Alley, R. B., Waddington, E. D., Iverson, N. A., Dunbar, N. W., Bay, R. C., Souney, J. M., Sigl, M., and McConnell, J. R.: The SP19 chronology for the South Pole Ice Core – Part 1: volcanic matching and annual layer counting, Clim. Past, 15, 1793-1808, 10.5194/cp-15-1793-2019, 2019.

Wolff, E. W., Fischer, H., Fundel, F., Ruth, U., Twarloh, B., Littot, G. C., Mulvaney, R., Rothlisberger, R., de Angelis, M., Boutron, C. F., Hansson, M., Jonsell, U., Hutterli, M. A., Lambert, F., Kaufmann, P., Stauffer, B., Stocker, T. F., Steffensen, J. P., Bigler, M., Siggaard-Andersen, M. L., Udisti, R., Becagli, S., Castellano, E., Severi, M., Wagenbach, D., Barbante, C., Gabrielli, P., and Gaspari, V.: Southern Ocean sea-ice extent, productivity and iron flux over the past eight glacial cycles, Nature, 440, 491-496, 10.1038/nature04614, 2006.

Wolff, E. W., Chappellaz, J., Blunier, T., Rasmussen, S. O., and Svensson, A.: Millennial-scale variability during the last glacial: The ice core record, Quaternary Science Reviews, 29, 2828-2838, 10.1016/j.quascirev.2009.10.013, 2010.

Wolff, E. W., Burke, A., Crick, L., Doyle, E. A., Innes, H. M., Mahony, S. H., Rae, J. W. B., Severi, M., and Sparks, R. S. J.: Frequency of large volcanic eruptions over the past 200,000 years, Clim. Past Discuss., 2022, 1-21, 10.5194/cp-2022-69, 2022.

Zanchettin, D., Khodri, M., Timmreck, C., Toohey, M., Schmidt, A., Gerber, E. P., Hegerl, G., Robock, A., Pausata, F. S. R., Ball, W. T., Bauer, S. E., Bekki, S., Dhomse, S. S., LeGrande, A. N., Mann, G. W., Marshall, L., Mills, M., Marchand, M., Niemeier, U., Poulain, V., Rozanov, E., Rubino, A., Stenke, A., Tsigaridis, K., and Tummon, F.: The Model Intercomparison Project on the climatic response to Volcanic forcing (VolMIP): experimental design and forcing input data for CMIP6, Geoscientific Model Development, 9, 2701-2719, 10.5194/gmd-9-2701-2016, 2016.

Zdanowicz, C. M., Zielinski, G. A., and Germani, M. S.: Mount Mazama eruption: Calendrical age verified and atmospheric impact assessed, Geology, 27, 621–624, 1999.

Zielinski, G. A., Mayewski, P. A., Meeker, L. D., Whitlow, S., Twickler, M. S., Morrison, M., Meese, D. A., Gow, A. J., and Alley, R. B.: RECORD OF VOLCANISM SINCE 7000-BC FROM THE GISP2 GREENLAND ICE CORE AND IMPLICATIONS FOR THE VOLCANO-CLIMATE SYSTEM, Science, 264, 948-952, 10.1126/science.264.5161.948, 1994.

Zielinski, G. A.: Stratospheric Loading and Optical Depth Estimates of Explosive Volcanism over the Last 2100 Years Derived from the Greenland-Ice-Sheet-Project-2 Ice Core, J. Geophys. Res.-Atmos., 100, 20937–20955, 1995.

Zielinski, G. A., Mayewski, P. A., Meeker, L. D., Whitlow, S., and Twickler, M. S.: A 110,000-yr record of explosive volcanism from the GISP2 (Greenland) ice core, Quaternary Research, 45, 109-118, 10.1006/qres.1996.0013, 1996.

Zuo, M., Zhou, T., Man, W., Chen, X., Liu, J., Liu, F., and Gao, C.: Volcanoes and Climate: Sizing up the Impact of the Recent Hunga Tonga-Hunga Ha'apai Volcanic Eruption from a Historical Perspective, Advances in Atmospheric Sciences, 10.1007/s00376-022-2034-1, 2022.

Chapter 2

Chapter contents

Magnitude, frequency and climate forcing of global volcanism during the last glacial period as seen in Greenland and Antarctic ice cores (60-9 ka)

Jiamei Lin[1], Anders Svensson[1], Christine S. Hvidberg[1], Johannes Lohmann[1], Steffen Kristiansen[1], Dorthe Dahl-Jensen[1,5], Jørgen P. Steffensen[1], Sune O. Rasmussen[1], Eliza Cook[1], Helle Astrid Kjær[1], Bo M. Vinther[1], Hubertus Fischer[2], Thomas Stocker[2], Michael Sigl[2], Matthias Bigler[2], Mirko Severi[3], Rita Traversi[3], Robert Mulvaney[4]

[1]Physics of Ice, Climate and Earth, Niels Bohr Institute, University of Copenhagen, 2100, Denmark

[2]Climate and Environmental Physics, Physics Institute & Oeschger Center for Climate Change Research, University of Bern, Sidlerstrasse 5, Bern, Switzerland

[3]Department of Chemistry, University of Florence, Florence, Italy

[4]British Antarctic Survey, Cambridge, UK

[5]Centre for Earth Observation Science, University of Manitoba, Winnipeg, Manitoba, Canada R3T 2N2

Corresponding authors: Jiamei Lin (jm.lin@nbi.ku.dk), Anders Svensson (as@nbi.ku.dk)

Received: 28 Jul 2021 – Discussion started: 09 Aug 2021 – Revised: 03 Dec 2021 – Accepted: 04 Jan 2022 – Published: 15 Mar 2022

Abstract. Large volcanic eruptions occurring in the last glacial period can be detected by their accompanying sulfuric acid deposition in continuous ice cores. Here we employ continuous sulfate and sulfur records from three Greenland and three Antarctic ice cores to estimate the emission strength, the frequency and the climatic forcing of large volcanic eruptions that occurred during the second half of the last glacial period and the early Holocene, 60-9 ka years before AD 2000 (b2k). Over most of the investigated interval the ice cores are synchronized making it possible to distinguish large eruptions with a global sulfate distribution from eruptions detectable in one hemisphere only. Due to limited data resolution and large variability in the sulfate background signal, particularly in the Greenland glacial climate, we only list Greenland sulfate depositions larger than 20 kg km^{-2} and Antarctic sulfate depositions larger than 10 kg km^{-2}. With those restrictions, we identify 1113 volcanic eruptions in Greenland and 740 eruptions in Antarctica within the 51ka period - where the sulfate deposition of 85 eruptions is found at both poles (bipolar eruptions). Based on the ratio of Greenland and Antarctic sulfate deposition, we estimate the latitudinal band of the bipolar eruptions and assess their approximate climatic forcing based on established methods. Twenty-five of the identified bipolar eruptions are larger

than any volcanic eruption occurring in the last 2500 years and 69 eruptions are estimated to have larger sulfur emission strengths than the Tambora, Indonesia eruption (1815 AD). Throughout the investigated period, the frequency of volcanic eruptions is rather constant and comparable to that of recent times. During the deglacial period (16-9 ka b2k), however, there is a notable increase in the frequency of volcanic events recorded in Greenland and an obvious increase in the fraction of very large eruptions. For Antarctica, the deglacial period cannot be distinguished from other periods. This confirms the suggestion that the isostatic unloading of the Northern Hemisphere (NH) ice sheets may be related to the enhanced NH volcanic activity. Our ice-core based volcanic sulfate records provide the atmospheric sulfate burden and estimates of climate forcing for further research on climate impact and understanding the mechanism of the Earth system.

2.1 Introduction

The dispersal of gas, aerosols and ash particles by volcanic eruptions play a major role in the climate system (Gao et al., 2007; Robock, 2000). Large volcanic eruptions injecting sulfuric gases into the stratosphere and forming sulfate aerosols have a global or hemispheric cooling effect of several degrees lasting for several years after the eruption (Sigl et al., 2015; Sinnl et al., CPD, 2021).

Estimations of volcanic stratospheric sulfur injections and of the timing and frequency of large volcanic eruptions are essential for the ability to understand and model past and future global climate conditions (Timmreck et al., 2016). For the last 1200 to 2500 years, the ice-core based volcanic forcing records derived from Greenland and Antarctica (Crowley and Unterman, 2013; Gao et al., 2008; Toohey and Sigl, 2017) provide an essential forcing record for climate model simulations (Jungclaus et al., 2017), supporting detection and attribution studies (Schurer et al., 2014) including those applied in the IPCC. However, so far the global ice-core based volcanic record of the last glacial period is poorly documented.

2.1.1 Ice-core records of volcanic sulfate deposition

Several studies have reconstructed the volcanic sulfate deposition for part or all of the Holocene in Greenland (Cole-Dai et al., 2009; Gao et al., 2008; Sigl et al., 2013) or in Antarctica (Kurbatov et al., 2006; Castellano et al., 2004; Plummer et al., 2012; Nardin et al., 2020; Cole-Dai et al., 2021). Sigl et al. (2015) applied accurately dated ice cores synchronized between the two hemispheres to reconstruct global volcanism over the last 2500 years. This so-called bipolar

synchronization allows to distinguish large global eruptions from those of hemispheric or more regional impact. During the last 2500 years, they identified 50 global (bipolar) volcanic eruptions, 5 of which had a sulfur emission strength larger or similar to the Tambora eruption occurring in Indonesia in 1815 CE. Prior to the last glacial maximum no bipolar volcanic sulfate deposition record is currently available from ice cores.

One conclusion drawn from historical eruptions is that there is a significant variability of the same volcanic event in the sulfate deposition records derived from different ice cores both on a regional and a local scale (Sigl et al., 2014; Gao et al., 2007). Part of this regional variability can be explained by the difference in sulfate deposition fluxes at different locations. For example, in Antarctica where geographical distances are large, the sulfate deposition at a specific site will be strongly dependent on the location of the eruption, governing wind patterns, seasonality, etc. Another reason for the lateral sulfate deposition variability is the amount and patchiness of snowfall, which may locally enhance the sulfate deposition for high snowfall areas compared to low snowfall areas for a volcanic event. Moreover, there may be more absent sulfate deposition events caused by post depositional processes on the snow surface, such as wind erosion (Gautier et al., 2016). The spatial variability of sulfate deposition in Antarctica was studied at 19 sites covering the past 2000 years by Sigl et al. (2014), and here both accumulation and post-deposition effects were found to be important factors. In particular, on the East Antarctic plateau where snow-accumulation is very low, the sulfate deposition is lower than at more coastal and higher accumulation sites in Antarctica. The snow accumulation effect is also observed in Greenland (Gao et al., 2007), although the effect is much less pronounced here, because the accumulation rates are less variable in Central Greenland than in different parts of Antarctica. In order to reduce the accumulation bias, Gao et al. (2008) selected five large low-latitude volcanic events from 54 Arctic and Antarctic ice cores and calculated the mean ratio of deposition in individual ice cores; they then applied the deposition ratio between different cores to correct the sulfate deposition for all events in all cores to obtain the Arctic and Antarctic mean sulfate depositions. In general, it is clear that more robust volcanic deposition patterns can be obtained when larger sets of ice cores are included, preferably ice cores from high-accumulation sites should be applied (Gao et al., 2007; Sigl et al., 2014).

One complication related to the derivation of volcanic sulfate deposition in ice cores is the thinning of the ice layers with increasing depth and age. Due to glacier flow, the annual layers and thus the volcano-derived sulfate deposition becomes thinned with depth; an effect that is most pronounced at high-accumulation sites and close to bedrock. In central Greenland, typical

thinning rates of annual layers in the 60-10 ka range are 50-90% depending on age and local flow conditions (Johnsen et al., 2001). To calculate the sulfate deposition of a specific eruption from a measured ice concentration a correction for the thinning at the corresponding depth is needed to obtain the past accumulation rate at the time of snowfall. Thinning functions are obtained from ice flow modelling, and thus, there is a site-specific dependency on accurate flow modelling associated with the sulfate deposition determination.

2.1.2 Studies of the frequency of volcanic eruptions

The volcanic sulfate record of the Greenland GISP2 ice core has been investigated by Zielinski et al. (1997), who found that there has been increased volcanic activity during the deglacial period (22-8 ka b2k) as compared to the average activity of the last glacial cycle. This is interpreted as being related to the tectonic isostatic response to the melting of the large ice sheets during that period. Based on the global volcanic databases (Siebert and Simkin, 2002; Bryson et al., 2006), Huybers and Langmuir (2009) found that volcanism increased two to six times during the deglacial period, 12-7 ka b2k, as compared to the average level of eruptions during 40-0 ka b2k interval.

In Antarctica, Castellano et al. (2004) determined the frequency of volcanic eruptions over the last 45 ka based on the EDC ice core. They found a rather constant level of volcanic activity throughout that period except for the most recent millennia, where the activity shows an increase. Kurbatov et al. (2006) detected volcanic signals during the last 12 ka in the Siple Dome A ice core from West Antarctica. They found that the number of volcanic sulfate signals is decreasing with age, possibly related to the relatively low sampling resolution in the deeper part of that core. Recently, Cole-Dai et al. (2021) used the high-accumulation WAIS Divide ice core to determine a fairly constant Holocene eruption frequency with larger-than-Tambora (1815 AD) events occurring approximately once per millennium. Note, however, that all these reconstructions differ in their volcanic signal detection method, which may lead to different trends in peak frequencies.

2.1.3 Volcanic events identified in ice cores with tephra and sulfate peak synchronization

The ice-core volcanic source identification is important as it helps to constrain the magnitude – interpreted here as sulfur emission strength rather than the mass of material erupted (Pyle, 2015) – and the climate forcing of the eruption. Furthermore, it allows for a more detailed comparison to modelling studies. In historical times, the volcanic origin of an ice-core acidity spike may be corroborated by a precise dating of the ice core (Sigl et al., 2015). Further back in time, as the

uncertainty of both the ice-core dating and the identification of the erupting volcanoes increases, the origin of a volcanic ice-core layer can only be determined if it is associated with a volcanic ash (tephra) deposition in the ice (Gronvold et al., 1995). However, tephra layers are not always coinciding with sulfate peaks (Davies et al., 2010) and most volcanic sulfate signals have no tephra associated with them.

In the last glacial period, many Greenland tephra deposits have been associated with Icelandic eruptions while around a dozen of identified tephra layers originate in North America and Eastern Asia (Abbott and Davies, 2012; Bourne et al., 2015; Davies et al., 2014). In Antarctica, tephra layers have been identified and associated with eruptions occurring within Antarctica and in the Southern Hemisphere (Narcisi et al., 2005; Narcisi et al., 2010; Narcisi et al., 2012). Recently, Mcconnell et al. (2017) identified tephra from the long-lasting and halogen-rich Antarctic Mount Takahe eruption that occurred around 17.80 ka. Tephra of the Oruanui eruption from the Taupo volcano in present-day New Zealand has been identified and dated to 25.32 ka BP1950 in the West Antarctic Ice Sheet Divide ice core (WDC) (Dunbar et al., 2017).

Volcanic eruptions generally do not deposit tephra in both Greenland and Antarctica, so the bipolar synchronization of sulfur spikes in the ice cores is dependent on an alternative matching technique. Svensson et al. (2020) applied annual layer counting in both Greenland and Antarctic ice cores to match patterns of volcanic eruptions leading to the identification of some 80 bipolar eruptions in the 60-12 ka interval. For the Holocene, a bipolar synchronization of volcanic eruptions was released with the AICC2012 time scale (Veres et al., 2013). Using sulfur isotopes, it has recently become possible to test if sulfate has indeed reached the stratosphere, which is a prerequisite for being globally distributed, as the sulfate undergoes characteristic isotope fractionation in the stratosphere (Burke et al., 2019; Gautier et al., 2018; Crick et al., 2021; Baroni et al., 2008), but these analyses are still scarce for the last glacial period.

2.1.4 Extending the ice-core volcanic record into the last glacial period

Here we extend the ice-core record of sulfate deposition in Greenland and Antarctica by employing sulfate records from three Greenland and three Antarctic ice cores in the interval 60-9 ka (in one core we use elemental sulfur measurements, but for the sake of brevity we will refer to sulfate records). We investigate the sulfur emission strengths (i.e. defining the climate impact potential) and the frequency of volcanic eruptions detected in either Greenland or Antarctica. For eruptions identified in both hemispheres, we estimate the climate forcing using modern analogues and determine the occurrence of very large eruptions.

2.2 Methods

2.2.1 Ice-core records

For Greenland we used the North Greenland Eemian Ice Drilling ice core (NEEM) (Dahl-Jensen et al., 2013), the North Greenland Ice Core Project ice core (NGRIP2) (Andersen et al., 2004), and the Greenland Ice Sheet Project 2 ice core (GISP2) (Grootes et al., 1993), and in Antarctica the WDC ice core (WAIS Divide Project Members, 2013; 2015), the EPICA Dome C ice core (EDC) (EPICA community, 2004), and the EPICA Dronning Maud Land ice core (EDML) (EPICA community, 2006).

The sulfate records were obtained by different analytical methods and with different temporal resolution as detailed in the Table S1. For NGRIP the SO_4^{2-} concentration was obtained by a Continuous Flow Analysis system (CFA) (Bigler, Thesis, 2004; Röthlisberger et al., 2000). For WDC, sulfur was measured by ICP-MS coupled to a CFA system (Sigl et al., 2016). For EDC and EDML, SO_4^{2-} was measured by Fast Ion Chromatography (FIC) coupled to a CFA system (Severi et al., 2015). For GISP2 and for a second NGRIP profile, SO_4^{2-} was obtained from discrete samples by Ion Chromatography (IC) (Clausen et al., 1997; Mayewski et al., 1993; Siggaard-Andersen, PhD thesis, 2004). The temporal resolution of the sulfate records decreases with ice-core depth and ranges from sub-annual for the CFA profiles to decadal for the lower-resolution discrete profiles (Table S1 and Fig. S2). The high-resolution NGRIP and WDC records have been resampled to annual resolution, which we see as an upper limit for the effective resolution during the oldest part of the analysis in last glacial. As discussed in section 3.4, we are also resampling these records to lower resolution in order to obtain comparable resolution throughout the investigated period and in order to investigate eruption occurrences among stadial and interstadial periods. Minor data gaps were interpolated using linear interpolation and larger gaps are indicated as missing data. Sulfur and sulfate records were corrected for the sea-salt-sulfur contribution based on sodium concentrations as sea salt tracer by assuming 0.084 for the ratio of Na/S (Bowen et al., 1979), except for EDC. In all cases, the sea-salt correction is less than 15% of the measured sulfate background signal, giving a slight change to the non-sea-salt-sulfur. In a previous study of WDC for the Holocene period, methanesulfonic acid (MSA) was used to make a minor correction of the Antarctic sulfur signal (Cole-Dai et al., 2021). As there are no continuous MSA records available for WDC over the investigated period, we do not make this correction here.

For the 12-9 ka interval, the Greenland sulfate deposition is based on the NGRIP and GISP2 records only, as the NEEM dataset is not available. Apart from using the sulfate records, the depth assignment of the volcanic peaks was occasionally assisted by application of other high-resolution records that also are indicators of volcanic sulfate deposition. Those include the Electrical Conductivity Measurement (ECM) profile, the Di-Electric Profiling (DEP) and the liquid conductivity records, that are also available for most of the applied cores (Table S1 for a complete list of records and references).

2.2.2 Background signal determination and volcanic peak detection

To determine the biogenic sulfate background level of the ice-core sulfate records and detect volcanic peaks above this background, we apply robust peak detection methods similar to those applied for Holocene records (Fischer et al., 1998; Karlof et al., 2005; Gao et al., 2007; Sigl et al., 2013), which allow for a change with sulfate background variability over time. A running median filter with a width of 50-180 years was applied to estimate the non-volcanic background signal. Due to the different depth resolution of the individual records, and because of the highly variable and abruptly changing background levels of the Greenland sulfate levels across DO-events, it has been necessary to apply different filter widths for different records (Fig. S2.1 (a-y) and Table S1). A second iteration of a reduced running median (RRM) filter using the same filter widths was applied after removal of the spikes identified in the first iteration. For the coarse-resolution NGRIP IC sulfate record, a continuous background determination was not possible and the background has been estimated manually for selected events only.

For all records, a volcanic detection threshold was estimated as RRM plus three times the running median of absolute deviations from the RRM (RMAD) using the same window widths as for the background determination (Fig. S2.1 (a-y)). In Greenland, the RMAD value varies strongly across DO-events due to the much greater background variability during stadial periods as compared to interstadials (Table S2). This implies that the volcanic spikes may not be detected for the time windows covering the fast transitions from stadials and interstadials (lasting on the order of decades to up to about 150 years, Capron et al. (2021)) when the background variability changes in a short time. Thus, the volcano frequency found in these short intervals may be impacted, but the volcanic frequency outside of these short intervals is not affected. The duration of a volcanic event is estimated from the depth interval of the sulfate spike that is above the RRM and the sulfate deposition associated with the event is calculated by integrating the

sulfate concentrations above the RRM across the duration of the event. The volcanic sulfate peak area S in kg km^{-2} is calculated as follows:

$$S = \int_{D1}^{D2} (y - RRM)dy * 0.917 \quad (1)$$

where y is the nss-sulfate concentration in units of ppb, 0.917 is the ice-water density in g cm^{-3}, and the sulfate layer in the ice core is constrained between the depths D1 and D2 in m ice equivalent. At shallow depth, the temporal duration of the sulfate deposition can be determined precisely, but in the last glacial period peak broadening by diffusion is hampering such a determination, that is not considered in this work.

2.2.3 Correction for ice flow / layer thinning

As the volcanic layer is buried in the ice sheet, the layer is being thinned by ice flow. In order to calculate the amount of sulfate deposited on the ice sheet at the time of the eruption a correction for the thinning of the volcanic layer in the ice must be applied.

$$SF = \frac{S}{T} \quad (2)$$

Here SF is the accumulated sulfate flux in kg km^{-2} and T is the layer thinning (the ratio between the layer thickness in the ice core and the original layer thickness). The layer thinning has been calculated by site-specific ice-flow models (thinning function) that we applied here (Table S1 and Fig. S2.2 (c)). During the last glacial period, the layer thinning can be significant. For the Greenland cores, the thinning rate ranges from a 60% reduction of the original layer thickness (T=0.4) at 12 ka b2k to as much as 90% (T=0.1) at 60 ka b2k (Table S1). For Antarctica, the thinning rate is most significant for the high-accumulation WDC core, where it approaches 95% (T=0.05) at 60 ka b2k (Fudge et al., 2016; Buizert et al., 2015), whereas the EDC core exhibits a modest thinning of 30% (T=0.7) at 60 ka b2k (Fig. S2.2 (c)). For the WDC core, we apply the thinning function of Fudge et al. (2016) for the upper 2800 m, whereas below 2800m we apply a simple linear fit to the gas-based thinning function (Buizert et al., 2015) that has large and possibly unrealistic wiggles (Fig. S2.2 (c)). As the volcanic sulfate deposition scales with the amount of thinning, an inaccurate thinning factor has large implications for the calculated sulfate depositions.

For high snow accumulation sites, such as those in Greenland and coastal Antarctica, it is quite likely that wet deposition is dominating the sulfate deposition at present day (Kreutz et al., 2000; Schupbach et al., 2018). During the last glacial period, dry deposition may have played a

more important role, giving rise to a potential bias of our glacial sulfate deposition estimates. We do not attempt to make any corrections for this effect.

2.2.4 Correction of volcanic signals for low resolution data

As the depth resolution of the sulfate records for the GISP2 and NEEM cores is relatively low (Fig. S2.2 (a)), adjacent acidity peaks may be merged into falsely large acidity spikes. We made a manual correction for this effect by comparing to the corresponding higher-resolution ECM and DEP recordsFi (depth resolution of 1 cm or higher) of the same core and removed or split falsely large peaks according to the associated ECM or DEP peaks. The specific correction for volcanic signals is indicated in Table S3.

2.2.5 Volcanic sulfate deposition records

We generate three lists of volcanic sulfate deposition for the 60-9 ka period: one for eruptions identified in the Greenland ice cores (Table S3), one for eruptions identified in the Antarctic ice cores (Table S4), and one for global (bipolar) eruptions identified in both Greenland and Antarctica (Table S5). The bipolar list contains the large global eruptions identified by Svensson et al. (2020) and also two large bipolar eruptions found in Veres et al. (2013) for the 12-9 ka period. Furthermore, two additional bipolar eruptions at 44.75 ka b2k and 44.76 ka b2k have been included, applying the same methods as described in Svensson et al. (2020). For the bipolar list, no bipolar eruptions were unambiguously identified in the 24.5-16.5 ka period, not because they may not have existed but because ice core synchronization is very difficult in this period. Therefore, the list covers only an effective period of 43 ka. The list of NH volcanism contains only volcanic deposits larger than 20 kg km^{-2} in any of the applied Greenland ice cores, and the list containing the Southern Hemisphere includes all deposition events larger than 10 kg km^{-2} for the Antarctic ice cores, which biases our list to larger eruptions. This cut-off is necessary because of the highly variable sulfate background in the Greenland cold periods of the last glacial predominantly associated with mineral dust (e.g. gypsum (Svensson et al., 2000)) (Table S2). A sulfate deposition of 20 kg km^{-2} corresponds to half the Greenland deposition from the 1815 AD Tambora eruption (Sigl et al., 2015), thus only quite large events in terms of total sulfur injections into the atmosphere are detected in this work. If the cut-off is set at a lower value, a large number of presumably non-volcanic spikes will be identified in stadial periods. A similar cut-off applied to the sulfate deposition record of the last 2000 years (Sigl et al., 2013) reduces the number of identified eruptions in Greenland from 138 to 49 events. Likewise, for Antarctica,

we are only identifying events that are referred to as 'large' or 'very large' by Cole-Dai et al. (2021).

When eruptions are detected in several ice cores in Greenland or Antarctica, we provide the sulfate deposition value for each core, the range spanned by all the cores, and the calculated average sulfate deposition value. The average Greenland sulfate deposition is calculated by the simple mean of the three cores due to their similar sulfate-deposition levels and proximity of the ice coring sites (Fig. S2.3). In Antarctica, however, the ice-core sites are far apart and the EDC core generally has the lowest sulfate deposition due to low snow accumulation or a reduced amount of sulfate reaching the remote EDC ice-coring site. Therefore, when there is only a sulfate signal present in one or two cores, the average sulfate deposition of Antarctica is calculated with a rescaling factor, similar to the method applied by Gao et al. (2008). The scaling factor is based on the relative ratio of sulfate deposition from the 30 largest eruptions (in terms of the sulfate deposition) in the three cores in the period of 60-9 ka. For the 30 largest eruptions identified in Antarctica, the ratio of the sulfate deposition among the three Antarctic cores is EDC:EDML:WDC =0.72:0.87:1.4 (Fig. S2.3).

The volcanic sulfate deposition uncertainty estimate is obtainted from the error propagation in formula (1) and (2). For NGRIP, NEEM, GISP2 and WDC, we apply an estimated 21% uncertainty of the sulfate concentration levels independent of the analytical method (Fig. S2.3 (e)), an estimated 10% uncertainty of the applied thinning functions, and a 15% uncertainty related to the varying temporal resolution of the sulfate records. This leads to an error estimate of up to 26% for individual deposition events that we apply as error estimate for all the derived sulfate depositions. For EDC and EDML, the low accumulation leads to an additional large local variability in sulfate deposition of up to 29% (Gautier et al., 2016), so for those cores we arrive at a combined error estimate of 40% for individual deposition events. When there are sulfate signals from three ice cores in one hemisphere, we used the standard deviation of the rescaled volcanic sulfate depositions for all ice cores to estimate the uncertainty for the average area volcanic sulfate deposition. When there is a common signal in fewer than three cores, we use the maximum uncertainty of the volcanic sulfate deposition from the individual cores.

2.2.6 Latitudinal band assignment of bipolar volcanic eruptions

The volcanic sulfate deposition in Greenland and Antarctica shows a distribution pattern related to the latitudinal band of the eruption site (Fig. 2.1) (Marshall et al., 2019). To estimate the latitudinal band of bipolar volcanic eruptions of unknown origin, we applied the Support Vector

Machine (SVM) classification model of Hastie et al. (2009) and Vapnik (1998) that is based on a kernel function generation and logistic regression. The model was trained using 4 eruptions from the last glacial period and 17 eruptions from the last two millennia for which the eruption site is known from the deposit tephra in the ice (Fig. 2.1(b) and Table S6). The input values of each eruption for the model on the training set are the average Greenland sulfate deposition, the average Antarctic sulfate deposition and the latitudinal band of the eruption site (above 40°N, 40°N-40°S, or below 40°S). The cross-validation is performed on the training set consisting of 10% of the total training eruptions selected at random. Then, this trained model is applied to give a best estimate of the latitudinal band of the bipolar eruptions for which the eruption site is unknown. The model output parameters - kernel scale, box constraints and Bayesian optimization - show that the model has good performance (Fig. S2.4). Due to the low number of known volcanoes erupted in the high latitudes of the Southern Hemisphere, the method does not allow unambiguous identification of eruptions potentially located in this region. The bipolar eruptions of unknown origin are thus predicted into two latitudinal bands – above 40°N (NHHL) and below 40°N (LL or SH) (Table S5). The latitudinal band assignment for the four bipolar eruptions at the onset of the Younger Drays period (Table S5) is similar to that expected from comparing the relative sulfate deposition in Greenland and Antarctica (Abbott et al., 2021). A weakness of the method is that the training set mostly consists of volcanic eruptions for which the sulfate deposition is much smaller than that of the large eruptions occurring during the last glacial period. Details of the SVM method are provided in Hastie et al. (2009), page 17.

2.3 Results

2.3.1 The Greenland volcanic sulfate deposition record (60-9 ka)

The sulfate deposition records derived from the NGRIP, NEEM and GISP2 ice cores are displayed in Fig. 2.2 and Fig. S2.1 (a-y). The background level of the sulfate signal in the Greenland cores is in the range of 50-200 ppb with both the absolute level and the signal variability being much higher in stadial periods than in interstadial periods (Table S2). At the abrupt climate transitions during the last glacial period the sulfate background changes abruptly, making it difficult to determine the background level and volcanic detection limits (see Section 2.2). The higher background level and variability during the stadial periods is partly due to the lower snow accumulation during these periods.

Using a 20 kg km^{-2} deposition threshold, 1113 volcanic events are identified in Greenland in total (Table S3). Table S7 shows the number of volcanoes detected from one, two or three Greenland ice cores, respectively. NGRIP has the highest event detection rate because of its superior depth resolution. Depth resolution becomes increasingly critical in the cold climate of the investigated period where annual layers get down to a few centimeters of layer thickness (Fig. S2.2 (d)).

The difference in sulfate deposition among the cores reflects to some degree the spatial variability in sulfate deposition within Greenland, but is also strongly influenced by the sulfate analytical measurement technique (IC, FIC, CFA), the data resolution, the thinning correction made for each site, and possibly the accumulation rates. A comparison of the sulfate deposition between NGRIP, NEEM and GISP2 for the 30 largest volcanoes with identified signals in Antarctica ice cores shows that there is a very large spread in the signal from event to event (Fig. S2.3 (a-d)). Due to the large variability of sulfate deposition values among the cores, we provide the full range of sulfate deposition values spanned by the cores as well as the average sulfate deposition value, when an eruption is identified in several ice cores.

Fig. S2.3 (e) shows a comparison between the 57 largest volcanic events identified in the NGRIP ice core, as derived from the high-resolution CFA SO_4^{2-} record and from the lower resolution IC SO_4^{2-} record, respectively (Table S5). This comparison illustrates the differences in calculated sulfate depositions due to the analytic method and record resolution only, as the sulfate deposition and the thinning factor uncertainties are eliminated. It is obvious from the comparison that the derived sulfate deposition of a single event in a single core should not be taken at face value; there are very large uncertainties in addition to the variability caused by the spatial distribution pattern. Still, being the first systematic compilation of large volcanic eruptions from the last glacial period, the estimated depositions provide a good estimate of the order of sulfur emission strength and the frequency of large volcanic eruptions in Greenland. Out of the 1113 volcanic events identified in Greenland we identify 10 very large events with sulfate deposition estimated to be larger than 300 kg km^{-2} – where 9 have an Antarctic counterpart indicating their global impact. We identify 87 volcanic events with sulfate deposition larger than 135 kg km^{-2}, thereby exceeding the Icelandic Laki eruption occurring in 1783 CE, which produced the largest Greenland sulfate deposition in the last 2500 years (Sigl et al., 2015). The largest sulfate deposition in Greenland is by far the North Atlantic Ash Zone (NAAZ II) event occurring at 55.38 ka b2k (Rutledal et al., 2020; Austin et al., 2004). The sulfate deposition of this event is in the range of 866-1436 kg km^{-2}, which is more than a factor of two higher than any

other event occurring in the investigated period. The second largest event is an unknown eruption occurring at 45.55 ka b2k with a sulfate deposition in the range 200-849 kg km^{-2}. Those and other large events will be discussed in more details in section 4.4.

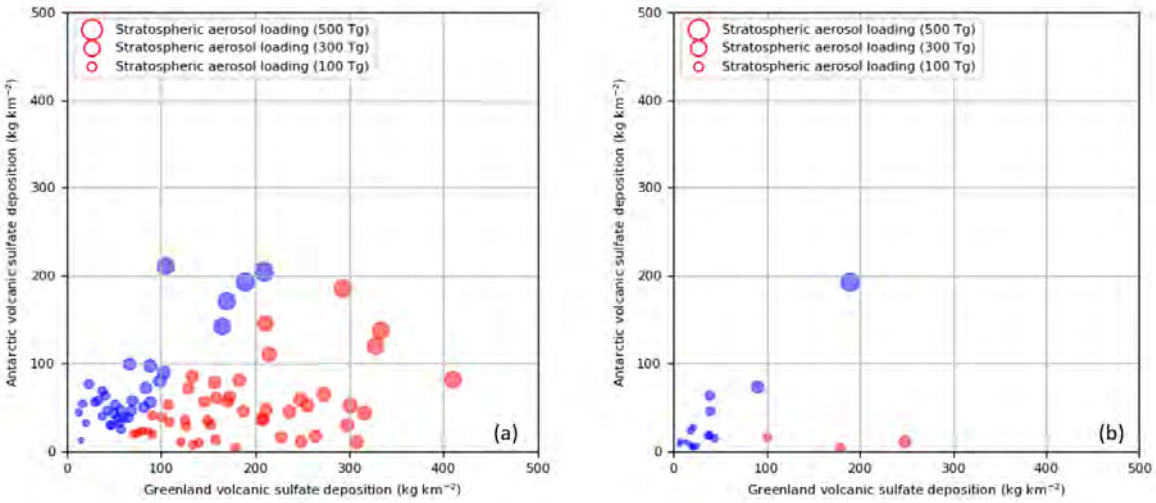

Figure 2.1. Relationship between Greenland and Antarctic volcanic sulfate deposition for the large bipolar volcanic eruptions. The size of the circle relates to the stratospheric sulfate aerosol loading. (a) Volcanoes in the last glacial period are classified by a Support Vector Machine (SVM) model with latitudinal bands: above 40°N in red circles, below 40°N in blue circles. (b) Volcanoes of the last 2500 years for which the eruption site is known (listed in Table S6) are classified with the latitudinal bands as for (a).

2.3.2 The Antarctic volcanic sulfate deposition record (60-9 ka)

The volcanic sulfate deposition extracted from the EDML, EDC and WDC ice cores are shown in Fig. 2.2 and Fig. S2.1 (a-y). The sulfate background level in Antarctica is comparable to that of Greenland (Table S2), but there is much less signal variability and an absence of abrupt shifts associated with Greenland DO transitions, making volcanic signal detection more robust. In total, 740 (350) volcanic sulfate deposition values estimated to be larger than 10 (20) kg km^{-2} are identified in the Antarctic ice cores (Table S4 and Table S7). WDC has the highest accumulation of the three records, but as the deepest part of the applied WDC record is close to bedrock, layer thinning becomes very significant here (Fudge et al., 2016), making the loss of measured ice-core temporal resolution (Table S1). Therefore, in the deepest section of the WDC core, fewer eruptions are detected as compared to EDML and EDC, and the derived WDC sulfate deposition has a very strong dependency on the applied thinning function. EDC has the lowest accumulation of the three and also the lowest temporal resolution of the sulfate record. Therefore, smaller

events are generally not detected in the EDC core, and the low accumulation contributes to some eruptions being partly or entirely absent from the record (Gautier et al., 2016).

The volcanic deposition of the 30 largest events in Antarctica are compared among the cores in Fig. S2.3. In general, there are large differences among the sulfate deposition in the different cores for the same events, primarily owing to the large gradient of accumulation rates and spatially different transport pathways over Antarctica (Sigl et al., 2014). The influence of different analytical techniques (FIC or CFA-ICP-MS) and the temporal resolution of the records may also accounts for some of the variability, as well as post-depositional processes (Gautier et al., 2018).

In the 60-9 ka period, there are 31 large volcanic events with a sulfate deposition larger than 78.2 kg km^{-2}, which is the largest volcanic deposition in Antarctica over the most recent 2500 years (Sigl et al., 2015). Forty-eight volcanic events have a sulfate deposition larger than 64 kg km^{-2} corresponding to the Antarctic sulfate deposition of the Kuwae 1458 CE eruption (Sigl et al., 2015). Among the 50 largest eruptions, 28 are also identified in Greenland ice cores. The largest volcanic signal detected in Antarctica is occurring at around 46.69 ka b2k with a sulfate deposition of 121.0-369.4 kg km^{-2}.

2.3.3 The bipolar volcanic sulfate deposition record (60-9 ka)

For the 60-9 ka period, the 85 bipolar volcanic eruptions that have been identified in both Greenland and Antarctic ice cores (Veres et al., 2013; Svensson et al., 2020) are listed separately in Table S5. We note that no bipolar eruptions have been identified in the interval 24.5-16.5 ka, because of the general difficulty to synchronize ice cores in this period (Seierstad et al., 2014). Twenty-eight out of the 85 bipolar eruptions have been identified in all six ice cores. Two of the bipolar volcanic eruptions are known from Greenland ice-core tephra deposits to be of Icelandic origin: The Vedde ash eruption (12.17 ka b2k) (Mortensen et al., 2005) and the NAAZ II eruption (55.38 ka b2k) (Rutledal et al., 2020). Furthermore, there are tephra deposits in Greenland from the Japanese Towada-H eruption (ca 15.68 ka b2k) (Bourne et al., 2016). In Antarctica there is tephra deposited from the New Zealand Oruanui, Taupo, eruption (ca 25.32 ka BP1950) (Dunbar et al., 2017) (Table S6). For the bipolar eruptions the volcanic forcing can be estimated using methods previously applied to Holocene eruptions (see section 4.3).

2.3.4. Relationship between data resolution and the volcanic eruption record of the last glacial (60-9 ka)

To investigate the frequency of different size categories of volcanic eruptions over time, we need to consider the sample resolution of the underlying sulfate records (Fig. S2.2 (a+b)). As we go back in time, the layer thinning becomes stronger which makes it increasingly difficult to detect smaller eruptions signals. Depending on the ice-core sample resolution, the apparent number of smaller eruptions decreases relatively faster with increasing age (or depth) than the larger eruptions, as the former will no longer exceed the detection threshold determined by the background signal due to smoothing of the records (Fig. S2.5). The effect is seen when the frequency of detected eruptions is separated into fractions of sulfate deposition sizes. We separated the eruptions according to the 0.7 and 0.9 quantiles of the volcanic sulfate deposition distribution, which for Greenland are 68 kg km^{-2} and 140 kg km^{-2} and for Antarctica are 25 kg km^{-2} and 50 kg km^{-2}. When considering the frequency of volcanic eruptions across the investigated period, we should preferably have the same or at least a comparable temporal sulfate sample resolution throughout the period in order to minimize this age (or depth) bias.
For Greenland, only the NGRIP sulfate record has high (sub-annual) resolution for most of the investigated interval (Fig. S2.2 (b)). Therefore, the number of eruptions detected in different periods will depend strongly on the NGRIP sample resolution. The NGRIP sulfate has an effective resolution of 8-20 mm due to smoothing of the record in the ice and – most importantly – by signal dispersion during the measurement. Using an approach similar to that of Rasmussen et al. (2005), we performed a spectral analysis of the NGRIP sulfate record to determine a signal cut-off of around 2 cm, which is comparable to that of other components analyzed with the same setup (Bigler et al., 2011) (Fig. S2.6). Two cm corresponds to about 2 annual layers in NGRIP in the climatically coldest and oldest sections of the investigated interval. In Table S8 and Fig. S2.5 we investigate the effect of increased smoothing of the NGRIP sulfate record for the detection of sulfate spikes. As expected the number of detected eruptions decreases with increased smoothing, however, with 3 years smoothing, the number of larger sulfate spikes starts to increase as adjacent sulfate peaks are being merged.

As a compromise between compensating for the decreasing resolution of the record with depth and at the same time avoiding a strong influence of the peak merging effect, we smoothed the NGRIP sulfate record to 2-year resolution for the eruption frequency analysis, knowing that this is eliminating a fraction of the smaller eruptions in the younger section of the record. With

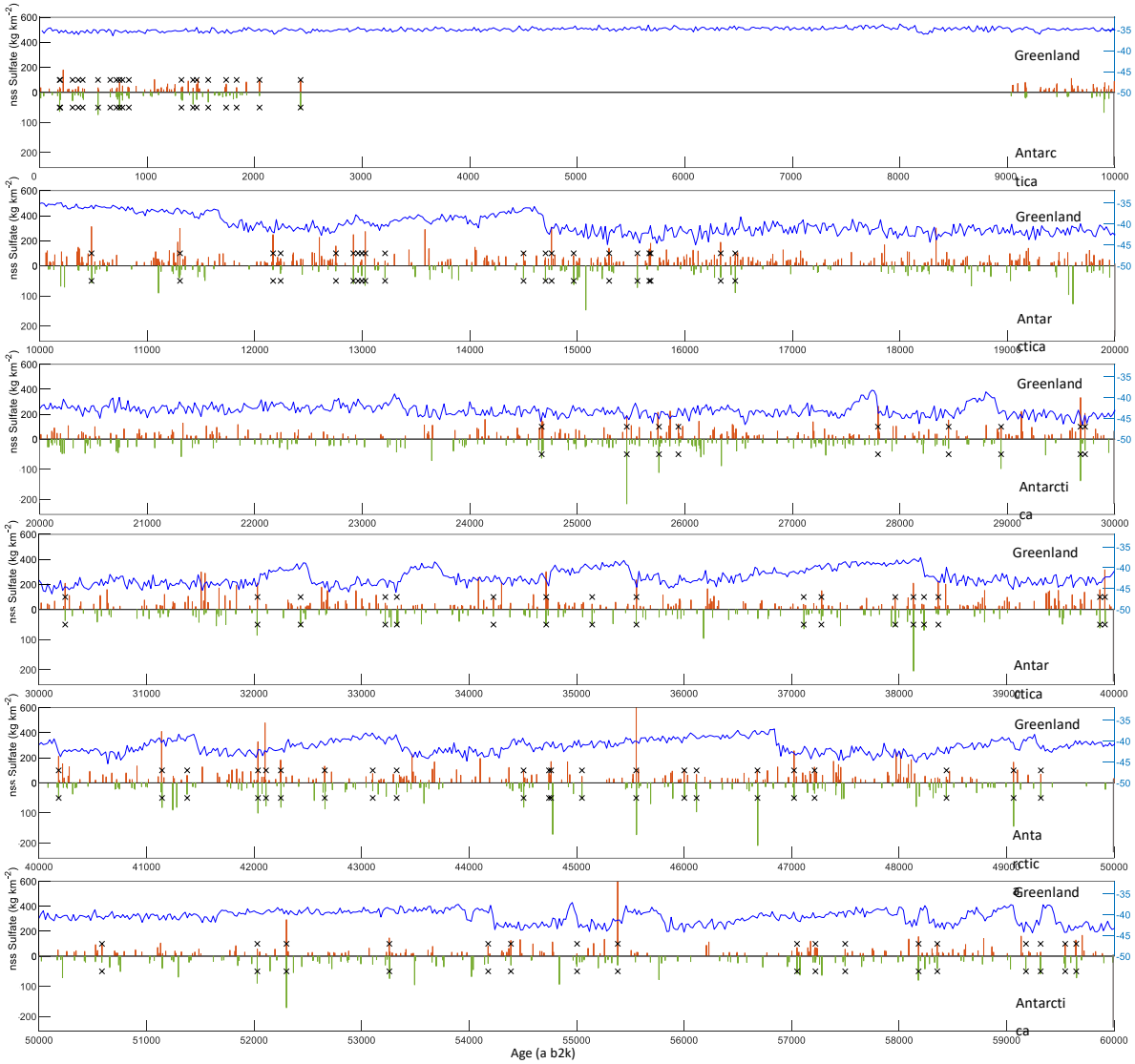

Figure 2.2. The average volcanic sulfate deposition in Greenland and Antarctica (60-9 ka; 2.5-0 ka adapted from Sigl et al., 2013, 2015). The blue curve shows $\delta^{18}O$ of the NGRIP core. Greenland volcanic sulfate depositions larger than 20 kg km^{-2} (cyan bars) and Antarctic volcanic sulfate deposition larger than 10 kg km^{-2} (black bars) are shown. Bipolar volcanic eruptions are indicated with an 'x'.

the 2-year smoothing there is probably still a bias towards a higher detection rate in the stadial periods due to the high signal variability of the sulfate record in those periods (see discussion in section 4.1). The GISP2 sulfate record has lower than 10-year resolution in the 60-14 ka period (Fig. S2.2), so in this period we can only use the GISP2 sulfate record to estimate the sulfate deposition of the larger eruptions. The NEEM sulfate record has a constant resolution of 10 years and we use this record throughout the investigated period. In Fig. 2.3 we show the records of

detected Greenland eruptions per millennium with the sulfate deposition grouped into three size fractions.

For Antarctica, EDML and EDC have fairly constant thinning rates for the 60-9 ka period (Fig. S2.2 (c)), whereas WDC has very strong thinning in the oldest part of the period, due to the high accumulation rate (Fig. S2.2 (c)). Spectral analysis of the Antarctic sulfate records shows the effective resolution (Table S1) and the signal cut-off is around 2 cm, 3 cm, and 1 cm for EDML, EDC and WDC, respectively (Fig. S2.6). In order to have comparable resolution throughout the investigated period, we smoothed the entire WDC sulfate record to 2-year resolution to homogenize the record resolution across the investigated period. For EDML the corresponding effective signal resolution is 1-2 year for the entire period, so we keep the original

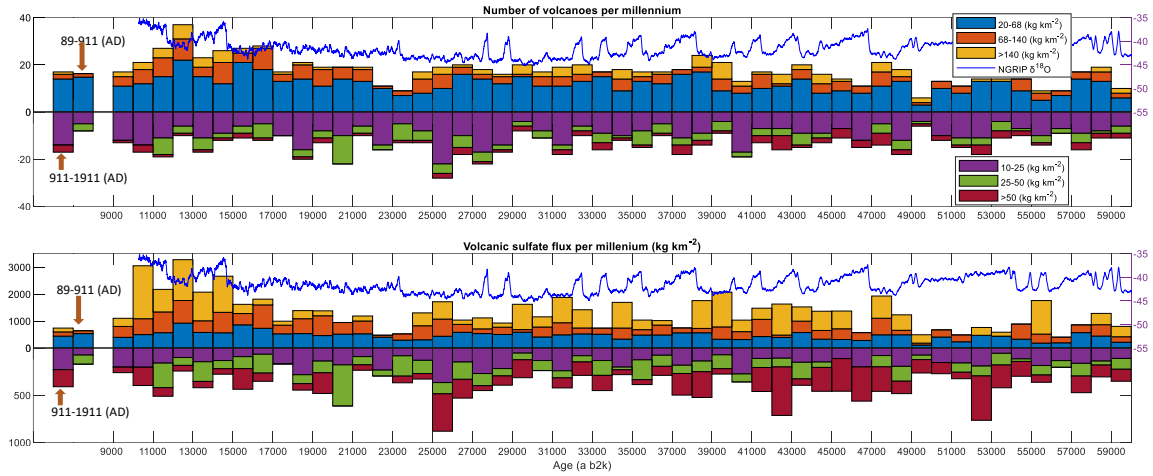

Figure 2.3. Number (top) and volcanic sulfate deposition (bottom) of volcanoes per millennium detected in Greenland and Antarctic ice-core sulfate records with relatively similar data resolution for the last 2500 years and the late glacial period. Positive values represent Greenland volcanoes and negative values represent Antarctic volcanoes. The volcanic eruptions are grouped into three size fractions based on the 0.7 and 0.9 quantiles of the volcanic sulfate deposition distribution. For Greenland the classes are separated at 68 kg km^{-2} and 140 kg km^{-2} and for Antarctica the separation is made at 25 kg km^{-2} and 50 kg km^{-2}. The magnitude of volcanoes is represented by the average volcanic sulfate deposition in Greenland or in Antarctica. The records used for the figure as follows: For the last 2000 years (911-1911 AD and 89-911 AD), the volcanic sulfate deposition is based on the NEEM S1 and NGRIP cores for Greenland and on the WDC core for Antarctica (Sigl et al. 2013) using smoothed 2-year resolution sulfate records. For the period 60-9 ka the Greenland sulfate deposition is derived from NEEM, GISP2 and NGRIP. For GISP2, the data was smoothed to 5 years in the period of 14-9 ka and for the period older than 14 ka only large volcanic sulfate signals are detected. The NGRIP sulfate record has been smoothed to 2-year resolution throughout. For the period 60-9 ka the Antarctic sulfate deposition is derived from EDML, EDC and WDC sulfate records. The WDC sulfate record has been smoothed to 2-year resolution.

resolution of the EDML sulfate record for the entire period. The EDC sulfate record has almost constant resolution, so we apply this record throughout the investigated period. The result of the frequency analysis is discussed in section 4.1.

2.4 Discussion

In the following we investigate possible climate-volcano links on different time scales, estimate the last glacial volcanic forcing, and compare the glacial volcanic record to that of the last 2500 years. Many studies have discussed a possible impact of climate on the frequency and magnitude of volcanic eruptions (Cooper et al., 2018). In particular, the melting of the large ice sheets at the end of the last glacial period and the corresponding sea-level rise are thought to have created crustal stress imbalances and increased the volcanic eruption frequency in that period (Watt et al., 2013; Huybers and Langmuir, 2009; Zielinski et al., 1996; Zielinski et al., 1997).

2.4.1 Millennium scale volcanic eruption variability

We investigate the variability in eruption frequency and sulfur emission strength with the DO cycles by separating the detected volcanic eruptions according to climate of 'cold' and 'milder' periods, applying the onset and termination of DO events defined by Rasmussen et al. (2014). 'Cold' periods constitute the stadial periods from 21 ka b2k to 60 ka b2k, covering a total of 21.8 ka. 'Mild' periods are the remaining periods that include all of the interstadial periods from 21 ka b2k to 60 ka b2k, adding up to 17.2 ka years. We grouped the detected eruptions according to the size of deposited sulfate and also investigated the effect of smoothing the NGRIP sulfate record to 1, 2, 3, and 5 years resolution (Fig. S2.7). For Antarctica, the number of detected eruptions (per millennium) is very similar for stadial and interstadial periods, independent of deposition size categories and record smoothing (Fig. 2.4). For Greenland, however, the number of volcanic eruptions is higher in stadial periods than in interstadial periods (Fig. 2.4), in the smaller deposition category (20-68 kg km^{-2}) this effect decreases with increasing NGRIP sulfate record smoothing (Fig. S2.7).

This observed difference leaves us two options: either there is a true millennium-scale volcanic eruption variability related to northern hemispheric climate variability during the last glacial period, or the dependency is an artefact caused by the very different properties of the Greenland sulfate record in stadial and interstadial periods. In Greenland, the variability of the sulfate background level is high in cold periods, stadials and the LGM, and low in milder periods such as interstadials (see section 3.1). We try to take this difference into account by employing

the variability-dependent RMAD to determine the eruption detection limit, but because of the very different character of the sulfate profiles in cold and milder periods there is still the possibility of having a climate related detection bias of sulfate spikes that is unrelated to the

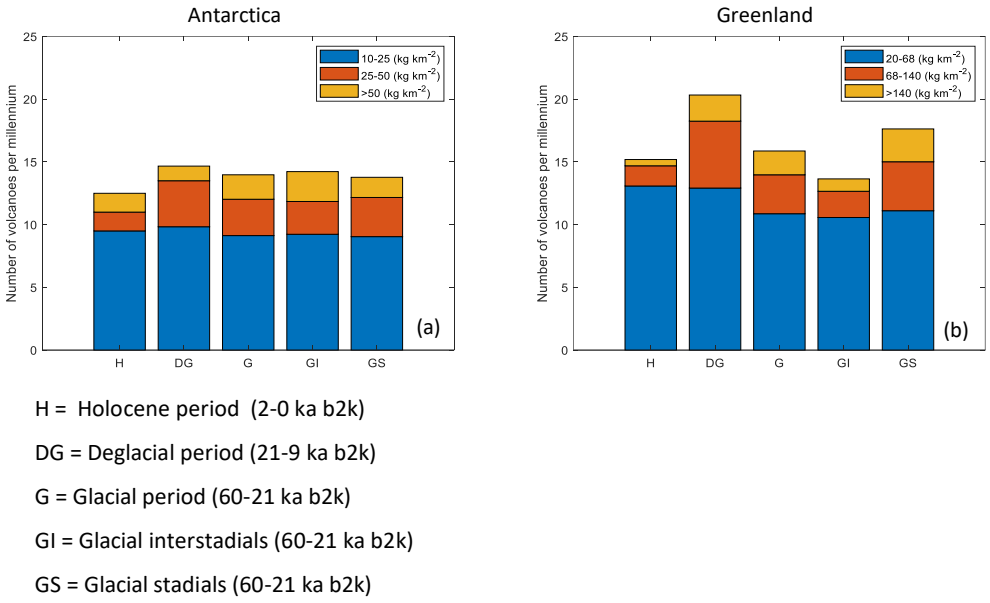

Figure 2.4. Comparison of the number of volcanic eruptions per millennium detected in Greenland and Antarctic ice cores grouped for different climatic periods with relatively similar data resolution for the last 2500 years and the late glacial period. The applied datasets and smoothing are the same as used for Fig. 2.3. The detected eruptions are classified into three size fractions similar to the approach of Fig. 2.3.

actual volcanic eruption record. For example, in cold periods, it could be that strong seasonal sulfate spikes associated with marine or terrestrial (non-volcanic) sulfate production could be detected as smaller volcanic eruptions. For recent times, Gao et al. (2007) has demonstrated that the volcanic sulfate deposition to some degree is accumulation dependent, with increased accumulation leading to higher sulfate deposition. Since, however, the highest accumulation occurs in the interstadial periods, this effect would lead to relatively higher sulfate deposition in interstadial periods, which is the opposite of what is observed.

We investigated the effect of a possible seasonal sulfate contributions of non-volcanic origin by a smoothing exercise where successively increased smoothing of the NGRIP sulfate record increasingly eliminates the detection of smaller short-lived (seasonal) sulfate spikes. Fig. S2.5, Fig. S2.7 and Table S8 show the number of sulfate spikes detected in stadial and interstadial periods as a function of the degree of smoothing. It is seen that for cold periods, the number of detected small and short-lived sulfate spikes decreases significantly with increased smoothing,

whereas the effect is almost absent for milder periods. This suggests that the higher number of detected sulfate spikes in cold periods is mainly due to spikes of periodic duration of sulfate background which we believe are less likely to be of volcanic origin. For volcanic eruptions that are large enough to inject sulfate into the stratosphere modern observations show that the sulfate fallout typically will last several years. We thus conclude that the apparent increased volcanism detected in cold periods is most likely an artefact caused by non-volcanic seasonal contributions from high-sulfate marine or terrestrial sources. It could for example be contributions from gypsum that is known to have high deposition fluxes in Greenland during stadial periods (Legrand and Mayewski, 1997). Indeed, for bipolar events we do observe a higher correlation in stadial periods than in interstadial periods between the volcanic sulfate deposition and both insoluble dust concentration and sodium concentration (Fig. S2.10). We cannot exclude, however, that other mechanisms such as different atmospheric circulation patterns, or different sulfate deposition process in terms of dry versus wet deposition, are also affecting the Greenland volcanic detection rates in stadial versus interstadial periods. We note that because an increased smoothing of the sulfate record mostly decreases the number of smaller detected sulfate depositions, the effect of smoothing on the large accumulated sulfate deposition over time is less important (Fig. S2.5 and Table S2.8).

2.4.2 Long-term volcanic eruption variability

In order to estimate the long-term pattern of volcanic activity, the accumulated number of volcanic eruptions and resulting sulfate deposition in Greenland and Antarctica over the investigated period are compared in Fig. 2.5 (same data as applied in Fig. 2.2). The cumulative volcanic number (sulfate deposition) in Greenland is larger than in Antarctica by a factor of 3.2 (4.7), considering only sulfate depositions larger than 20 kg km^{-2} at both poles. We attributed this mainly to the larger number of volcanoes situated in the NH, but it is possibly also related to the proximity of Iceland to Greenland and to other volcanic regions located upwind of Greenland, as well as to the differing atmospheric circulation patterns between the two hemispheres (Toohey et al., 2019). In terms of cumulated volcanic number there is some temporal variability that could be climate related, but overall the eruption frequency is rather constant in comparison to the geological record from Large Magnitude Explosive Volcanic Eruptions (LaMEVE) database (Brown et al., 2014), most likely because the ice-core preservation and identification are much more homogeneous over time than that of radiometrically dated eruptions.

The number of volcanic eruptions per millennium shows a fairly constant level both for Greenland and for Antarctica (Fig. 2.3, Fig. S2.8 and Fig. S2.9). The Early Holocene increase in global volcanism as suggested by Watt et al. (2013) is not identified in our record. Neither is the periodicity of Campanian eruptions as identified by Kutterolf et al. (2019), but this pattern could be masked by eruptions from elsewhere.

Based on the EDC sulfate record, Castellano et al. (2004) determined the Antarctic volcanic sulfate deposition to be fairly constant over the last 45 ka, except for an increase during the last 2000 years. The eruption frequency level of 5-10 eruptions per millennium determined in that study is on the low side compared to the present study, in particular for the older part of the period (Fig. 2.3). This is likely because the EDC sulfate record has low resolution and could not pick up all of the smaller short-lived eruptions, also because the low accumulation at the EDC site does not record some eruptions (see methods/results section). Over the 60-9 ka interval we have detected 224 volcanic eruptions in EDC as compared to 513 and 496 in the higher resolution WDC and EDML records, respectively (Table S2.4).

Recently, Cole-Dai et al. (2021) compiled a Holocene volcanic record from the high-resolution sulfate record of the high-accumulation WDC ice core. The authors determine a fairly constant Holocene volcanic activity with identification of 426 eruptions of which 162 and 44 have sulfate depositions larger than 10 kg km^{-2} and 30 kg km^{-2}, respectively. Those numbers are very comparable to our findings for Antarctica in the period of 11-9 ka (Fig. 2.3).

Based on the same GISP2 sulfate dataset as applied in the present study and after introducing a rescaling to compensate for the decreasing sample resolution with depth, Zielinski et al. (1996, 1997) identified an enhanced northern hemispheric volcanic eruption frequency in the deglacial period (17-6 ka) compared to the 60-0 ka average. In our 3-core Greenland sulfate deposition compilation, we also found an increased volcanic eruption frequency over the deglacial period, which is 34% higher than the late Holocene period (2-0 ka), especially for the fraction of large sulfate deposition events (Fig. 2.3 and Fig. 2.4). In Antarctica, neither the detected eruption frequency nor the total sulfate deposition over the deglacial period are higher than the average for the full 60-9 ka interval. We therefore conclude that the increased number of large eruptions occurring in the deglacial period are mostly of northern hemispheric origin. This hypothesis is supported by the elevated number of tephra deposits identified in Iceland records (Maclennan et al., 2002) and in Greenland during the deglacial period mostly of Icelandic origin, a few from Japanese and unknow origins (Bourne et al., 2016; Zielinski et al., 1997; Mortensen et al., 2005; Gronvold et al., 1995). Van Vliet-Lanoe et al. (2020) found that the enhanced volcanic activity in

southern Iceland is most likely related to stress unlocking during deglaciation events and related to rifting events at the melting margin of the ice sheet. In the period of 14.6-13.1 ka in Southeast Alaska, an enhanced volcanic activity from the Mount Edgecumbe Volcanic Field has also been observed by Praetorius et al. (2016).

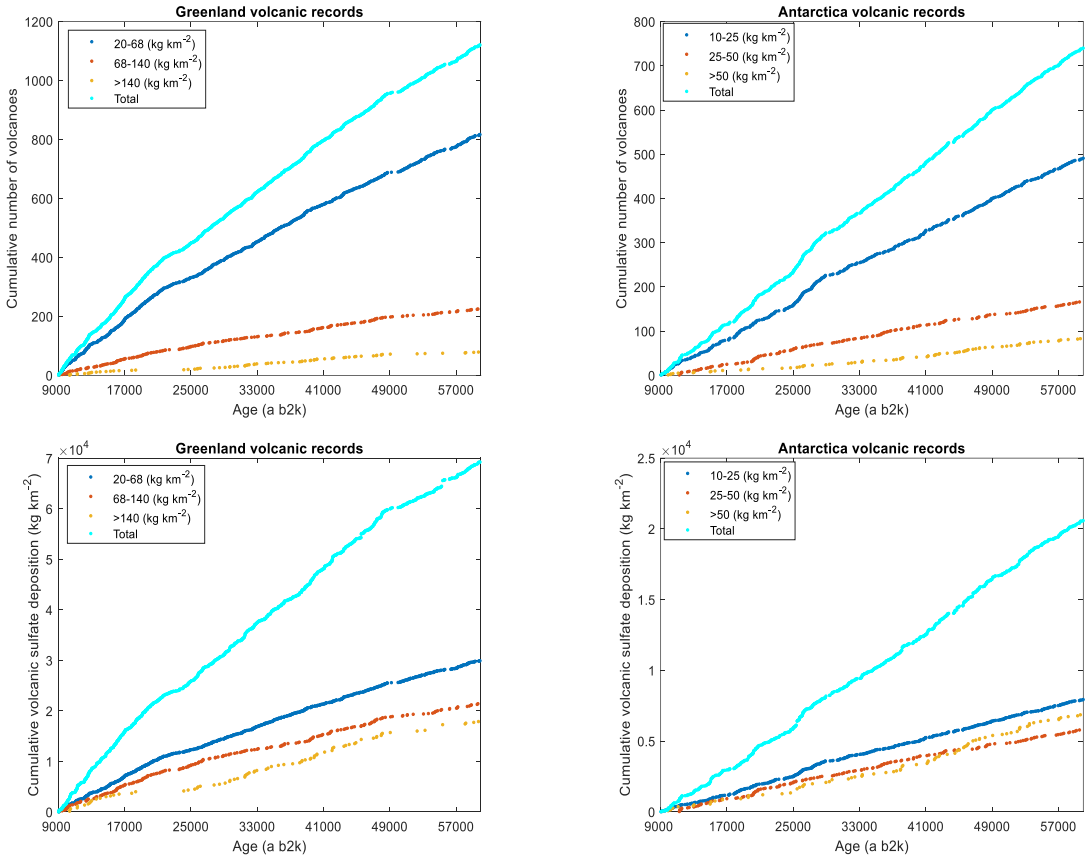

Figure 2.5. Cumulative number and sulfate deposition of volcanoes with time (same as in Fig. 2.2 and Tables S2.3 and S2.4) for three classified size fractions (same fractions as in Fig. 2.3) of volcanoes for Greenland and Antarctica (60-9 ka).

For the glacial period (60-21 ka), the frequency of detected eruptions is similar to that of the last 2000 years, when comparing the same sulfate deposition fractions (Fig. 2.4). We note that for the last 2000 years only eruptions with sulfate depositions larger than 20 kg km^{-2} are included and in order to make the profiles comparable - the sulfate records have been smoothed with a two-year filter. The apparent increase in global volcanism over the last millennia in the geologic records (Brown et al., 2014) is therefore most likely due to an under-representation of older eruption identifications in that study (Papale, 2018; Deligne et al., 2010). When it comes to

sulfur emission strengths of eruptions and accumulated sulfate deposition, however, the last 2000 years appear to be under-represented in very large eruptions as compared to long periods of the last glacial period (Table 2.1).

2.4.3 Estimating the volcanic forcing of the last glacial 60-9 ka

To estimate the volcanic radiative forcing from eruptions occurring in the last glacial and early Holocene we need to (i) constrain the sulfate stratospheric aerosol loading (we applied the method of Gao et al. (2007)), (ii) convert the stratospheric aerosol loading into the global mean stratospheric aerosol optical depth (SAOD) (we applied the methods of Crowley and Unterman. (2013) and that of Aubry et al. (2020)), and (iii) convert global mean SAOD to the global mean radiative forcing (we applied the methods of Hansen et al. (2005) and that of Marshall et al. (2020)). The global stratospheric sulfate aerosol loading requires a separation of NH high-latitude eruptions from other eruptions, as the two eruption groups are scaled differently (Gao et al., 2007). We defined NH high latitude eruption as eruptions that occurred at a latitude above 40° N. To identify the NH high latitude eruptions, we applied a Support Vector Machine learning classifier model (SVM – see methods section), that is trained by the bipolar sulfate deposition of volcanic eruptions for which the eruption site is known. We applied 17 Holocene and 4 glacial volcanic eruptions of known origin (Table S2.6) to predict that 50 out of 85 bipolar eruptions of unknown origin are likely to have occurred in the NH high latitudes (Fig. 2.1 and Fig. 2.6). We then reconstruct the volcanic radiative forcing using three different approaches:

	Absolute number of eruptions		**Eruptions per millennium**	
	0-2.5 ka	**9-16.5 ka 24.5-60 ka**	**0-2.5 ka**	**9-16.5 ka 24.5-60 ka**
< -13.2 W m^{-2} (Oruanui, Taupo)	0	3	0	0.07
< -9.5 W m^{-2} (EU 426 BC)	1	25	0.4	0.58
< -6.5 W m^{-2} (Tambora)	6	69	2.4	1.60

Table 2.1. The number and frequency of large bipolar volcanic eruptions for the last 2500 years and for the last glacial and early Holocene (this study). The climate forcing is calculated using the SAOD scaling of Aubry et al. (2020) and the radiative forcing conversion from Marshall et al. (2020).

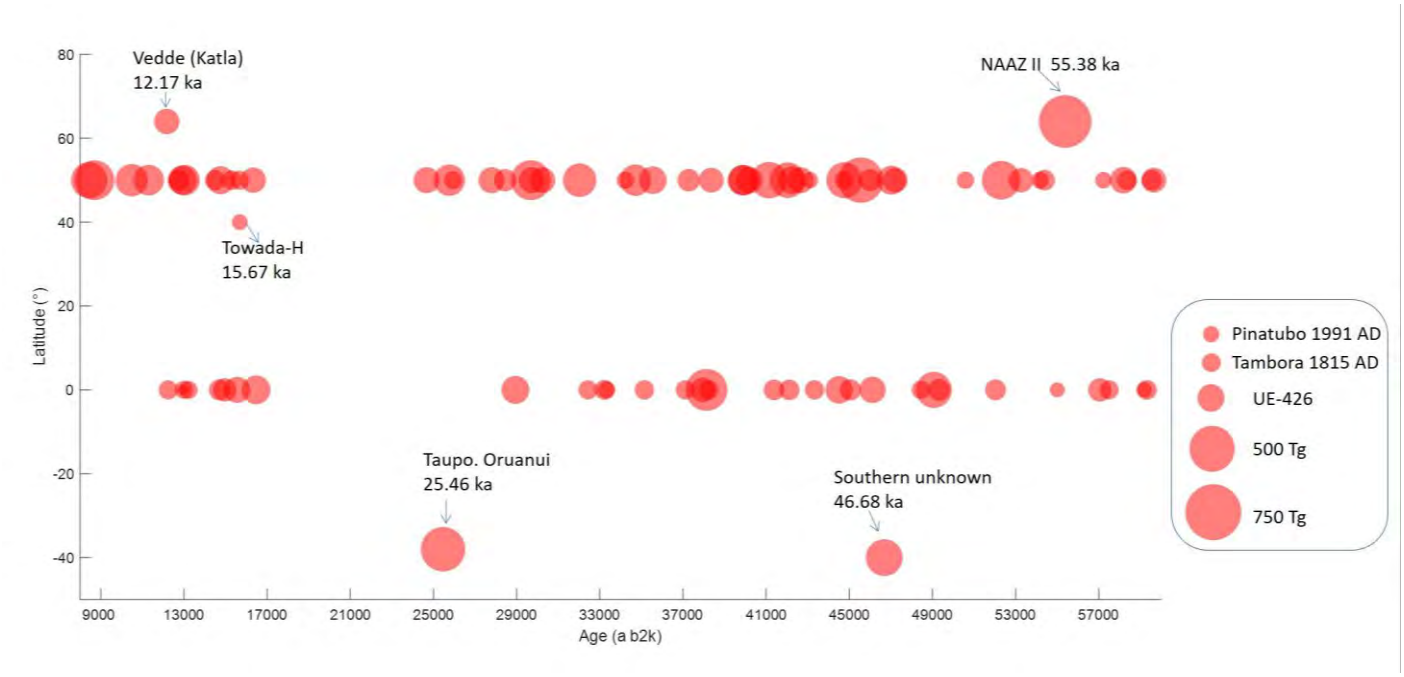

Figure 2.6. Schematic of the latitudinal location for the identified bipolar volcanic eruptions (Table S2.5). Volcanoes for which the eruption site is predicted above 40°N are marked at 50°N and those predicted below 40°N are marked at Equator. Volcanic locations that are known from ice-core tephra deposits are indicated by name and age of the eruption (Table S2.5). Due to its high relative sulfate deposition in Antarctica, the eruption at 46.68 ka, marked at 40°S in the figure, is very likely from the Southern Hemisphere but the eruption site is unknown. The size of the circles represents the strength of volcanic stratospheric aerosol loading.

1) The global mean SAOD is obtained using the method of Crowley and Unterman. (2013) and the radiative forcing calculation applies the scaling factor of Hansen et al. (2005). Here the volcanic radiative forcing is calibrated against Pinatubo 1991 AD (at 15°N). This approach is similar to the one used by Sigl et al. (2015).

2) The global mean SAOD is obtained using the scaling factor of Aubry et al. (2020) and the radiative forcing calculation applies the scaling factor of Hansen et al. (2005). This approach is similar as IPCC AR5.

3) The global mean SAOD is obtained using the scaling factor of Aubry et al. (2020) and the radiative forcing calculation applies the scaling factor of Marshall et al. (2020), which considers rapid aerosol adjustment for large volcanic eruptions.

All of the reconstructed volcanic radiative forcings are calibrated and evaluated based on modern volcanic eruptions, and they are therefore potentially biased when applied to the eruptions occurring in the very different glacial climate (see section 4.1). Table S2.5 and Fig. S2.11 present the reconstructed volcanic radiative forcing of individual volcanic events using the

three approaches. The reconstructed volcanic forcing obtained by methods 2) and 3) is significantly weaker than that obtained by method 1) by a factor of 1.3 and 2.8, respectively, when integrated over all events. In the following, we adopt method 3) to present the reconstructed volcanic forcing values.

Having estimated the volcanic forcing of the glacial and early Holocene eruptions, we can compare it to the well-constrained eruptions that occurred over the last 2500 years (Sigl et al., 2015). In Table 2.1 we compare the number of eruptions with a climate forcing larger than Oruanui, Taupo, 25.32 ka BP1950; the unidentified eruption of 426 BC, and Tambora, 1815 AD for the periods of 2.5-0 ka, and 60-9 ka. Note that the investigated period of the last glacial and the early Holocene covers some 43 ka (60-9 ka minus the section of no identified bipolar eruptions 24.5 to 16.5 ka). Among the 85 bipolar events investigated in the last glacial and early Holocene, three eruptions are found to be larger than Oruanui, Taupo, and 25 eruptions are found to be larger than the largest eruption of the past 2500 years.

Based on geological evidence, the occurrence of large volcanic eruptions was estimated in terms of their VEI (Volcanic explosivity index), which is based on the volume of ejected magma. The average occurrence rate of VEI-7 (VEI-8) volcanoes discovered in the last 125 ka BP (2600 ka BP) is 0.3 (0.01) per millennium, respectively, based on databases of LaMEVE and GVP (Papale, 2018). From ice-core records, we cannot directly derive the VEI index, but the estimated volcanic radiative forcing is likely to be another good indicator of volcanic eruption magnitude. The average rate of volcanoes in the 60-9 ka interval with a climate forcing larger than the 1815 AD Tambora eruption (VEI-7) is 1.60 per millennium (Table 2.1). In the same interval, we have 4 eruptions with a climate forcing larger or equal to the 25.32 ka BP1950 Taupo Oruanui (VEI-8) eruption. Of those, the Icelandic 55.38 ka NAAZ II volcanic event is likely to be overestimated due to its proximity to Greenland (see section 4.4.). Thus, we identify three eruptions with a climate forcing larger than or equal to Taupo Oruanui 25.47 ka, occurring at a rate of 0.07 eruptions per millennium. Those ice-core based eruption frequency estimates are thus about 5.3 times larger than those based on geological evidence for Tambora 1815 AD, and 7 times larger as Taupo Oruanui 25.32 ka BP1950 resting on the observation that there exists a positive relationship between the volume of ejected magma and the emission of sulfur gas for a volcanic eruption (Table S2.6).

2.4.4 Large and notable volcanic eruptions of the last glacial period (60-9 ka)

The largest eruptions of the last glacial period and early Holocene are ranked by the average climate forcing in Table 2.2. The highest ranking on the list is the Icelandic eruption associated with the NAAZ II occurring in GS-15.2 at 55.4 ka b2k (Gronvold et al., 1995; Zielinski et al., 1997). The sulfate deposition in Greenland from this eruption is enormous (almost 15 times higher than the deposition for Laki 1783 AD), but none or only very little sulfate is deposited in Antarctica. With its close proximity to Greenland, it is therefore likely that a large fraction of the sulfate was transported to Greenland through the troposphere and thus the estimated climatic forcing of –15.9 W m^{-2} is probably overestimated and should not be taken at face value. From the marine sediment records, the NAAZ II layer consists of different Icelandic events (Rutledal et al., 2020). For the above reasons, the eruption should not be considered as the largest eruption of the last 60 ka in a global context. The very wide range of sulfate deposition of 866.2-1435.6 kg km^{-2} among the Greenland ice-core records (Table S2.5) is probably due to a combination of 1) a true geographical variability in deposition in Greenland, 2) the quite significant and possibly inaccurate correction for layer thinning at great depth in the ice cores for this eruption, and 3) an unexplained difference related to the different analytical methods applied (see results section). The second largest event on the list occurred in GI-12 at 45.56 ka b2k and is identified in all Greenland and Antarctic ice cores, but the deposition at EDC is very low, most likely due to its low accumulation and the low time-resolution of the sulfate record. The eruption is of unknown origin, but based on its relative Greenland and Antarctic sulfate deposition, it occurred in the NH extratropical area and its climate forcing is estimated to be -15.0 W m^{-2}.

Number three on the list of large eruptions occurred at 38.13 ka b2k; 100 years after the onset of GI-8 and 11 years before the occurrence of the Faroe Marine Ash Zone III (FMAZ III) tephra in Greenland (Davies et al., 2012). The eruption is detected in all ice cores (but there is a data gap for the WDC sulfur in this interval), and with very similar Greenland and Antarctic sulfate depositions this is most likely a low-latitude eruption with an estimated average climate forcing of −13.6 W m^{-2}, about 2 times that of Tambora (1815 CE).

The forth largest bipolar ice-sheet sulfate deposits are from the New Zealand Taupo, Oruanui, eruption that occurred in GS-3 at 25.32 ka BP1950, verified by the presence of a tephra deposit in Antarctica (Dunbar et al., 2017). The estimated average climate forcing of the eruption is -13.2 W m^{-2}, about 1.5 times that of Samalas 1257AD (-9.1 W m^{-2}) (Sigl et al., 2015), which caused large variability of atmospheric temperature of global climate for several years (Lim et al., 2016), prolonged the drought in North American and leading to the famine (Herweijer et al.,

2007). Despite its magnitude, the sulfate deposition of the eruption is undetected in the Greenland GISP2 ice core, which has the lowest temporal sulfate-data resolution of all the used cores in this time period.

In GS-5.1 at 29.68 ka b2k there is a pair of volcanic eruptions separated by some 40 years, of which the younger event ranks seventh on the list of the largest eruptions. The estimated climatic forcing of this eruption is -12.5 W m^{-2} and it has a clear NH signature in the bipolar sulfate distribution. There is no associated tephra deposit in the ice cores, but we speculate the event originates from the Italian Campi Flegrei Y-3 eruption, being the only bipolar volcanic eruption of that magnitude within a range of several millennia. The Y-3 eruption is independently Carbon-14 dated to 29.0 ka b2k (Albert et al., 2015).

Number 8 on the list of the largest eruptions occurred at 46.68 ka b2k in GI-12 and is the only eruption in this study apart from the 25.32 ka BP1950 Taupo, Oruanui, eruption that has a clear southern hemispheric origin. The Antarctic sulfate deposition of the eruption is approximately twice that in Greenland (Fig. 2.1) and the eruption has an average estimated climatic forcing of -12.3 W m^{-2} or about 0.9 times that of Oruanui.

Right after the onset of GS-9 at 39.92 ka b2k there is another pair of large eruptions separated by some 46 years. Those are ranking respectively number 14 (39,915 a b2k; -10.6 W m^{-2}) and number 38 (39,869 a b2k; -8.8 W m^{-2}) of the large eruptions listed in Table 2.2. Both eruptions have bipolar sulfate distributions suggesting a NH eruption. Because of their magnitude and their stratigraphic setting right at the onset of GS-9 these volcanic events are both possible candidates for the Italian Y-5 Campanian Ignimbrite eruption. There is no tephra evidence for this suggestion in the ice cores, but tephra from this eruption has been identified in the Black Sea in very similar stratigraphic setting at the onset of GS-9 and the eruption is independently dated by Ar/Ar to 39.9 ± 0.1 ka b2k (Giaccio et al., 2017).

In the late GI-1 right before the onset of GS-1 / Younger Dryas there is a quadruple of bipolar eruptions covering a period of 110 years (Svensson et al., 2020). The oldest (13,028 a b2k; -10.5 W m^{-2}) and the youngest (12,917 a b2k; -10.0 W m^{-2}) of those eruptions are number 16 and 17 on the list of large eruptions. Both eruptions are likely to have occurred in the NH at above 40°N. The 12,917 b2k eruption has been suggested as a candidate for the Laacher See Eruption (LSE) that occurred in the East Eifel region in present-day Germany (Brauer et al., 1999; Baldini et al., 2018), but no tephra has been identified in the ice cores from this eruption. A recent publication, however, suggested that the LSE was around 130 years older (Reinig, et al., 2021) and is synchronous instead (within age uncertainty) with the oldest event of this quadruple of

Table 2.2. The largest bipolar volcanic eruptions of the last glacial period and early Holocene ranked by the volcanic aerosol forcing that is derived from the average Greenland and Antarctic volcanic sulfate depositions. The stratospheric aerosol loading was estimated according to Gao et al. (2007) and the radiative volcanic aerosol forcing was reconstructed with a scaling factor of SAOD obtained from Aubry et al. (2020) and a scaling factor to obtain the radiative forcing following Marshall et al. (2020) (section 4.3). 'NHHL' refers to high-latitude northern-hemisphere locations of volcanoes, meaning above 40° N; 'LL or SH' refers to low latitude or southern hemisphere locations, meaning below 40° N. 'Number of ice cores' refers to the number of ice cores in Greenland and Antarctica in which the volcanic sulfate signal has been detected.

Rank	Age (b2k)	Greenland volc. depo. (kg/km^2)	Antarctic volc. depo. (kg/km^2)	Stratospheric aerosol loading (Tg)	Global climate forcing	Prediction of volcanic site	Number of ice cores	
							Greenland	Antarctica
1	55383	1117.4	16.5	653.4	-15.9	NHHL	3	2
2	45555	652.6	172.7	544.7	-15.0	NHHL	3	3
3	38133	209.4	204.5	413.9	-13.6	LL or SH	3	2
4	25460	189.5	192.8	382.3	-13.2	LL or SH	2	3
5	52302	293.0	185.4	352.4	-12.8	NHHL	3	3
6	44763	169.7	171.0	340.7	-12.7	LL or SH	2	3
7	29680	333.3	137.6	327.5	-12.5	NHHL	2	3
8	46683	105.1	211.1	316.2	-12.3	LL or SH	2	3
9	41144	410.0	81.8	315.5	-12.3	NHHL	3	3
10	49065	164.9	142.3	307.2	-12.1	LL or SH	3	3
11	42037	327.7	119.8	306.6	-12.1	NHHL	2	3
12	32032	210.8	145.6	265.8	-11.4	NHHL	3	3
13	25759	214.8	110.6	233.1	-10.8	NHHL	3	3
14	39915	316.0	44.0	224.1	-10.6	NHHL	3	3
15	34718	301.0	52.5	224.1	-10.6	NHHL	2	3
16	13028	272.8	65.0	220.5	-10.5	NHHL	3	3
17	12917	248.1	59.4	200.8	-10.0	NHHL	3	3
18	11305	297.8	30.1	199.8	-10.2	NHHL	2	3
19	47023	255.4	52.3	197.9	-10.0	NHHL	3	3
20	16469	102.9	89.8	192.7	-9.9	LL or SH	2	3
21	14761	307.8	10.7	186.2	-9.7	NHHL	3	3
22	28942	88.4	97.5	185.9	-9.7	LL or SH	1	3
23	42250	183.0	80.9	185.2	-9.7	NHHL	2	3
24	35556	236.4	45.4	180.1	-9.5	NHHL	3	3
25	44507	98.6	80.3	178.9	-9.5	LL or SH	1	2
26	40183	211.5	47.5	168.1	-9.2	NHHL	3	3
27	58182	156.9	78.6	168.1	-9.2	NHHL	1	3
28	27797	263.9	17.6	168.0	-9.2	NHHL	2	3
29	46116	66.5	99.4	165.9	-9.2	LL or SH	3	3
30	42658	133.1	85.6	161.5	-9.0	NHHL	3	3
31	24669	172.9	62.1	160.7	-9.0	NHHL	3	3
32	15559	84.0	72.2	156.2	-8.9	LL or SH	2	3
33	30244	208.7	36.3	155.2	-8.9	NHHL	3	2
34	29722	206.1	36.8	154.3	-8.8	NHHL	2	2
35	10481	170.6	56.7	153.9	-8.8	NHHL	2	3
36	12170	248.6	11.2	153.0	-8.8	NHHL	3	2
37	16334	187.5	45.8	152.7	-8.8	NHHL	3	3
38	39869	158.5	61.2	151.6	-8.8	NHHL	1	2
39	38366	227.6	16.0	145.7	-8.6	NHHL	3	3
40	59647	129.0	72.0	145.6	-8.6	NHHL	1	3
41	37965	88.7	56.0	144.7	-8.6	LL or SH	3	2
42	53259	146.1	56.8	140.0	-8.4	NHHL	3	3
43	14966	81.7	50.5	132.1	-8.2	LL or SH	2	3
44	57051	69.6	57.6	127.2	-8.0	LL or SH	2	2
45	37277	149.3	35.3	120.4	-7.8	NHHL	2	2

bipolar eruptions, but also with some minor sulfate signals. Stratospheric sulfur injections and changes in aerosol optical depth have recently been independently estimated in the late GI-1 based on a subset of four ice cores with less stringent cut-off criteria (Abbott et al., 2021) indicating this time period experienced stronger volcanic forcing than any other comparable period during the Common Era.

The Vedde Ash layer (number 36 in Table 2.2) originates from a significant euption from Katla, Iceland with widespread tephra deposition in Greenland (Mortensen et al., 2005; Gronvold et al., 1995) and the North Atlantic region in the middle of GS-1 / Younger Dryas at 12.17 ka (Lane et al., 2012). Surprisingly, this Icelandic eruption not only deposited large amounts of sulfate in Greenland but also a much smaller amount in Antarctica, where it is identified in the WDC and EDML sulfate profiles suggesting that it had a large stratospheric injection. The average volcanic forcing is estimated to about -8.8 W m^{-2}, but this value has to be taken with the caution as some of the sulfate could have made it to Greenland through the troposphere.

2.5 Conclusion

We have employed three Greenland and three Antarctic sulfate/sulfur ice-core records to document the global volcanic activity over the period 60-9 ka b2k. Detection of volcanic signals in the last glacial is challenging due to extensive layer thinning of the ice cores with depth and a highly variable sulfate background level in the Greenland ice cores across DO events. Due to those challenges, we limited ourselves to identify Greenland (Antarctica) eruptions with sulfate deposition larger than 20 (10) kg km^{-2}, which for Greenland is about half the volcanic sulfate deposition of the Tambora 1815 AD and for Antarctica comparable to the Pinatubo 1991 AD eruption.

With those restrictions we identified 1113 volcanic eruptions in Greenland and 740 volcanic eruptions in Antarctica verifying the NH to be the most volcanic active. Of those, 85 volcanic eruptions had global impact (bipolar volcanos) as they were previously identified in Greenland and Antarctic ice-core records. Compared to the past 2500 years, the ratio of bipolar volcanoes to total identified volcanic events is very low in last glacial period, highlighting the challenges of robust synchronization over the glacial period. Based on the hemispheric partitioning of sulfate deposition following well-known historical eruptions, we determined if the bipolar volcanoes are likely to be situated above or below 40 ° N latitude. We then estimated their climatic impact potential in terms of radiative forcing based on established methods. Throughout the investigated

period, we find that 69 volcanoes are larger than the Tambora 1815 AD eruption, and one unknown volcano occurring at 45.56 ka b2k in the NH and one unknown volcano at 38.13 ka b2k in low latitude or in the Southern Hemisphere are larger than the Taupo, Oruanui, eruption occurring at 25.32 ka BP1950 in present day New Zealand. The Icelandic NAAZ II eruption (55.38 ka b2k) has by far left the largest sulfate deposition in Greenland, but due to its minor sulfate deposition in Antarctica, it is thought that only a fraction of the sulfur gases was injected into the stratosphere. In general, we observe significantly higher occurrences of very large eruptions (VEI 7 or larger) than estimated from the geological record, indicating that ice cores provide a more complete picture of volcanic activity in the past.

Overall, the frequency of volcanic eruptions per millennium is rather constant throughout the investigated period and comparable to that of the most recent millennia. In agreement with previous studies, however, we find elevated levels of volcanic activity in the NH during the deglacial period (16-9 ka b2k). In particular, many very large eruptions occurred in this interval, quite likely associated with the redistribution of mass related to the melt down of the major glacial ice sheets in this period. In contrast, an apparent increase of Northern Hemispheric volcanic activity in cold stadial periods as compared to milder interstadial periods is likely to be an artefact due to the highly variable nature of the Greenland sulfate signal of those periods. It is unlikely to be related to the sea level variations occurring in parallel to stadial/interstadial changes, which are much smaller than the sea level increases that occurred over the glacial termination.

Data availability: The high-resolution NGRIP CFA sulfate dataset is available as supplementary information for this publication. All other applied datasets are available elsewhere.

Supplement. The supplement related to this article is available online at: https://doi.org/10.5194/cp-18-485-2022-supplement.

2.6 References

Abbott, P. M. and Davies, S. M.: Volcanism and the Greenland ice-cores: the tephra record, Earth-Science Reviews, 115, 173-191, 10.1016/j.earscirev.2012.09.001, 2012.

Abbott, P. M., Niemeier, U., Timmreck, C., Riede, F., McConnell, J. R., Severie, M., Fischer, H., Svensson, A., Toohey, M., Reinig, F., Sigl, M.: Volcanic climate forcing preceding the inception of the Younger Dryas: Implications for tracing the Laacher See eruption, Quaternary Science Reviews, 274, 1-9, 10.1016/j.quascirev.2021.107260, 2021.

Albert, P. G., Hardiman, M., Keller, J., Tomlinson, E. L., Smith, V. C., Bourne, A. J., Wulf, S., Zanchetta, G., Sulpizio, R., Muller, U. C., Pross, J., Ottolini, L., Matthews, I. P., Blockley, S. P. E., and Menzies, M. A.: Revisiting the Y-3 tephrostratigraphic marker: a new diagnostic glass geochemistry, age estimate, and details on its climatostratigraphical context, Quaternary Science Reviews, 118, 105-121, 10.1016/j.quascirev.2014.04.002, 2015.

Andersen, K. K., Azuma, N., Barnola, J. M., Bigler, M., Biscaye, P., Caillon, N., Chappellaz, J., Clausen, H. B., DahlJensen, D., Fischer, H., Fluckiger, J., Fritzsche, D., Fujii, Y., Goto-Azuma, K., Gronvold, K., Gundestrup, N. S., Hansson, M., Huber, C., Hvidberg, C. S., Johnsen, S. J., Jonsell, U., Jouzel, J., Kipfstuhl, S., Landais, A., Leuenberger, M., Lorrain, R., Masson-Delmotte, V., Miller, H., Motoyama, H., Narita, H., Popp, T., Rasmussen, S. O., Raynaud, D., Rothlisberger, R., Ruth, U., Samyn, D., Schwander, J., Shoji, H., Siggard-Andersen, M. L., Steffensen, J. P., Stocker, T., Sveinbjornsdottir, A. E., Svensson, A., Takata, M., Tison, J. L., Thorsteinsson, T., Watanabe, O., Wilhelms, F., White, J. W. C., and Project, N. G. I. C.: High-resolution record of Northern Hemisphere climate extending into the last interglacial period, Nature, 431, 147-151, 10.1038/nature02805, 2004.

Aubry, T. J., Toohey, M., Marshall, L., Schmidt, A., & Jellinek, A. M. (2020). A New Volcanic Stratospheric Sulfate Aerosol Forcing Emulator (EVA_H): Comparison With Interactive Stratospheric Aerosol Models. Journal of Geophysical Research-Atmospheres, 125(3). doi:10.1029/2019jd031303

Austin, W. E. N., Wilson, L. J., and Hunt, J. B.: The age and chronostratigraphical significance of North Atlantic Ash Zone II, Journal of Quaternary Science, 19, 137-146, 10.1002/jqs.821, 2004.

Baldini, J. U. L., Brown, R. J., and Mawdsley, N.: Evaluating the link between the sulfur-rich Laacher See volcanic eruption and the Younger Dryas climate anomaly, Climate of the Past, 14, 969-990, 10.5194/cp-14-969-2018, 2018.

Baroni, M., Savarino, J., Cole-Dai, J. H., Rai, V. K., and Thiemens, M. H.: Anomalous sulfur isotope compositions of volcanic sulfate over the last millennium in Antarctic ice cores, Journal of Geophysical Research-Atmospheres, 113, 10.1029/2008jd010185, 2008.

Bazin, L., Landais, A., Lemieux-Dudon, B., Kele, H. T. M., Veres, D., Parrenin, F., Martinerie, P., Ritz, C., Capron, E., Lipenkov, V., Loutre, M. F., Raynaud, D., Vinther, B., Svensson, A., Rasmussen, S. O., Severi, M., Blunier, T., Leuenberger, M., Fischer, H., Masson-Delmotte, V., Chappellaz, J., and Wolff, E.: An optimized multi-proxy, multi-site Antarctic ice and gas orbital chronology (AICC2012): 120-800 ka, Climate of the Past, 9, 1715-1731, 10.5194/cp-9-1715-2013, 2013.

Bigler, M., Svensson, A., Kettner, E., Vallelonga, P., Nielsen, M. E., and Steffensen, J. P.: Optimization of High-Resolution Continuous Flow Analysis for Transient Climate Signals in Ice Cores, Environmental Science & Technology, 45, 4483-4489, 10.1021/es200118j, 2011.

Bigler, M.: Hochauflösende Spurenstoffmessungen an polaren Eisbohrkernen: Glazio-chemische und klimatische Prozessstudien, 2004.Ph.D. dissertation, Physics Institute, University of Bern, Switzerland, 2004.

Bourne, A. J., Abbott, P. M., Albert, P. G., Cook, E., Pearce, N. J. G., Ponomareva, V., Svensson, A., and Davies, S. M.: Underestimated risks of recurrent long-range ash dispersal from northern Pacific Arc volcanoes, Scientific Reports, 6, 10.1038/srep29837, 2016.

Bourne, A. J., Cook, E., Abbott, P. M., Seierstad, I. K., Steffensen, J. P., Svensson, A., Fischer, H., Schupbach, S., and Davies, S. M.: A tephra lattice for Greenland and a reconstruction of volcanic events spanning 25-45 ka b2k, Quaternary Science Reviews, 118, 122-141, 10.1016/j.quascirev.2014.07.017, 2015.

Bowen, H. J. M. (1979), Environmental Chemistry of the Elements, 333 pp., Academic Press, London.

Brauer, A., Endres, C., and Negendank, J. F. W.: Lateglacial calendar year chronology based on annually laminated sediments from Lake Meerfelder Maar, Germany, Quaternary International, 61, 17-25, 10.1016/s1040-6182(99)00014-2, 1999.

Brown, S.K., Crosweller, H.S., Sparks, R.S.J., Cottrell. E, Deligne, N.I., Guerrero, N.O., Hobbs, L., Kiyosugi, K., Loughlin, S.C., Siebert, L., Takarada, S.: Characterisation of the Quaternary eruption record: analysis of the Large Magnitude Explosive Volcanic Eruptions (LaMEVE) database. J Appl. Volcanol. 3, 5, https://doi.org/10.1186/2191-5040-3-5, 2014.

Bryson, R.U., Bryson, R.A., Ruter, A.: A calibrated radiocarbon database of late Quaternary volcanic eruptions. eEarth Discuss. 1, 123–134, 10.5194/eed-1-123-2006 2006.

Buizert, C., Cuffey, K. M., Severinghaus, J. P., Baggenstos, D., Fudge, T. J., Steig, E. J., Markle, B. R., Winstrup, M., Rhodes, R. H., Brook, E. J., Sowers, T. A., Clow, G. D., Cheng, H., Edwards, R. L., Sigl, M., McConnell, J. R., and Taylor, K. C.: The WAIS Divide deep ice core WD2014 chronology - Part 1: Methane synchronization (68-31 kaBP) and the gas age-ice age difference, Climate of the Past, 11, 153-173, 10.5194/cp-11-153-2015, 2015.

Burke, A., Moore, K. A., Sigl, M., Nita, D. C., McConnell, J. R., and Adkins, J. F.: Stratospheric eruptions from tropical and extra-tropical volcanoes constrained using high-resolution sulfur isotopes in ice cores, Earth and Planetary Science Letters, 521, 113-119, 10.1016/j.epsl.2019.06.006, 2019.

Capron, E., Rasmussen, S. O., Popp, T. J., Erhardt, T., Fischer, H., Landais, A., Pedro, J. B., Vettoretti, G., Grinsted, A., Gkinis, V., Vaughn, B., Svensson, A., Vinther, B. M., and White, J. W. C.: The anatomy of past abrupt warmings recorded in Greenland ice, Nature Communications, 12, 10.1038/s41467-021-22241-w, 2021.

Castellano, E., Becagli, S., Jouzel, J., Migliori, A., Severi, M., Steffensen, J. P., Traversi, R., and Udisti, R.: Volcanic eruption frequency over the last 45 ky as recorded in Epica-Dome C ice core (East Antarctica) and its relationship with climatic changes, Global and Planetary Change, 42, 195-205, 10.1016/j.gloplacha.2003.11.007, 2004.

Clausen, H. B., Hammer, C. U., Hvidberg, C. S., DahlJensen, D., Steffensen, J. P., Kipfstuhl, J., and Legrand, M.: A comparison of the volcanic records over the past 4000 years from the Greenland Ice Core Project and Dye 3 Greenland Ice Cores, Journal of Geophysical Research-Oceans, 102, 26707-26723, 10.1029/97jc00587, 1997.

Cole-Dai, J., Ferris, D. G., Kennedy, J. A., Michael, S., and McConnell, J.: Comprehensive Record of Volcanic Eruptions in the Holocene (11,000□years) From the WAIS Divide, Antarctica Ice Core, Journal of Geophysical Research-Atmospheres, 126, 10.1029/2020JD032855, 2021.

Cole-Dai, J., Ferris, D., Lanciki, A., Savarino, J., Baroni, M., and Thiemens, M. H.: Cold decade (AD 1810-1819) caused by Tambora (1815) and another (1809) stratospheric volcanic eruption, Geophysical Research Letters, 36, 10.1029/2009gl040882, 2009.

Cooper, C. L., Swindles, G. T., Savov, I. P., Schmidt, A., and Bacon, K. L.: Evaluating the relationship between climate change and volcanism, Earth-Science Reviews, 177, 238-247, 10.1016/j.earscirev.2017.11.009, 2018.

Crick, L., Burke, A., Hutchison, W., Kohno, M., Moore, K., A., S., J., Doyle, E. A., Mahony, S., Kipfstuhl, S., Rae, J. W. B., and Steele, R. C. J., Sparks, R. S. J., and Wolff, E. W.: New insights into the ~74 ka Toba eruption from sulfur isotopes of polar ice cores, Clim. Past Discuss, https://doi.org/10.5194/cp-2021-38, in review, 2021, 2021.

Crowley, T. J. and Unterman, M. B.: Technical details concerning development of a 1200 yr proxy index for global volcanism, Earth System Science Data, 5, 187-197, 10.5194/essd-5-187-2013, 2013.

Dahl-Jensen, D., Albert, M. R., Aldahan, A., Azuma, N., Balslev-Clausen, D., Baumgartner, M., Berggren, A. M., Bigler, M., Binder, T., Blunier, T., Bourgeois, J. C., Brook, E. J., Buchardt, S. L., Buizert, C., Capron, E., Chappellaz, J., Chung, J., Clausen, H. B., Cvijanovic, I., Davies, S. M., Ditlevsen, P., Eicher, O., Fischer, H., Fisher, D. A., Fleet, L. G., Gfeller, G., Gkinis, V., Gogineni, S., Goto-Azuma, K., Grinsted, A., Gudlaugsdottir, H., Guillevic, M., Hansen, S. B., Hansson, M., Hirabayashi, M., Hong, S., Hur, S. D., Huybrechts, P., Hvidberg, C. S., Iizuka, Y., Jenk, T., Johnsen, S. J., Jones, T. R., Jouzel, J., Karlsson, N. B., Kawamura, K., Keegan, K., Kettner, E., Kipfstuhl, S., Kjaer, H. A., Koutnik, M., Kuramoto, T., Kohler, P., Laepple, T., Landais, A., Langen, P. L., Larsen, L. B., Leuenberger, D., Leuenberger, M., Leuschen, C., Li, J., Lipenkov, V., Martinerie, P., Maselli, O. J., Masson-Delmotte, V., McConnell, J. R., Miller, H., Mini, O., Miyamoto, A., Montagnat-Rentier, M., Mulvaney, R., Muscheler, R., Orsi, A. J., Paden, J., Panton, C., Pattyn, F., Petit, J. R., Pol, K., Popp, T., Possnert, G., Prie, F., Prokopiou, M., Quiquet, A., Rasmussen, S. O., Raynaud, D., Ren, J., Reutenauer, C., Ritz, C., Rockmann, T., Rosen, J. L., Rubino, M., Rybak, O., Samyn, D., Sapart, C. J., Schilt, A., Schmidt, A. M. Z., Schwander, J., Schupbach, S., Seierstad, I., Severinghaus, J. P., Sheldon, S., Simonsen, S. B., Sjolte, J., Solgaard, A. M., Sowers, T., Sperlich, P., Steen-Larsen, H. C., Steffen, K., Steffensen, J. P., Steinhage, D., Stocker, T. F., Stowasser, C., Sturevik, A. S., Sturges, W. T., Sveinbjornsdottir, A., Svensson, A., Tison, J. L., Uetake, J., Vallelonga, P., van de Wal, R. S. W., van der Wel, G., Vaughn, B. H., Vinther, B., Waddington, E., Wegner, A., Weikusat, I., White, J. W. C., Wilhelms, F., Winstrup, M., Witrant, E., Wolff, E. W., Xiao, C., Zheng, J., and Community, N.: Eemian interglacial reconstructed from a Greenland folded ice core, Nature, 493, 489-494, 10.1038/nature11789, 2013.

Dansgaard, W., Johnsen, S. J., Clausen, H. B., Dahljensen, D., Gundestrup, N. S., Hammer, C. U., Hvidberg, C. S., Steffensen, J. P., Sveinbjornsdottir, A. E., Jouzel, J., and Bond, G.: EVIDENCE FOR GENERAL INSTABILITY OF PAST CLIMATE FROM A 250-KYR ICE-CORE RECORD, Nature, 364, 218-220, 10.1038/364218a0, 1993.

Davies, S. M., Abbott, P. M., Pearce, N. J. G., Wastegard, S., and Blockley, S. P. E.: Integrating the INTIMATE records using tephrochronology: rising to the challenge, Quaternary Science Reviews, 36, 11-27, 10.1016/j.quascirev.2011.04.005, 2012.

Davies, S. M., Wastegard, S., Abbott, P. M., Barbante, C., Bigler, M., Johnsen, S. J., Rasmussen, T. L., Steffensen, J. P., and Svensson, A.: Tracing volcanic events in the NGRIP ice-core and synchronising North Atlantic marine records during the last glacial period, Earth and Planetary Science Letters, 294, 69-79, 10.1016/j.epsl.2010.03.004, 2010.

Davies, S. M., Abbott, P. M., Meara, R. H., Pearce, N. J. G., Austin, W. E. N., Chapman, M. R., Svensson, A., Bigler, M., Rasmussen, T. L., Rasmussen, S. O., and Farmer, E. J.: A North Atlantic tephrostratigraphical framework for 130-60 ka b2k: new tephra discoveries, marine-based correlations, and future challenges, Quaternary Science Reviews, 106, 101-121, 10.1016/j.quascirev.2014.03.024, 2014.

Deligne, N. I., Coles, S. G., and Sparks, R. S. J.: Recurrence rates of large explosive volcanic eruptions, Journal of Geophysical Research-Solid Earth, 115, 10.1029/2009jb006554, 2010.

Dunbar, N. W., Iverson, N. A., Van Eaton, A. R., Sigl, M., Alloway, B. V., Kurbatov, A. V., Mastin, L. G., McConnell, J. R., and Wilson, C. J. N.: New Zealand supereruption provides time marker for the Last Glacial Maximum in Antarctica, Scientific Reports, 7, 10.1038/s41598-017-11758-0, 2017.

Eliza Cook, Siwan M. Davies, Peter M. Abbott, Nick J.G. Pearce, Seyedhamidreza Mojtabavi, Anders Svensson, Anna J. Bourne, Rhian H. Meara, Sune O. Rasmussen, Joseph Harrison, Elliott Street, Inger K. Seierstad, Bo M. Vinther, Jørgen Peder Steffensen, An updated record of volcanism in Greenland's ice between 12.1 and 17.4 ka b2k: A new tephrochronology framework based on cryptotephra deposits in three ice cores (in preparation).

Fischer, H., Wagenbach, D., and Kipfstuhl, J.: Sulfate and nitrate firn concentrations on the Greenland ice sheet - 2. Temporal anthropogenic deposition changes, Journal of Geophysical Research-Atmospheres, 103, 21935-21942, 10.1029/98jd01886, 1998.

Fudge, T. J., Markle, B. R., Cuffey, K. M., Buizert, C., Taylor, K. C., Steig, E. J., Waddington, E. D., Conway, H., and Koutnik, M.: Variable relationship between accumulation and temperature in West Antarctica for the past 31,000 years, Geophysical Research Letters, 43, 3795-3803, 10.1002/2016GL068356, 2016.

Fudge, T. J., Steig, E. J., Markle, B. R., Schoenemann, S. W., Ding, Q. H., Taylor, K. C., McConnell, J. R., Brook, E. J., Sowers, T., White, J. W. C., Alley, R. B., Cheng, H., Clow, G. D., Cole-Dai, J., Conway, H., Cuffey, K. M., Edwards, J. S., Edwards, R. L., Edwards, R., Fegyveresi, J. M., Ferris, D., Fitzpatrick, J. J., Johnson, J., Hargreaves, G., Lee, J. E., Maselli, O. J., Mason, W., McGwire, K. C., Mitchell, L. E., Mortensen, N., Neff, P., Orsi, A. J., Popp, T. J., Schauer, A. J., Severinghaus, J. P., Sigl, M., Spencer, M. K., Vaughn, B. H., Voigt, D. E., Waddington, E. D., Wang, X. F., Wong, G. J., and Members, W. D. P.: Onset of deglacial warming in West Antarctica driven by local orbital forcing, Nature, 500, 440-+, 10.1038/nature12376, 2013.

Gao, C. C., Robock, A., and Ammann, C.: Volcanic forcing of climate over the past 1500 years: An improved ice core-based index for climate models, Journal of Geophysical Research-Atmospheres, 113, 10.1029/2008jd010239, 2008.

Gao, C. H., Oman, L., Robock, A., and Stenchikov, G. L.: Atmospheric volcanic loading derived from bipolar ice cores: Accounting for the spatial distribution of volcanic deposition, Journal of Geophysical Research-Atmospheres, 112, 10.1029/2006jd007461, 2007.

Gautier, E., Savarino, J., Erbland, J., and Farquhar, J.: SO2 Oxidation Kinetics Leave a Consistent Isotopic Imprint on Volcanic Ice Core Sulfate, Journal of Geophysical Research-Atmospheres, 123, 9801-9812, 10.1029/2018jd028456, 2018.

Gautier, E., Savarino, J., Erbland, J., Lanciki, A., and Possenti, P.: Variability of sulfate signal in ice core records based on five replicate cores, Climate of the Past, 12, 103-113, 10.5194/cp-12-103-2016, 2016.

Giaccio, B., Hajdas, I., Isaia, R., Deino, A., and Nomade, S.: High-precision C-14 and Ar-40/Ar-39 dating of the Campanian Ignimbrite (Y-5) reconciles the time-scales of climatic-cultural processes at 40 ka, Scientific Reports, 7, 10.1038/srep45940, 2017.

Gronvold, K., Oskarsson, N., Johnsen, S. J., Clausen, H. B., Hammer, C. U., Bond, G., and Bard, E.: ASH LAYERS FROM ICELAND IN THE GREENLAND GRIP ICE CORE CORRELATED WITH OCEANIC AND LAND SEDIMENTS, Earth and Planetary Science Letters, 135, 149-155, 10.1016/0012-821x(95)00145-3, 1995.

Grootes, P. M., Stuiver, M., White, J. W. C., Johnsen, S., and Jouzel, J.: COMPARISON OF OXYGEN-ISOTOPE RECORDS FROM THE GISP2 AND GRIP GREENLAND ICE CORES, Nature, 366, 552-554, 10.1038/366552a0, 1993.

Hansen, J., Sato, M., Ruedy, R., Nazarenko, L., Lacis, A., Schmidt, G. A., Russell, G., Aleinov, I., Bauer, M., Bauer, S., Bell, N., Cairns, B., Canuto, V., Chandler, M., Cheng, Y., Genio, A. Del, Faluvegi, G., Fleming, E., Friend, A., Hall, T., Jackman, C., Kelley, M., Kiang, N., Koch, D., Lean, J., Lerner, J., Lo, K., Menon, S., Miller, R., Minnis, P., Novakov, T., Oinas, V., Perlwitz, J., Perlwitz, J., Rind, D., Romanou, A., Shindell, D., Stone, P., Sun, S., Tausnev, N., Thresher, D., Wielicki, B., Wong, T., Yao, M., Zhang, S.: Efficacy of climate forcings, Journal of Geophysical Research 110(D18), D18104, 2005.

Herweijer, C., Seager, R., Cook, E. R., and Emile-Geay, J.: North American droughts of the last millennium from a gridded network of tree-ring data, Journal of Climate, 20, 1353-1376, 10.1175/jcli4042.1, 2007.

Huybers, P. and Langmuir, C.: Feedback between deglaciation, volcanism, and atmospheric CO2, Earth and Planetary Science Letters, 286, 479-491, 10.1016/j.epsl.2009.07.014, 2009.

Hvidberg, C. S., DahlJensen, D., and Waddington, E. D.: Ice flow between the Greenland Ice Core Project and Greenland Ice Sheet Project 2 boreholes in central Greenland, Journal of Geophysical Research-Oceans, 102, 26851-26859, 10.1029/97jc00268, 1997.

Johnsen, S. J., DahlJensen, D., Gundestrup, N., Steffensen, J. P., Clausen, H. B., Miller, H., . . . White, J. (2001). Oxygen isotope and palaeotemperature records from six Greenland ice-core stations: Camp Century, Dye-3, GRIP, GISP2, Renland and NorthGRIP. *Journal of Quaternary Science, 16*(4), 299-307. doi:10.1002/jqs.622

Jungclaus, J. H., Bard, E., Baroni, M., Braconnot, P., Cao, J., Chini, L. P., Egorova, T., Evans, M., Gonzalez-Rouco, J. F., Goosse, H., Hurtt, G. C., Joos, F., Kaplan, J. O., Khodri, M., Goldewijk, K. K., Krivova, N., LeGrande, A. N., Lorenz, S. J., Luterbacher, J., Man, W. M., Maycock, A. C., Meinshausen, M., Moberg, A., Muscheler, R., Nehrbass-Ahles, C., Otto-Bliesner, B. I., Phipps, S. J., Pongratz, J., Rozanov, E., Schmidt, G. A., Schmidt, H., Schmutz, W., Schurer, A., Shapiro, A. I., Sigl, M., Smerdon, J. E., Solanki, S. K., Timmreck, C., Toohey, M., Usoskin, I. G., Wagner, S., Wu, C. J., Yeo, K. L., Zanchettin, D., Zhang, Q., and Zorita, E.: The PMIP4 contribution to CMIP6-Part 3: The last millennium, scientific objective, and experimental design for the PMIP4 past1000 simulations, Geoscientific Model Development, 10, 4005-4033, 10.5194/gmd-10-4005-2017, 2017.

Karlof, L., Oigard, T. A., Godtliebsen, F., Kaczmarska, M., and Fischer, H.: Statistical techniques to select detection thresholds for peak signals in ice-core data, Journal of Glaciology, 51, 655-662, 10.3189/172756505781829115, 2005.

Kreutz, K. J., Mayewski, P. A., Meeker, L. D., Twickler, M. S., and Whitlow, S. I.: The effect of spatial and temporal accumulation rate variability in West Antarctica on soluble ion deposition, Geophysical Research Letters, 27, 2517-2520, 10.1029/2000gl011499, 2000.

Kurbatov, A. V., Zielinski, G. A., Dunbar, N. W., Mayewski, P. A., Meyerson, E. A., Sneed, S. B., and Taylor, K. C.: A 12,000 year record of explosive volcanism in the Siple Dome Ice Core, West Antarctica, Journal of Geophysical Research-Atmospheres, 111, 10.1029/2005jd006072, 2006.

Kutterolf, S., Schindlbeck, J. C., Jegen, M., Freundt, A., and Straub, S. M.: Milankovitch frequencies in tephra records at volcanic arcs: The relation of kyr-scale cyclic variations in volcanism to global climate changes, Quaternary Science Reviews, 204, 1-16, 10.1016/j.quascirev.2018.11.004, 2019.

Lane, C. S., Blockley, S. P. E., Mangerud, J., Smith, V. C., Lohne, O. S., Tomlinson, E. L., Matthews, I. P., and Lotter, A. F.: Was the 12.1 ka Icelandic Vedde Ash one of a kind?, Quaternary Science Reviews, 33, 87-99, 10.1016/j.quascirev.2011.11.011, 2012.

Legrand, M. and Mayewski, P.: Glaciochemistry of polar ice cores: A review, Reviews of Geophysics, 35, 219-243, 10.1029/96rg03527, 1997.

Legrand, M., Hammer, C., DeAngelis, M., Savarino, J., Delmas, R., Clausen, H., and Johnsen, S. J.: Sulfur-containing species (methanesulfonate and SO4) over the last climatic cycle in the Greenland Ice Core Project (central Greenland) ice core, Journal of Geophysical Research-Oceans, 102, 26663-26679, 10.1029/97jc01436, 1997.

Lim, H. G., Yeh, S. W., Kug, J. S., Park, Y. G., Park, J. H., Park, R., and Song, C. K.: Threshold of the volcanic forcing that leads the El Nino-like warming in the last millennium: results from the ERIK simulation, Climate Dynamics, 46, 3725-3736, 10.1007/s00382-015-2799-3, 2016.

Maclennan, J., Jull, M., McKenzie, D., Slater, L., and Gronvold, K.: The link between volcanism and deglaciation in Iceland, Geochemistry Geophysics Geosystems, 3, 10.1029/2001gc000282, 2002.

Marshall, L., Johnson, J. S., Mann, G. W., Lee, L., Dhomse, S. S., Regayre, L., . . . Schmidt, A. (2019). Exploring How Eruption Source Parameters Affect Volcanic Radiative Forcing Using Statistical Emulation. Journal of Geophysical Research-Atmospheres, 124(2), 964-985. doi:10.1029/2018jd028675

Marshall, L. R., Smith, C. J., Forster, P. M., Aubry, T. J., Andrews, T., & Schmidt, A. (2020). Large Variations in Volcanic Aerosol Forcing Efficiency Due to Eruption Source Parameters and Rapid Adjustments. Geophysical Research Letters, 47(19). doi:10.1029/2020gl090241

Mayewski, P. A., Holdsworth, G., Spencer, M. J., Whitlow, S., Twickler, M., Morrison, M. C., Ferland, K. K., and Meeker, L. D.: ICE-CORE SULFATE FROM 3 NORTHERN-HEMISPHERE SITES - SOURCE AND TEMPERATURE FORCING IMPLICATIONS, Atmospheric Environment Part a-General Topics, 27, 2915-2919, 10.1016/0960-1686(93)90323-q, 1993.

Mayewski, P. A., Meeker, L. D., Twickler, M. S., Whitlow, S., Yang, Q. Z., Lyons, W. B., and Prentice, M.: Major features and forcing of high-latitude northern hemisphere atmospheric circulation using a 110,000-year-long glaciochemical series, Journal of Geophysical Research-Oceans, 102, 26345-26366, 10.1029/96jc03365, 1997.

McConnell, J. R., Burke, A., Dunbar, N. W., Kohler, P., Thomas, J. L., Arienzo, M. M., Chellman, N. J., Maselli, O. J., Sigl, M., Adkins, J. F., Baggenstos, D., Burkhart, J. F., Brook, E. J., Buizert, C., Cole-Dai, J., Fudge, T. J., Knorr, G., Graf, H. F., Grieman, M. M., Iverson, N., McGwire, K. C., Mulvaney, R., Paris, G., Rhodes, R. H.,

Saltzman, E. S., Severinghaus, J. P., Steffensen, J. P., Taylor, K. C., and Winckler, G.: Synchronous volcanic eruptions and abrupt climate change similar to 17.7 ka plausibly linked by stratospheric ozone depletion, Proceedings of the National Academy of Sciences of the United States of America, 114, 10035-10040, 10.1073/pnas.1705595114, 2017.

Mortensen, A. K., Bigler, M., Gronvold, K., Steffensen, J. P., and Johnsen, S. J.: Volcanic ash layers from the Last Glacial Termination in the NGRIP ice core, Journal of Quaternary Science, 20, 209-219, 10.1002/jqs.908, 2005.

Narcisi, B., Petit, J. R., and Chappellaz, J.: A 70 ka record of explosive eruptions from the TALDICE ice core (Talos Dome, East Antarctic plateau), Journal of Quaternary Science, 25, 844-849, 10.1002/jqs.1427, 2010.

Narcisi, B., Petit, J. R., Delmonte, B., Basile-Doelsch, I., and Maggi, V.: Characteristics and sources of tephra layers in the EPICA-Dome C ice record (East Antarctica): Implications for past atmospheric circulation and ice core stratigraphic correlations, Earth and Planetary Science Letters, 239, 253-265, 10.1016/j.epsl.2005.09.005, 2005.

Narcisi, B., Petit, J. R., Delmonte, B., Scarchilli, C., and Stenni, B.: A 16,000-yr tephra framework for the Antarctic ice sheet: a contribution from the new Tabs Dome core, Quaternary Science Reviews, 49, 52-63, 10.1016/j.quascirev.2012.06.011, 2012.

Nardin, R., Amore, A., Becagli, S., Caiazzo, L., Frezzotti, M., Severi, M., Stenni, B., and Traversi, R.: Volcanic Fluxes Over the Last Millennium as Recorded in the Gv7 Ice Core (Northern Victoria Land, Antarctica), Geosciences, 10, 10.3390/geosciences10010038, 2020.

Nordhausen, K. The Elements of Statistical Learning: Data Mining, Inference, and Prediction, Second Edition by Trevor Hastie, Robert Tibshirani, Jerome Friedman; Springer: New York, NY, USA, 2009; pp. 37–38. doi:10.1111/j.1751-5823.2009.00095_18.x

Parrenin, F., Petit, J. R., Masson-Delmotte, V., Wolff, E., Basile-Doelsch, I., Jouzel, J., Lipenkov, V., Rasmussen, S. O., Schwander, J., Severi, M., Udisti, R., Veres, D., and Vinther, B. M.: Volcanic synchronisation between the EPICA Dome C and Vostok ice cores (Antarctica) 0-145 kyr BP, Climate of the Past, 8, 1031-1045, 10.5194/cp-8-1031-2012, 2012.

Papale, P.: Global time-size distribution of volcanic eruptions on Earth, Scientific Reports, 8, 10.1038/s41598-018-25286-y, 2018.

Plummer, C. T., Curran, M. A. J., van Ommen, T. D., Rasmussen, S. O., Moy, A. D., Vance, T. R., Clausen, H. B., Vinther, B. M., and Mayewski, P. A.: An independently dated 2000-yr volcanic record from Law Dome, East Antarctica, including a new perspective on the dating of the 1450s CE eruption of Kuwae, Vanuatu, Climate of the Past, 8, 1929-1940, 10.5194/cp-8-1929-2012, 2012.

Praetorius, S., Mix, A., Jensen, B., Froese, D., Milne, G., Wolhowe, M., Addison, J., and Prahl, F.: Interaction between climate, volcanism, and isostatic rebound in Southeast Alaska during the last deglaciation, Earth and Planetary Science Letters, 452, 79-89, 10.1016/j.epsl.2016.07.033, 2016.

Pyle, D. M.: Chapter 13 - Sizes of Volcanic Eruptions. In: The Encyclopedia of Volcanoes (Second Edition), Sigurdsson, H. (Ed.), Academic Press, Amsterdam, 2015.

Rasmussen, S. O., Abbott, P. M., Blunier, T., Bourne, A. J., Brook, E., Buchardt, S. L., Buizert, C., Chappellaz, J., Clausen, H. B., Cook, E., Dahl-Jensen, D., Davies, S. M., Guillevic, M., Kipfstuhl, S., Laepple, T., Seierstad, I. K., Severinghaus, J. P., Steffensen, J. P., Stowasser, C., Svensson, A., Vallelonga, P., Vinther, B. M., Wilhelms,

F., and Winstrup, M.: A first chronology for the North Greenland Eemian Ice Drilling (NEEM) ice core, Climate of the Past, 9, 2713-2730, 10.5194/cp-9-2713-2013, 2013.

Rasmussen, S. O., Andersen, K. K., Johnsen, S. J., Bigler, M., and McCormack, T.: Deconvolution-based resolution enhancement of chemical ice core records obtained by continuous flow analysis, Journal of Geophysical Research-Atmospheres, 110, 10.1029/2004jd005717, 2005.

Rasmussen, S. O., Bigler, M., Blockley, S. P., Blunier, T., Buchardt, S. L., Clausen, H. B., Cvijanovic, I., Dahl-Jensen, D., Johnsen, S. J., Fischer, H., Gkinis, V., Guillevic, M., Hoek, W. Z., Lowe, J. J., Pedro, J. B., Popp, T., Seierstad, I. K., Steffensen, J. P., Svensson, A. M., Vallelonga, P., Vinther, B. M., Walker, M. J. C., Wheatley, J. J., and Winstrup, M.: A stratigraphic framework for abrupt climatic changes during the Last Glacial period based on three synchronized Greenland ice-core records: refining and extending the INTIMATE event stratigraphy, Quaternary Science Reviews, 106, 14-28, 10.1016/j.quascirev.2014.09.007, 2014.

Reinig, F. et al.: Precise date for the Laacher See eruption synchronizes the Younger Dryas, Nature, 595, 66–69, 2021.

Robock, A.: Volcanic eruptions and climate, Reviews of Geophysics, 38, 191-219, 10.1029/1998rg000054, 2000.

Rutledal, S., Berben, S. M. P., Dokken, T. M., van der Bilt, W. G. M., Cederstrom, J. M., and Jansen, E.: Tephra horizons identified in the western North Atlantic and Nordic Seas during the Last Glacial Period: Extending the marine tephra framework, Quaternary Science Reviews, 240, 10.1016/j.quascirev.2020.106247, 2020.

Ruth, U., Barnola, J. M., Beer, J., Bigler, M., Blunier, T., Castellano, E., Fischer, H., Fundel, F., Huybrechts, P., Kaufmann, P., Kipfstuhl, S., Lambrecht, A., Morganti, A., Oerter, H., Parrenin, F., Rybak, O., Severi, M., Udisti, R., Wilhelms, F., and Wolff, E.: "EDML1": a chronology for the EPICA deep ice core from Dronning Maud Land, Antarctica, over the last 150 000 years, Climate of the Past, 3, 475-484, 10.5194/cp-3-475-2007, 2007.

Ruth, U., Wagenbach, D., Steffensen, J. P., and Bigler, M.: Continuous record of microparticle concentration and size distribution in the central Greenland NGRIP ice core during the last glacial period, Journal of Geophysical Research-Atmospheres, 108, 10.1029/2002jd002376, 2003.

Röthlisberger, R., Bigler, M., Hutterli, M., Sommer, S., Stauffer, B., Junghans, H. G., and Wagenbach, D.: Technique for continuous high-resolution analysis of trace substances in firn and ice cores, Environmental Science & Technology, 34, 338-342, 2000.

Sinnl, G., Winstrup, M., Erhardt, T., Cook, E., Jensen, C., Svensson, A., Vinther, B. M., Muscheler, R., and Rasmussen, S. O.: A multi-ice-core, annual-layer-counted Greenland ice-core chronology for the last 3800 years: GICC21, Clim. Past Discuss. [preprint], https://doi.org/10.5194/cp-2021-155, in review, 2021.

Schupbach, S., Fischer, H., Bigler, M., Erhardt, T., Gfeller, G., Leuenberger, D., Mini, O., Mulvaney, R., Abram, N. J., Fleet, L., Frey, M. M., Thomas, E., Svensson, A., Dahl-Jensen, D., Kettner, E., Kjaer, H., Seierstad, I., Steffensen, J. P., Rasmussen, S. O., Vallelonga, P., Winstrup, M., Wegner, A., Twarloh, B., Wolff, K., Schmidt, K., Goto-Azuma, K., Kuramoto, T., Hirabayashi, M., Uetake, J., Zheng, J., Bourgeois, J., Fisher, D., Zhiheng, D., Xiao, C., Legrand, M., Spolaor, A., Gabrieli, J., Barbante, C., Kang, J. H., Hur, S. D., Hong, S. B., Hwang, H. J., Hong, S., Hansson, M., Iizuka, Y., Oyabu, I., Muscheler, R., Adolphi, F., Maselli, O., McConnell, J., and Wolff, E. W.: Greenland records of aerosol source and atmospheric lifetime changes from the Eemian to the Holocene, Nature Communications, 9, 10.1038/s41467-018-03924-3, 2018.

Schurer, A. P., Tett, S. F. B., and Hegerl, G. C.: Small influence of solar variability on climate over the past millennium, Nature Geoscience, 7, 104-108, 10.1038/ngeo2040, 2014.

Seierstad, I. K., Abbott, P. M., Bigler, M., Blunier, T., Bourne, A. J., Brook, E., Buchardt, S. L., Buizert, C., Clausen, H. B., Cook, E., Dahl-Jensen, D., Davies, S. M., Guillevic, M., Johnsen, S. J., Pedersen, D. S., Popp, T. J., Rasmussen, S. O., Severinghaus, J. P., Svensson, A., and Vinther, B. M.: Consistently dated records from the Greenland GRIP, GISP2 and NGRIP ice cores for the past 104 ka reveal regional millennial-scale delta O-18 gradients with possible Heinrich event imprint, Quaternary Science Reviews, 106, 29-46, 10.1016/j.quascirev.2014.10.032, 2014.

Severi, M., Becagli, S., Castellano, E., Morganti, A., Traversi, R., Udisti, R., Ruth, U., Fischer, H., Huybrechts, P., Wolff, E., Parrenin, F., Kaufmann, P., Lambert, F., and Steffensen, J. P.: Synchronisation of the EDML and EDC ice cores for the last 52 kyr by volcanic signature matching, Climate of the Past, 3, 367-374, 10.5194/cp-3-367-2007, 2007.

Severi, M., Becagli, S., Traversi, R., and Udisti, R.: Recovering Paleo-Records from Antarctic Ice-Cores by Coupling a Continuous Melting Device and Fast Ion Chromatography, Analytical Chemistry, 87, 11441-11447, 10.1021/acs.analchem.5b02961, 2015.

Siebert, L., Simkin, T.: Volcanoes of the world: an illustrated catalog of Holocene volcanoes and their eruptions. Smithsonian Institution, Global Volcanism Program, Digital Information Series. GVP-3, 2002.

Sigl, M., McConnell, J. R., Layman, L., Maselli, O., McGwire, K., Pasteris, D., Dahl-Jensen, D., Steffensen, J. P., Vinther, B., Edwards, R., Mulvaney, R., and Kipfstuhl, S.: A new bipolar ice core record of volcanism from WAIS Divide and NEEM and implications for climate forcing of the last 2000 years, Journal of Geophysical Research-Atmospheres, 118, 1151-1169, 10.1029/2012jd018603, 2013.

Sigl, M., McConnell, J. R., Toohey, M., Curran, M., Das, S. B., Edwards, R., Isaksson, E., Kawamura, K., Kipfstuhl, S., Kruger, K., Layman, L., Maselli, O. J., Motizuki, Y., Motoyama, H., Pasteris, D. R., and Severi, M.: Insights from Antarctica on volcanic forcing during the Common Era, Nature Climate Change, 4, 693-697, 10.1038/nclimate2293, 2014.

Sigl, M., Winstrup, M., McConnell, J. R., Welten, K. C., Plunkett, G., Ludlow, F., Buntgen, U., Caffee, M., Chellman, N., Dahl-Jensen, D., Fischer, H., Kipfstuhl, S., Kostick, C., Maselli, O. J., Mekhaldi, F., Mulvaney, R., Muscheler, R., Pasteris, D. R., Pilcher, J. R., Salzer, M., Schupbach, S., Steffensen, J. P., Vinther, B. M., and Woodruff, T. E.: Timing and climate forcing of volcanic eruptions for the past 2,500 years, Nature, 523, 543-+, 10.1038/nature14565, 2015.

Sigl, M., Fudge, T. J., Winstrup, M., Cole-Dai, J., Ferris, D., McConnell, J. R., Taylor, K. C., Welten, K. C., Woodruff, T. E., Adolphi, F., Bisiaux, M., Brook, E. J., Buizert, C., Caffee, M. W., Dunbar, N. W., Edwards, R., Geng, L., Iverson, N., Koffman, B., Layman, L., Maselli, O. J., McGwire, K., Muscheler, R., Nishiizumi, K., Pasteris, D. R., Rhodes, R. H., and Sowers, T. A.: The WAIS Divide deep ice core WD2014 chronology - Part 2: Annual-layer counting (0-31 ka BP), Clim. Past., 12, 769-786, 10.5194/cp-12-769-2016, 2016.

Siggaard-Andersen, M. L. (2004): Analysis of soluble ions from dust and sea salt over the last glacial cycle in polar deep ice cores , PhD thesis, University of Bremen.

Svensson, A., Biscaye, P. E., and Grousset, F. E.: Characterization of late glacial continental dust in the Greenland Ice Core Project ice core, Journal of Geophysical Research-Atmospheres, 105, 4637-4656, 10.1029/1999jd901093, 2000.

Svensson, A., Dahl-Jensen, D., Steffensen, J. P., Blunier, T., Rasmussen, S. O., Vinther, B. M., Vallelonga, P., Capron, E., Gkinis, V., Cook, E., Kjaer, H. A., Muscheler, R., Kipfstuhl, S., Wilhelms, F., Stocker, T. F., Fischer, H., Adolphi, F., Erhardt, T., Sigl, M., Landais, A., Parrenin, F., Buizert, C., McConnell, J. R., Severi, M., Mulvaney, R., and Bigler, M.: Bipolar volcanic synchronization of abrupt climate change in Greenland and Antarctic ice cores during the last glacial period, Climate of the Past, 16, 1565-1580, 10.5194/cp-16-1565-2020, 2020.

Taylor, K. C., Alley, R. B., Lamorey, G. W., and Mayewski, P.: Electrical measurements on the Greenland Ice Sheet Project 2 core, Journal of Geophysical Research-Oceans, 102, 26511-26517, 10.1029/96jc02500, 1997.

Timmreck, C., Pohlmann, H., Illing, S., and Kadow, C.: The impact of stratospheric volcanic aerosol on decadal-scale climate predictions, Geophysical Research Letters, 43, 834-842, 10.1002/2015gl067431, 2016.

Toohey, M. and Sigl, M.: Volcanic stratospheric sulfur injections and aerosol optical depth from 500 BCE to 1900 CE, Earth System Science Data, 9, 809-831, 10.5194/essd-9-809-2017, 2017.

Toohey, M., Kruger, K., Schmidt, H., Timmreck, C., Sigl, M., Stoffel, M., and Wilson, R.: Disproportionately strong climate forcing from extratropical explosive volcanic eruptions, Nature Geoscience, 12, 100-+, 10.1038/s41561-018-0286-2, 2019.

Van Vliet-Lanoe, B., Bergerat, F., Allemand, P., Innocentd, C., Guillou, H., Cavailhes, T., Gudmundsson, A., Chazot, G., Schneider, J. L., Grandjean, P., Liorzou, C., and Passot, S.: Tectonism and volcanism enhanced by deglaciation events in southern Iceland, Quaternary Research, 94, 94-120, 10.1017/qua.2019.68, 2020.

Vapnik V. (1998) The Support Vector Method of Function Estimation. In: Suykens J.A.K., Vandewalle J. (eds) Nonlinear Modeling. Springer, Boston, MA. https://doi.org/10.1007/978-1-4615-5703-6_3

Veres, D., Bazin, L., Landais, A., Kele, H. T. M., Lemieux-Dudon, B., Parrenin, F., Martinerie, P., Blayo, E., Blunier, T., Capron, E., Chappellaz, J., Rasmussen, S. O., Severi, M., Svensson, A., Vinther, B., and Wolff, E. W.: The Antarctic ice core chronology (AICC2012): an optimized multi-parameter and multi-site dating approach for the last 120 thousand years, Climate of the Past, 9, 1733-1748, 10.5194/cp-9-1733-2013, 2013.

Watt, S. F. L., Pyle, D. M., and Mather, T. A.: The volcanic response to deglaciation: Evidence from glaciated arcs and a reassessment of global eruption records, Earth-Science Reviews, 122, 77-102, 10.1016/j.earscirev.2013.03.007, 2013.

Wolff, E. W.: The Antarctic ice core chronology (AICC2012): an optimized multi-parameter and multi-site dating approach for the last 120 thousand years, Climate of the Past, 9, 1733-1748, 10.5194/cp-9-1733-2013, 2013.

Zielinski, G. A., Mayewski, P. A., Meeker, L. D., Whitlow, S., and Twickler, M. S.: A 110,000-yr record of explosive volcanism from the GISP2 (Greenland) ice core, Quaternary Research, 45, 109-118, 10.1006/qres.1996.0013, 1996.

Zielinski, G. A., Mayewski, P. A., Meeker, L. D., Gronvold, K., Germani, M. S., Whitlow, S., Twickler, M. S., and Taylor, K.: Volcanic aerosol records and tephrochronology of the Summit, Greenland, ice cores, Journal of Geophysical Research-Oceans, 102, 26625-26640, 10.1029/96jc03547, 1997.

Chapter 3

Chapter contents

Pinpointing the ~74 ka Toba eruption from ice cores and estimating the volcanic radiative forcing of the 74.8-73.8 ka period

Jiamei Lin[1], Peter M. Abbott[2], Michael Sigl[2], Jørgen P. Steffensen[1], Robert Mulvaney[3], Mirko Severi[4], Anders Svensson[1]

[1]Physics of Ice, Climate and Earth, Niels Bohr Institute, University of Copenhagen, 2100, Denmark

[2]Climate and Environmental Physics, Physics Institute & Oeschger Center for Climate Change Research, University of Bern, Sidlerstrasse 5, Bern, Switzerland

[3]British Antarctic Survey, Cambridge, UK

[4]Department of Chemistry, University of Florence, Florence, Italy

Corresponding authors: Jiamei Lin (jm.lin@nbi.ku.dk), Anders Svensson (as@nbi.ku.dk)

This manuscript is under review at Quaternary Science Reviews. Date of submission: 01 May 2022

Abstract. The Younger Toba Tuff eruption occurring ~74 ka ago in Indonesia is among the largest known supereruptions in the Quaternary and its potential impact on the climate system and on human evolution remains controversially debated. The eruption is dated radiometrically to 73.88 ± 0.32 ka (1σ, Storey et al., 2012) and is known to have occurred at the abrupt cooling transition from Greenland Interstadial 20 to Greenland Stadial 20. The precise stratigraphic position of volcanic fallout detected in ice cores from both polar ice sheets has previously been narrowed down to four potential candidates. Here, we compile all available Greenland and Antarctic sulfate records, together with electrical conductivity records and recently obtained sulfur isotope records to quantify and characterize these Toba candidates in terms of their likely latitudinal position of eruption, sulfur emission strength and radiative forcing. We identify the youngest event of the four candidates to be composed of two separate eruptions, both likely located in the extra-tropical Northern Hemisphere. We deem the two older events unlikely candidates for the Toba eruption because of their limited sulfur emission strengths. The second youngest event is larger regarding sulfur output than the other Toba candidates, and it is also larger than any other volcanic event identified in ice core records over the last 60 kyr. Comparable amounts of sulfate deposits in Greenland and Antarctica strongly suggest a tropical

source. We thus propose the second youngest event to be most likely associated with the Toba eruption. A recent age revision for the Los Chocoyos supereruption occurred in Guatemala (74.8 ± 1.8 ka (1σ, Cisneros de León 2021)) may assign that eruption to one of the second older events. The estimated stratospheric sulfate aerosol loading of the proposed Toba eruption is 535 ± 96 Tg, which is 3.3 times that of Samalas 1258 CE, 6.3 times that of Tambora 1815 CE and 9.7 times that of Pinatubo 1991 CE. We derive the continuous time-series of volcanic sulfate deposition, sulfur emission strength and radiative forcing over the 74.8 - 73.8 ka time window, suitable for conducting experiments with climate models that either require prescribed forcing field or interactively reproduce aerosol processes. We estimate the cumulative volcanic sulfur emission strength and the radiative forcing of the two younger events that are found to be much stronger than those at the onset of the Youngers Dryas and those preceding the Little Ice Age. Stacked Greenland water isotopes record show an accelerated transition trend and abrupt shift after the proposed Toba eruption and suggest that the Greenland moisture source moved southward shortly after the Toba eruption. The Toba eruption may thus have an amplifying effect on the cooling transition leading to Greenland Stadial 20.

3.1 Introduction

The Youngest Toba Tuff (Toba) eruption in Indonesia is among the largest known supereruptions over the past 2.5 million years with 2500–3000 kg m^3 of magma deposited (Rose and Chesner, 1987; Chesner et al., 1991). The eruption has been accurately dated by $^{40}Ar/^{39}Ar$ to occur at 73.88 ± 0.32 ka in Malaysia (1σ, Storey et al., 2012) and at 75.0 ± 0.9 ka in India (1σ, Mark et al., 2014). Ash from the eruption was widely discovered in marine sediments from the Arabian Sea (Von Rad et al., 2001), the Indian Ocean (Shane et al., 1995) and the South China Sea (Song et al., 2000; Huang et al., 2001; Liu et al., 2006; Buhring et al., 2000), in lake sediment at Lake Malawi in Africa (Lane et al., 2013), and across Indian peninsular (Pearce et al., 2014). Although, to date, no tephra has been identified in ice cores (Abbott et al., 2012), the identified ash layers in the marine sediment records of the Arabian Sea strongly suggests that the eruption occurred at the cooling transition from Greenland Interstadial 20 (GI-20) to Greenland Stadial 20 (GS-20) (Schulz et al., 1998; Deplazes et al., 2013). In this interval, four volcanic sulfate events identified in both Greenland and Antarctic ice cores have been proposed as Toba candidates (named T1, T2, T3 and T4; Svensson et al., 2013) that are dated to 74,057, 74,156, 74,358 and 74,484 a b2k, respectively, using the Greenland GICC05modelext time scale.

Recently, Antarctic ice-core sulfur isotope analysis has been applied to determine the T1 and T2 events as the most likely candidates for the Toba eruption (Crick et al., 2021).

A large explosive eruption can heavily disturb the regional and global climate through direct impact of the stratospheric sulfate aerosol burden and also through feedbacks involving the ocean and atmospheric circulations (Robock, 2000; Pausata et al., 2015; Mcconnell et al., 2020; Sigl et al., 2015). It has been suggested that the Toba eruption is associated with a human population bottleneck that occurred in the period of 50-100 ka period (Rampino and Self, 1993; Ambrose, 1998). However, this hypothesis has been challenged as continued human activity is suggested (Ge and Gao, 2020), and modern humans appeared not to be strongly impacted by the Toba eruption at a South African site (Smith et al., 2018; Jackson et al., 2015) as well as in India (Clarkson et al., 2020; Mark et al., 2014) indicating the cooling impact on those areas may have been less severe.

The magnitude of the stratospheric sulfate loading from past eruptions, commonly derived from the volcanic sulfate depositions on the polar ice sheets, is key to estimate the cooling effect of past eruptions. For the recent volcanic eruptions occurred in the last 2500 years, Sigl et al. (2015) established a strong relationship between the reconstructed post-eruption temperature cooling estimated from tree ring records and the enhanced stratospheric sulfate aerosol burden estimated from ice cores. The sulfur emission strength of the Toba eruption, estimated using petrological evidence, has a wide range from 105 Tg to 9,900 Tg of emitted sulfate, that is almost 10 to 360 times that of the Mt Pinatubo 1991 CE eruption (Chesner and Luhr, 2010; Scaillet et al., 1998; Oppenheimer, 2002). The debate on the climatic consequences of the Toba eruption is strongly tied to the poorly constrained sulfur emission strength in model simulations. Model simulations of the Toba eruption applying 5 - 900 times the SO_2 emission of the 1991 Pinatubo eruption used the idealized stratospheric chemistry or aerosol micro-physics mechanism and suggested a 2.3 -17.0 °C mean global cooling following the eruption (Osipov et al., 2020; Black et al., 2021; Robock et al., 2009), in comparsion to the ~0.5 °C global cooling following the 1991 Pinatubo eruption.

Whether a single volcanic eruption could have triggered abrupt climate change, such as the onset of Dansgaard-Oeschger (DO) events in glacial period (Lohmann et al., 2022; Baldini et al., 2015), or have accelerated the deglaciation in the Southern Hemisphere (Mcconnell et al., 2017), or whether a cluster of volcanic eruptions could lead to an extended period of climate cooling and ice growth (Abbott et al., 2021; Miller et al., 2012) are topics currently being debated. Pinpointing the precise position of the Toba eruption in the cooling transition leading to GS-20

will help to explore these questions and to decipher the involved mechanisms. A recent dating of the Los Chocoyos eruption of Atitlán volcano that occurred in Guatemala at 75 ± 2 ka (Cisneros De León et al., 2021) opens the possibility that two supereruptions occurred close to the onset of GS-20 and, in combination, could have triggered the GS-20 cooling (Paine et al., 2021). Volcanic forcing needs to be better constrained and incorporated in model simulations to better understand the role of volcanism associated with the onset of GS-20 and other abrupt climate transitions in the glacial period.

In this study, we compile all available sulfate, conductivity and electrical conductivity measurement (ECM) records from Greenland and Antarctic ice cores to reassess the Toba candidates and estimate the associated volcanic sulfate deposition in Greenland and Antarctica. Sulfate records from three Greenland and two Antarctic ice cores are firstly utilised to derive the volcanic sulfate deposition. Although Toba candidates have been previously identified from polar ice cores (Svensson et al., 2013) and the ice-core sulfur isotope signal has been used to indicate the altitude of eruption plume (Crick et al., 2021), the exact position of the Toba eruption in the ice-core records has not been determined. Here, we predict the latitudinal band of eruption site based on the method of Lin et al., (2022) and use the sulfur emission strength from our reconstruction to pinpoint the Toba eruption. Furthermore, we estimate the sequenced sulfur emission strengths and reconstruct the spatial-temporal volcanic radiative forcing at the cooling transition to GS-20 (74.8-73.8 ka b2k) using the synchronized sulfate records of Greenland and Antarctic ice cores. Unless otherwise stated, all ages in this study are referring to the model extended Greenland Ice Core Chronology 2005 (GICC05) (Rasmussen et al., 2014) using the datum 2000 AD (b2k).

3.2 Methods

We employed five sulfate records from three Greenland ice cores – an Ion Chromatography (IC) sulfate record of the Greenland Ice Core Project (GRIP) ice core (this work), a Fast Ion Chromatography (FIC) sulfate record of the North Greenland Eemian Ice Drilling (NEEM) ice core (Schupbach et al., 2018), a CFA record from the North Greenland Ice Core Project (NGRIP) ice core (Svensson et al., 2013) and two IC sulfate records from the Greenland Ice Sheet Project 2 (GISP2) ice core (Mayewski et al., 1997; Yang et al., 1996). Four sulfate records from two Antarctic ice cores are used - two records measured by FIC and IC from the EPICA Dome C (EDC) ice core (Crick et al., 2021; Svensson et al., 2013) and two records measured by FIC and IC from the EPICA Dronning Maud Land (EDML) ice core (Svensson et

al., 2013; Crick et al., 2021) (Fig. S1, Table S1 and Table S2). From those records, we derive the polar volcanic sulfate depositions for the period 74,800-73,800 a b2k (Fig. S2 and Table S3). For Greenland, the effective time resolution of sulfate measurements range is 1-2 years for NGRIP (Svensson et al., 2013), 1-5 years for GISP2 (Yang et al., 1996), 5-10 years for GRIP (this work), 10 years for NEEM (Schupbach et al., 2018) and 50-150 years for GISP2 (Mayewski et al., 1997). For Antarctica, the temporal time resolution of EDML and EDC sulfate measurements fall in the range of 1-3 years (Svensson et al., 2013). The EDML and EDC sulfate records from Crick et al. (2021) were solely sampled for Toba candidate peaks, as identified by Svensson et al. (2013), in 1-8 years temporal time resolution. Due to the magnitude of the Toba candidates, those events are detectable in sulfate records of lower temporal resolution.

Using the T1-T4 Toba candidates identified in the NGRIP, GRIP, GISP2, EDC and EDML ice cores by Svensson et al. (2013), we linearly interpolated the GICC05 time scale for the period of 74.8-73.8 ka b2k for those cores. For the NEEM core, we apply the volcanic synchronizations between the NEEM and NGRIP cores (Rasmussen et al., 2013) to the identify Toba candidates in NEEM and make a similar linear interpolation. We then identify all of the volcanic sulfate events in Greenland and Antarctic ice cores during the 74.8-73.8 ka b2k period. If volcanic sulfate signals are identified in both Greenland and Antarctic ice cores within the annual layer counting uncertainty, we define them as bipolar volcanic events, otherwise, we classify them as unipolar events.

We applied established methods to distinguish volcanic sulfate signals from sulfate background and derive the volcanic sulfate content of the ice (Fischer et al., 1998; Gao et al., 2007; Karlof et al., 2005; Sigl et al., 2013; Lin et al., 2022). For each core, an ice-core flow model is applied to correct for layer thinning and to obtain volcanic sulfate deposition (Table S2; Bazin et al., 2013; Johnsen et al., 2001; Hvidberg et al., 1997; Rasmussen et al., 2013; Lin et al., 2022). The average volcanic sulfate deposition in Greenland is obtained by averaging all of the sulfate records for the same volcanic event. Due to the large distance among the Antarctic ice-core sites and the accumulation dependence of the sulfate deposition, we apply weighing factors for the two involved ice cores to obtain the average volcanic sulfate deposition following the approach of Lin et al. (2022). These weighing factors are based on the relative ratio of volcanic sulfate depositions in three synchronized (Buizert et al., 2018) Antarctic ice cores (WAIS Divide Ice Core, EDML and EDC) for the 30 largest bipolar eruptions occurred in the 60-9 ka period. The derived weighing factors for EDML and EDC are 1.15 and 1.39, respectively. The relative sulfate deposition in Greenland and Antarctica can be used to estimate the latitudinal band of the

eruption site for bipolar volcanic events. We applied the same method as Lin et al. (2022) to classify the volcanic latitudinal bands - above 40°N, Northern Hemisphere High Latitude (NHHL), and below 40°N, Low Latitude or Southern Hemisphere (LL or SH) - for bipolar events (Table 3.1 and Table S3.3). From the polar volcanic sulfate depositional values, the stratospheric sulfate loading can be estimated and the associated volcanic radiative forcing can be reconstructed (Toohey and Sigl, 2017; Gao et al., 2008). We estimate the stratospheric sulfate loading by the transfer function of Gao et al. (2007). We then apply the EVA_H model to estimate the stratospheric sulfate aerosol optical depth (SAOD) from the stratospheric sulfate loading (Aubry et al., 2020) using default parameters for plume height and source location taken from historical analogue eruptions. For the EVA_H model, the injection conditions - altitude and latitude parameters - for unipolar eruptions follow an Eldgjá 939 CE like eruption (12.5 km altitude, 60°N or 60°S), for the bipolar (NHHL) eruptions an Okmok 43 BCE like eruption (24 km altitude, 40°N) is applied, and for the bipolar (LL or SS) eruptions a Tambora 1815 CE like eruption (24 km altitude, 0°N) is applied. The tropopause height is defined as the average value of tropopause height from 1979 to 2016 (Thomason et al., 2018). The eruption date of unknown volcanoes is set to 1 January consistent with previous work (Crowley and Unterman, 2013; Toohey and Sigl, 2017). To obtain the aerosol radiative forcing from SAOD we use the scaling factor of Marshall et al. (2020).

3.3 Results and Discussion

3.3.1 Zooming in on the Toba candidates

We compile multiple ice-core sulfate, ECM and conductivity records and derive the related volcanic sulfate deposition for the four Toba candidates - T1, T2, T3 and T4 (Fig. S3.1, Table S3.2 and Fig. S3.2). For the EDC sulfate records, one volcanic sulfate peak, originally labelled as T4b by Crick et al., (2021), is repositioned at the T4 event due to a correction of that dataset (see corrigendum to Crick et al., 2021). Using the high-resolution NGRIP sulfate record and the high-resolution conductivity records of NEEM and NGRIP, it becomes evident that the Greenland T1 event is composed of two separate volcanic sulfate peaks, named as T1a and T1b, that are separated by about 12 years (peak to peak) (Fig. S3.3 (a)). There is a ‘dead’ period (no volcanic sulfate signal above background) of around 6 years duration between the two events, confirming that the T1 event is composed of two distinct volcanic events (Fig. S3.3 (a)). Adjacent volcanic sulfate peaks can be merged in low-resolution sulfate records, but such occurrences can be

identified in high-resolution DEP or ECM records of the same core. We manually separate the merged sulfate peak of the T1 events detected in the GISP2 and NEEM sulfate records by the associated area ratio of high-resolution DEP or ECM peaks of the same core and derive the volcanic sulfate depositions (Fig. S3.1 and Table S3.2).

As only one volcanic sulfate peak of the T1 event is detected in Antarctic ice cores (EDC and EDML), the counterpart signal in Greenland is proposed to be the T1b event. This is based on the annual layer counting, for which the period between the T2 and T1 events in Antarctica (EDML) is 84 ± 7 yrs and in Greenland (NGRIP) the period between the T2 and T1b events is 87 ± 6 yrs (Fig.7 in Svensson et al. (2013)). As the annual layer counting between the T1a and T1b events in Greenland (NGRIP) is 12 years, it is most likely that T1b is the bipolar volcanic event. However, as exact annual layer counting is challenging at this depth, we can not firmly rule out that the T1a event is related to the T1 event in Antarctica.

*Table 3.1 Volcanic sulfate deposition of Greenland and Antarctica, stratospheric aerosol loading and erupted latitude prediction for Toba candidates, compared to well-known eruptions-Pinatubo, Tambora, Salamas, Taupo and the largest unknown eruption at 45.56 ka b2k. * represents the largest eruption in the period of 60-0 ka.*

Eruption	Volc. age GICC05	Volc. duration	Antarctic volc. SO4	Greenland volc. SO4	Predicted erupted latitude	Stratospheric sulfate loading	Aerosol optical depth	Global aerosol radiative forcing	Number of ice cores		
	a b2k	yrs	kg km^{-2}	kg km^{-2}		Tg		W m^{-2}	Greenland	Antarctica	Reference
T1a	74045	10		292.6	Unipolar	166.8	0.59	-9.19	5		This study
T1b	74057	5-16	97.6	212.7	Bipolar (NHHL)	218.9	0.70	-10.46	5	4	This study
T2	74156	7-18	290.0	244.5	Bipolar (LL or SH)	534.6	1.28	-14.92	4	4	This study
T3	74358	4-15	150.6	73.6	Bipolar (LL or SH)	224.2	0.71	-10.57	3	4	This study
T4	74484	5-12	207.2	115.4	Bipolar (LL or SH)	322.6	0.91	-12.38	3	4	This study
Pinatubo	1991 CE	0.5-2	18.2	37.2	15°8'N, 120°21'E	55.4	0.28	-5.08	1	1	Sigl et al., 2013
Tambora	1815 CE	2-3	45.8	39.7	8°15'S, 118°E	85.5	0.38	-6.49	1	2	Sigl et al., 2015
Salamas	1258 CE	2.4-3.8	90.4	73.2	8°42'S, 116°24′E	163.6	0.58	-9.10	1	2	Sigl et al., 2015
Taupo	24.46 ka b2k	3-7	192.8	189.5	Bipolar (LL or SH)	382.3	1.02	-13.24	2	3	Lin et al., 2022
Unknown*	45.56 ka b2k	6-14	172.7	652.6	Bipolar (NHHL)	544.7	1.29	-15.01	3	3	Lin et al., 2022

3.3.2 Tracing the Toba eruption

In the following, we will combine multiple lines of evidence to propose the likeliest candidate for the Toba event from the four Toba candidates. From the Greenland and Antarctic sulfate deposition derived in this study, we have estimated the sulfur emission strength of the individual eruptions. The ratio of volcanic sulfate deposition in Greenland and Antarctica provides an

approach to predict the latitudinal band of the eruption site (NHHL, and LL or SH). In addition, the ice-core sulfur isotopic composition of the Toba candidates indicates whether the eruption plume reached the stratosphere and provides an indication of the height of the eruption plume (Savarino et al., 2003; Crick et al., 2021).

As discussed in section 3.3.1, the T1 event is suggested to be associated with two separate events (T1a and T1b), of which the T1b event is most likely to be related to the Antarctic T1 event, and the T1a event is proposed to be a Northern Hemisphere extratropical eruption with no imprint in Antarctic ice cores (NHHL). Independent of which of the two Greenland events is bipolar, the rather low T1 Antarctic sulfate deposition compared to the T1a or T1b sulfate depositions in Greenland strongly suggests that both events are related to eruptions that occurred above 40°N. The clear Northern Hemispheric dominance of the T1a and the T1b events thus makes both of them unlikely to originate from the Toba eruption.

The T2 event has by far the largest stratospheric sulfate loading of the four Toba candidates (Fig.3.1 (b)). It is also stronger than any bipolar eruption signal identified from ice cores in the 60-9 ka period (Lin et al., 2022). The even distribution of sulfate deposition between the two

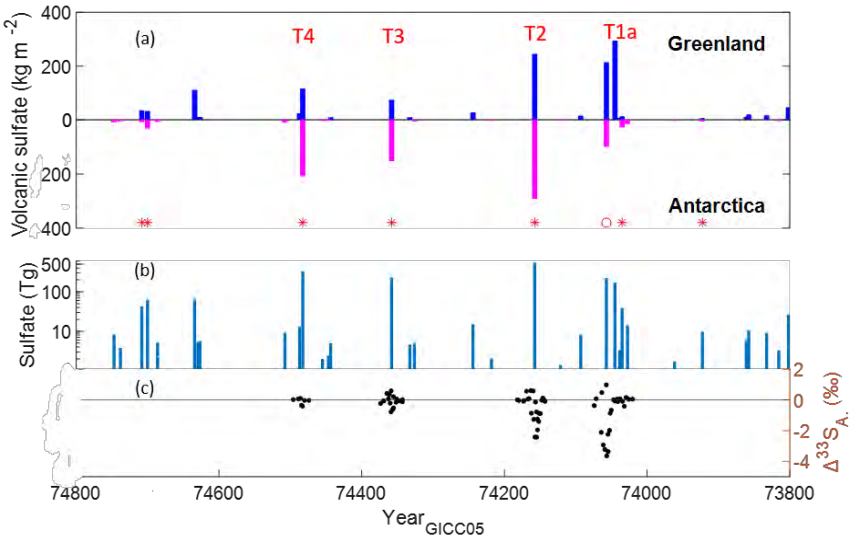

Figure 3.1 Ice-core derived volcanic sulfate depositions in Greenland and Antarctica. '' denotes that the predicted latitudinal band of eruption site occurred below 40°N (LL or SH) and 'o' denotes ones occurred above 40°N (NHHL) for bipolar volcanic eruptions. (b) The stratospheric sulfate loading derived from Greenland and Antarctic volcanic sulfate depositions list. (c) The sulfur isotope $\Delta^{33}S$ measured by Crick et al. (2021) from Antarctic ice cores for the Toba candidates.*

hemispheres (Greenland versus Antarctica) suggests the event occurred at low latitudes (Fig.3.1 (a) and Table 3.1). The Antarctic sulfur isotopic composition shows that the eruption plume

reached the stratosphere and that the top of plume height may have exceeded 45 km (Crick et al., 2021). Therefore, the T2 event fulfils all criteria for being related to the Toba eruption.

The T3 event has a sulfur emission strength about four times that of the Pinatubo, 1991 CE eruption, but it is weaker than those of the T2 and T4 events. The hemispheric sulfate distribution of the T3 event suggests that the event occurred below 40°N. The Antarctic sulfur isotopic signals of the T3 event suggests that the eruption plume reached the stratosphere, but the top of the plume height is lower than those of the T2 and T1 events (Fig.3.1 (c) (Crick et al., 2021). Overall, this implies that the T3 event was not of a sufficient magnitude to be associated with the Toba eruption.

The sulfate emission strength of the T4 event is larger than that of the T3 event but smaller than that of the T2 event. The relative hemispheric sulfate depositions in Greenland and Antarctica implies that the eruption site was most likely in the tropics or the Southern Hemisphere. The magnitude of the Antarctic sulfur isotopic signals suggests that the eruption plume of the T4 event did not reach the ozone layer (Crick et al., 2021) (Fig.3.1 (c)). For this reason, the T4 event is unlikely to be associated with the Toba eruption.

A recent (U–Th)/He dating age of the Los Chocoyos (LC) eruption of the Atitlán volcano, that occurred in present-day Guatemala, is 75 ± 2 ka (Cisneros De León et al., 2021) suggesting that the eruption may have occurred close to or within the cooling transition leading to GS-20 and thus close to the Toba eruption (Paine et al., 2021). As the stratigraphic setting of the Toba eruption is right at the cooling transition leading to GS-20 in several marine records (Fig. S6 in Deplazes et al., 2013; Fig. 3 in Schulz et al., 1998), we know for certain that the Toba eruption has to be found among the T1-T4 events. With the T2 event is being associated with the Toba eruption that event can not be related to the LC eruption. An additional argument for the T2 event being related to the Toba eruption is the magnitude and the relative dimensions of the Toba and LC calderas. The Toba eruption is suggested to be the largest known eruption in the Quaternary with a magnitude of 8.8 compared to the LC eruption with an estimated magnitude of 8.1 (Kutterolf et al., 2016; Storey et al., 2012; Paine et al., 2021). The Toba caldera is 100×30 km, ~900 m depth (Rose et al., 1987) and the Atitlán caldera is 18×12 km, ~600 m depth (Newhall, 1987). If the T2 event is the Toba eruption, the T1a and T1b events are related to the NH extratropical eruptions, and the eruption plume of the T4 is mostly constrained to the troposphere, the T3 event appears the most likely candidate for the LC eruption. Another option is that the LC eruption could be related to another large volcanic signal outside our investigated time frame.

The stratospheric aerosol loading of the T2 event is estimated to be 1.4 times that of the Oruanui,Taupo (New Zealand, VEI-8) supereruption dated 25.37± 0.25 ka in the annual-layer counted WD2014 chronology from Antarctica (Sigl et al., 2016), which remains the only supereruption ever identified in an ice core through cryptotephra fingerprinting (Dunbar et al., 2017) and its sulfur emission strength is ranked fourth in the ice-core volcano list of the last 60 ka (Lin et al., 2022). In terms of stratospheric aerosol loading, the T2 eruption is comparable to the largest eruption identified in the 60-9 ka period, that occurred at 45.56 ka b2k. However, as the 45.56 ka b2k eruption most likely occurred in the extratropical NH (Lin et al., 2022), the T2 event is suspected to have the strongest volcanic impact of the two based on the assumption that the sulfate aerosol burden time of tropical eruptions is longer than that of extratropical NH eruptions (Marshall et al., 2019). The climatic impact of these most recent large bipolar eruptions - Samalas 1257 CE, Tambora 1815 CE and Pinatubo 1991CE – was a lowering of the global mean temperature of 0.5-1.2°C, which lasted for several years (Brazdil et al., 2010; Parker et al., 1996; Guillet et al., 2017). The stratospheric aerosol loading of the T2 event is 3.3 times that of Samalas, 6.3 times that of Tambora and 9.7 times that of Pinatubo, indicating that a more extreme cooling could have followed the Toba eruption (Table 3.1).

Compared to the wider range of the sulfur emission strength estimated from petrological evidence (10 to 360 times that of the Pinatubo eruption), we estimate a stratospheric sulfate loading of 535 ± 96 Tg derived from ice cores for the Toba eruption, that is 8-10 times that of the Pinatubo eruption. This estimate supports the relatively low sulfur emission scenarios in model simulations for the Toba eruption (Black et al., 2021; Osipov et al., 2021; Robock et al., 2009; Timmreck et al., 2012). Black et al. (2021) found that 300 Tg of stratospheric sulfate loading led to a 2.3 ± 0.4 °C lowering of the annual mean global surface temperature.

3.3.3 Volcanic forcing at the GS-20 onset and comparison with other periods of enhanced volcanic activity

There are 35 volcanic eruptions identified from polar ice cores in the investigated period of 74.8-73.8 ka b2k (Table S3.3). Among them, eight volcanic sulfate signals are identified as bipolar volcanic eruptions with stratospheric sulfate loading above 10 Tg. Fourteen volcanic sulfate signals are only identified in Greenland ice cores and 13 volcanic sulfate signals are identified only in Antarctica. The global mean and the 30°- 90°N mean of the SAOD as well as the radiative forcing are reconstructed over this period (Table S3.4).

We define the 'Toba' period at the end of the cooling transition leading to GS-20 as 74,158-74,045 a b2k, and we compare this interval to younger periods of enhanced volcanic activity that are associated with long-term cooling and ice growth. The 'Toba' interval contains three major eruptions (T1a, T1b and T2). The three periods selected for comparison are located at the onset of Youngers Dryas event (YD_S, 13030-12921 a b2k), at the start of the Little Ice Age (LIA_S, 1171-1286 CE) and at the end of the Little Ice Age (LIA_E, 1783-1890 CE), following

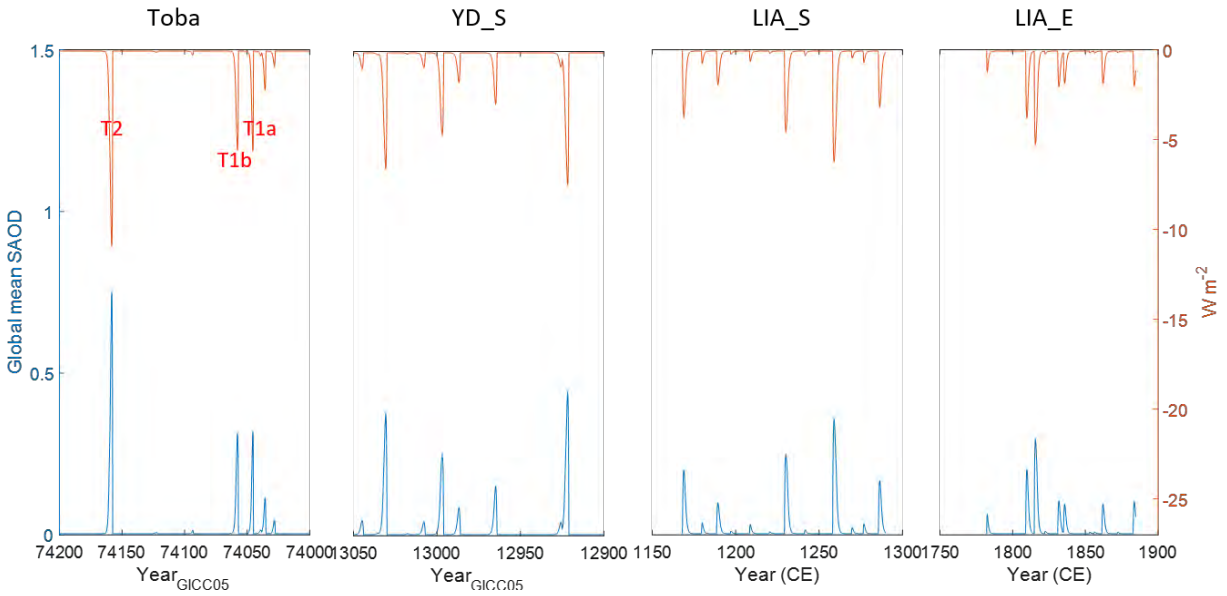

Figure 3.2 Comparison of monthly global mean SAOD and estimated volcanic radiative forcing for the enhanced volcanic period of 74158-74045 (a b2k) including the Toba candidates (T2, T1a and T1b) to the three well investigated periods – at the onset of Youngers Dryas (13030-12921 a b2k; Abbott et al., 2021; labelled as YD_S), the Little Ice Age (1171-1286 CE; labelled as LIA_S), and Little Ice Age (1783-1890 CE; labelled as LIA_E; Toohey & Sigl, 2017).

the approach of Abbott et al. (2021) (Fig. 3.2 and Table S3.5). For these three volcanically enhanced periods, we applied the same approach as Lin et al. (2022) to estimate the stratospheric aerosol loading and to reconstruct the volcanic radiative forcing from the published Greenland and Antarctic volcanic sulfate deposition records (Abbott et al., 2021; Sigl et al., 2013; Table S5). The results presented here differ from those of Abbott et al. (2021) due to the different weighing of the Greenland volcanic sulfate deposition applied to derive the stratospheric aerosol loading for extratropical NH bipolar eruptions. Here we assume that volcanic sulfate transport and deposition over Greenland is influenced by the polar vortex transport patterns (Gao et al., 2007). Using this approach, the centennial cumulative stratospheric aerosol loading for the volcanic active periods - YD_S, LIA_S and LIA_E - are respectively 40%, 8% and 7% lower

than those estimated by Abbott et al. (2021) and Toohey and Sigl (2017). The centennial cumulative stratospheric aerosol loading, the mean global SAOD and the mean SAOD at 30-90°N of the 'Toba' period is much stronger than those of the other three periods (Table S3.5). Due to the distinct volcanic cluster and the extreme volcanic forcing at the onset of the GS-20, we speculate in the following about the possibility of an amplified and prolonged cooling beyond the stratospheric sulfate aerosol burden induced cooling.

3.3.4 Potential longer-term climatic impact of the T1 and T2 eruptions

The behaviour of the ice-core water isotopic proxies - $\delta^{18}O$ and deuterium excess (d-excess) - at the T1 and T2 events may provide clues about the climatic impact of those eruptions in both hemispheres.

For Greenland, we calculate the anomaly of the water isotopic signal over the period of 75.0-73.0 ka b2k by quantifying the integration of the negative peak area of the NGRIP and NEEM $\delta^{18}O$ records in 5 cm resolution (3-18 yrs temporal resolution) below a 101 and 201-yrs moving average, respectively (Fig. S3.4). A merged negative peak is detected in both $\delta^{18}O$ records following the T1a and T1b events. In terms of the empirical cumulative distribution of the magnitude of negative peaks for the NEEM and NGRIP $\delta^{18}O$ records, the fractions of the merged peak related to the T1a and T1b events are both below 10%, while there is no obvious dip following the T2 event (Fig. S3.4). The reason for the stronger Greenland impact of the T1a and T1b events may be that both are predicted to have occurred above 40°N as opposed to the T2 event that originates in the tropics.

Using the stacked $\delta^{18}O$ record from four $\delta^{18}O$ records of the NGRIP (North Greenland Ice Core Project members, 2004), GISP2 (Grootes and Stuiver, 1997), NEEM (Gkinis et al., 2021) and GRIP (Johnsen et al., 2001) cores (Fig. S3.5 (d-g)), we observe an accelerated cooling transition (a steepening of the isotopic trend) right after the T2 event for a 110 yrs period leading to the GS-20 (Fig.3.3 (c)). The interpretation of this increased cooling trend could be that the very large volcanic eruption induced a cooling of the atmosphere and the upper mixed ocean, leading to increased sea-ice cover in the North Atlantic. This hypothesis is supported by the NGRIP and NEEM d-excess records (Svensson et al., 2013; Gkinis et al., 2021), a proxy for the temperature of the Greenland vapor source areas (Steffensen et al., 2008). Both the individual and the stacked d-excess records show an abrupt shift right at the T2 eruption (Fig. 3.3 (a) and Fig. S3.5 (b, c)), suggesting a southern shift of the water vapor source resulting from the extended sea ice cover.

The $\delta^{18}O$ records of the EDML (EPICA community members, 2006), EDC (EPICA community members, 2004), and Dome F (Kawamura et al., 2007) ice cores in Antarctica do not indicate any extended cooling following the T2 eruption (Fig.3.3 (d) and Fig. S3.5 (h)). However, there is a short-term warming after the T1 eruption recorded only in the EDC $\delta^{18}O$ record (Fig. S3.5 (i)), indicating the uneven regional temperature followed the T1 eruption in Antarctica. An interpretation of this behaviour is that the Greenland and Antarctic temperature proxies follow a 'bipolar seesaw' pattern and the NH extended sea ice cover triggered by the T2 eruption may weaken the Atlantic meridional overturning circulation and induce a delayed

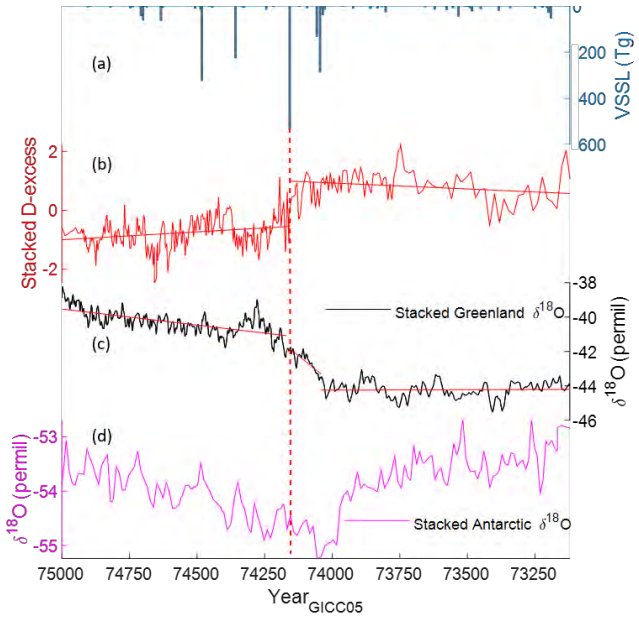

Figure 3.3 Abrupt climate variability at the termination of GI-20. (a), The volcanic stratospheric sulfate loading (VSSL). (b), The stacked normalized NGRIP and NEEM deuterium excess records. Two disconnected linear fits (intervals: >74156, 74156-73121) represent in red color. (c), The stacked δ18O records of NGRIP, NEEM, GISP2 and GRIP ice cores in Greenland. Three disconnected linear fits (intervals: >74156, 74156-74041, 74041-73121) represent in red color. (d), The stacked $\delta^{18}O$ records of EDC, EDML and DF ice cores in Antarctica.

warming in Antarctica that is most likely perturbed by the strong T1 eruption. This mechanism is in an agreement with the interpretation of Stocker and Johnsen. (2003) and with model simulation results (Robock et al., 2009; Timmreck et al., 2012).

3.4 Conclusions

We pinpoint the Toba eruption from ice-core records with the combined information from synchronized high-resolution impurity records, the sulfur isotopic signals, the sulfate emission strength and the estimated latitudinal band of eruption sites. From the previously identified Toba

candidates - T1, T2, T3 and T4, we propose the T2 event to be related to the Toba eruption, because the T2 event has a clear tropical origin and its sulfur emission strength is larger than the other Toba candidates and than any other volcanic events identified in ice core records over the last 60 kyr. Previous estimates of the Toba eruption using a single ice-core, mineral chemistry or experimental petrology have produced a wide range of emitted sulfate from 105 Tg to 9,900 Tg. Here, the estimated stratospheric sulfate loading of the proposed Toba eruption is 535 ± 96 Tg, which is 3.3 times that of Samalas 1258 CE, 6.3 times that of Tambora 1815 CE and 9.7 times that of Pinatubo 1991 CE. Further support for this proposition could be gained if tephra from the Toba eruption was found in direct association with the T2 chemical signal, however, tephra investigations of NGRIP for all the Toba candidates did not yield any glass shards (Abbott et al., 2012).

Within one thousand years of volcanic reconstruction at the cooling transition to Greenland Stadial 20, thirty-five volcanic eruptions have been identified. Towards the end of this period, three major eruptions -T1a, T1b and T2 – show an extreme volcanic forcing that is unparalleled in later periods such as at the onset of the Younger Dryas period and the Little Ice Age. Following the proposed Toba eruption, an abrupt shift is observed in Greenland temperature proxies, suggesting that the climatic forcing of the Toba eruption has accelerated the cooling transition leading to the extremely cold GS-20 period, possibly due to an extended sea-ice extension in the North Atlantic. The reconstructed volcanic forcing can be incorporated in model simulations in order to investigate mechanisms of abrupt climate change, and to quantify the global climatic impact of the Toba eruption and the volcanic cluster occurring at the cooling transition leading to GS-20.

3.5 References

Abbott, P. M., Niemeier, U., Timmreck, C., Riede, F., McConnell, J. R., Severi, M., Fischer, H., Svensson, A., Toohey, M., Reinig, F., and Sigl, M.: Volcanic climate forcing preceding the inception of the Younger Dryas: Implications for tracing the Laacher See eruption, Quaternary Science Reviews, 274, 10.1016/j.quascirev.2021.107260, 2021.

Abbott, P.M., Davies, S.M., Steffensen, J.P., Pearce, N.J.G., Bigler, M., Johnsen, S.J., Seierstad, I.K., Svensson, A., Wastegård, S. (2012) "A Detailed Framework of Marine Isotope Stage 4 and 5 Volcanic Events recorded in two Greenland Ice-cores", Quaternary Science Reviews 36, 59-77.

Ambrose, S. H.: Late Pleistocene human population bottlenecks, volcanic winter, and differentiation of modern humans, Journal of Human Evolution, 34, 623-651, 10.1006/jhev.1998.0219, 1998.

Aubry, T. J., Toohey, M., Marshall, L., Schmidt, A., and Jellinek, A. M.: A New Volcanic Stratospheric Sulfate Aerosol Forcing Emulator (EVA_H): Comparison With Interactive Stratospheric Aerosol Models, Journal of Geophysical Research-Atmospheres, 125, 10.1029/2019jd031303, 2020.

Baldini, J. U. L., Brown, R. J., and McElwaine, J. N.: Was millennial scale climate change during the Last Glacial triggered by explosive volcanism?, Scientific Reports, 5, 10.1038/srep17442, 2015.

Bazin, L., Landais, A., Lemieux-Dudon, B., Kele, H. T. M., Veres, D., Parrenin, F., Martinerie, P., Ritz, C., Capron, E., Lipenkov, V., Loutre, M. F., Raynaud, D., Vinther, B., Svensson, A., Rasmussen, S. O., Severi, M., Blunier, T., Leuenberger, M., Fischer, H., Masson-Delmotte, V., Chappellaz, J., and Wolff, E.: An optimized multi-proxy, multi-site Antarctic ice and gas orbital chronology (AICC2012): 120-800 ka, Climate of the Past, 9, 1715-1731, 10.5194/cp-9-1715-2013, 2013.

Birkett, C. M. and Mason, I. M.: A NEW GLOBAL LAKES DATABASE FOR A REMOTE-SENSING PROGRAM STUDYING CLIMATICALLY SENSITIVE LARGE LAKES, Journal of Great Lakes Research, 21, 307-318, 10.1016/s0380-1330(95)71041-3, 1995.

Brazdil, R., Demaree, G. R., Deutsch, M., Garnier, E., Kiss, A., Luterbacher, J., Macdonald, N., Rohr, C., Dobrovolny, P., Kolar, P., and Chroma, K.: European floods during the winter 1783/1784: scenarios of an extreme event during the 'Little Ice Age', Theoretical and Applied Climatology, 100, 163-189, 10.1007/s00704-009-0170-5, 2010.

Black, B. A., Lamarque, J. F., Marsh, D. R., Schmidt, A., and Bardeen, C. G.: Global climate disruption and regional climate shelters after the Toba supereruption, Proceedings of the National Academy of Sciences of the United States of America, 118, 10.1073/pnas.2013046118, 2021.

Buizert, C., Sigl, M., Severi, M., Markle, B. R., Wettstein, J. J., McConnell, J. R., Pedro, J. B., Sodemann, H., Goto-Azuma, K., Kawamura, K., Fujita, S., Motoyama, H., Hirabayashi, M., Uemura, R., Stenni, B., Parrenin, F., He, F., Fudge, T. J., and Steig, E. J.: Abrupt ice-age shifts in southern westerly winds and Antarctic climate forced from the north, Nature, 563, 681-+, 10.1038/s41586-018-0727-5, 2018.

Buhring, C., Sarnthein, M., and Leg 184 Shipboard Sci, P.: Toba ash layers in the South China Sea: Evidence of contrasting wind directions during eruption ca. 74 ka, Geology, 28, 275-278, 10.1130/0091-7613(2000)028<0275:Talits>2.3.Co;2, 2000.

Burke, A., Moore, K. A., Sigl, M., Nita, D. C., McConnell, J. R., and Adkins, J. F.: Stratospheric eruptions from tropical and extra-tropical volcanoes constrained using high-resolution sulfur isotopes in ice cores, Earth and Planetary Science Letters, 521, 113-119, 10.1016/j.epsl.2019.06.006, 2019.

Cisneros de León, A., Mittal, T., de Silva, S. L., Self, S., Schmitt, A. K., and Kutterolf, S.: On Synchronous Supereruptions, Frontiers in Earth Science, 10, 10.3389/feart.2022.827252, 2022.

Chesner, C. A. and Luhr, J. F.: A melt inclusion study of the Toba Tuffs, Sumatra, Indonesia, Journal of Volcanology and Geothermal Research, 197, 259-278, 10.1016/j.jvolgeores.2010.06.001, 2010.

Chesner, C. A., Rose, W. I., Deino, A., Drake, R., and Westgate, J. A.: Eruptive history of Earth's largest Quaternary caldera (Toba, Indonesia) clarified, Geology, 19, 200-203, 10.1130/0091-7613(1991)019<0200:Ehoesl>2.3.Co;2, 1991.

Clarkson, C., Harris, C., Li, B., Neudorf, C. M., Roberts, R. G., Lane, C., Norman, K., Pal, J., Jones, S., Shipton, C., Koshy, J., Gupta, M. C., Mishra, D. P., Dubey, A. K., Boivin, N., and Petraglia, M.: Human occupation of northern India spans the Toba super-eruption similar to 74,000 years ago, Nature Communications, 11, 10.1038/s41467-020-14668-4, 2020.

Crick, L., Burke, A., Hutchison, W., Kohno, M., Moore, K. A., Savarino, J., Doyle, E. A., Mahony, S., Kipfstuhl, S., Rae, J. W. B., Steele, R. C. J., Sparks, R. S. J., and Wolff, E. W.: New insights into the similar to 74 ka Toba eruption from sulfur isotopes of polar ice cores, Climate of the Past, 17, 2119-2137, 10.5194/cp-17-2119-2021, 2021.

Crowley, T. J. and Unterman, M. B.: Technical details concerning development of a 1200 yr proxy index for global volcanism, Earth System Science Data, 5, 187-197, 10.5194/essd-5-187-2013, 2013.

Deplazes, G., Luckge, A., Peterson, L. C., Timmermann, A., Hamann, Y., Hughen, K. A., Rohl, U., Laj, C., Cane, M. A., Sigman, D. M., and Haug, G. H.: Links between tropical rainfall and North Atlantic climate during the last glacial period, Nature Geoscience, 6, 213-217, 10.1038/ngeo1712, 2013.

Dunbar, N. W., Iverson, N. A., Van Eaton, A. R., Sigl, M., Alloway, B. V., Kurbatov, A. V., Mastin, L. G., McConnell, J. R., and Wilson, C. J. N.: New Zealand supereruption provides time marker for the Last Glacial Maximum in Antarctica, Scientific Reports, 7, 10.1038/s41598-017-11758-0, 2017.

EPICA community members: Eight glacial cycles from an Antarctic ice core, Nature, 429, 623–628, 2004.

EPICA community members: One-to-one coupling of glacial climate variability in Greeland and Antartctica, Nature, 444, 195–198, 2006.

Erhardt, T., Bigler, M., Federer, U., Gfeller, G., Leuenberger, D., Stowasser, O., Röthlisberger, R., Schüpbach, S., Ruth, U., Twarloh, B., Wegner, A., Goto-Azuma, K., Kuramoto, T., Kjær, H. A., Vallelonga, P. T., Siggaard-Andersen, M.-L., Hansson, M. E., Benton, A. K., Fleet, L. G., Mulvaney, R., Thomas, E. R., Abram, N., Stocker, T. F., and Fischer, H.: High-resolution aerosol concentration data from the Greenland NorthGRIP and NEEM deep ice cores, Earth Syst. Sci. Data, 14, 1215–1231, https://doi.org/10.5194/essd-14-1215-2022, 2022.

Fischer, H., Wagenbach, D., and Kipfstuhl, J.: Sulfate and nitrate firn concentrations on the Greenland ice sheet - 2. Temporal anthropogenic deposition changes, Journal of Geophysical Research-Atmospheres, 103, 21935-21942, 10.1029/98jd01886, 1998.

Gao, C. C., Robock, A., and Ammann, C.: Volcanic forcing of climate over the past 1500 years: An improved ice core-based index for climate models, Journal of Geophysical Research-Atmospheres, 113, 10.1029/2008jd010239, 2008.

Gao, C. H., Oman, L., Robock, A., and Stenchikov, G. L.: Atmospheric volcanic loading derived from bipolar ice cores: Accounting for the spatial distribution of volcanic deposition, Journal of Geophysical Research-Atmospheres, 112, 10.1029/2006jd007461, 2007.

Ge, Y. and Gao, X.: Understanding the overestimated impact of the Toba volcanic super-eruption on global environments and ancient hominins, Quaternary International, 559, 24-33, 10.1016/j.quaint.2020.06.021, 2020.

Gkinis, V., Vinther, B. M., Popp, T. J., Quistgaard, T., Faber, A. K., Holme, C. T., Jensen, C. M., Lanzky, M., Lutt, A. M., Mandrakis, V., Orum, N. O., Pedersen, A. S., Vaxevani, N., Weng, Y. B., Capron, E., Dahl-Jensen, D., Horhold, M., Jones, T. R., Jouzel, J., Landais, A., Masson-Delmotte, V., Oerter, H., Rasmussen, S. O., Steen-Larsen, H. C., Steffensen, J. P., Sveinbjornsdottir, A. E., Svensson, A., Vaughn, B., and White, J. W. C.: A 120,000-year long climate record from a NW-Greenland deep ice core at ultra-high resolution, Scientific Data, 8, 10.1038/s41597-021-00916-9, 2021.

Grootes, P. M. and Stuiver, M.: Oxygen 18/16 variability in Greenland snow and ice with 10^{-3} - 10^{5}-year time resolution, J. Geophys. Res., 102, 26455–26470, 1997.

Guillet, S., Corona, C., Stoffel, M., Khodri, M., Lavigne, F., Ortega, P., Eckert, N., Sielenou, P. D., Daux, V., Churakova, O. V., Davi, N., Edouard, J. L., Zhang, Y., Luckman, B. H., Myglan, V. S., Guiot, J., Beniston, M., Masson-Delmotte, V., and Oppenheimer, C.: Climate response to the Samalas volcanic eruption in 1257 revealed by proxy records, Nature Geoscience, 10, 123-+, 10.1038/ngeo2875, 2017.

Huang, C. Y., Zhao, M. X., Wang, C. C., and Wei, G. J.: Cooling of the South China Sea by the Toba eruption and correlation with other climate proxies similar to 71,000 years ago, Geophysical Research Letters, 28, 3915-3918, 10.1029/2000gl006113, 2001.

Hvidberg, C. S., DahlJensen, D., and Waddington, E. D.: Ice flow between the Greenland Ice Core Project and Greenland Ice Sheet Project 2 boreholes in central Greenland, Journal of Geophysical Research-Oceans, 102, 26851-26859, 10.1029/97jc00268, 1997.

Jackson, L. J., Stone, J. R., Cohen, A. S., and Yost, C. L.: High-resolution paleoecological records from Lake Malawi show no significant cooling associated with the Mount Toba supereruption at ca. 75 ka, Geology, 43, 823-826, 10.1130/g36917.1, 2015.

Johnsen, S. J., DahlJensen, D., Gundestrup, N., Steffensen, J. P., Clausen, H. B., Miller, H., Masson-Delmotte, V., Sveinbjornsdottir, A. E., and White, J.: Oxygen isotope and palaeotemperature records from six Greenland ice-core stations: Camp Century, Dye-3, GRIP, GISP2, Renland and NorthGRIP, Journal of Quaternary Science, 16, 299-307, 10.1002/jqs.622, 2001.

Karlof, L., Oigard, T. A., Godtliebsen, F., Kaczmarska, M., and Fischer, H.: Statistical techniques to select detection thresholds for peak signals in ice-core data, Journal of Glaciology, 51, 655-662, 10.3189/172756505781829115, 2005.

Kawamura, K., Parrenin, F., Lisiecki, L., Uemura, R., Vimeux, F., Severinghaus, J. P., Hutterli, M. A., Nakazawa, T., Aoki, S., Jouzel, J., Raymo, M. E., Matsumoto, K., Nakata, H., Motoyama, H., Fujita, S., Goto-Azuma, K., Fujii, Y., and Watanabe, O.: Northern Hemisphere forcing of climatic cycles in Antarctica over the past 360,000 years, Nature, 448, 912–914, doi:10.1038/nature06015, 2007.

Kutterolf, S., Schindlbeck, J. C., Anselmetti, F. S., Ariztegui, D., Brenner, M., Curtis, J., Schmid, D., Hodell, D. A., Mueller, A., Perez, L., Perez, W., Schwalb, A., Frische, M., and Wang, K. L.: A 400-ka tephrochronological

framework for Central America from Lake Peten Itza (Guatemala) sediments, Quaternary Science Reviews, 150, 200-220, 10.1016/j.quascirev.2016.08.023, 2016.

Lane, C. S., Chorn, B. T., and Johnson, T. C.: Ash from the Toba supereruption in Lake Malawi shows no volcanic winter in East Africa at 75 ka, Proceedings of the National Academy of Sciences of the United States of America, 110, 8025-8029, 10.1073/pnas.1301474110, 2013.

Liu, Z. F., Colin, C., and Trentesaux, A.: Major element geochemistry of glass shards and minerals of the Youngest Toba Tephra in the southwestern South China Sea, Journal of Asian Earth Sciences, 27, 99-107, 10.1016/j.jseaes.2005.02.003, 2006.

Mark, D. F., Petraglia, M., Smith, V. C., Morgan, L. E., Barfod, D. N., Ellis, B. S., Pearce, N. J., Pal, J. N., and Korisettar, R.: A high-precision Ar-40/Ar-39 age for the Young Toba Tuff and dating of ultra-distal tephra: Forcing of Quaternary climate and implications for hominin occupation of India, Quaternary Geochronology, 21, 90-103, 10.1016/j.quageo.2012.12.004, 2014.

Marshall, L., Johnson, J. S., Mann, G. W., Lee, L., Dhomse, S. S., Regayre, L., Yoshioka, M., Carslaw, K. S., and Schmidt, A.: Exploring How Eruption Source Parameters Affect Volcanic Radiative Forcing Using Statistical Emulation, Journal of Geophysical Research-Atmospheres, 124, 964-985, 10.1029/2018jd028675, 2019.

Marshall, L. R., Smith, C. J., Forster, P. M., Aubry, T. J., Andrews, T., and Schmidt, A.: Large Variations in Volcanic Aerosol Forcing Efficiency Due to Eruption Source Parameters and Rapid Adjustments, Geophysical Research Letters, 47, 10.1029/2020gl090241, 2020.

Mayewski, P. A., Meeker, L. D., Twickler, M. S., Whitlow, S., Yang, Q. Z., Lyons, W. B., and Prentice, M.: Major features and forcing of high-latitude northern hemisphere atmospheric circulation using a 110,000-year-long glaciochemical series, Journal of Geophysical Research-Oceans, 102, 26345-26366, 10.1029/96jc03365, 1997.

McConnell, J. R., Sigl, M., Plunkett, G., Burke, A., Kim, W. M., Raible, C. C., Wilson, A. I., Manning, J. G., Ludlow, F., Chellman, N. J., Innes, H. M., Yang, Z., Larsen, J. F., Schaefer, J. R., Kipfstuhl, S., Mojtabavi, S., Wilhelms, F., Opel, T., Meyer, H., and Steffensen, J. P.: Extreme climate after massive eruption of Alaska's Okmok volcano in 43 BCE and effects on the late Roman Republic and Ptolemaic Kingdom, Proceedings of the National Academy of Sciences of the United States of America, 117, 15443-15449, 10.1073/pnas.2002722117, 2020.

Miller, G. H., Geirsdottir, A., Zhong, Y. F., Larsen, D. J., Otto-Bliesner, B. L., Holland, M. M., Bailey, D. A., Refsnider, K. A., Lehman, S. J., Southon, J. R., Anderson, C., Bjornsson, H., and Thordarson, T.: Abrupt onset of the Little Ice Age triggered by volcanism and sustained by sea-ice/ocean feedbacks, Geophysical Research Letters, 39, 10.1029/2011gl050168, 2012.

Newhall, C. G.: GEOLOGY OF THE LAKE ATITLAN REGION, WESTERN GUATEMALA, Journal of Volcanology and Geothermal Research, 33, 23-55, 10.1016/0377-0273(87)90053-9, 1987.

North Greenland Ice Core Project members: High-resolution record of Northern Hemisphere climate extending into the last interglacial period, Nature, 431, 147–151, 2004.

Oppenheimer, C.: Limited global change due to the largest known Quaternary eruption, Toba approximate to 74 kyr BP?, Quaternary Science Reviews, 21, 1593-1609, 10.1016/s0277-3791(01)00154-8, 2002.

Osipov, S., Stenchikov, G., Tsigaridis, K., LeGrande, A. N., and Bauer, S. E.: The Role of the SO2 Radiative Effect in Sustaining the Volcanic Winter and Soothing the Toba Impact on Climate, Journal of Geophysical Research-Atmospheres, 125, 10.1029/2019jd031726, 2020.

Paine, A. R., Wadsworth, F. B., and Baldini, J. U. L.: Supereruption doublet at a climate transition, Communications Earth & Environment, 2, 219, 10.1038/s43247-021-00293-6, 2021.

Parker, D. E., Wilson, H., Jones, P. D., Christy, J. R., and Folland, C. K.: The impact of Mount Pinatubo on world-wide temperatures, International Journal of Climatology, 16, 487-497, 10.1002/(sici)1097-0088(199605)16:5<487::Aid-joc39>3.0.Co;2-j, 1996.

Pausata, F. S. R., Chafik, L., Caballero, R., and Battisti, D. S.: Impacts of high-latitude volcanic eruptions on ENSO and AMOC, Proceedings of the National Academy of Sciences of the United States of America, 112, 13784-13788, 10.1073/pnas.1509153112, 2015.

Rampino, M. R. and Self, S.: BOTTLENECK IN HUMAN-EVOLUTION AND THE TOBA ERUPTION, Science, 262, 1955-1955, 10.1126/science.8266085, 1993.

Rasmussen, S. O., Abbott, P. M., Blunier, T., Bourne, A. J., Brook, E., Buchardt, S. L., Buizert, C., Chappellaz, J., Clausen, H. B., Cook, E., Dahl-Jensen, D., Davies, S. M., Guillevic, M., Kipfstuhl, S., Laepple, T., Seierstad, I. K., Severinghaus, J. P., Steffensen, J. P., Stowasser, C., Svensson, A., Vallelonga, P., Vinther, B. M., Wilhelms, F., and Winstrup, M.: A first chronology for the North Greenland Eemian Ice Drilling (NEEM) ice core, Climate of the Past, 9, 2713-2730, 10.5194/cp-9-2713-2013, 2013.

Rasmussen, S. O., Bigler, M., Blockley, S. P., Blunier, T., Buchardt, S. L., Clausen, H. B., Cvijanovic, I., Dahl-Jensen, D., Johnsen, S. J., Fischer, H., Gkinis, V., Guillevic, M., Hoek, W. Z., Lowe, J. J., Pedro, J. B., Popp, T., Seierstad, I. K., Steffensen, J. P., Svensson, A. M., Vallelonga, P., Vinther, B. M., Walker, M. J. C., Wheatley, J. J., and Winstrup, M.: A stratigraphic framework for abrupt climatic changes during the Last Glacial period based on three synchronized Greenland ice-core records: refining and extending the INTIMATE event stratigraphy, Quaternary Science Reviews, 106, 14-28, 10.1016/j.quascirev.2014.09.007, 2014.

Robock, A.: Volcanic eruptions and climate, Reviews of Geophysics, 38, 191-219, 10.1029/1998rg000054, 2000.

Robock, A., Ammann, C. M., Oman, L., Shindell, D., Levis, S., and Stenchikov, G.: Did the Toba volcanic eruption of similar to 74 ka BP produce widespread glaciation?, J. Geophys. Res.- Atmos., 114, D10107, doi:10.1029/2008jd011652, 2009.

Rose, W. I., Newhall, C. G., Bornhorst, T. J., and Self, S.: QUATERNARY SILICIC PYROCLASTIC DEPOSITS OF ATITLAN CALDERA, GUATEMALA, Journal of Volcanology and Geothermal Research, 33, 57-80, 10.1016/0377-0273(87)90054-0, 1987.

Savarino, J., Romero, A., Cole-Dai, J., Bekki, S., and Thiemens, M. H.: UV induced mass-independent sulfur isotope fractionation in stratospheric volcanic sulfate, Geophysical Research Letters, 30, 10.1029/2003gl018134, 2003.

Scaillet, B., Clemente, B., Evans, B. W., and Pichavant, M.: Redox control of sulfur degassing in silicic magmas, Journal of Geophysical Research-Solid Earth, 103, 23937-23949, 10.1029/98jb02301, 1998.

Sigl, M., Winstrup, M., McConnell, J. R., Welten, K. C., Plunkett, G., Ludlow, F., Buntgen, U., Caffee, M., Chellman, N., Dahl-Jensen, D., Fischer, H., Kipfstuhl, S., Kostick, C., Maselli, O. J., Mekhaldi, F., Mulvaney, R., Muscheler, R., Pasteris, D. R., Pilcher, J. R., Salzer, M., Schupbach, S., Steffensen, J. P., Vinther, B. M., and Woodruff, T. E.: Timing and climate forcing of volcanic eruptions for the past 2,500 years, Nature, 523, 543-+, 10.1038/nature14565, 2015.

Sigl, M., Fudge, T. J., Winstrup, M., Cole-Dai, J., Ferris, D., McConnell, J. R., Taylor, K. C., Welten, K. C., Woodruff, T. E., Adolphi, F., Bisiaux, M., Brook, E. J., Buizert, C., Caffee, M. W., Dunbar, N. W., Edwards, R., Geng, L.,

Iverson, N., Koffman, B., Layman, L., Maselli, O. J., McGwire, K., Muscheler, R., Nishiizumi, K., Pasteris, D. R., Rhodes, R. H., and Sowers, T. A.: The WAIS Divide deep ice core WD2014 chronology - Part 2: Annual-layer counting (0-31 ka BP), Climate of the Past, 12, 769-786, 10.5194/cp-12-769-2016, 2016.

Schulz, H., von Rad, U., and Erlenkeuser, H.: Correlation between Arabian Sea and Greenland climate oscillations of the past 110,000 years, Nature, 393, 54-57, 10.1038/31750, 1998.

Schupbach, S., Fischer, H., Bigler, M., Erhardt, T., Gfeller, G., Leuenberger, D., Mini, O., Mulvaney, R., Abram, N. J., Fleet, L., Frey, M. M., Thomas, E., Svensson, A., Dahl-Jensen, D., Kettner, E., Kjaer, H., Seierstad, I., Steffensen, J. P., Rasmussen, S. O., Vallelonga, P., Winstrup, M., Wegner, A., Twarloh, B., Wolff, K., Schmidt, K., Goto-Azuma, K., Kuramoto, T., Hirabayashi, M., Uetake, J., Zheng, J., Bourgeois, J., Fisher, D., Zhiheng, D., Xiao, C., Legrand, M., Spolaor, A., Gabrieli, J., Barbante, C., Kang, J. H., Hur, S. D., Hong, S. B., Hwang, H. J., Hong, S., Hansson, M., Iizuka, Y., Oyabu, I., Muscheler, R., Adolphi, F., Maselli, O., McConnell, J., and Wolff, E. W.: Greenland records of aerosol source and atmospheric lifetime changes from the Eemian to the Holocene, Nature Communications, 9, 10.1038/s41467-018-03924-3, 2018.

Shane, P., Westgate, J., Williams, M., and Korisettar, R.: NEW GEOCHEMICAL EVIDENCE FOR THE YOUNGEST TOBA-TUFF IN INDIA, Quaternary Research, 44, 200-204, 10.1006/qres.1995.1064, 1995.

Sigl, M., McConnell, J. R., Layman, L., Maselli, O., McGwire, K., Pasteris, D., Dahl-Jensen, D., Steffensen, J. P., Vinther, B., Edwards, R., Mulvaney, R., and Kipfstuhl, S.: A new bipolar ice core record of volcanism from WAIS Divide and NEEM and implications for climate forcing of the last 2000 years, Journal of Geophysical Research-Atmospheres, 118, 1151-1169, 10.1029/2012jd018603, 2013.

Smith, E. I., Jacobs, Z., Johnsen, R., Ren, M., Fisher, E. C., Oestmo, S., Wilkins, J., Harris, J. A., Karkanas, P., Fitch, S., Ciravolo, A., Keenan, D., Cleghorn, N., Lane, C. S., Matthews, T., and Marean, C. W.: Humans thrived in South Africa through the Toba eruption about 74,000 years ago, Nature, 555, 511-+, 10.1038/nature25967, 2018.

Song, S. R., Chen, C. H., Lee, M. Y., Yang, T. F., Iizuka, Y., and Wei, K. Y.: Newly discovered eastern dispersal of the youngest Toba Tuff, Marine Geology, 167, 303-312, 10.1016/s0025-3227(00)00034-7, 2000.

Steffensen, J. P., Andersen, K. K., Bigler, M., Clausen, H. B., Dahl-Jensen, D., Fischer, H., Goto-Azuma, K., Hansson, M., Johnsen, S. J., Jouzel, J., Masson-Delmotte, V., Popp, T., Rasmussen, S. O., Rothlisberger, R., Ruth, U., Stauffer, B., Siggaard-Andersen, M. L., Sveinbjornsdottir, A. E., Svensson, A., and White, J. W. C.: High-resolution Greenland Ice Core data show abrupt climate change happens in few years, Science, 321, 680-684, 10.1126/science.1157707, 2008.

Storey, M., Roberts, R. G., and Saidin, M.: Astronomically calibrated Ar-40/Ar-39 age for the Toba supereruption and global synchronization of late Quaternary records, Proceedings of the National Academy of Sciences of the United States of America, 109, 18684-18688, 10.1073/pnas.1208178109, 2012.

Stocker, T. F., and S. J. Johnsen, A minimum thermodynamic model for the bipolar seesaw,Paleoceanography,18(4), 1087,doi:10.1029/2003PA000920, 2003.

Svensson, A., Bigler, M., Blunier, T., Clausen, H. B., Dahl-Jensen, D., Fischer, H., Fujita, S., Goto-Azuma, K., Johnsen, S. J., Kawamura, K., Kipfstuhl, S., Kohno, M., Parrenin, F., Popp, T., Rasmussen, S. O., Schwander, J., Seierstad, I., Severi, M., Steffensen, J. P., Udisti, R., Uemura, R., Vallelonga, P., Vinther, B. M., Wegner, A., Wilhelms, F., and Winstrup, M.: Direct linking of Greenland and Antarctic ice cores at the Toba eruption (74 ka BP), Climate of the Past, 9, 749-766, 10.5194/cp-9-749-2013, 2013.

Thomason, L. W., Ernest, N., Millan, L., Rieger, L., Bourassa, A., Vernier, J. P., Manney, G., Luo, B. P., Arfeuille, F., and Peter, T.: A global space-based stratospheric aerosol climatology: 1979-2016, Earth System Science Data, 10, 469-492, 10.5194/essd-10-469-2018, 2018.

Timmreck, C., Graf, H. F., Zanchettin, D., Hagemann, S., Kleinen, T., and Kruger, K.: Climate response to the Toba super-eruption: Regional changes, Quaternary Int., 258, 30–44, doi:10.1016/j.quaint.2011.10.008, 2012.

Toohey, M. and Sigl, M.: Volcanic stratospheric sulfur injections and aerosol optical depth from 500 BCE to 1900 CE, Earth System Science Data, 9, 809-831, 10.5194/essd-9-809-2017, 2017.

Yang, Q., Mayewski, P. A., Zielinski, G. A., Twickler, M., and Taylor, K. C.: Depletion of atmospheric nitrate and chloride as a consequence of the Toba volcanic eruption, Geophysical Research Letters, 23, 2513-2516, 10.1029/96gl02201, 1996.

Chapter 4

Chapter contents

Recurrence rates and probability of global sulfur-rich volcanism as seen from ice cores

Jiamei Lin[1], Anders Svensson[1], Johannes Lohmann [1]
[1]Physics of Ice, Climate and Earth, Niels Bohr Institute, University of Copenhagen, 2100, Denmark

Abstract:
Large sulfur-rich explosive volcanic eruptions are globally disruptive events. The return times and probability of occurrence of future large eruptions are poorly constrained due to the limit number of observations. Here, two ice-core based datasets of global volcanism with bi-hemisphere volcanic sulfate depositions are compiled to estimate the probability and recurrence rate for different size categories in terms of their stratospheric sulfate injections. The first dataset is an existing bi-hemispheric volcanic record that includes eruptions with stratospheric sulfate injections above 3 Tg. The second dataset combines the Holocene dataset with a composite record from the last glacial period covering a total of 16,670 years (composite duration), but only with stratospheric sulfate injections above 30 Tg due to the fact that smaller eruptions cannot be reliably identified in the glacial period. Overall, we find the distribution of the return times of the global sulfur-rich explosive eruptions at different scales to be close to exponential. For eruptions with volcanic stratospheric sulfate injections of 3-30 Tg, the estimated mean return time is 63 years. The mean return time is 129 years for volcanic eruptions with stratospheric sulfate injections between those of the Pinatubo 1991 AD and the Tambora 1815 AD eruptions. Over the next 100 years, the probability of an eruption recurrence of magnitude between that of the Tambora and the Samalas 1257 AD is 19-21%. These results constrain the likelihood of impending eruptions in different size categories and underlines the need to engage in volcanic emergency management for human society.

4.1 Introduction:

Explosive sulfur-rich volcanic eruptions with stratospheric sulfur injections impose numerous regional and global impacts on climate, the biosphere and human society through reduction of the flux of solar radiation to the Earth's surface (Robock, 2000). To first order, the cooling induced by volcanic eruption is proportional to the magnitude of the volcanic stratospheric sulfate loading (VSSL). The VSSL can be reconstructed from ice cores when volcanic sulfate

deposits have occurred in both the Greenland and Antarctica (Sigl et al., 2015; Toohey et al., 2019). The well-observed Pinatubo eruption that occurred in 1991 AD injected 55 Tg of sulfate into the stratosphere as estimated from ice-core records at both poles (Sigl et al., 2013; Lin et al., 2022). This eruption was responsible for a multi-annual global cooling (Guillet et al., 2017; Sigl et al., 2015; Tejedor et al., 2021), that led to crop failure and famines (Huhtamaa and Helama, 2017). The largest volcanic eruption of the past 500 years – the Tambora 1815 AD, Indonesia - ejected about 86 Tg sulfate into the stratosphere (Sigl et al., 2015), resulting in 'the year without a summer' with the global mean surface temperature lowering by 0.4-0.7 °C (Stothers, 1984; Oppenheimer, 2003). In the past 2000 years, the largest well-known volcanic eruption - the Samalas 1257 AD, Indonesia - ejected 164 Tg sulfate into the stratosphere (Sigl et al., 2015). This event led to extreme cooling in the year 1259 AD of -1.2 °C cooling in the Northern Hemisphere (Guillet et al., 2017). Compared to the cooling induced by La Niña (Morice et al., 2012), the cooling episodes following such eruptions are more severe and persistent. If a volcanic eruption of that magnitude or larger would occur today, society would be severely impacted by the induced cooling and ensuring hazards. Thus, we need to forecast the probability and manage such large eruptions.

Existing analyses of return times and eruption rates are based on global volcanism databases of emitted magma summarized by the volcanic explosivity index (VEI). One such database contains 9517 individual eruptions over the past 2 Ma, and includes a quantitative description of the time and size distribution of global volcanism (Papale et al., 2021; Papale, 2018; Rougier et al., 2018; Mason et al., 2004). However, such volcanic lists are incomplete, as they are based on discontinuous geological records. In contrast, ice-core based volcanic sulfate deposition records are continuous, although their extension back in time is limited to the last glacial cycle, that is time span covered by the Greenland ice core records. Furthermore, the detection threshold for the identification of volcanic eruptions increases with age and it is generally not possible to assign geological information about a volcano to the individual acidity spikes of the ice core records (Lin et al., 2022).

Here, we apply for the first time two datasets of bi-hemisphere (bipolar) volcanic records with eruption date and VSSL derived from polar ice cores. A quantitative description of the return times and probability of occurrence of global sulfur-rich volcanism is obtained for different size categories of volcanic eruptions.

4.2 Results and discussion

4.2.1 Two continuous bi-hemispheric eruption datasets

We apply two datasets of bipolar volcanism with the eruption date and the VSSL based on Greenland and Antarctic ice-core sulfate or sulfur records.

The first dataset, BiVol-1, is published by Sigl et al., 2022 and covers the Holocene period (100-11,550 a b2k, before 2000 AD). The dataset contains 328 bipolar volcanic events with a VSSL above 3 Tg, which is the lower detection limit from the applied ice core records (Fig. S4.1 (a) and Table S4.1).

The second dataset, BiVol-2, is a composite of several time intervals consisting of the Holocene, as well as nine intervals from the last glacial period of which two are published and the others are applied here for the first time. The two published datasets cover the inception of the Younger Dryas cold event (12,752-13,225 a b2k) (Abbott et al., 2021), and the 'Toba interval' related to volcanic enhanced activity in which the Indonesian Toba mega-eruption is likely to have occurred (73,800-74,800 a b2k) (Lin et al., 2022, under review). The seven remaining periods for which bipolar volcanoes are identified continuously from Greenland and Antarctic ice cores, are 14,467-15,723 a b2k, 19,500-24,700 a b2k, 37,890-38,406 a b2k, 40,700-41,405 a b2k, 41,715-42,250 a b2k, 57,074-57,509 a b2k and 59,100-59,800 a b2k (Fig. S4.2). The method we applied to identify continuous bipolar volcanic signals exploits unique pattern of volcanic spikes and the same counting years between adjacent volcanic tie-points, that have been applied to synchronize global volcanic signals from polar ice cores (Svensson et al., 2013; Svensson et al., 2020). There have been 85 bipolar volcanic match points identified from the Greenland and Antarctic ice cores (Lin et al., 2022; Svensson et al., 2020). As annual layer counting in the younger half of the last glacial period has been employed for Greenland and Antarctic ice cores (Svensson et al., 2008; Svensson et al., 2020; Sigl et al., 2016), it is possible to continuously identify bipolar volcanic sulfate signals. Here, we identify continuous bipolar volcanic signals when the uncertainty of the counted annual layers between the published adjacent bipolar volcanic tie-points is below 18 years, that equals to the lowest resolution of ice core impurities (Fig. S4.2). The last glacial maximum (19,500-24,700 b2k) is generally difficult to synchronize using bipolar volcanic tie-points (Svensson et al., 2020). However, recently two new bipolar ^{10}Be match points have been discovered in Greenland and Antarctic ice cores at 24.4 ka and 21.7 ka b2k, respectively (Sinnl et al., 2022, under review), enabling us to synchronize this interval (Methods, 4.4.1).

For the last glacial period, it is not possible to detect weaker volcanic signals, because the glacial impurity levels in Greenland ice cores and the sulfate background are higher and more variable than in the Holocene. For the BiVol-2, the lower detection limit of volcanic sulfate deposition is 20 kg km^{-2} for Greenland and 10 kg $km^{-2}$for Antarctica. We therefore apply the lower limit of VSSL of 30 Tg converted from Greenland and Antarctic lower detection limit by the established method of Gao et al. (2007). The BiVol-2 contains 151 bipolar volcanic events with the VSSL above 30 Tg of which 68 are in the Holocene and 83 are in the glacial period (Table S4.2 and Fig. S4.1 (b)). The total duration of the composite dataset is about 22,220 years.

Several factors may contribute to the uncertainty of the estimated VSSL: a) Different approachs have been applied to identify volcanic signals from ice-core sulfate background over the investigated period. B) The VSSL is derived from ice-core volcanic sulfate depositions, based on the established transfer function (Gao et al., 2007). This function may be influenced by injection altitudes, latitudes, seasons and the meteorological conditions in the volcanic cloud dispersal and deposition process (Toohey et al., 2013). c) The number of ice-core sulfate or sulfur records and the related data resolutions varies over the investigated period.

4.2.2 Features of cumulative volcanic eruptions

Footprints of global volcanism and climatic conditions are preserved in ice cores from both poles. Whether volcanic activities are influenced by climate change, such as the warm of the Holocene pr the cold last glacial period. To adress this question, we compare the global volcanic records of the Holocene period to those of the last glacial period based on the BiVol-2. We test the distributions of volcanic eruptions in these two climate states using the two-sample Kolmogorov-Smirnov test (Hodges, J.L. Jr, 1958). The p-value = 0.18 (statistics = 0.17) suggests that we can not reject the consistent volcanic occurrence over the Holocene and the last glacial periods.

We further test whether the volcanic event process is similar over all investigated time intervals of the last glacial period. We assume that the volcanic occurrence is homogenous and that the volcanic events are independent of each other, yielding a Poisson process as null hypothesis. We estimate the mean eruption rate over the investigated period, then calculate the 90% confidence level based on the Poisson distribution at the given fixed rate. The result is shown in Fig. 4.1. The number of volcanoes in 4 (thousand-year) intervals is out of the 90% confidence level among 25 time periods. Two outliers are in the transition to the Youngers Dryas and in the final stage of last glacial period, respectively, one is at the beginning of the Last

Glacial Maximum, and the last is in an abrupt transition from a warm to a cold state. An enhanced volcanic activity in the last deglacial period has been observed from Greenland volcanic records and tephra deposits of Icelandic records (Lin et al., 2022; Maclennan et al., 2002). We could not rule out that these four volcanic active intervals may be associated to the abrupt climate changes. However, the volcanic occurrence doesn't change significantly over the last glacial period, when there are three outliers expected to follow the Poisson distribution.

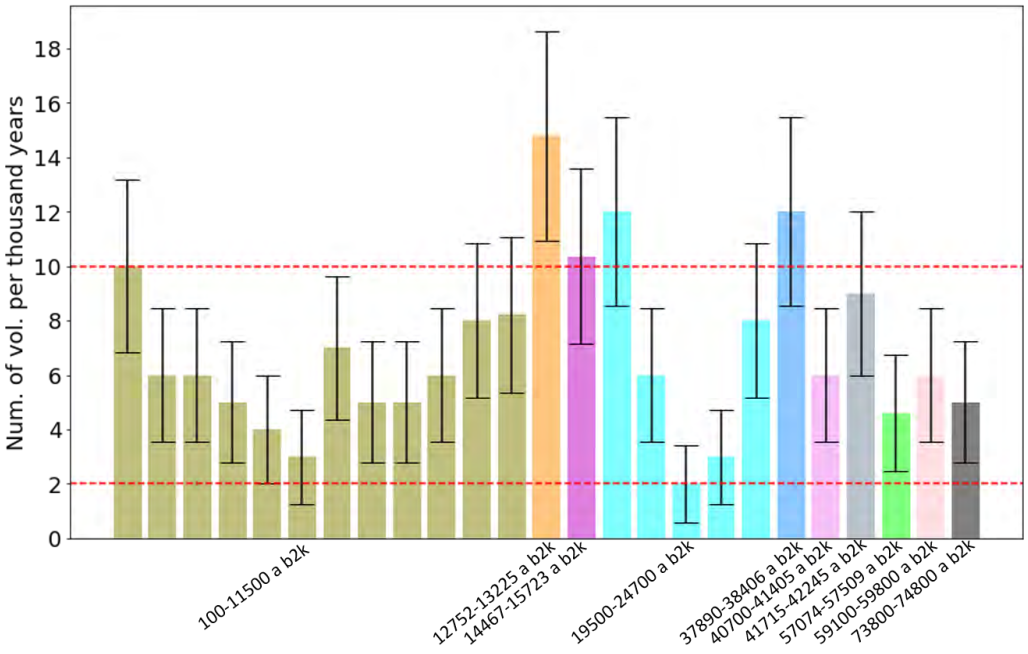

Figure 4.1 Number of bipolar volcanic eruptions per thousand years over the investigated periods in the last glaical period based on the BiVol-2. The colors represent the volcanic records collected from different periods, that are labelled on the horizontal axis. The red dash line stands for the upper and lower bound of the 95% confidential interval.

We categorize volcanic eruptions in five size classes according to the volcanic sulfate magnitude (Methods 4.4.2, Table 4.2). The recorded numbers of Large, Very Large and Super Large volcanic events are comparable, only 14 Super Large events are recorded in the Holocene, 28 in the last glacial period (Fig. 4.2). The Small events are more frequent compared to the other recorded eruptions of larger size categories. For the Holocene, the volcanic eruptions of the Small and Moderate categories show a higher frequency (BiVol-1). However, this can not be compared to the last glacial period, as the volcanic detection limit (VSSL of 30 Tg from BiVol-2) is higher. The cumulative number of volcanic eruptions of all size categories shows a linear trend that indicates a stationary process (Fig. 4.2), similar to the cumulative number of eruptions classified by the VEI (Papale, 2018; Rougier et al., 2018; Nishimura et al., 2016).

Long return times (gaps) in the plot of the cumulative number of eruptions versus time are observed in 15-17 ka of Very Large events on a 'composite continuous' timescale (Fig. 4.2 (e)), and in 13-18 ka of Super Large events on a 'composite continuous' timescale Fig. 4.2 (f). These gaps possibly represent either the natural variability of the volcanic occurrence, or due to down recording that may be misinterpreted as long pauses between eruptions.

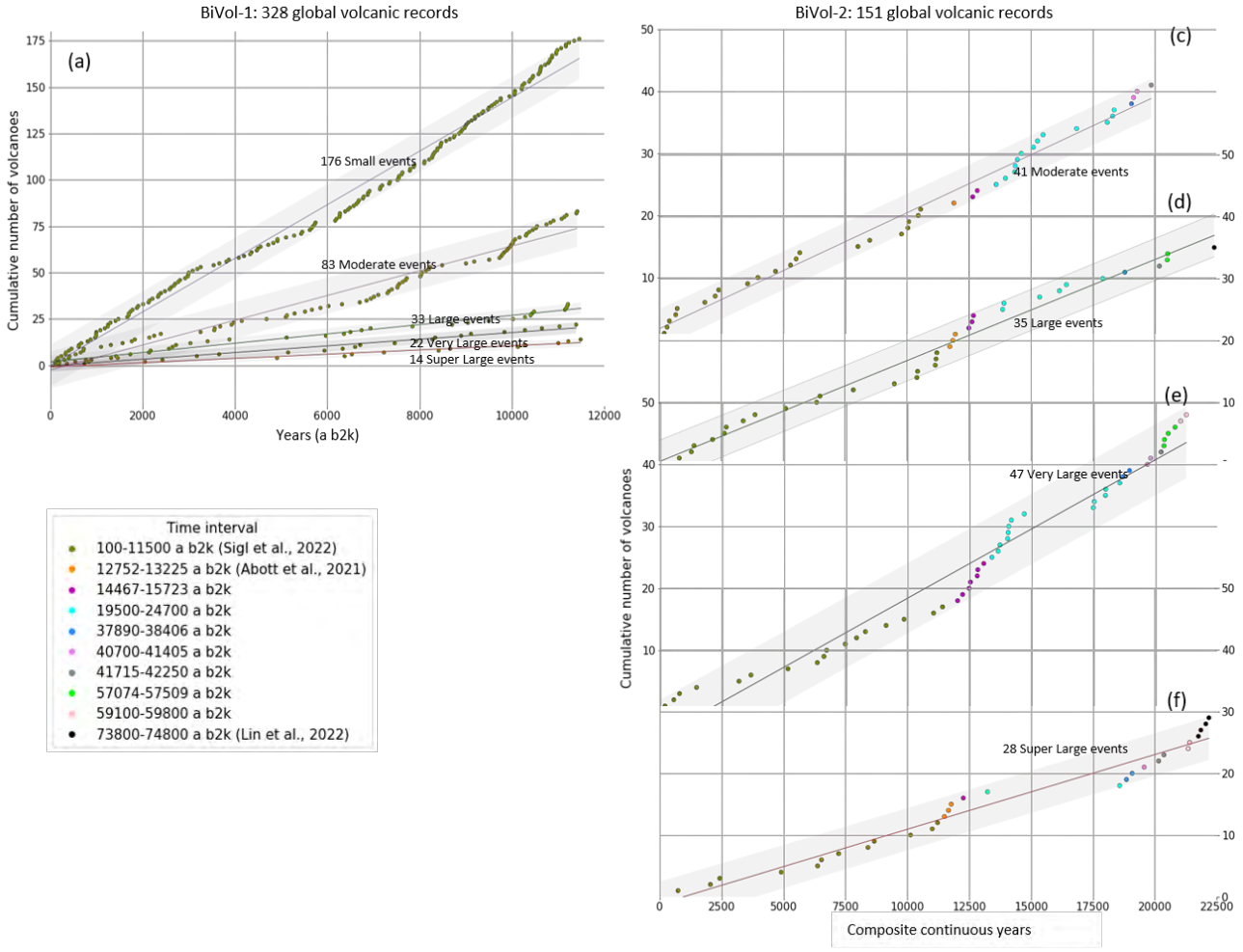

Figure 4.2 Cumulative number of all size categories of volcanic eruptions with time for the BiVol-1 (a) and BiVol-2 (b-e) datasets. The horizontal axis of (a) represents years before 2000 AD from the BiVol-1. The horizontal axis of (b-e) represents 'composite continous years' for the disconnected time intervals from the BiVol-2 (see 4.2.1). Linear fits are represented by thick lines and the confidential bands are shown as shadow bands in the same colors.

4.2.3 Estimation of the volcanic eruption rate

Using the historical volcanic eruptions to forecast the recurrence rate and probability of volcanic eruptions requires a statistical approach. We use the exponential model to fit the complementary cumulative distribution of the return times for all size categories of eruptions. The eruption rate parameters are estimated by the maximum likelihood estimation (MLE) (Table 4.1), that is

described in Section 4.4.4-4.4.6. These complementary cumulative distributions approximate the theoretical curve of the exponential distribution (Fig. 4.3), although some of the Anderson-Darling (A-D) test are not within some significance level. The deviation of points is not evenly distributed around the exponential fitting line (Fig. 4.3). This systemic deviation may be caused by: a) the enhanced volcanic activity that is related to climate change such as the high number of volcanoes in the deglacial period (Fig. 4.1), b) misinterpretation of the return times from bipolar ice-core synchronization, c) the magnitude estimation that is biased in different climatic conditions, such as the Holocene and the last glaciation. In order to evaluate the bias, the confidential interval (0.05 and 0.95 quantile) for the estimated eruption rate for each size category of eruptions is estimated using the bootstrapping method (Table 4.1, Methods, 4.4.3).

The current estimation of the eruption rate for all size categorise is based on the statistical model, that is not much destroy on the effective estimation. Another trial of the fit to estimate the volcanic eruption rate is to use the log-normal model, that is close to exponential distribution. The log-normal model is more complex and needs two parameters to estimate the mean return times. The fitting results and systematic deviations are shown in Fig. S4.4. As this model needs one additional parameter and the fitting quality is not in high confidence, we prefer to apply the sample exponential model.

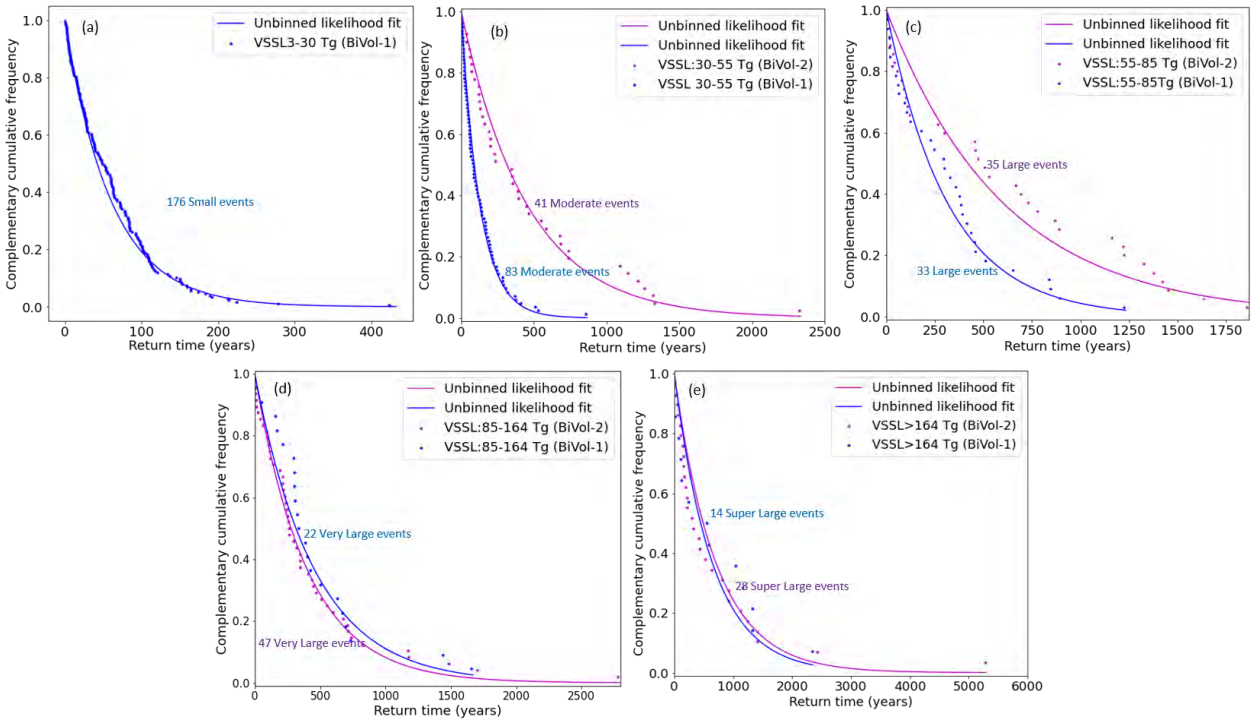

Figure 4.3 The complementary cumulative frequency of return times of each category of global volcanic eruptions (dots) and their fitted models (thick line). The blue color dots represent the volcanic records from the BiVol-1, the puple dots are from the BiVol-2. The estimated eruption rates for each category eruptions are shown in Table 4.1.

MLE of rate parameters lambda (year^{-1})					
Size/Magnitude (Tg)	**Mean (λ)**	**0.95 quantile**	**0.05 quantile**	**A-D test**	**Dataset**
Super Large (>164)	1.46E-03	9.93E-04	2.57E-03	10%	
Very Large (85-164)	2.11E-03	1.58E-03	2.93E-03	2.5%	
Large (55-85)	3.08E-03	2.42E-03	4.14E-03	rejected	BiVol-1
Moderate (30-55)	7.74E-03	6.38E-03	9.60E-03	rejected	
Small (3-30)	1.59E-02	1.42E-02	1.80E-02	10%	
Super Large (>164)	1.41E-03	9.47E-04	2.37E-03	1%	
Very Large (85-164)	2.30E-03	1.78E-03	3.13E-03	rejected	BiVol-2
Large (55-85)	1.62E-03	1.30E-03	2.16E-03	rejected	
Moderate (30-55)	2.14E-03	1.67E-03	2.91E-03	rejected	

Table 4.1 The eruption rate parameters are estimated by the maximum likelihood estimation (MLE). The mean return time is equal to 1/λ. The 0.95 quantile and 0.05 quantile are estimated for the mean return times using the bootstrap resampling method. The method for estimating eruption rate parameters are described in sections 4.2.3-4.2.7. The A-D test provide significant level for the exponetial fitting.

The mean return times for the Small, Moderate, Large and Very Large events are estimated to 63, 129, 323 and 470 years, respectively, from the BiVol-1 (Fig. 4.4 (a)). The mean return times for the Super Large events are estimated at 676(689) years based on the BiVol-1 (BiVol-2) (Fig. 4.4 (a)). This is 0.24 times that of the VEI 7 eruptions estimated from the geological database,

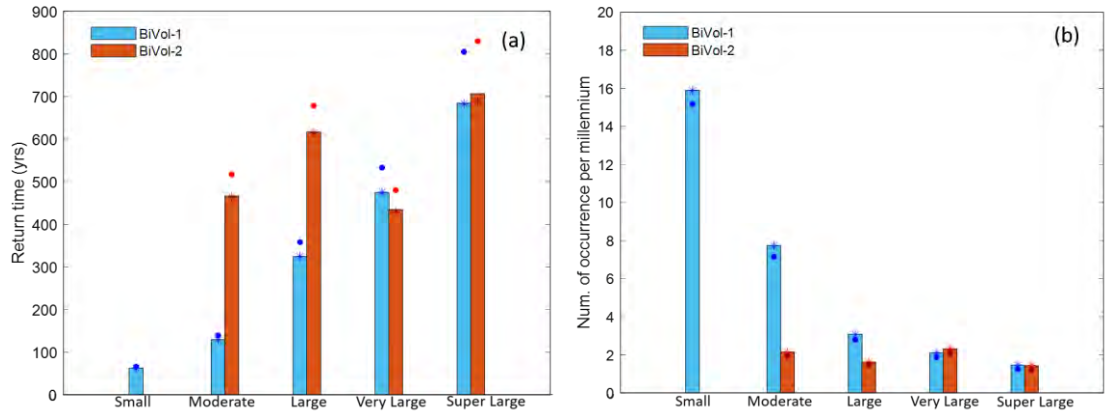

Figure 4.4 (a) represents the mean return time of each size category of eruptions estimated from the BiVol-1 and BiVol-2. (b) indicates the number of bipolar volcanoes will occur in the next millennium for each size category based on the BiVol-1 and BiVol-2. Dots and star markers represent 75th quantile and the median values.

whose mean return time is 2,810 years based on the observations back to 125 ka (Papale, 2018). The mean return times of the Moderate and Large size eruptions of the BiVol-1 are much shorter

than those of the BiVol-2. This is because the detection limit of the volcanic events is 30 Tg in the BiVol-2 and no Small events are included.

4.2.4 Probabilistic volcanic hazard assessment

Our two datasets and the statistical model allow us to forecast the number of global volcanic eruptions at certain magnitude in the next millennium. As is shown in Fig. 4.4 (b), on average 16 Small events, and 8 Moderate events are expected to occur in the next millennium based on the BiVol-1. For the Large, Very Large and Super Large events, 1-3 number eruptions are expected to occur in the next millennium according to the estimates from the BiVol-1 and BiVol-2 (Fig. 4.4 (b)).

It is possible to quantitatively assess the probability of the occurrence of volcanic hazards of different magnitudes over a certain length of time, as the distribution of the return times of volcanic eruptions is close to the exponential model (Methods, 4.4.7). The probabilistic volcanic hazard assessment is shown in Fig. 4.5. In the next year, the probability of the occurrence is below 2% for the Small events based on the BiVol-1, and decreasing to 0.1-0.2% for the Very Large and Super Large events. In the next 10 years, the probability of the occurrence is up to15% for the Small eruptions.

Very Large events are suspected to trigger extreme weather and will damage transport, energy, food and finance around the world, as the sulfate magnitude is above that of the Tambora 1815 eruption. In the next 100 years, the probability of observing the Very Large events is 19-21%, that is only 5-7% higher than that of the Super Large events. In the next 500 years, the probability is expected to be 65-68%.

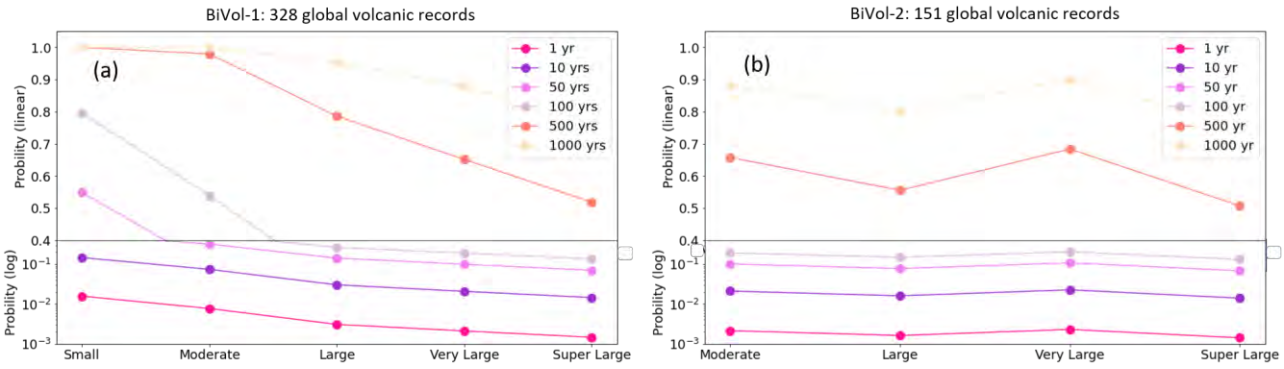

Figure 4.5 The probability of occurrence for all size categories of eruptions based on the BiVol-1 (a) and BiVol-2 (b) datasets. It is calculated based on the exponential fitting of the return times (Table 4.2, Methods 4.4.7).

Compared to the estimate from geological evidence, the probability of occurrence is 3.6% for the VEI-7 eruptions in a 100-year time window. This estimation is 4-5 times lower than the probability of the Very Large events based on the ice-core volcanic records. To monitor and

forecasting a sulfate magnitude related to the VEI 8 size volcanic eruption is certainly difficult due to the limited observations of bipolar volcanic sulfate records.

4.3 Conclusion

Two datasets of sulfur-rich explosive eruptions are complied from ice cores, one covering the Holocene period and the other covering the Holocene and selected sections of the last glacial periods. The density distribution of return times for different sizes of volcanic eruptions, that quantified by the magnitude of volcanic stratospheric sulfate loading comparable to the well-known eruptions, is approximated by an exponential distribution function. This finding support that the occurrence of volcanic eruptions follows a random process. In recent time, the smaller sulfur-rich eruptions have occurred frequently and well observed, but the larger eruptions are rare and have not occurred in the satellite era. Here, based on the volcanic records from ice cores over the Holocene and the last glacial period, the frequency and probability of occurrence of all size categories of volcanic eruptions are estimated in a statistical approach. For volcanic eruptions larger than the Tambora 1815 AD eruption, the mean return time is estimated to 434 years. In the next 100 years, the probability of observing such event is above 19%, rising above 65% for the next 500 years. Volcanic eruption could disrupt the global trade and economy and would trigger a strong climate anomaly. The next volcanic hazard is not far from human civilization. The governments should develop strategies to defend it.

4.4 Methods

4.4.1 Bipolar synchronization of the last glacial maximum (19.5-24.5 ka)

With synchronized bipolar volcanic tie-points (Svensson et al., 2022, in preparation) and applied linear interpolation, there are 38 bipolar volcanic match points identified in the LGM (19.5-24.5 ka b2k), that are consistent to the two ^{10}Be match points (Sinnl et al., 2022 undereview; Table S4.3 and Fig. S4.3). However, with this method, mis-matched bi-hemispheric volcanic markers, composed by two close hemispheric volcanic signals can occur. The further step for cross validation of these bipolar match points is using the smooth curve passing through all bipolar match points between ice cores, assuming the relative stable annual snow accumulation as seen from water isotope record of NGRIP (Fig. S4.3).

4.4.2 Volcanic eruption size categories

Volcanic eruption sizes are commonly quantified and represented in terms of the magnitude of the emitted magma volume or mass. A widely used classification index is the volcanic explosivity index (VEI), that is based on the volume of lava and the plume height of column (Newhall and Self, 1982). The VEI does not necessarily represent the magnitude of volcanic eruption in terms of sulfur emissions, however, as the relationship between the volcanic sulfur-containing gas and the magma mass/volume is complex. For volcanic eruption size classifications from ice-core volcanic records, it is convenient to classify the eruption magnitude in terms of the VSSL that can be estimated for all bipolar events that directly related to the climatic cooling effect of the eruption. The VSSL of well-known volcanic eruptions can be used as a metric to separate eruptions into different size categories for understanding volcanic impact and aiding assessment of volcanic hazards. The climate response to the sufur-rich explosive volcanic eruptions is a complex process and the VSSL does not exclusively measure their climatic impact. However, the magnitude of VSSL is proportional to the volcanic induced cooling, observed in tree-ring width records (Toohey et al., 2019), suggesting that the VSSL is a good indicator. We use the VSSL of the well-known eruptions – 30 Tg of half magnitude of the Pinatubo 1991, 55 Tg of the Pinatubo 1991, 85 Tg of the Tambora 1815, and 164 Tg of the Samalas 1257 eruptions- as measures to categorize the volcanoes in five size eruptions. We use terms of 'Small', 'Moderate', 'Large', 'Very Large' and 'Super Large' to represent the eruption-size categories (Fig. S4.1). The number of events for each size category for the BiVol-1 and the BiVol-2 is shown in Table 4.2.

Size	Categorization	VSSL (Tg)	BiVol-1	BiVol-2
Super Large	Samalas (1257)	>164	14	28
Very Large	Tambora (1815) - Samalas (1257)	85-164	22	47
Large	Pinatubo (1991) - Tambora (1815)	55-85	33	35
Moderate	0.5*Pinatubo (1991) - Pinatubo (1991)	30-55	83	41
Small	0.5*Pinatubo (1991)	3-30	176	
Total			328	151

Table 4.2 Classification of ice-core volcanic records into different size categories. The values of the VSSL are the sulfate magnitudes of the categorized eruptions. The number of events refers to the related eruption size for the BiVol-1 and BiVol-2 that is shown in the column 'BiVol-1' and 'BiVol-2'.

4.4.3 Bootstrapping

To quantify the uncertainty for the mean return time of each size category eruption, we applied bootstrapping to resample the return times with replacement.

This process has 5000 iterations. For each iteration, the return times are chosen at random, and the resampled datasets are identical in size to the original dataset. The mean return time is calculated with each iteration. The confidence interval can be calculated from the distribution of the mean return times of 5000 iterations.

4.4.4 Exponential density function of volcanic return times

The variable x represents the return times of volcanic eruptions, that has an exponential distribution. $\lambda > 0$ being the rate parameter of the distribution. $1/\lambda$ is the mean return time of volcanic eruption.

$$f(x;\lambda) = \lambda e^{-\lambda x} \quad x \geq 0$$

The complementary cumulative distribution (CCD) of return times of volcanic eruptions can be obtained as follows:

$$F(x;\lambda) = 1 - \int_0^x f(x;\lambda) = e^{-\lambda x} \quad x \geq 0$$

This function can also be seen as memoryless function

$$f(x > s + T | x > s) = \frac{f((x > s + T) \cap (x > s))}{f(x > s)} = \frac{e^{-\lambda(s+T)}}{e^{-\lambda s}} = e^{-\lambda T} \ (T > s)$$

Here 'T'and 's' are interpreted as the two return times.

This CCD function or memoryless function is employed in Fig. 4.2 for the BiVol-1 and BiVol-2.

4.4.5 Maximum likelihood estimation (MLE)

The MLE is a method to estimate the most likely parameters for the fitted exponential model. The most likely parameters from the maximum joint probability based on the probability of the observed data in a joint CCD or memoryless distributions governed by a set of parameters.

The joint exponential density function is defined as:

$L_n(\theta) = L_n(\theta; x)$,

Where $\theta = [\lambda_1, \lambda_2, \ldots, \lambda_k]^T$ is the parameter vector and $x = [x_1, x_2, \ldots, x_n]^T$ is the observed return times of volcanic eruptions. The maximized parameter of λ is to obtained from an equation of

$\frac{d}{d\theta} ln(L_n(\theta)) = 0$

4.4.6 Anderson–Darling test (A–D test)

The A-D test is used to quantify the distance between the CCD model and the empirical distribution function, which is used to estimate the goodness of fit.

4.4.7 Probabilistic assessment in certain time-windows

The possibility of occurrence of volcanic eruptions (P_s) in 1, 10, 50, 100, 500 and 1000-year time lengths, that is represented by T_s.

$$P_s = 1 - e^{-\lambda T_s}$$

4.5 References

Abbott, P. M., Niemeier, U., Timmreck, C., Riede, F., McConnell, J. R., Severi, M., Fischer, H., Svensson, A., Toohey, M., Reinig, F., and Sigl, M.: Volcanic climate forcing preceding the inception of the Younger Dryas: Implications for tracing the Laacher See eruption, Quaternary Science Reviews, 274, 10.1016/j.quascirev.2021.107260, 2021.

Ambrose, S. H.: Late Pleistocene human population bottlenecks, volcanic winter, and differentiation of modern humans, Journal of Human Evolution, 34, 623-651, 10.1006/jhev.1998.0219, 1998.

Black, B. A., Lamarque, J. F., Marsh, D. R., Schmidt, A., and Bardeen, C. G.: Global climate disruption and regional climate shelters after the Toba supereruption, Proceedings of the National Academy of Sciences of the United States of America, 118, 10.1073/pnas.2013046118, 2021.

Gao, C. H., Oman, L., Robock, A., and Stenchikov, G. L.: Atmospheric volcanic loading derived from bipolar ice cores: Accounting for the spatial distribution of volcanic deposition, Journal of Geophysical Research-Atmospheres, 112, 10.1029/2006jd007461, 2007.

Huhtamaa, H. and Helama, S.: Distant impact: tropical volcanic eruptions and climate-driven agricultural crises in seventeenth-century Ostrobothnia, Finland, Journal of Historical Geography, 57, 40-51, 10.1016/j.jhg.2017.05.011, 2017.

Lin, J. M., Svensson, A., Hvidberg, C. S., Lohmann, J., Kristiansen, S., Dahl-Jensen, D., Steffensen, J. P., Rasmussen, S. O., Cook, E., Kjaeer, H. A., Vinther, B. M., Fischer, H., Stocker, T., Sigl, M., Bigler, M., Severi, M., Traversi, R., and Mulvaney, R.: Magnitude, frequency and climate forcing of global volcanism during the last glacial period as seen in Greenland and Antarctic ice cores (60-9 ka), Climate of the Past, 18, 485-506, 10.5194/cp-18-485-2022, 2022.

Maclennan, J., Jull, M., McKenzie, D., Slater, L., and Gronvold, K.: The link between volcanism and deglaciation in Iceland, Geochemistry Geophysics Geosystems, 3, 10.1029/2001gc000282, 2002.

Mason, B. G., Pyle, D. M., and Oppenheimer, C.: The size and frequency of the largest explosive eruptions on Earth, Bulletin of Volcanology, 66, 735-748, 10.1007/s00445-004-0355-9, 2004.

Morice, C. P., Kennedy, J. J., Rayner, N. A., and Jones, P. D.: Quantifying uncertainties in global and regional temperature change using an ensemble of observational estimates: The HadCRUT4 data set, Journal of Geophysical Research: Atmospheres, 117, https://doi.org/10.1029/2011JD017187, 2012.

Newhall, C. G. and Self, S.: The volcanic explosivity index (VEI) an estimate of explosive magnitude for historical volcanism, Journal of Geophysical Research: Oceans, 87, 1231-1238, https://doi.org/10.1029/JC087iC02p01231, 1982.

Nishimura, T., Iguchi, M., Hendrasto, M., Aoyama, H., Yamada, T., Ripepe, M., and Genco, R.: Magnitude–frequency distribution of volcanic explosion earthquakes, Earth, Planets and Space, 68, 125, 10.1186/s40623-016-0505-2, 2016.

Oppenheimer, C.: Climatic, environmental and human consequences of the largest known historic eruption: Tambora volcano (Indonesia) 1815, Progress in Physical Geography-Earth and Environment, 27, 230-259, 10.1191/0309133303pp379ra, 2003.

Papale, P.: Global time-size distribution of volcanic eruptions on Earth, Scientific Reports, 8, 10.1038/s41598-018-25286-y, 2018.

Papale, P., Marzocchi, W., and Garg, D.: Global Volume Distribution for Subaerial Volcanism on Earth, Journal of Geophysical Research-Solid Earth, 126, 10.1029/2021jb021763, 2021.

Robock, A.: Volcanic eruptions and climate, Reviews of Geophysics, 38, 191-219, 10.1029/1998rg000054, 2000.

Rougier, J., Sparks, R. S. J., Cashman, K. V., and Brown, S. K.: The global magnitude-frequency relationship for large explosive volcanic eruptions, Earth and Planetary Science Letters, 482, 621-629, 10.1016/j.epsl.2017.11.015, 2018.

Sigl, M., Toohey, M., McConnell, J. R., Cole-Dai, J., and Severi, M.: Volcanic stratospheric sulfur injections and aerosol optical depth during the Holocene (past 11,500 years) from a bipolar ice core array, Earth Syst. Sci. Data Discuss., 2022, 1-45, 10.5194/essd-2021-422, 2022.

Sigl, M., McConnell, J. R., Layman, L., Maselli, O., McGwire, K., Pasteris, D., Dahl-Jensen, D., Steffensen, J. P., Vinther, B., Edwards, R., Mulvaney, R., and Kipfstuhl, S.: A new bipolar ice core record of volcanism from WAIS Divide and NEEM and implications for climate forcing of the last 2000 years, Journal of Geophysical Research-Atmospheres, 118, 1151-1169, 10.1029/2012jd018603, 2013.

Sigl, M., McConnell, J. R., Toohey, M., Curran, M., Das, S. B., Edwards, R., Isaksson, E., Kawamura, K., Kipfstuhl, S., Kruger, K., Layman, L., Maselli, O. J., Motizuki, Y., Motoyama, H., Pasteris, D. R., and Severi, M.: Insights from Antarctica on volcanic forcing during the Common Era, Nature Climate Change, 4, 693-697, 10.1038/nclimate2293, 2014.

Sigl, M., Winstrup, M., McConnell, J. R., Welten, K. C., Plunkett, G., Ludlow, F., Buntgen, U., Caffee, M., Chellman, N., Dahl-Jensen, D., Fischer, H., Kipfstuhl, S., Kostick, C., Maselli, O. J., Mekhaldi, F., Mulvaney, R., Muscheler, R., Pasteris, D. R., Pilcher, J. R., Salzer, M., Schupbach, S., Steffensen, J. P., Vinther, B. M., and Woodruff, T. E.: Timing and climate forcing of volcanic eruptions for the past 2,500 years, Nature, 523, 543-+, 10.1038/nature14565, 2015.

Sigl, M., Fudge, T. J., Winstrup, M., Cole-Dai, J., Ferris, D., McConnell, J. R., Taylor, K. C., Welten, K. C., Woodruff, T. E., Adolphi, F., Bisiaux, M., Brook, E. J., Buizert, C., Caffee, M. W., Dunbar, N. W., Edwards, R., Geng, L., Iverson, N., Koffman, B., Layman, L., Maselli, O. J., McGwire, K., Muscheler, R., Nishiizumi, K., Pasteris, D. R., Rhodes, R. H., and Sowers, T. A.: The WAIS Divide deep ice core WD2014 chronology - Part 2: Annual-layer counting (0-31 ka BP), Climate of the Past, 12, 769-786, 10.5194/cp-12-769-2016, 2016.

Sinnl, G., Winstrup, M., Erhardt, T., Cook, E., Jensen, C. M., Svensson, A., Vinther, B. M., Muscheler, R., and Rasmussen, S. O.: A multi-ice-core, annual-layer-counted Greenland ice-core chronology for the last 3800 years: GICC21, Clim. Past, 18, 1125-1150, 10.5194/cp-18-1125-2022, 2022.

Stothers, R. B.: THE GREAT TAMBORA ERUPTION IN 1815 AND ITS AFTERMATH, Science, 224, 1191-1198, 10.1126/science.224.4654.1191, 1984.

Svensson, A., Bigler, M., Blunier, T., Clausen, H. B., Dahl-Jensen, D., Fischer, H., Fujita, S., Goto-Azuma, K., Johnsen, S. J., Kawamura, K., Kipfstuhl, S., Kohno, M., Parrenin, F., Popp, T., Rasmussen, S. O., Schwander, J., Seierstad, I., Severi, M., Steffensen, J. P., Udisti, R., Uemura, R., Vallelonga, P., Vinther, B. M., Wegner, A., Wilhelms, F., and Winstrup, M.: Direct linking of Greenland and Antarctic ice cores at the Toba eruption (74 ka BP), Climate of the Past, 9, 749-766, 10.5194/cp-9-749-2013, 2013.

Svensson, A., Dahl-Jensen, D., Steffensen, J. P., Blunier, T., Rasmussen, S. O., Vinther, B. M., Vallelonga, P., Capron, E., Gkinis, V., Cook, E., Kjaer, H. A., Muscheler, R., Kipfstuhl, S., Wilhelms, F., Stocker, T. F., Fischer, H., Adolphi, F., Erhardt, T., Sigl, M., Landais, A., Parrenin, F., Buizert, C., McConnell, J. R., Severi, M., Mulvaney, R., and Bigler, M.: Bipolar volcanic synchronization of abrupt climate change in Greenland and Antarctic ice cores during the last glacial period, Climate of the Past, 16, 1565-1580, 10.5194/cp-16-1565-2020, 2020.

Toohey, M., Kruger, K., and Timmreck, C.: Volcanic sulfate deposition to Greenland and Antarctica: A modeling sensitivity study, Journal of Geophysical Research-Atmospheres, 118, 4788-4800, 10.1002/jgrd.50428, 2013.

Toohey, M., Kruger, K., Schmidt, H., Timmreck, C., Sigl, M., Stoffel, M., and Wilson, R.: Disproportionately strong climate forcing from extratropical explosive volcanic eruptions, Nature Geoscience, 12, 100-+, 10.1038/s41561-018-0286-2, 2019.

Chapter 5

5.1 Conclusion

This thesis employs continuous sulfate and sulfur records from polar ice cores to estimate the emission strength, frequency, and climatic forcing from large volcanic eruptions that occurred during the early Holocene and the last glacial period (60-9 ka). In addition, the global volcanic records are identified from ice cores and applied to forecast the recurrence rate and probability of volcanic eruptions at different scales. The main results are summarized in the following.

There are 1113 volcanic eruptions in Greenland and 740 eruptions in Antarctica identified over the period 60-9 ka b2k (before 2000 AD) with volcanic sulfate deposition. Among them, the sulfate deposition of 85 eruptions is quantified at both poles, defined as bipolar eruptions.

Twenty-five of the identified bipolar eruptions are larger than any volcanic eruption occurring in the last 2500 years, and 69 eruptions are estimated to have stronger sulfur emission strengths than that of the Tambora, Indonesia eruption (1815 AD).

Two largest sulfur-rich volcanic eruptions are identified over the investigated period – one occurred at 45.56 ka b2k, with the eruption latitude predicted in the Northern Hemisphere, and the other one occurred at 38.13 ka b2k, with the eruption site predicted in low latitude or in the Southern Hemisphere. Both are larger than the Taupo, Oruanui, eruption, that occurred at 25.32 ka BP1950, in present day New Zealand.

Volcanic activity in the Northern Hemisphere is more enhanced compared to the Southern Hemisphere because more volcanic sulfate signals are identified in Greenland ice cores than in Antarctic ice cores. Besides, we found increased volcanic frequency in the Northern Hemisphere during the deglacial period, which is related to the induced stochastic state of the plate due to the melt down of the major glacial ice sheet.

For the largest volcanic eruption in the quaternary period, the ~74 ka Toba eruption, the proposed stratigraphic position in polar ice cores is pinpointed. The estimated stratospheric sulfate injection of the proposed candidate is 535 ± 96 Tg, that is 3.3 times that of the Samalas 1258 AD, 6.3 times that of the Tambora 1815 AD and 9.7 times that of the Pinatubo 1991 AD.

Two datasets of bipolar volcanic records with eruption dates and stratospheric sulfate injections are collected from ice cores, one covering the Holocene period and the other covering the Holocene and the last glacial periods. The density distribution of return times of eruptions at different scales, defined by the magnitude of known eruptions, is close to the exponential distribution.

According to statistical analysis, volcanic eruption larger than the Tambora 1815 AD is characterized by low eruption rate and a conservative mean return time is estimated to be 434 years. Over the next 100 years, the probability of observing such an event exceeds 19%, rising above 65% in the next 500 years. An eruption of this scale could disrupt global trade and economies and trigger climate anomalies. Human society should prepare for such hazards.

5.2 Outlook

Call for multiple high-quality ice-core sulfate records

During the last glacial cycle, three deep ice core records in Antarctica and three deep ice core records in Greenland were used to derive volcanic sulfate deposition. However, in the common era, there were 10-25 ice cores in Antarctica that were applied to have a better estimate of regional average volcanic sulfate depositions (Sigl et al., 2014). Therefore, the uncertainty of the volcanic sulfate depositions in the last glacial cycle is larger. More high-resolution sulfur or sulfate records need to be developed from ice cores, that can provide a more precise estimation for the regional volcanic sulfate fallout. This is more needed in Antarctica due to the long distance between ice core sites and the large spatial variability of the sulfate fallout process.

Improve the reconstruction of volcanic sulfate fallout through climate models

The detection of volcanic sulfate signals is challenging in the last glacial period due to the high sulfate background in Greenland ice cores, which is related to glacial climate conditions in the Northern Hemisphere. What causes this mechanism has not yet been addressed. For further research, the magnitude of sulfur-rich volcanism can be more accurately quantified through improved understanding of the atmospheric and ocean circulation, the wet and dry deposition processes in the polar area, the volcanic cloud transport and dispersal process, and the hemispheric partitioning of sulfate deposition. The climate model with chemistry-aerosol and microphysics modules would be a useful tool to test this process and understand the relationship between sulfur injecition altitude and the amount of deposition in the Greenland and Antarctic ice sheets.

To investigate volcanic features (the plume height and the source)

It has recently become possible to test whether sulphate does reach the stratosphere, a prerequisite for global distribution, where it undergoes a characteristic isotopic differentiation (Burke et al., 2019; Gautier et al., 2018; Crick et al., 2021). But these analyses are still scarce for the last glacial period. More measurements need to be performed to improve features for large volcanic eruptions in the last glacial period.

The ice-core volcanic source identification is important as it helps to distinguish bipolar volcanoes from regional volcanoes and has a better constraint on the volcanic radiative forcing. Tephra layers are not always coincident with sulfate peaks (Davies et al., 2010) and most volcanic sulfate signals have no tephra associated with them. The number of bipolar volcanoes identified from bipolar ice-core synchronization is lower compared to that in the Holocene

period, due to the ice layer thinning with depth and more offset between Greenland and Antarctic ice-core timescales. More age markers need to be investigated to better constrain the polar ice-core timescale and identify more bipolar volcanoes.

5.3 References

Burke, A., Moore, K. A., Sigl, M., Nita, D. C., McConnell, J. R., and Adkins, J. F.: Stratospheric eruptions from tropical and extra-tropical volcanoes constrained using high-resolution sulfur isotopes in ice cores, Earth and Planetary Science Letters, 521, 113-119, 10.1016/j.epsl.2019.06.006, 2019.

Crick, L., Burke, A., Hutchison, W., Kohno, M., Moore, K. A., Savarino, J., Doyle, E. A., Mahony, S., Kipfstuhl, S., Rae, J. W. B., Steele, R. C. J., Sparks, R. S. J., and Wolff, E. W.: New insights into the similar to 74 ka Toba eruption from sulfur isotopes of polar ice cores, Climate of the Past, 17, 2119-2137, 10.5194/cp-17-2119-2021, 2021.

Gautier, E., Savarino, J., Erbland, J., and Farquhar, J.: SO2 Oxidation Kinetics Leave a Consistent Isotopic Imprint on Volcanic Ice Core Sulfate, Journal of Geophysical Research-Atmospheres, 123, 9801-9812, 10.1029/2018jd028456, 2018.

Sigl, M., McConnell, J. R., Toohey, M., Curran, M., Das, S. B., Edwards, R., Isaksson, E., Kawamura, K., Kipfstuhl, S., Kruger, K., Layman, L., Maselli, O. J., Motizuki, Y., Motoyama, H., Pasteris, D. R., and Severi, M.: Insights from Antarctica on volcanic forcing during the Common Era, Nature Climate Change, 4, 693-697, 10.1038/nclimate2293, 2014.

Appendix

Fig. S3.1

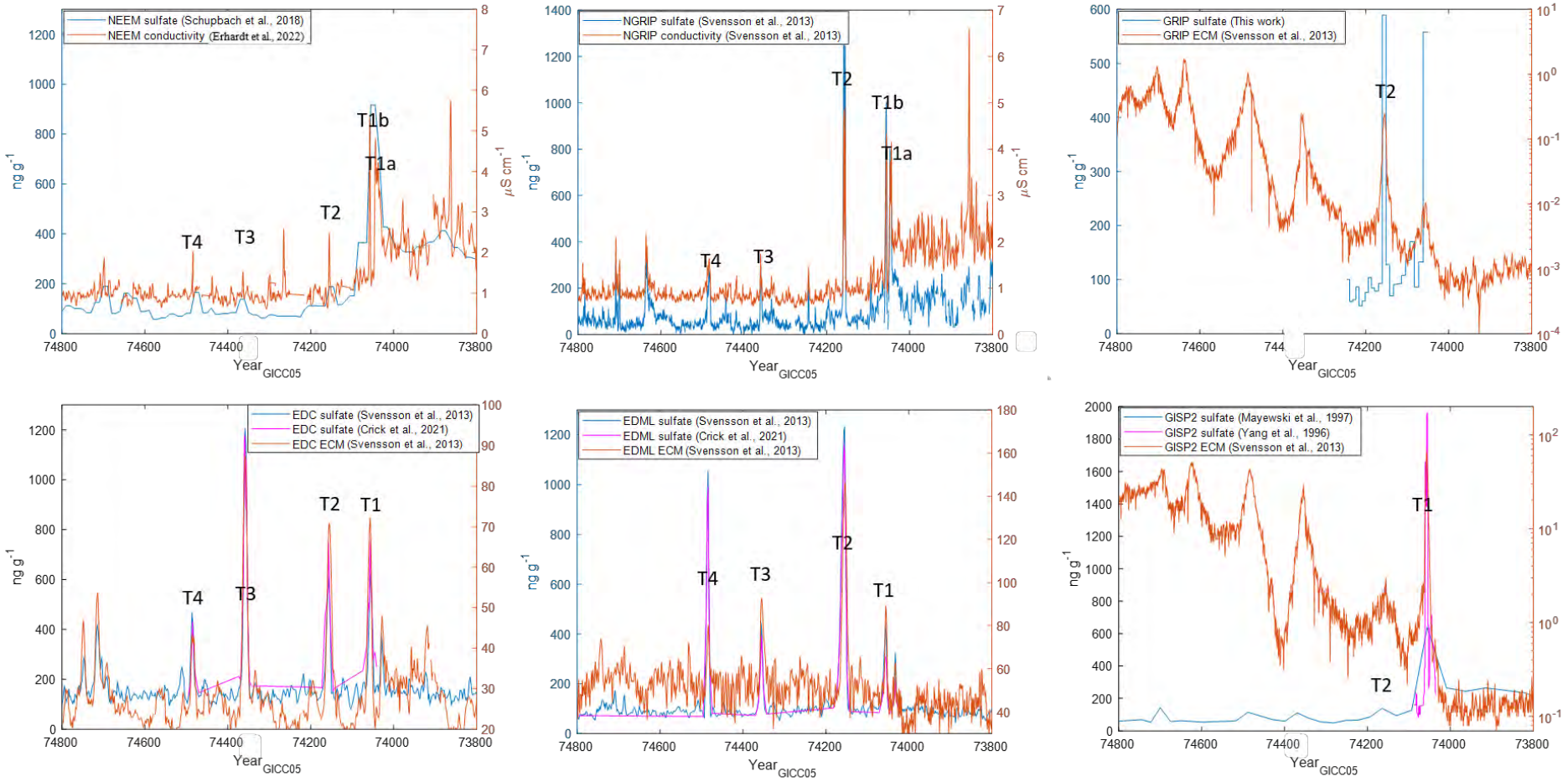

The sulfate, ECM and conductivity records derived from the ice cores of Greenland and Antarctica.

Appendix

Fig. S3.2

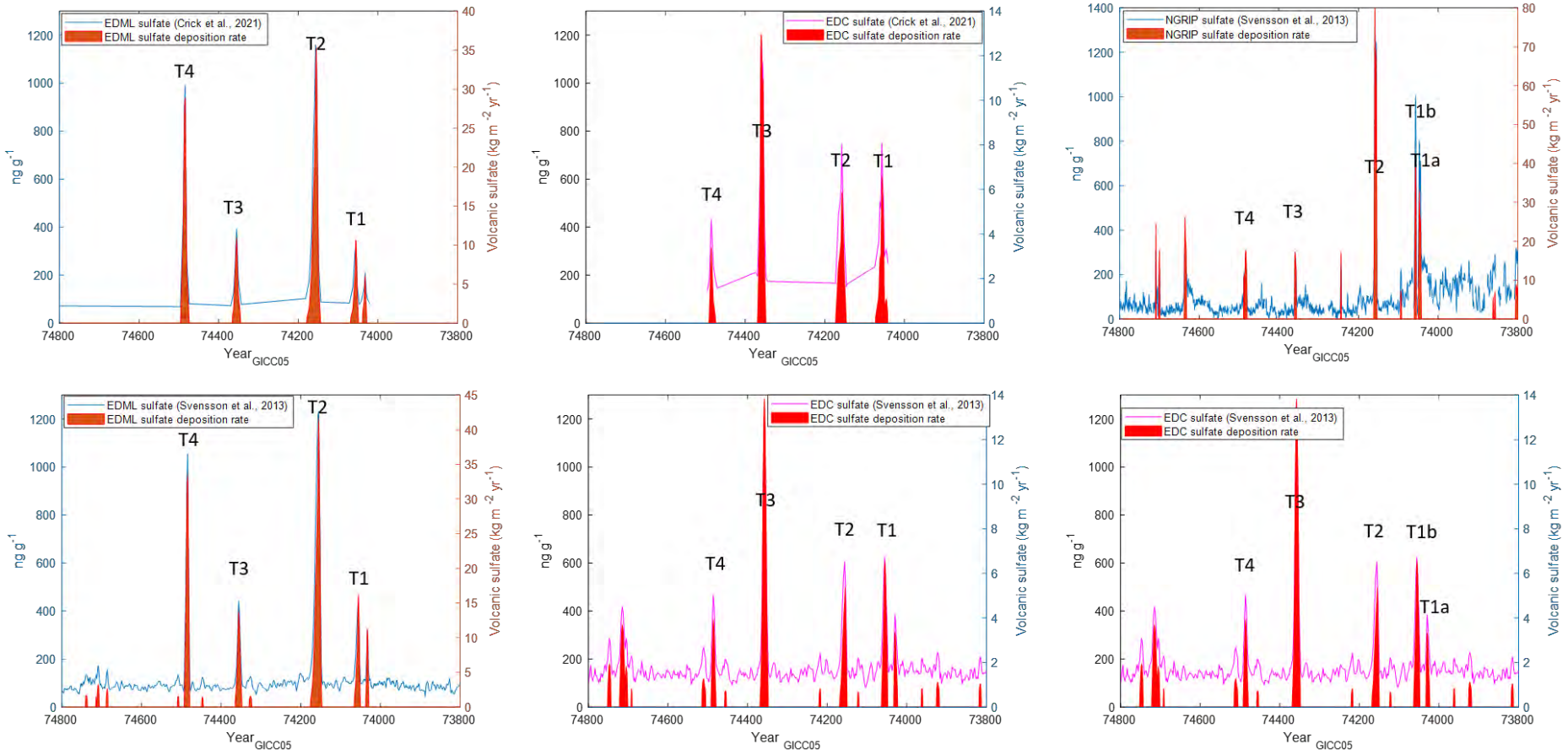

The ice-core sulfate records and the annual volcanic sulfate deposition rates derived from the corresponding sulfate records of Greenland and Antarctica.

Fig. S3.3

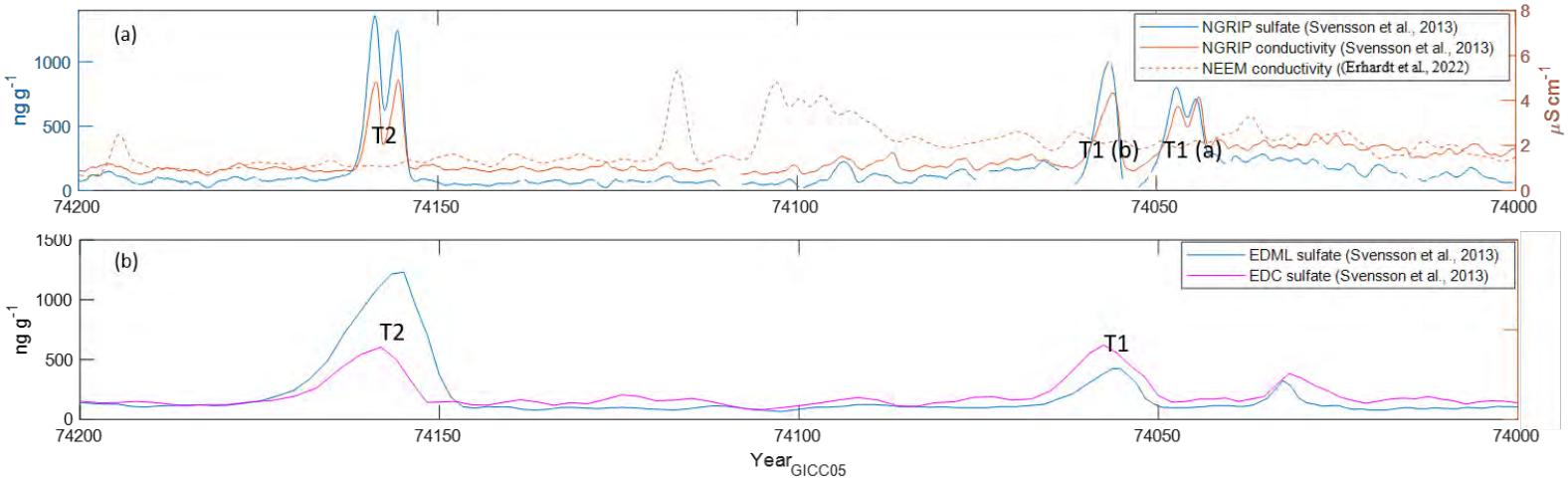

Detailed information of Toba candidates - T1a, T1b and T2 on the high-resolution NGRIP sulfate record, NGRIP conductivity, NEEM conductivity, EDC sulfate and EDML sulfate records.

Fig. S3.4

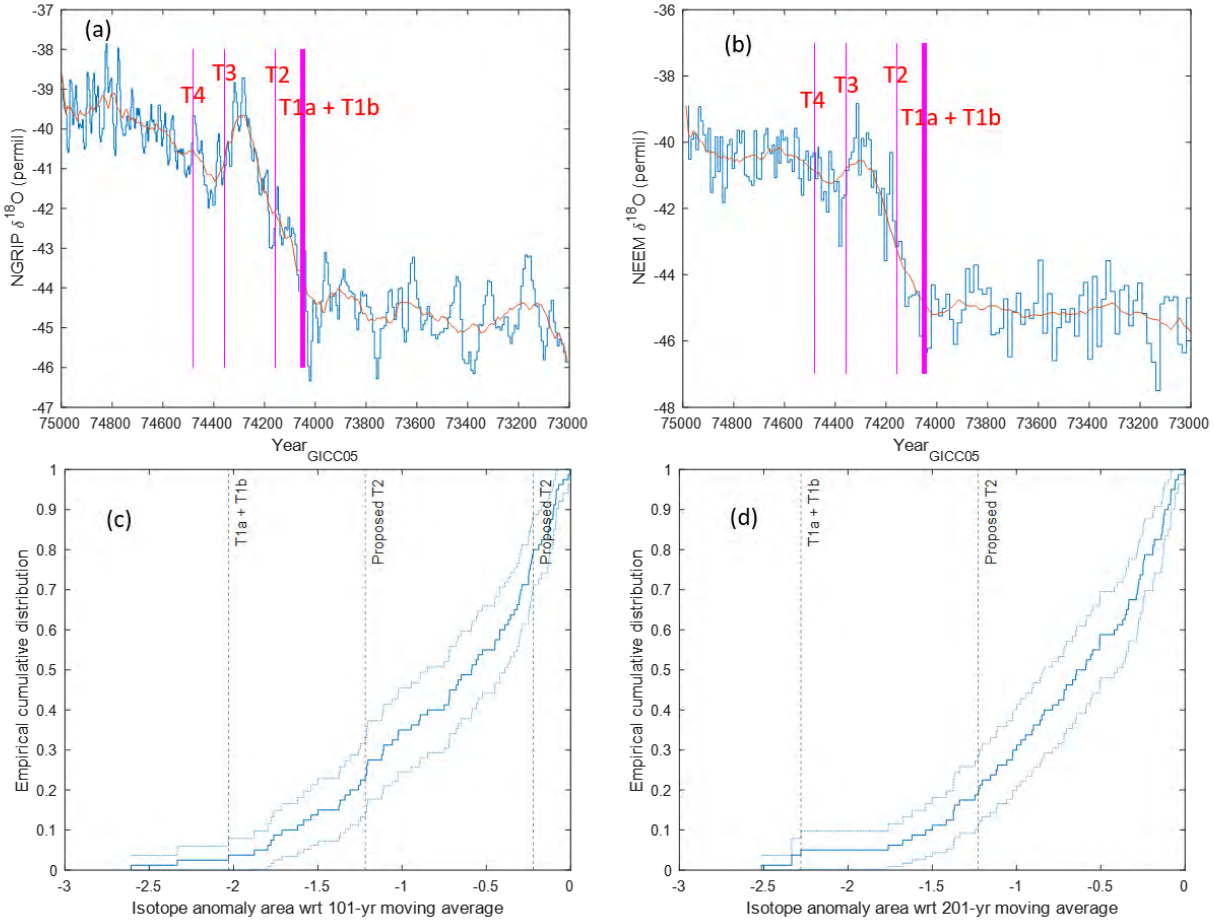

(a), The NGRIP δ18O record with the 101-yrs moving average smooth. (b), The NEEM δ18O record with the 201-yrs moving average smooth. (c-d), The empirical cumulative distribution of negative isotopic magnitude, that is derived by integrating the negative peak area of the NGRIP and NEEM δ18O records in 5 cm (3-18 yrs temporal resolution; red line). NGRIP (c) and NEEM (d). The proposed T2 event is the negative isotopic peaks close to the T2 event. The width of magenta bar represents the volcanic duration of ice-core.

Fig. S3.5

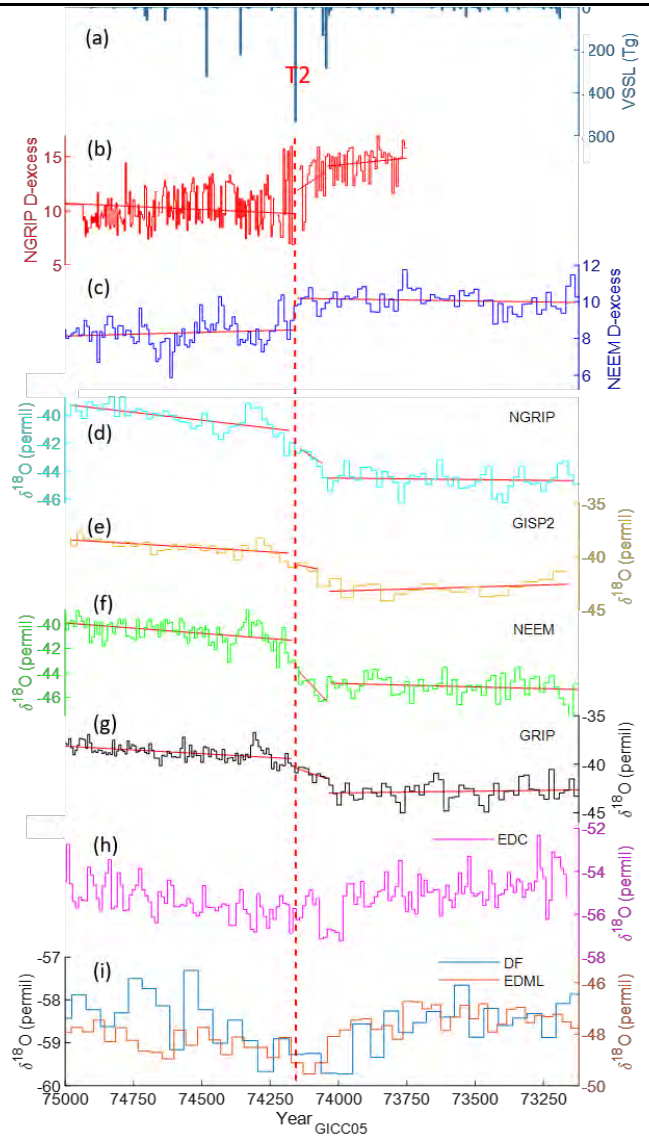

Abrupt climate variability at the termination of GI-20. (a), The volcanic stratospheric sulfate loading (VSSL). (b), NGRIP deuterium excess record. Three disconnected linear fits (intervals: >74156, 74156-74041, 74041-73760) represent in red color. (c), NEEM deuterium excess record. Two disconnected linear fits (intervals: >74156, 74156-73121) represent in red color. (d-g), The δ18O records of the NGRIP, NEEM, GISP2 and GRIP ice cores in Greenland. Three disconnected linear fits (intervals: >74156, 74156-74041, 74041-73121). (h-i), The $\delta^{18}O$ records of EDC, EDML and DF ice cores in Antarctica.

Figure S4.1

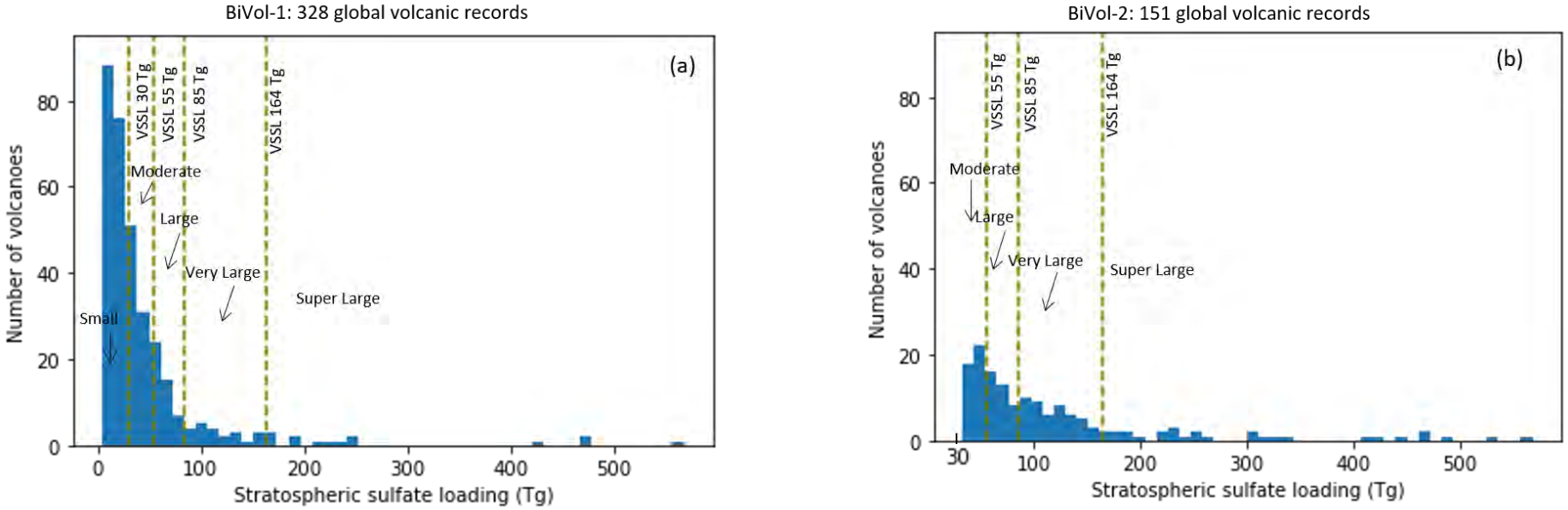

Magnitude and number of global volcanic records from ice cores.

(a) VSSL of global volcanic records derived from Greenland and Antarctic ice cores for the Holocene (100-11,550 a b2k; Sigl et al., 2022). Volcanoes are classified into five eruption-size groups (Small : VSSL 3-30 Tg, 176 events; Moderate: VSSL 30-55 Tg, 83 events; Large: VSSL 55-85 Tg, 33 events;Very Large: VSSL 85-164 Tg, 22 events; Super Large: VSSL>164 Tg, 14 events).

(b) VSSL derived from Greenland and Antarctic ice cores , covering the periods of 100-11,550, 12,752-13,225, 14,467-15,723, 19,500-24,700, 37,890-38,406, 40,700-41,405, 41,715-42,250, 57,074-57,509, 59,100-59,800, and 73,800-74,800 a b2k. Detection limit for VSSL is the Greenland volcanic sulfate deposits larger than 20 kg km^{-2} and Antarctic volcanic sulfate deposits above 10 kg km^{-2}. Volcanoes are classified into four eruption-size groups (Moderate: VSSL 30-55 Tg, 41 events; Large: VSSL 55-85 Tg, 35 events; Very Large: VSSL 85-164 Tg, 47 events; Super Large: VSSL>164 Tg, 28 events).

Figure S4.2

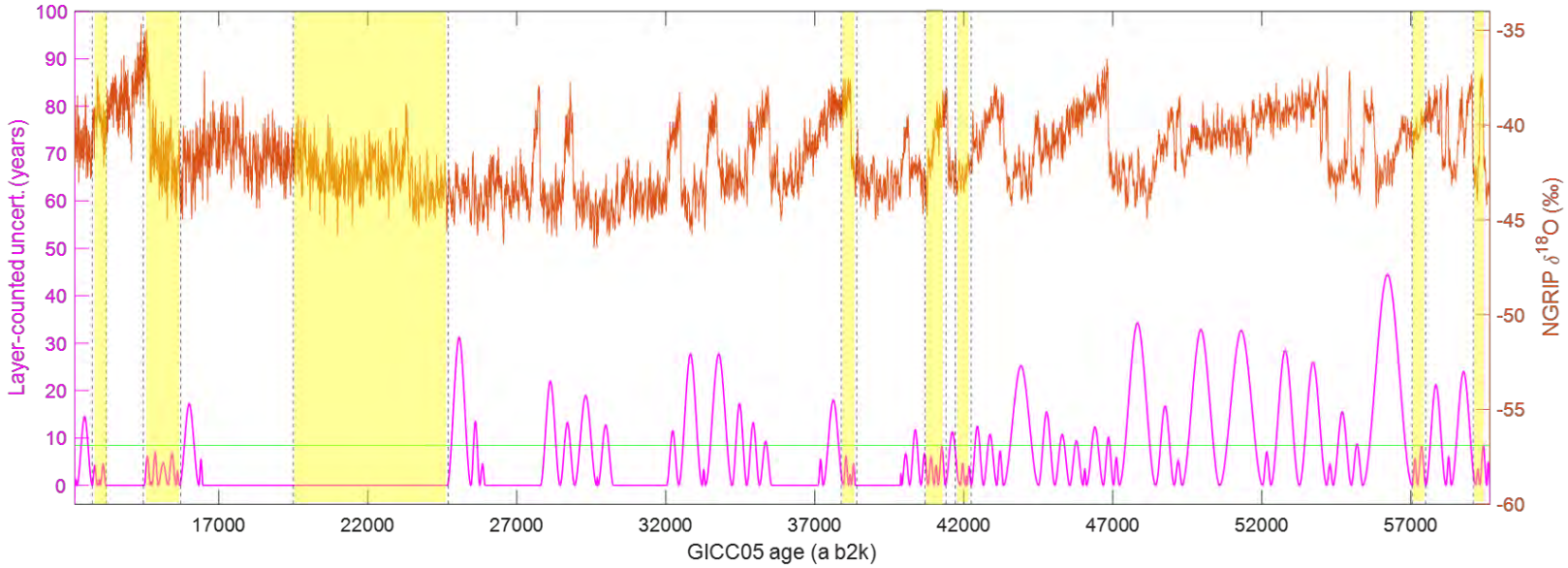

The uncertainty of layer counted between adjacent bipolar volcanic tie-points. New bipolar volcanic sulfate signals are identified over the 'highlight' periods. The 'zero year' keeping more than one years represents no ice-layer counted (Svensson et al., 2020). The green line stands for threshold of layer counted uncertainty years (18 years).

Figure S4.3 LGM bipolar match points

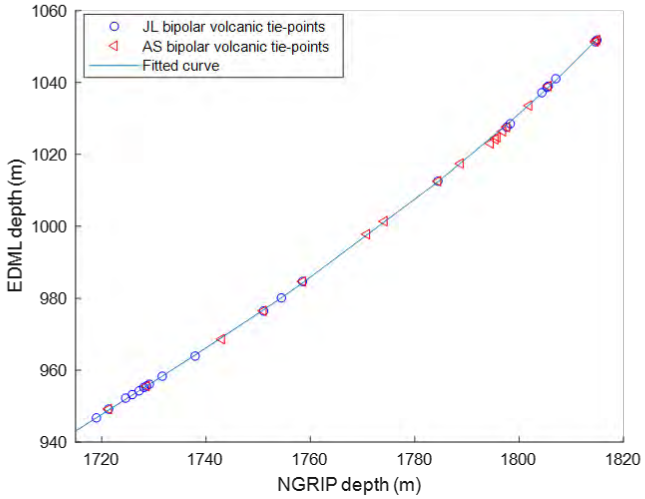

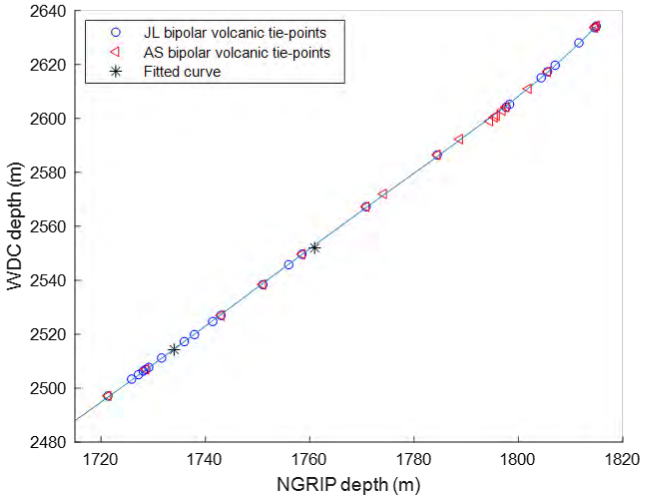

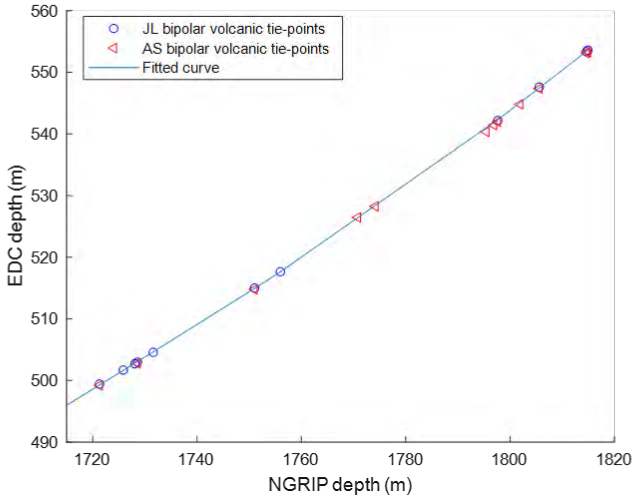

Bipolar match points identified in polar ice cores in last glacial maximum. Thirteen bipolar volcanic tie points in the last glacial maximum (19.5-24.5 ka b2k) are synchronized by Svensson et al. (2022 in prepare, labelled with red Δ). Two newly ^{10}Be match points are discovered in Greenland and Antarctic ice cores (Sinnl et al., 2022 undereview; labelled with *).
Forty-two bipolar volcanic match points are identified using the linear interpolation of timescale and the same timing of volcanic events (labelled with blue circle).

Figure S4.5

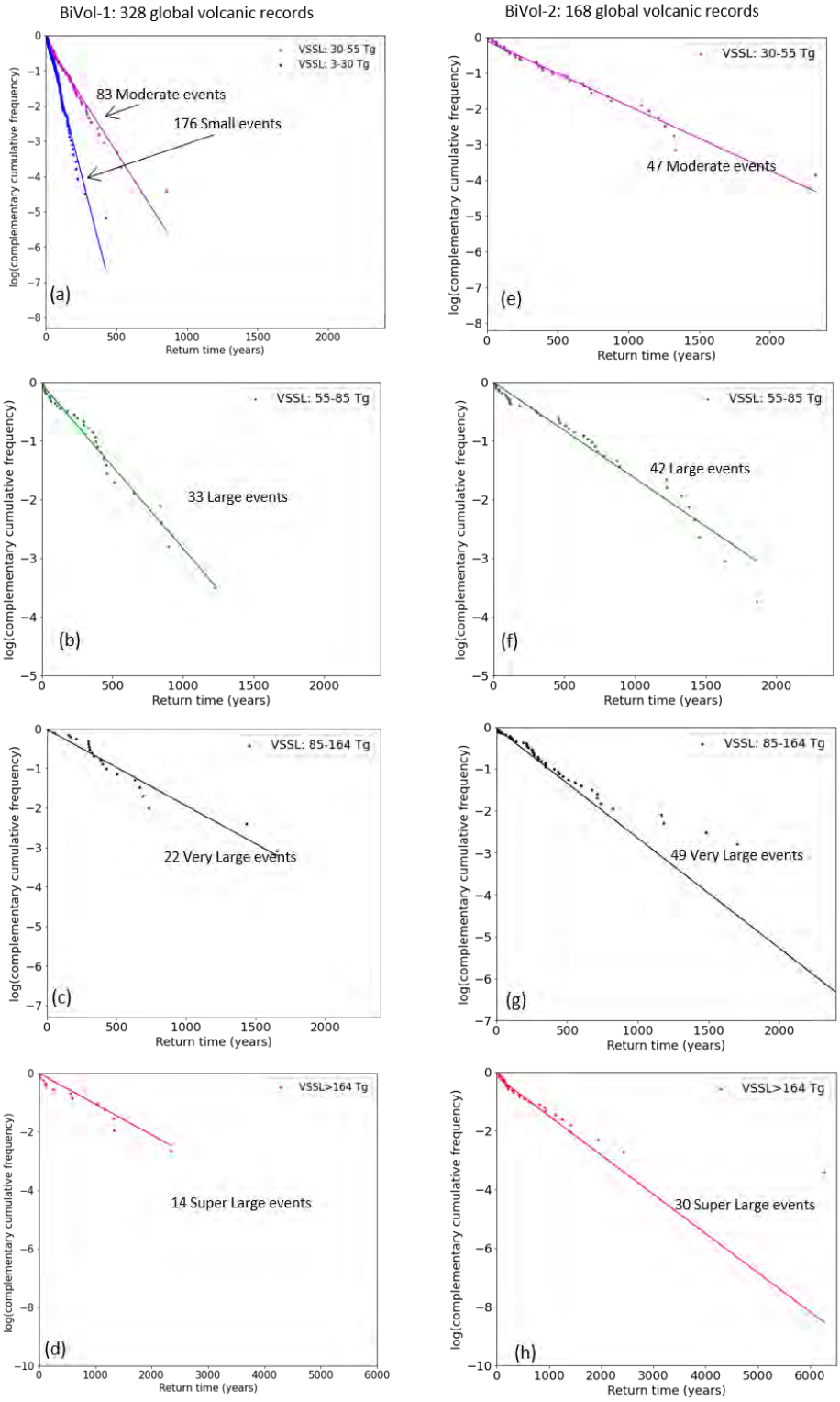

The log normal of complementary cumulative distribution of return times of each size categories of global volcanic eruptions. The fits are represented by thick lines in the same colors.